HYDRO-MECHANICAL ANALYSIS OF EXPANSIVE CLAYS CONSTITUTIVE AND NUMERICAL MODELLING

by

Daniel Felipe Ruiz Restrepo

A thesis submitted in partial fulfilment of the
requirements for the degree of
Doctor of Philosophy

Department of Civil and Environmental Engineering
Section of Geotechnical Engineering and Geosciences
Technical University of Catalonia
BARCELONATECH

Supervisors:
Antonio Gens Solé
Jean Vaunat

Barcelona
March 2020

To the little man who inspire me to be the best version of myself,

Thiago.

*"I'll tell you what freedom is to me. **No fear**."*

Nina Simone

*"If you are going through hell, **keep going**."*

Winston S. Churchill

Abstract

Bentonite-based materials are being currently considered in several countries as a backfill component in the multi-barrier concept for deep geological disposal of radioactive waste. The bentonite barrier fulfils several important functions: i) high swelling capacity to fill gaps and compress the excavation damaged zone and ii) very low hydraulic conductivity and important retention capacity which retards significantly radionuclides transport. Small-scale testing in geotechnical laboratories and in-situ experiments in underground research laboratories (URL) have demonstrated that initial state, water supply conditions and volume constrictions are the main aspects affecting the behaviour of bentonites.

In this context, the main objective of the present study is the numerical simulation of the hydro-mechanical behaviour of expansive clays. For this purpose, a constitutive model has been developed to characterise the bentonite-based materials. The modelling of these materials is a quite challenging task. They exhibit a marked double-porosity system in which the swelling/shrinkage mechanism occurs at clay aggregate level and the collapsible behaviour comes from granular-like skeleton formed by the aggregates. In addition, several material configuration, with even more intricate fabric, have been proposed for the emplacement works of seals and plugs. The explicit consideration of two structural levels for the constitutive model seems to be suitable. Mechanical interaction and water mass exchanges between them can explain the short- and long-term behaviour. The model has been formulated using concepts of elasto-plasticity for strain hardening materials and generalized plasticity theory. The formulation has been implemented in the finite element code program CODE-BRIGHT and has been used to solve a variety of problems. The results provide relevant insights into the hydro-mechanical behaviour of double structure porous media, and they indicated the main aspects affecting the responses of expansive barriers. In particular, the relevance of the structural levels interaction has been demonstrated.

Acknowledgements

Quiero expresar mi agradecimiento, en primer lugar, a los directores de esta tesis doctoral. Trabajar junto a ellos ha sido una experiencia enriquecedora. A Antonio Gens por su capacidad de escuchar y aportar nuevas ideas en momentos críticos de este proceso. Su visión crítica y asertiva de la ingeniería geotécnica ha sido una gran lección. A Jean Vaunat por nunca guardarse nada en las extensas asesorías y explicaciones y lo más importante por su amistad.

Agradezco también a otros miembros del Departamento de Ingeniería del Terreno. A Antonio Lloret por siempre tener la puerta de su oficina abierta para resolver dudas y brindar conocimiento. A Sebastián Olivella por su constante asesoría y efectiva ayuda durante este tiempo. Probablemente la persona más inteligente que he conocido.

Special mention to Prof. Anne-Catherine Dieudonné and Prof Vicente Navarro, who agreed to review this work and took part in the examination jury.

I want to express my gratitude to Prof. Christophe Dano, Dr. Andry Razakamanantsoa and Dr. Didier Virely. Sometimes the doctoral work development takes a different course. Nevertheless, the research stays in Nantes and Toulouse make me a better researcher and person.

Quiero agradecer también a José Manuel Gesto por poner sobre ruedas la parte inicial de esta investigación y por sus asesorías. A Ramon B. de Vasconcelos por ser un compañero de "batalla" en la modelación de arcillas expansivas; todas nuestras discusiones sobre esta investigación y el libre acceso sus avances e ideas de manera desinteresada han sido vitales. A Miguel Mánica por sus continuas orientaciones en implementación numérica y hacerme participe de sus investigaciones en el comportamiento de rocas arcillosas. A Mauricio Alvarado con quien compartimos piso "geotécnico" por ocho años y terminamos siendo familia.

Agradezco también a quienes desde la distancia se han interesado por este trabajo, especialmente a Manuel R. Villarraga y Edilma Goméz por su confianza y estímulo a lo largo de estos años.

Finalmente, un especial agradecimiento a mi familia. A mis padres y hermana quienes desde Colombia han sido espectadores y animadores en este proceso. A Claudia por su acompañamiento incondicional y constante ayuda personal y académica, y a Thiago por recargarme las baterías en los momentos más duros.

Este trabajo ha sido posible gracias al apoyo económico recibido por parte de diferentes instituciones. En primer lugar, mi gratitud a la Agència de Gestió d'Ajust Universitaris i de Recerca (AGAUR), a través del programa de becas FI-DRG 2013. También quiero agradecer el apoyo económico recibido durante estos años por parte de ANDRA y el proyecto europeo BEACON, a través del CIMNE, y a la compañía consultora INTEINSA.

Content

List of Publications

This is a detailed list of all work published, submitted or to be submitted, related to this PhD.

Peer reviewed journals

Ruiz, D.F., Gens, A., Vaunat, J., Vasconcelos R.B., Gesto, J.M., (in preparation). Enhanced double structure plasticity model for expansive clays.

Ruiz, D.F., Rorato, R., Gens, A., (in preparation). Discrete modelling of micro-macro mechanical interactions in expansive media.

Mánica, M., Gens, A., Vaunat, J., **Ruiz, D.F.**, 2018. Nonlocal plasticity modelling of strain localization in stiff clays. Comput. Geotech. 103, 138–150.

Mánica, M., Gens, A., Vaunat, J., **Ruiz, D.F.**, 2017. A time-dependent anisotropic model for argillaceous rocks. Application to an underground excavation in Callovo-Oxfordian claystone. Comput. Geotech. 85, 341–350.

Mánica, M.A., Gens, A., Vaunat, J., **Ruiz, D.F.**, 2016. A cross-anisotropic formulation for elasto-plastic models. Géotechnique Letters 6, 1–7.

Book Chapters

Manica, M-A., **Ruiz, D.F.**, Vaunat, J., Gens, A., 2019. Geomechanics of Shale Repositories: Mechanical Behavior and Modeling. In Shale: Subsurface Science and Engineering. American Geophysical Union, AGU.

Conference proceedings

Vasconcelos R.B., Gens, A., **Ruiz, D.F.**, Villar, M.V., 2019. Modelling a heating-hydration bentonite-based column test using a double porosity approach. In: XV International Conference on Computational Plasticity Fundamentals and Applications (Eds E.

Oñate, D.R.J. Owen, D. Peric, M. Chiumenti and E. de Souza Neto). Barcelona. CIMNE.

Ruiz, D.F., Vaunat, J., Gens, A., Mánica, M., 2018. Hydro-Mechanical modelling of an unsaturated seal structure. In: NUMGE 2018, IX European Conference on Numerical Methods in Geotechnical Engineering. Porto, Portugal. 10 p.

Ruiz, D.F., Vaunat, J., Gens, A., Mánica, M., 2017. Analysis of the hydration of an unsaturated seal. In: II Pan-American conference on unsaturated soils International. Dallas, USA. pp. 329–338.

Mánica, M., Gens, A., Vaunat, J., **Ruiz, D.F.**, 2017. Analysis of localized deformation around deep excavations in argillaceous rocks. In: VII International Conference on Clays in Natural and Engineered Barriers for Radioactive Waste Confinement. Davos, Swiss.

Ruiz, D.F., Vaunat, J., Gens, A., Mánica, M., 2017. Hydro-mechanical modelling of a gallery sealing over the entire life of a deep repository. In: GEOPROC 2017, VI International Conference on coupled THMC processes in geosystems. Paris, France, 4 p.

Mánica, M., Gens, A., Vaunat, J., **Ruiz, D.F.**, 2017. Analysis of strain localization with a nonlocal plasticity model. In: XIV International Conference on Computational Plasticity Fundamentals and Applications (Eds E. Oñate, D.R.J. Owen, D. Peric, and M. Chiumenti). Barcelona. CIMNE. pp. 606–612.

Mánica, M., Gens, A., Vaunat, J., **Ruiz, D.F.**, 2017. Hydromechanical modelling of a tunnel excavated in argillaceous rock. In: EURO:TUN 2017, IV International Conference on Computational Methods in Tunneling and Subsurface Engineering. Innsbruck: Universität Innsbruck. pp. 491-496.

Gens, A., Mánica, M., Vaunat, J., **Ruiz, D.F.**, 2017. Modelling the mechanical behaviour of Callovo-Oxfordian argillite. Formulation and application. In: Advance in Laboratory Testing and Modelling of Soils and Shales (Eds A. Ferrari and L. Laloui). pp. 37–44.

Ruiz, D.F., 2015. Insights into the response of a gallery sealing over the entire life of a deep repository. In: W(H)YDOC 2015, 5th International Workshop of Young Doctors in Geomechanics. Paris, France, Presentation.

Mánica, M., Gens, A., Vaunat, J., **Ruiz, D.F.**, 2015. Anisotropic failure criterion for an argillaceous rock. In: XIII International Conference on Computational Plasticity Fundamentals and Applications (Eds E. Oñate, D.R.J. Owen, D. Peric, and M. Chiumenti). Barcelona. CIMNE. pp. 654–660.

Ruiz, D.F., Vaunat, J., Gens, A., Pasteu, A., 2015. Insights into the response of a gallery sealing over the entire life of a deep repository. In: 7th Workshop of CODE_BRIGHT, 4 p.

Posters

Ruiz, D.F., Vaunat, J., Gens, A., Mánica, M., Pasteau, A., 2015. Insights into the response of a gallery sealing over the entire life of a deep repository. 6th International Conference on Clays in Natural and Engineered Barriers for Radioactive Waste Confinement, Brussels, Belgium, Poster presentation.

Mánica, M., Gens, A., Vaunat, J., **Ruiz, D.F.,** Seyedi, D. & Armand, G., 2015. Numerical modelling of drifts excavated in stiff clays. 6th International Conference on Clays in Natural and Engineered Barriers for Radioactive Waste Confinement, Brussels, Belgium, Poster presentation.

Technical reports

Ruiz, D.F., Vaunat, J., Gens, A., 2014. Coupled hydro-mechanical simulation of the sealing system for the ANDRA deep nuclear waste repository. Project "SCELLEMENTS". Annual Report 1, Base case modelling.

Ruiz, D.F., Vaunat, J., Gens, A., 2015. Coupled hydro-mechanical simulation of the sealing system for the ANDRA deep nuclear waste repository. Project "SCELLEMENTS". 1th Report,

Sensitivity analysis of the base case model and contact effects modelling.

Ruiz, D.F., Vaunat, J., Gens, A., 2015. Coupled hydro-mechanical simulation of the sealing system for the ANDRA deep nuclear waste repository. Project “SCELLEMENTS”. Report 3, Advanced modelling.

Ruiz, D.F., Gens, A., 2018. Coupled hydro-mechanical modelling of unsaturated expansive clays. Project BEACON (Bentonite Mechanical Evolution). Deliverable 3.1., Constitutive model formulation.

Ruiz, D.F., Gens, A., 2019. Coupled hydro-mechanical modelling of unsaturated expansive clays. Project BEACON (Bentonite Mechanical Evolution). Deliverable 3.2., Model improvement.

List of Figures

List of Tables

Chapter 1

Introduction

'Classical soil mechanics has evolved around a few simplified models which do not fit the properties of most real soils sufficiently for useful and safe predictions to be made...Since we cannot change the soil to fit the soil mechanics, perhaps we should change the soil mechanics to fit the soil. The theory which fails to fit their behaviour is problematic, not the soil.'

Professor P.R. Vaughan, (1999)

1.1. General

Expansive clays are materials that increase strongly in volume when they are exposed to water and adsorption of water molecules takes place in the mineral structure (Gens and Alonso, 1992; Mitchell and Soga, 2005). In case of very active clays, cation exchange also plays a key role in their mechanical response (Guimaraes et al., 2013).

The active clays have been historically of main concern for geotechnical engineers, as illustrated by the series of International Conference on Expansive Soils from the initial one in Texas in 1965 to the last version, again in Texas, in 1992 (Table 1-1) and focused on the description of field cases where pavements, foundations or buildings were affected by strong and seasonal volume changes of soil.

Table 1-1. Series of International Conference on Expansive Soils (Fredlund and Rahardjo, 1993).

	Date	Location
1st Int. Conf. on Expansive Soils	1965	College Station, Texas
2nd Int. Conf. on Expansive Soils	1969	College Station, Texas
3rd Int. Conf. on Expansive Soils	1973	Haifa, Israel
4th Int. Conf. on Expansive Soils	1980	Denver, Colorado
5th Int. Conf. on Expansive Soils	1984	Adelaide, Australia
6th Int. Conf. on Expansive Soils	1987	Delhi, India
7th Int. Conf. on Expansive Soils	1992	Dallas, Texas

With the advance in time and knowledge, aspects on the link between microstructural features, swelling mechanisms and soil origin and properties started to emerge as the focus of fundamental investigations on the mechanisms underlying the response of these materials.

The geological origin of expansive clay soils typically comes from the development of residual soil profiles from mudstones or claystones. In an interesting study, Fityus and Smith (2004) found that the chemical and mineralogical characteristics of the parent rock are very similar to those

of its derived expansive clay soils. This indicates that the main factor releasing the expansive potential in residual soils is related to weathering rather than changes in mineralogy.

The main consequence of the geological origin of expansive clays is the extensive areas in the world covered by clay soils with high swelling potential. Planning the transportation system in these areas involves the use of clay as subgrade and fill materials for roads and railways. Kassiff et al. (1969) exposed a classification system and swelling potential evaluation for the design and construction of pavements in arid and semi-arid regions where clays exist in unsaturated condition and, thus, their moisture changes are associated to seasonal climate. With the development in time of transport infrastructures, the geotechnical community has been continuously facing this kind of problems which, as pointed by Sánchez et al. (2014), favoured the development of phenomenological studies, constitutive models and numerical tools to perform back-analyses and predict future behaviour.

Another important practical topic concerns the foundations on expansive soils. In that case, the engineering approach is essentially oriented to assess field performance with emphasis to design criteria, construction specifications and economical solutions to avoid structure damage due to foundation movement. Drilled pile foundation, moisture control, soil replacements and chemical stabilization were some of the techniques employed (Peck et al., 1974; Chen, 1988).

Conversely, some features of the active clays have been founded useful to use them as an “engineering material”. For their low hydraulic properties, high plasticity, swelling and absorptive capacity of contaminants, active clays are suitable materials to prevent the migration of contaminant to the environment. As such, they are used as natural barriers to isolate any kinds of contaminants from the biosphere. Mitchell (1991) presented in his Rankine lecture the key role of fluid flow, chemicals and energy in contaminant transfer through these types of soils.

In particular, Compacted Clay Liners (CCL) have been implemented as barriers for controlling the contaminant transport in municipal solid waste (MSW), a crucial societal issue. Since a long time, active clays for

barriers have been the catalyser for open questions, consequent advances in research and specialized publications generation (Di Emidio et al., 2017). Rowe (2005) described for example in his Rankine lecture several field cases that provided experimental and numerical data on the long-term performance of GCL in front of environmental actions, leachate contaminants and heat fluxes generated by the waste degradation.

Another crucial societal issue concerns the disposal of nuclear waste because of the associated potential risk and the necessity to perform analyses at very long time scales related to radioactive substance decay rates (Gens, 2003). The current solution relies on disposal in multi-barrier system within deep geological formations, which isolate the radioactive waste from the human environment and insure that radionuclide release rates remain below prescribed limits (Chapman and Mc Kinley, 1987). A typical scheme for an underground mined repository involves the sinking of deep shafts or ramps down to a depth of several hundred metres according to local geological conditions. Shafts and ramps will provide access to a network of excavated horizontal drifts that constitutes the main repository area.

Gens (2003) pointed out the main uses of expansive clays in the multi-barrier system installed in this kind of repositories. The multi-barrier system considers essentially three main types of barriers: the container itself, the "engineered barrier" made of compacted expansive clay and the host formation. The expansive clay barrier is generally made of active clay (bentonite) and fulfils several important functions: its very low hydraulic conductivity limits water inflow into the contained, its low diffusion coefficient retards solute transport, and it is additionally afforded with sorption effects. The barrier should also provide a favourable chemical environment and be able to self-heal if subjected to damaging effect like cracking and fissuring. In addition, because of the heat emitted by the residues during hydration, clay materials with be the seat of a strong thermo-hydro-mechanical (THM) loading. Laboratory experimentation, highly instrumented mock-up tests and consistent numerical modelling have probed the technical feasibility of the multi-barrier concept (Gens, 2010).

Additionally, prior to repository closure, it will be necessary to seal and backfill access tunnels and shafts so that they do not become preferential

radionuclide migration pathways. The design of seal structures has as main purposes: i) to conform low permeability plugs ii) to maintain long term mechanical support for the underground openings, iii) to act as additional spots for radionuclide sorption, and iv) to prevent some protection against human intrusion. Again, the bentonites seals are at present the preferred option because of their high sealing capacity. The issues concerning seal behaviour are similar to those arising in the design of multi-barriers, with the important difference that no high temperatures are expected. Ruiz et al. (2017a), Ruiz et al. (2017b) and Ruiz et al. (2018) have shown that the performance of these structures must be assessed for the entire life of the deep repository and that their hydro-mechanical evolution takes thousands of years.

Whatever is the geotechnical issue and the final use contemplated for expansive clays, whatever they are defined as “problematic soils” or “engineering material”, expansive clays can be handled with a common conceptual framework. The framework proposed by Gens and Alonso, (1992) has provided a strong foundation for the development of constitutive models and their implementation in finite element codes (Alonso et al., 1999; Guimaraes, 2002; Sánchez, 2004; Gens et al., 2011).

1.2. Aims of the research

The driving force of this thesis has been the understanding and modelling of expansive clays under hydro-mechanical actions. Specifically, the objective of this doctoral research are:

- The identification of physical features, material responses and conditions to be considered in a hydro-mechanical formulation for expansive clays. This works is essentially based on a detailed literature review and the previous experience of the geomechanical research group of the Technical University of Catalonia (UPC) on the multi-physical modelling of geomaterials (Gens, 2010; Gens and Alonso, 1992; Olivella, 1995; Olivella et al., 1994).

- The development of a hydro-mechanical double-structure model able to reproduce the behaviour of compacted bentonite. Important components of this constitutive model are a water retention

formulation taking into account the two porosity levels and the various interactions between the two structural levels.

- The numerical implementation of the constitutive model in the finite element code CODE-BRIGH and its verification and validation through simple modelling cases.

- The application of the developed double-structure model to reproduce laboratory tests focussed in different responses as stress-path dependency, swelling pressure development and homogenization.

1.3. Thesis layout

The thesis is organized in six Chapters and three Appendices (see Figure 1-1). The main contents of each Chapter are as follows:

Chapter 2 presents physical features of expansive clayey and the theoretical approaches used to describe them in the framework of double-structure porous media. The field equations that define their hydro-mechanical behaviour are then formulated and completed with restrictions and constitutive equations.

Chapter 3 starts with a brief discussion on suction and stress concepts. Afterwards an enhanced constitutive double structure model is presented. The formulations for macro- and microstructural levels are displayed separately and their hydro-mechanical interactions established.

In Chapter 4, the discrete formulation of the balance equations is presented and important insights about the numerical treatment of water transfer between structural levels are given. Afterwards, the integration of the constitutive model through an explicit scheme with final drift correction is detailed and verified at the level of Gauss point.

Model validations are shown in the Chapter 5. The modelling at elementary and laboratory scales allows the comparison of the modelling outputs against known monitory data that involves particular conditions (e.g. bentonite configurations, hydraulic conditions, time evolution, among others). It should be stressed that all experimental cases come

from the research of the nuclear waste disposal. This is the research activity that accounts heavily instrumented laboratory and field test.

Finally, Chapter 6 gives a summary of the work carried out in this Thesis through general conclusions and some insights for further research.

Appendix A contains the experimental water retention curves of well-knows bentonites and their interpretation through a multimodal water retention model. Appendix B provides important insights about the micro-Macro mechanical interaction using discrete element analysis.

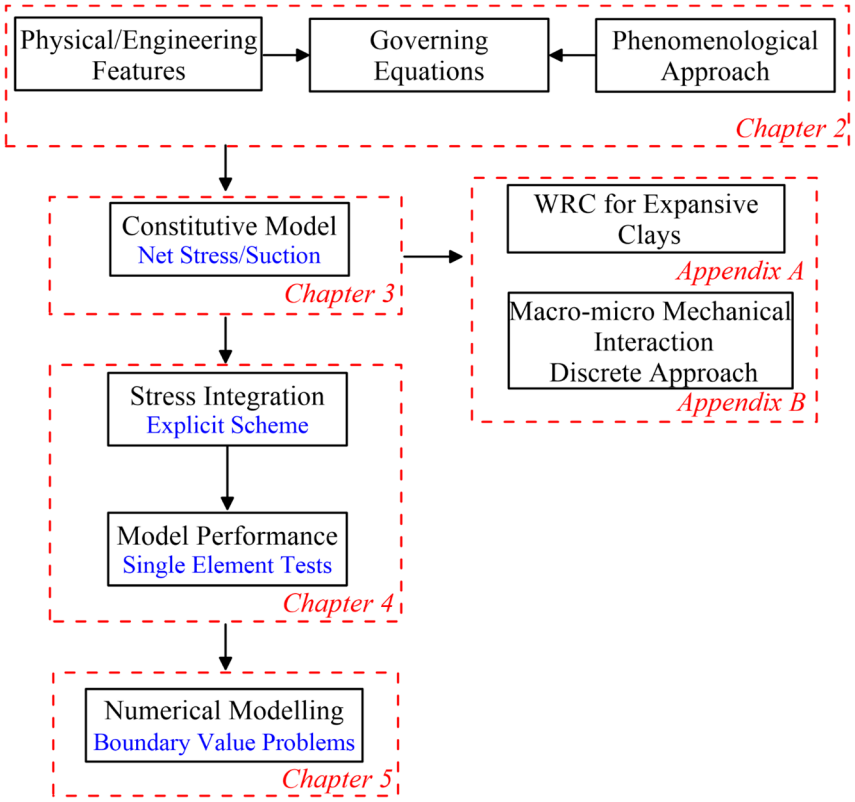

Figure 1-1. Thesis structure

1.4. References

Alonso, E.E., Vaunat, J., Gens, A., 1999. Modelling the mechanical behaviour of expansive clays. Eng. Geol. 54, 173–183.

Chapman, N.A., Mc Kinley, I.G., 1987. The geological disposal of nuclear waste. Chichester:John Wiley.

Chen, F.H., 1988. Foundations on Expansive Soils. Amsterdam: Elsevier.

Di Emidio, G., Katsumi, T., Touze-Foltz, N., Bouazza, A., 2017. Special Issue: Modified Clays for Barriers. Appl. Clay Sci. 142, 1–185.

Fityus, S.G., Smith, D.W., 2004. The development of a residual soil profile from a mudstone in a temperate climate. Eng. Geol. 74, 39–56.

Fredlund, D.G., Rahardjo, H., 1993. Soil Mechanics for Unsaturated Soils.

Gens, A., 2010. Soil–environment interactions in geotechnical engineering. Géotechnique 60, 3–74.

Gens, A., 2004. The role of geotechnical engineering for nuclear energy utilisation, in: Vanicek I. et Al., Editors. Proc. 13th European Conference on Soil Mechanics and Geotechnical Engineering, Vol. 3. Prague: CGtS. pp. 25–67.

Gens, A., Alonso, E.E., 1992. A framework for the behaviour of unsaturated expansive clays. Can. Geotech. J. 29, 1013–1032.

Gens, A., Valleján, B., Sánchez, M., Imbert, C., Villar, M.V., Van Geet, M., 2011. Hydromechanical behaviour of a heterogeneous compacted soil: experimental observations and modelling. Géotechnique 61, 367–386.

Guimaraes, L.D.N., 2002. Analisis multi-componente no isotermo en medio poroso deformable no saturado (in spanish). PhD Thesis, Universitat Politecnica de Catalunya, Spain.

Guimaraes, L.D.N., Gens, A., Sanchez, M., Olivella, S., 2013. A chemo-mechanical constitutive model accounting for cation exchange in expansive clays. Geotechnique 63, 221–234.

Kassiff, G., Livneh, M., Wiseman, G., 1969. Pavements on Expansive Clays. Jerusalem: Academic Press.

Mitchell, J.K., 1991. Conduction phenomena: from theory to geotechnical practice. Géotechnique 41, 299–340.

Mitchell, J.K., Soga, K., 2005. Fundamentals of Soil Behavior. 3rd ed. Hoboken, NJ: Wiley.

Olivella, S., 1995. Non-isothermal multiphase flow of brine and gas through saline media. PhD Thesis, Universitat Politecnica de Catalunya, Spain.

Olivella, S., Carrera, J., Gens, A., Alonso, E.E., 1994. Non-isothermal multiphase flow of brine and gas through saline media. Transp. Porous Media 15, 271–293.

Peck, R.B., Hanson, W.E., Thornburn, T.H., 1974. Foundation engineering. 2nd ed. USA:John Wiley & Sons, Inc.

Ruiz, D.F., Vaunat, J., Gens, A., Mánica, M., 2018. Hydro-mechanical modelling of an unsaturated seal structure, in: Proceedings of the 9th European Conference on Numerical Methods in Geotechnical Engineering (NUMGE 2018) Cardoso et Al (Eds). Porto, Portugal. pp. 757-764. Volume 1.

Ruiz, D.F., Vaunat, J., Gens, A., Mánica, M., 2017a. Analysis of the hydration of an unsaturated seal, in: Second Pan-American Conference on Unsaturated Soils, PanAm-UNSAT 2017. Dallas, USA. pp. 1–11.

Ruiz, D.F., Vaunat, J., Gens, A., Mánica, M., 2017b. Hydro-mechanical modelling of a gallery sealing over the entire life of a deep repository, in: 6th International Conference on Coupled THMC Processes in Geosystems, GeoProc 2017. París, France. pp. 120–121.

Sánchez, M., 2004. Thermo-Hydro-Mechanical coupled analysis in low permeability media. PhD Thesis, Universitat Politecnica de Catalunya, Spain.

Sánchez, M., Wang, D., Briaud, J.L., Douglas, C., 2014. Typical geomechanical problems associated with railroads on shrink-swell soils. Transp. Geotech. 1, 257–274.

Chapter 2

Expansive Clays as Double-Structure Materials

'Nature is indifferent towards the difficulties it causes to a mathematician.'

J. Fourier

2.1. Introduction

The characteristics that define the expansive clays as potential barriers in the nuclear waste disposal activities (e.g. low hydraulic, plasticity, swelling and absorptive capacity for contaminants) have their roots in the underlying physico-chemical features of the clays. Therefore, the numerical modelling of such kind of materials requires a complete understanding of these aspects.

Due to the large timescales involved in nuclear waste disposal, it is necessary to consider the physical mechanisms of the materials instead of some empirical bases of classical soil mechanics. The governing equations and constitutive models should obey the physical features, material structure and its evolution during the period involved (several hundred or thousand years).

Based on the above statements, the next items should be the main basis of a theoretical framework to deal with active clays (Gens, 2010):

- The expansive clay is a multiphase porous media.
- The microstructure is implicitly considered as an aid to understanding.
- New additional variables are required to describe fully soil behaviour.
- The relevant phenomena are often coupled phenomena, leading to coupled analysis.

This chapter is organised in the following way: first, the physical features of expansive clays are presented. Information on origin, mineralogical composition, particle arrangement, swelling mechanism and stress-strain response is given. Then, a theoretical framework is defined and the governing equations are formulated according to the physical aspects described previously. Finally, the constitutive laws close the overall hydro-mechanical (HM) formulation.

The set of partial differential equations that constitute the governing equations are the starting point for the formulation of a hydro-mechanical constitutive model, the implementation in a finite element scheme and the numerical modelling of boundary value problems.

2.2. Physical features

Fityus and Buzzi, (2009) presented direct and indirect physical evidence, which recognizes that natural expansive clays remains perpetually saturated despite the moisture changes due to environmental actions. Perpetual saturation state arises from the small particles of clays, which in the structural arrangement generates very small pores and high air entry pressure value. This characteristic is not true for the case of compacted expansive clays and extreme environmental conditions (e.g. arid and desert climate or the nuclear waste disposal environment). The backfilling of galleries and excavation of nuclear waste repositories requires compacted clays in particular conditions like granular mixtures (pellets) or blocks. The compaction of dry expansive clay powder to obtain pellets and blocks will generate unsaturated states. Likewise, the high thermal loads imposed by nuclear waste can desaturate the expansive clay.

As pointed out by Gens, (2010), unsaturated soils are simply soils in which pore space is occupied by more than one fluid, normally liquid and gas. They are not a special type of soil. The theoretical formulation and constitutive models should represent the soil behaviour over the entire range of possible stress, pore pressure and saturation degree. From here on, the expansive clays will treated as multiphase porous media.

2.2.1. Origin of expansive soils

The origin of expansive soils is related to a specific combination of conditions and processes that result in formation of clay minerals prone to expand in contact with water due to their particular chemical composition. Variations in those conditions and processes may also produce other non-expansive clay minerals. The factors that determine the clay mineralogy include composition of parent material and degree of physical and chemical weathering to which the material is subjected.

Chen, (1988) classified the parent materials that can be associated with expansive soils in two groups. The first group comprises the basic igneous rocks and the second group comprises sedimentary rocks that contain montmorillonite as a constituent (shales and claystones). From this fact,

expansive clays are widespread throughout the world. Some examples are:

- Fityus and Smith, (2004) described the development of an expansive residual clay from the weathering of argillaceous formation located in Maryland, Australia. They found the key role of physical weathering, structural evolution of the parent rock, in the increasing expansive potential.

- The FoCa clay (Fourges-Cahaignes clay) is a sedimentary clay from the Paris Basin. It is composed by an interstratified calcium-clay, kaolinite, quartz, gypsum and calcite. This material has been selected for the sealing of the experimental shaft in the Belgium repository within the RESEAL project (Van Geet et al., 2009).

- The Serrata clay is a bentonite coming from the Cortijo de Archidona deposit (Almería, Spain). Typically, it is named FEBEX bentonite, due to its use for the FEBEX Project in the in-situ (Grimsel, Switzerland) and the mock-up (Madrid, Spain) tests.

- Finally, the North American Wyoming bentonite, MX-80, has been tested as reference buffer material in several European underground research laboratories.

Typically, the conditioning of the bentonite in the quarry, and later in the factory, is strictly mechanical, consisting of homogenization, removal of rock fragments, drying at 60ºC (to avoid mineral changes) and crumbling of clods. From here, the configuration of bentonite can be powder, compacted blocks or pellets.

2.2.2. Clay mineralogy and swelling mechanism

In general, the minerals contained in clay soils are alumina-silicates, while quartz, calcite and other minerals are found in coarse-grained soils. Mitchell and Soga, (2005) pointed out the two fundamental structural elements in clay minerals: the silicon-oxygen (SiO_4) tetrahedron and aluminium-oxygen (AlO_2) octahedron (see Figure 2-1).

The kaolinite minerals are composed of alternating silica and octahedral sheets (1:1 minerals) as shown schematically in Figure 2-1. Mineral

particles consist of the basic units staked in the same direction. The bonding between layers is by both van der Waals forces and hydrogen bonds (Mitchell and Soga, 2005). This bonding is sufficiently strong that there is no interlayer swelling in presence of water.

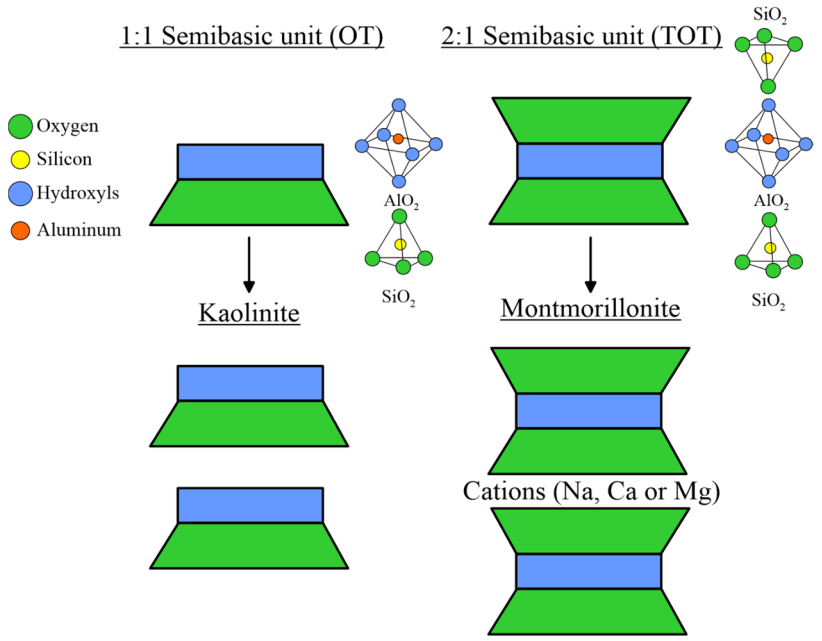

Figure 2-1. Schematic diagrams of structures of kaolinite and montmorillonite minerals (modified from Mitchell and Soga, 2005).

The mineral structure of *smectite* group (montmorillonite) is the main reason of the swelling mechanism. It consist of an octahedral sheet sandwiched between two silica sheets (Figure 2-1). As explained in Murad and Cushman, (2000), these minerals have a negative charge which is neutralized by exchangeable cations (Na—sodium, Ca—calcium or Mg—magnesium). When a montmorillonite is exposed to water, the water penetrates the superimposed layers and forces them to separate causing swelling. The attraction (hydrophilicity) of montmorillonite to water is one of the causes of swelling. Hydration causes the water properties to vary with the proximity to the solid surface. The interlaminar water is termed adsorbed water (or vicinal water) to distinguish it from its bulk or free-phase counterpart (i.e. water free of any adsorptive force). The properties of vicinal water depend in a complex way on the structure of surfaces and distance between surfaces.

Certain relationships exist between soil properties (e.g. the Atterberg limits) and the nature of the absorbed cations (Table 2-1). Empirical or indirect methods has been defined to determine the swelling potential of the expansive soils (e.g. Atterberg limits, linear shrinkage test, colloid content test, among others). Plasticity index and liquid limit are useful indices for determining the swelling characteristics of most clays (Table 2-2). Since liquid limit and swelling of clays both depend on the amount of water a clay tries to absorb, it is not surprising that they are related.

Table 2-1. Atterberg limits values of expansive clay minerals as a function of their exchangeable cations (after Lambe and Whitman, 1969).

Exchangeable cations	Liquid Limit (%)	Plasticity index (%)
Na—sodium (MX-80)	710	656
K—potassium	660	562
Ca—calcium (FoCa and FEBEX)	510	429
Mg—magnesium	410	350
Fe—iron	290	215
Fe[a]—iron	140	67

Table 2-2. Relationship between swelling potential of soils and plasticity index (from Chen, 1988).

Swelling potential	Plasticity index
Low	0-15
Medium	10-35
High	20-55
Very high	>35

The activity of clays, as was first presented by Skempton, (1953) has been widely used to express the type of clay minerals in clayey soils and correlate the with the swelling potential (Figure 2-2). It is defined as:

$$\text{Activity} = \frac{\text{Plasticity Index}}{\text{Clay Fraction}} \qquad \text{(Eq. 2-1)}$$

Where the clay fraction is the percentage by weight of particles finer than 2 μm.

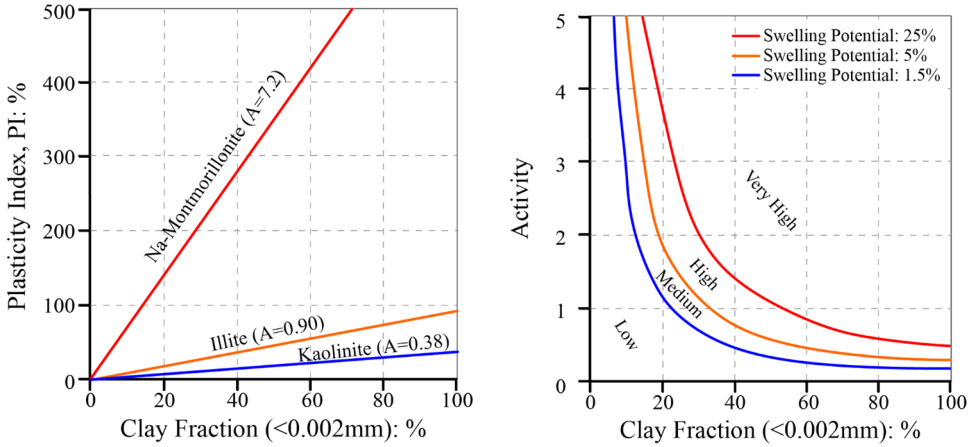

Figure 2-2. Relation between plastic index and clay fraction (from Skempton, 1953) and classification chart for swelling potential (modified from Seed et al., 1962).

Recently, Buzzi et al., (2011) use dimensional analysis to predict the amount of swelling of compacted unsaturated clays. Influencing factors such as initial water content, initial dry density and vertical stress are taken into account.

The empirical methods have been successful and often used in civil engineering applications. They demonstrate that the swelling depends strongly on physicochemical interaction between minerals. However, this fact does not explain the overall engineering behaviour of the expansive clays. Thus, it is convenient account for the key role of the clay structure.

2.2.3. Particles size, inter-particle forces and clay structure

Geomaterials are particulate materials and clays are not an exception. The fundamental understanding of expansive clays behaviour begins by recognizing their particulate nature and the immediate implications: inter-particle arrangement, occluded or interconnected porosity, inherently non-linear non-elastic contact phenomena and particle forces (Santamarina et al., 2001).

Clay falls within a specific range of particle sizes. Typically, they are smaller than 1μm (10^{-3} mm) but larger than molecular size. In this colloidal magnitude, the surface forces become dominant and prevail on

gravitational forces. Furthermore, mineralogy and pore fluid determine the chemo-electrical features on mineral surfaces, the subsequent particle forces and fabric formation (Santamarina et al., 2001).

We define the specific surface as the total surface of all soil particles contained in one gram of soil. It captures the combined effects of particle size and slenderness in a measurement that is independent and complementary to the grain-size distribution (Santamarina et al., 2002). Table 2-3 shows some schematic structure details of kaolinite and montmorillonite minerals. Both minerals have a classical platy shape of the clay particles. However, montmorillonite occurs as equidimensional flakes that are so thin as to appear more like films and its specific surface can be very large.

Table 2-3. Sheet silicate minerals (modified from Lambe and Whitman, 1969).

Mineral	Specific surface (m^2/g)	Particle shape	Particle size
Kaolinite	10-20	Platy	d=0.3 to 3μm t=1/3 to 1/10d
Montmorillonite	800	Platy	d=0.1 to 1μm t=1/100d

All material particles, including soil particles, carry electrical charge on their surface. It is well established that both attractive and repulsive forces of electrical nature exist among clay particles. The van der Waals force is the predominant attractive phenomenon in the clay-water system. The opposite side is the double-layer repulsion generated by the electrostatic interactions between the unbalanced negative surface charges and the ions contained in the water solute.

Santamarina et al., (2001) analysed the fabric formation under particle-fluid interactions. The pH and concentration influence the inter-particle forces and they drive the hierarchical arrangement of the expansive soils. The particle packings are generated by flocculation and/or aggregation of clay particles. Group of associated particles form aggregates, which in turn form the porous medium with macroscale implications. Multiphase flow (air and water) produces interfacial tensions (menisci) and capillary forces at clay particles packs and aggregates due to their coarse-grained nature (Figure 2-3).

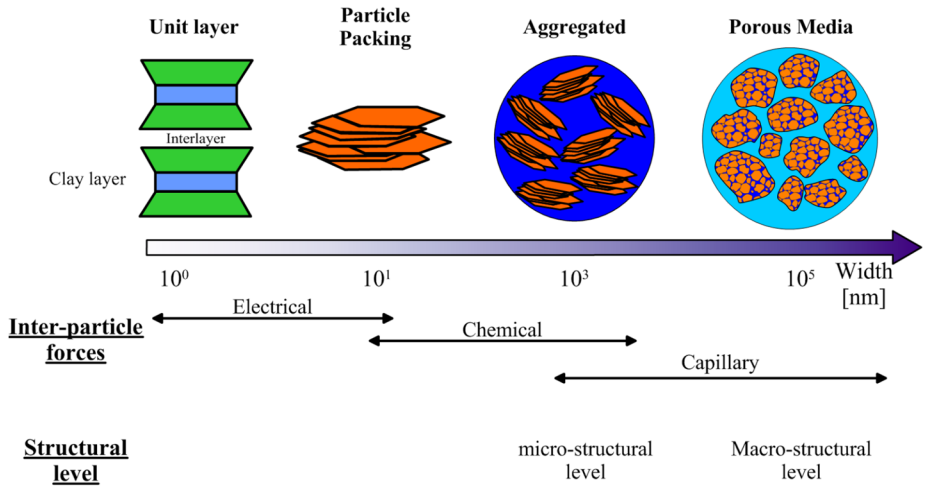

Figure 2-3. Hierarchical structure of expansive clays.

The fabric of active clays identified as a mixture of macroparticles (clay aggregates) formed by clay platelets has been examined through well-known experimental techniques:

- Qualitative observations from the former Scanning Electron Microscopy (SEM) (Collins and McGownn, 1974) to the innovative Environmental Scanning Electron Microscopy (ESEM)(Romero and Simms, 2008).

- Mercury Intrusion Porosimetry (MIP) which offers a convenient way to study quantitatively the pore size distribution (Romero and Simms, 2008). According to the described fabric components, natural and compacted expansive clays will tend to exhibit a marked bimodal distribution of voids: a large mode corresponding to inter-aggregate pores (macro-pores) and small one associated to intra-aggregate void space (micro-pores) (Figure 2-4 and Figure 2-5).

Indirect measures of intra- and inter-aggregates void ratios can be obtained from the water retention behaviour of bentonites. Navarro et al., (2015) proposed a methodology that relates higher suction values to the microstructural water content and micro-structural pores. By extrapolating this model to low suction, micro-structural and Macro-structural water contents were separated to obtain the Macro-structural water content and inter-aggregates pores.

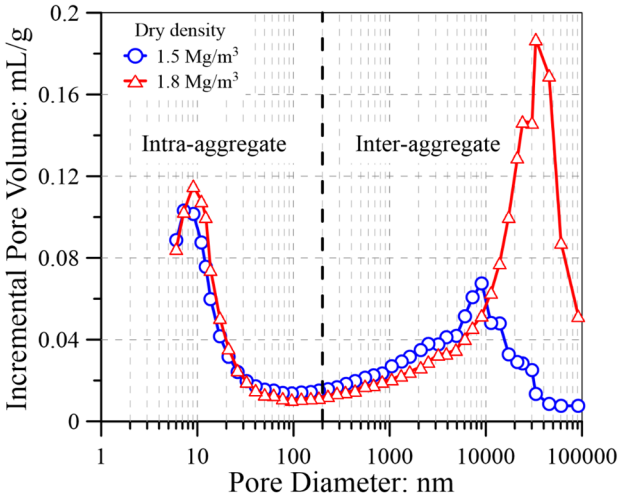

Figure 2-4. Distribution of incremental pore volume for compacted FEBEX bentonite at different dry densities (Lloret et al., 2003).

This double-porosity system is filled, total or partially, with water adsorbed to the aggregates or in bulk state. Concerning to inter-particle "bonding", Alonso et al., (1987) and Alonso et al., (1990) proved that water menisci, in the unsaturated state, acts as cohesive factor. Thereby, it is convenient to define the expansive clays as double-structure porous media (Figure 2-3 and Figure 2-5). The micro-structural level is intrinsically related to the aggregates governed by physico-chemical phenomena occurring at particle clay level and the Macro-structural level is the granular-like skeleton formed by the aggregates (Gens and Alonso, 1992; Alonso et al., 1999; Sánchez et al., 2005; Gens et al., 2011).

The consideration of two pore families may be an oversimplification of the complex structure of the expansive clays. The compaction processes can generate several pore size categories. Wang et al., (2014) identify four pore families, which include inaccessible pores (<6nm), small pores (6nm-40nm), medium pores (40nm-2μm) and large pores (>2μm) for compacted bricks of MX-80 bentonite. Granular mixtures made of high-density pellets of bentonite shows a three-mode MIP curve with characteristic pore sizes of 13nm (intra-aggregate), 3μm (inter-aggregate) and 250μm (inter-pellets) (Hoffmann et al., 2007). Certainly, the physical description of the expansive clays has to be as accurate as possible through available experimental techniques. Nevertheless, defining the role of each structural-level and the relationship between them are not

straightforward tasks. The identification of the predominant pore families and their implication on the hydro-mechanical behaviour of these porous media is an engineering challenge.

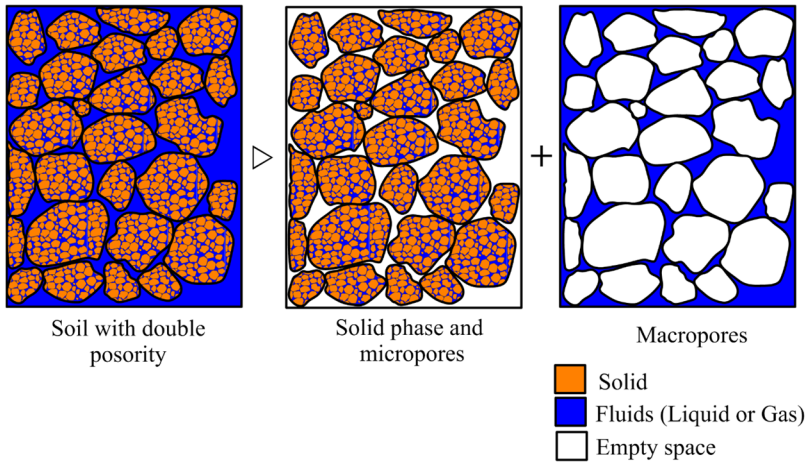

Figure 2-5. Schematic representation of the double-structure porous medium as the addition of two media: aggregates composed by solid and micro-pores filled by fluids and macro-pores also occupied by fluids. (After Coussy, 2004; Borja and Koliji, 2009; Borja and Choo, 2016).

The hydro-mechanical behaviour of the expansive clays as double-structure material is poorly explained considering only the swelling mechanism of a basic clay element. The diffuse double layer (DDL) theory has been proposed to predict the swelling of clays. This theory is based on the microscopic physico-chemical concept of the clay-water interaction for a two-clay platelet system. However, this system is more representative of clay particles packings or clay aggregates and it does not explain many mechanisms occurring at macroscopic scale.

According to Alonso et al., (1987) the mixture of clay aggregations and their connectors (water menisci) is prone to collapse. Consequently, the joint swelling-collapse behaviour of many natural and compacted expansive clays is interpreted as follows: under low external loads and upon wetting, expansion take place at elementary particle arrangements located within the aggregates. These tend to maintain its original structure as long as the external load is not significantly increased. If the external stresses increases, connectors break down, slippage takes place at aggregation contacts and aggregations deform so that the inter-aggregate pores are occupied by the (deformed) aggregates (Figure 2-6). Therefore,

the aggregates interact with each other much like rigid grains interact in a granular materials. Unlike sand or silt particles, however, the aggregates may experience volume changes.

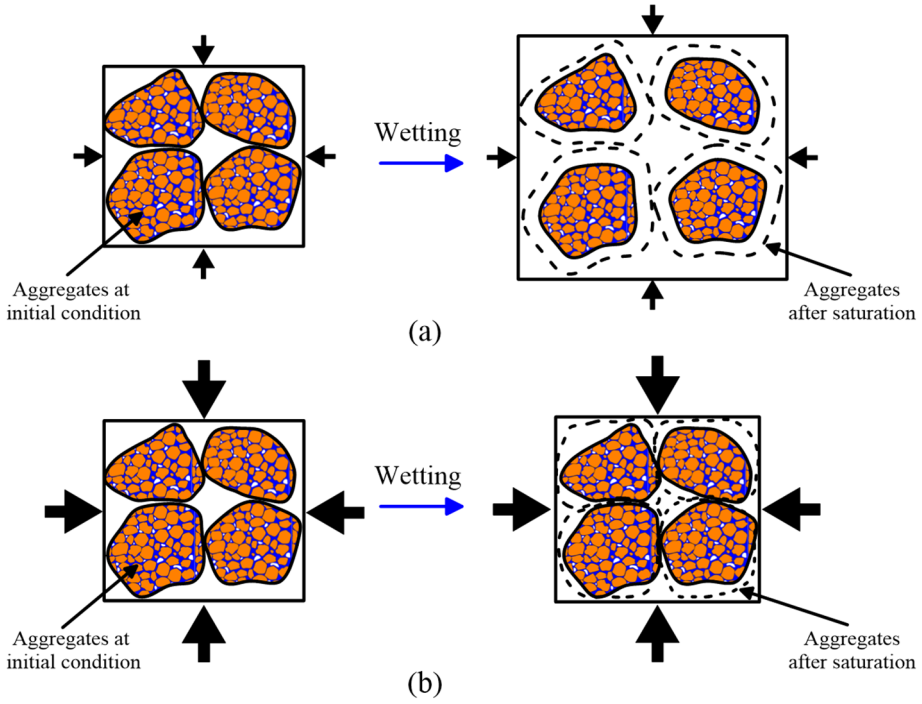

Figure 2-6. Deformation mechanism of expansive clays upon wetting. a) Low external stresses and b) High external stresses.

The above mechanism, derived from the double-structure of expansive clays, generates a very complex engineering behaviour. The following item presents the macroscopic material response due to environmental loads (mechanical and hydraulic).

2.2.4. Engineering behaviour of expansive clays

At the beginning of the research on the expansive clays, most of the efforts tried to identify the "swelling potential" of the soil. This term refers either to the swelling volumetric deformation or to the swelling pressure measured along wetting paths. The specific paths imposed usually involve an ever-decreasing value of the suction applied and different sequences of vertical load. As a consequence, stress and particularly suction reversals were uncommon (Gens and Alonso, 1992).

Pioneer experimental works performed by Brackley, (1973, 1975) and (Pousada, 1984) demonstrated: a) swelling pressure was essentially related to the void ratio, b) the stress-path dependency and c) the existence of reversible and irreversible strains components under cycles of suction reversals. Afterwards, the development of new experimental techniques (ESEM, MIP, X-ray tomography, digital image correlation, among others) allowed to identify the structural evolution of these porous media, the time evolution of the hydro-mechanical processes and the homogenization of the heterogeneous expansive clays.

2.2.4.1. Strain irreversibility and stress-path dependency

Because the physico-chemical phenomena occurring at particle level are fully reversible, one would expect expansive clay behaviour to be reversible and possibly stress path independent. In fact, it is not.

Strain irreversibility and stress path dependency are attributed to the effects of micro-structural deformation on the macro-structure (Gens and Alonso, 1992). A mechanical coupling between both structural levels can be described as follow: the reversible micro-structural behaviour is independent of the macro-structural deformation. However, there is an important influence of the micro-structure on the macro-structural response. The MIP reported by Lloret et al., (2003b) reveals small changes (almost zero) of the micro-structural level due to the macro-structural deformations. Mechanical compaction affects mainly the pore structure of the larger inter-aggregates pores (Macro-structural level) (see Figure 2-4).

Monitoring micro-structural change along hydraulic paths has been one of the main application of ESEM observations. Romero and Simms, (2008) show the swelling behaviour of bentonite through this technique. Figure 2-7 presents the paths followed by wetting-drying tests on bentonite. The control on relative humidity is equivalent of total suction variations. This study specifically investigates the reversibility or irreversibility features of the volume change behaviour at both structural levels after one wetting-drying cycle. At macroscopic scale, the volume change is directly measured on soil cylindrical sample (38 mm in diameter and 40 mm high). On the other hand, the swelling and

shrinking response at aggregate scale is observed directly by ESEM combined with digital image correlation (DIC).

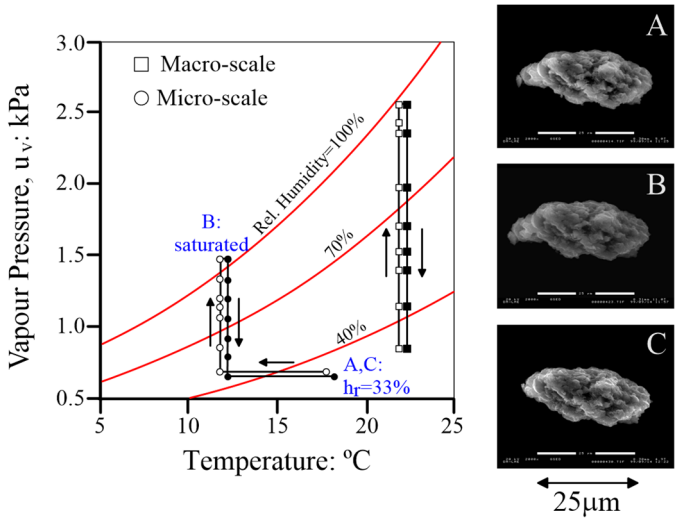

Figure 2-7. Paths followed on wetting-drying tests performed at micro- and macro-structural scales and direct observation of an aggregate in the ESEM (modified from Romero and Simms, 2008).

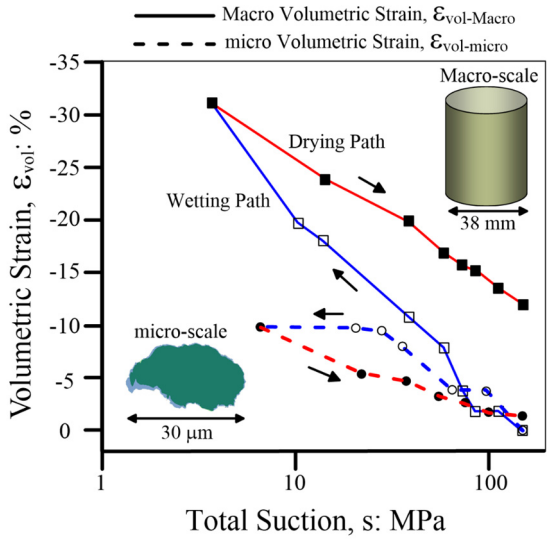

Figure 2-8. Volume change response along wetting-drying cycle at micro- and macro-scale. Volume changes at micro-structural level are tracking by ESEM observations (modified from Romero and Simms, 2008).

Reversible and irreversible volume change features of both micro- and macro-scales are observed in (Figure 2-8) for the wetting and drying paths followed. Strains at micro-scale are almost reversible, enclosing a hysteretic loop. At macroscopic scale, there is a marked irreversibility of the volume change. These experimental observations demonstrate the influence of the micro-structural deformation on the Macro-structural level.

The structural levels interaction is the core of the mechanical behaviour of expansive clays. Gens and Alonso, (1992) formulated empirical relationships that express the magnitude of macro-structural irreversible strains caused by micro-structural strains. They are dependent on the stress state and the dry density (or porosity) of the expansive clays. Chapter 3 and Appendix B give further insights on this mechanical mechanism.

Wetting-drying cycles in suction-controlled tests result in the accumulation of irrecoverable deformation take place. Figure 2-9 shows the relationship between the volumetric strains and suction cycle number. Wang and Wei, (2015) decomposed the volumetric strain (ε_{vs}) into two different components, a reversible swelling-shrinkage strain component (ε_{vs_Rev}) and an irreversible swelling-shrinkage strain component (ε_{vs_Irrev}). The accumulation of wetting-drying cycles converges to an elastic-like behaviour. The majority of the accumulated plastic volumetric strains occurs during the first cycles. Subsequently, the rate of volumetric strain accumulation reduces, and the samples tend towards a nearly reversible behaviour. The strain accumulation trend depends on the applied stress, as pointed out by Pousada, (1984). The volumetric contraction reported by Alonso et al., (2005) contrasts with the continuous expansion of the experiment performed by Nowamooz et al., (2009).

Stress-path dependency of swelling strains and swelling pressures exhibited by expansive soils have been long recognized (Gens and Alonso, 1992). Stress-path dependency of swelling deformations are illustrated by the test results reported by Brackley, (1975) (Figure 2-10) where three techniques to predict heave under a given load (50kPa) are considered: a) free swell and subsequent loading, b) loading to 50kPa and swell under pressure and c) saturation at constant volume and subsequent unloading

to 50kPa. The first method yields the maximum swelling (segment d-a), the third method gives the smallest deformation (segment d-c) and the second method results in and intermediate swelling value (segment d-b).

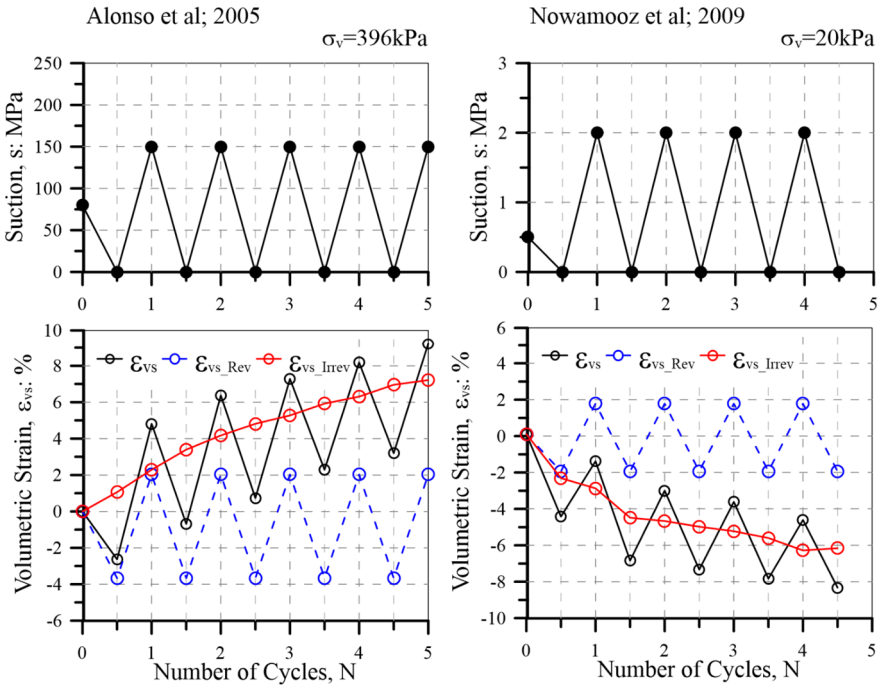

Figure 2-9. Decomposition of volumetric strain induced by cyclic wetting-drying tests (modified from Wang and Wei, 2015).

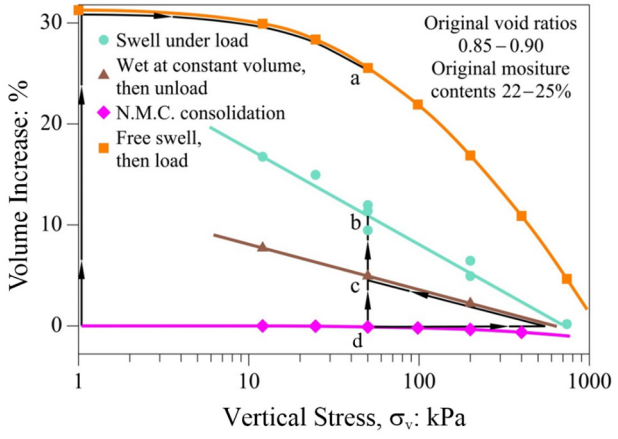

Figure 2-10. Procedures for swell prediction (after Brackley, 1975).

Lloret et al., (2003) described a testing programme performed on FEBEX bentonite and using oedometers especially designed to apply a very large range of suctions. Besides the initial and final equilibration stages, the actions applied on the samples were load increments at constant suction and changes of suction at constant load. The initial conditions of the test correspond to a dry density close to 1.70 Mg/m^3 and gravimetric water content near the 13 %. The various load or suction changes were applied in stages as shown in Figure 2-11.

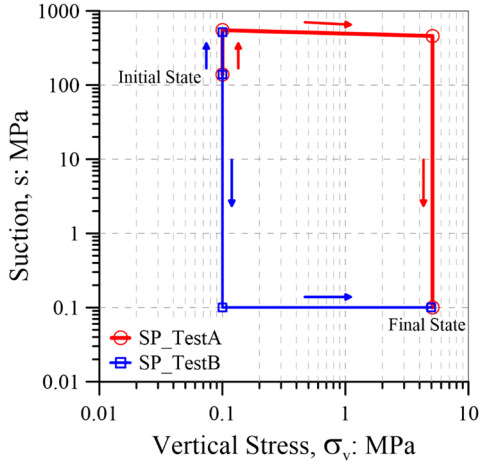

Figure 2-11. Generalized stress path followed by TestA and TestB (modified from Lloret et al., 2003b).

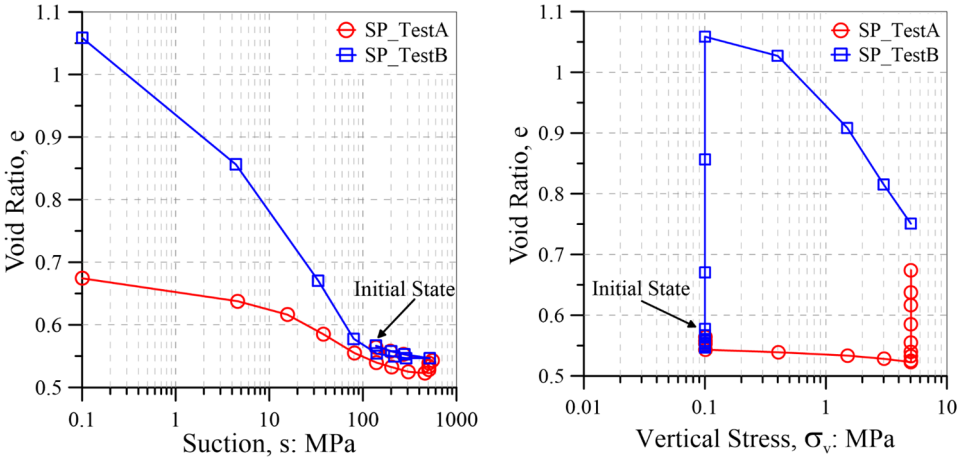

Figure 2-12. Variation of void ratio against suction and vertical net stress. TestA and TestB (modified from Lloret et al., 2003b).

The variations of void ratio during the stages at which the vertical stress was maintained constant and suction was varied are presented in Figure 2-12(a). The effects of applied load are very noticeable. Large void ratio changes are observed in the specimens where wetting took place at 0.1 MPa (Test B), whereas in the samples wetted under 5.1 MPa load the volume changes are quite small (Test A).

Figure 2-12(b) shows the void ratio variation for the two specimens, Test A and Test B, along the entire stress-paths. These tests share the initial and final stress points but they have followed different stress paths. It can be noted that the final void ratio is different, so there is a measure of stress-path dependency. In accordance with other cases (Brackley, 1973; Pousada, 1984), the final void ratio of the sample wetted under low stresses is higher. The disruption of the macrostructure would be more severe in this case because of the larger swelling strains developed during wetting, inducing large Macro-structural volume changes that cannot be recovered upon subsequent (Lloret et al., 2003).

2.2.4.2. Fabric evolution

A key aspect on the behaviour of bentonite is that its fabric is not static during hydration or load; it is subjected to change.

An experimental study related to the changes in the fabric of the FEBEX bentonite during wetting and drying is briefly presented here (Villar et al., 2004). Vapour pressure and temperature are applied around the samples in an ESEM (Environmental Scanning Electron Microscope). In addition, some samples have been observed using the scanning electron microscope (SEM) after a process of freeze-drying. The changes in the clay fabric originated by the progressive wetting of compacted bentonite with an initial dry density of 1.40 g/cm^3 can be observed in Figure 2-13. Suction changes under isochoric conditions were applied to samples before the observations. The differences in final dry density are due to the rebound experienced by the bentonite after unloading. The progressive occlusion of the inter-aggregate pores due to particle swelling can be easily noted. During hydration the clay fabric exhibits a dynamic character that can affect strongly the kinetics of hydration, especially if confined conditions prevail.

Although the observations mainly provide qualitative information, the use of this technique allows the improvement of the knowledge of the fabric changes due to hydration.

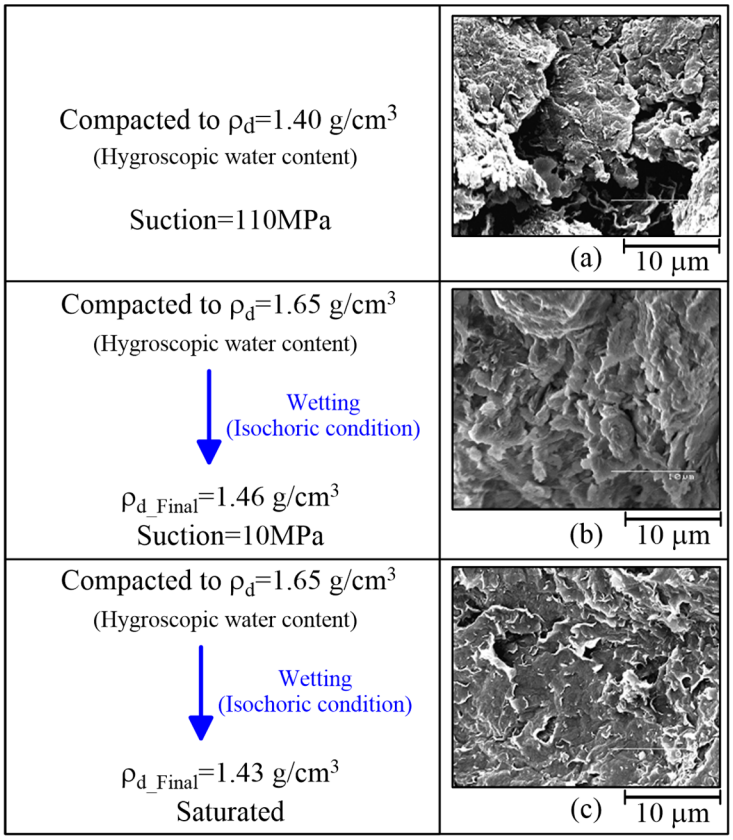

Figure 2-13. SEM micrographs of compacted FEBEX bentonite (modified from Villar et al., 2004).

Quantitative measurements of clay fabric evolution are done via mercury intrusion porosimetry (MIP). Recently, Sun et al., (2018) have presented a meticulous experimental analysis of the structural evolution of the Czech bentonite B75 due to wetting-dying cycles. The transition pore size between the micro-pores (intra-aggregate) and macro-pores (inter-aggregate) was found to be suction dependent. Only largest micro-pores are affected by moisture change and the intra-aggregate pore space is practically insensitive to compaction (Figure 2-14), as observed Lloret et al., (2003) (Figure 2-4).

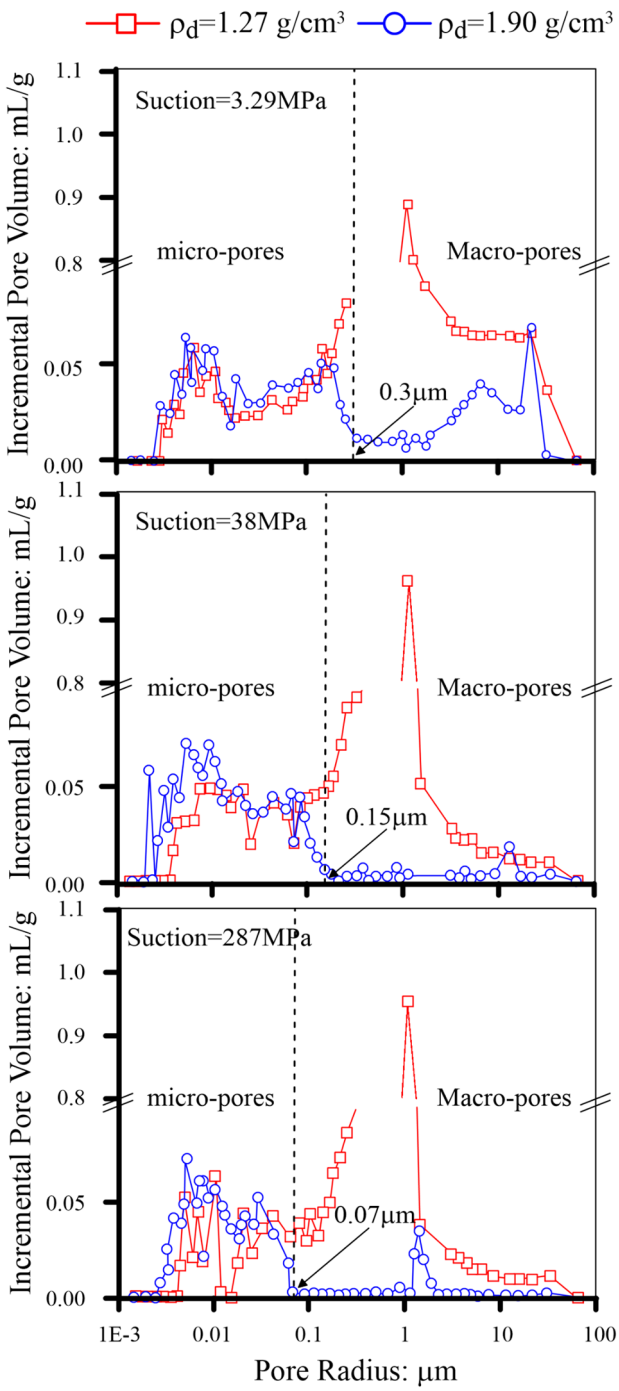

Figure 2-14. Distribution of incremental pore volume for compacted the Czech bentonite B75. Effect of dry density and micro-macro transition due to the effect of suction (Sun et al., 2019).

2.2.4.3. Time evolution of the HM processes

Swelling pressure and swelling strains evolution

The development of swelling pressure and swelling strains requires time. A typical relationship is presented in Figure 2-15 which refers to the swelling of expansive clay under various vertical loads. It is apparent that there is a "primary" consolidation process followed by a "secondary" one which was not finished at the time the test was ended. In general, the values of permeability explain the time evolution of the primary swelling. However the "secondary" strains, that would be normally attributed to viscosity effects, in the case of active clays are consequence of the micro-structural evolution.

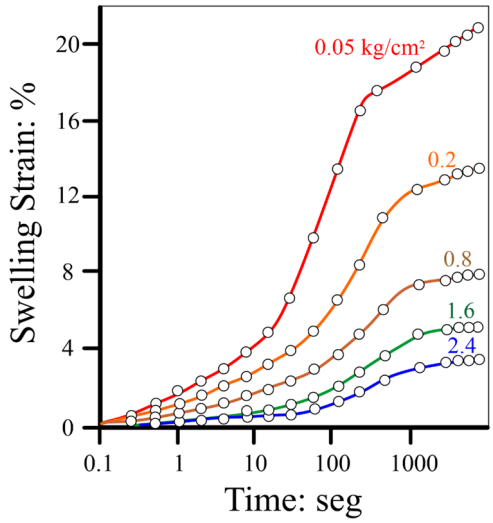

Figure 2-15. Swelling strain vs time relationship under various vertical loads (Modified from Mazurik and Komornik, 1973).

Figure 2-16 shows the results of the oedometer swelling pressure tests on compacted powder/pellets bentonite mixture (Gens et al., 2011). Specimens with different lengths (5, 10, 12 cm) was compacted to a common dry density of 1.60 g/cm^3. Several remarks were given from the experimental research:

- The time evolution of swelling pressure is very characteristic suggesting a rather complex pattern of behaviour. Swelling pressure increases rapidly at the beginning of the test, until reaching a peak

value. Afterwards, the measured pressure drops to a minimum value (macro-structural collapse) to start later a new increase until reaching a stationary swelling pressure value at the end of the test.

- There is a clear influence of the sample length on the rate of the development of the swelling pressure. The longer specimen, the slower the hydration kinetics. This fact should be taken into account when transferring laboratory test results to field conditions where scale and hydration paths are bound to be quite different (e.g. engineering barriers and seal structures for nuclear waste repositories).

- The final swelling pressure at the end of the test is similar for the three samples, irrespective of length. Indeed, it has been found that final swelling pressure depends basically on dry density.

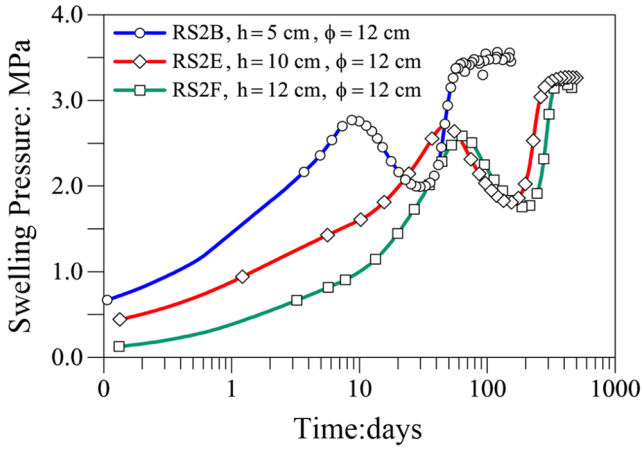

Figure 2-16. Swelling pressure vs. time relationship for various sample sizes. FoCa Clay (Gens et al., 2011).

The dependence of swelling pressure on compacted dry density has been examined by a large number of tests performed in conventional oedometers (wetting applied in a single step) and suction controlled equipment. It is reassuring that no spurious effects due to the equipment appear to affect the results of the swelling pressure tests (Lloret et al., 2003). From this fact, the large experimental database of well-known bentonites reveals an exponential trend (or lineal in semi-log plots) of the swelling pressure value with dry density (Figure 2-17). Hydraulic conductivity is also related to dry density in compacted granular bentonite (Hoffmann et al., 2007).

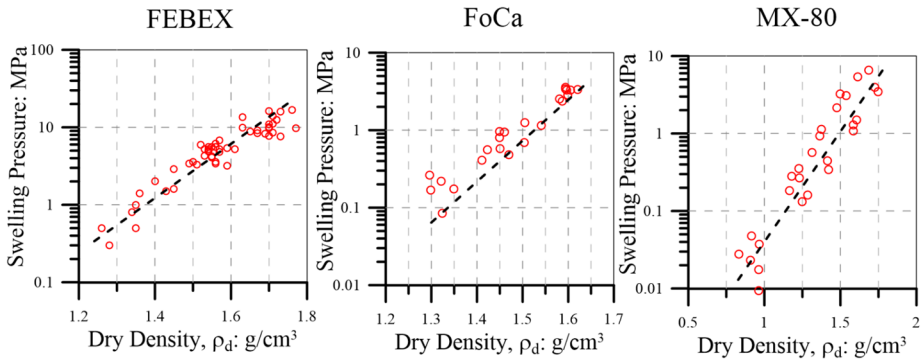

Figure 2-17. Swelling pressure as a function of dry density for FEBEX bentonite (Lloret et al., 2003), FoCa bentonite (Gens et al., 2011) and MX-80 bentonite (Karnland et al., 2008).

Delayed water transfer

A better understanding of the development of swelling pressure (and swelling strains) in time can be achieved considering separately the swelling of the macro-structure and the swelling of the micro-structure. The larger pores of the macro-structure are partially filled with water that move in accordance with Darcy's law. The rate of water movement is then controlled by the permeability. If the initial hydraulic state of the soil is altered (for instance by wetting the sample in a swelling test), the suction at a particular point of the macro-structure may be different from the one at the microstructure. Therefore, water will migrate from one structural level to the other one ensuring the hydration of the active minerals which then expand. A progressive hydration will result in a suction equilibrium. In fact, this mechanism can act in either direction, either in expansion or shrinkage. The hydraulic equilibrium between structural levels is a particular state of the expansive clay. Fityus and Buzzi, (2009) have shown water retention curves of the natural expansive clay samples indicating air entry value of approximately 10 MPa, while they argue that micro-structural level could theoretically (double layer theory) resist air entry suctions great as 80 to 100 MPa.

It is assumed that only matric and gravitational potential contribute to the total potential of the macro-structure but an additional osmotic component may also contribute to the microstructural potential (Gens, 2010). As water exchange is local in space, the gravitational potential will

be the same for the two structural levels. Water exchange will therefore be driven only by suction differences (Gens et al., 2011).

The full-saturation of aggregates even at high suction has been suggested by several physical evidence and theoretical works (Martin, 1960; Gens and Alonso, 1992; Alonso et al., 1999 and Fityus and Buzzi, 2009). Sun et al., (2019) evaluated the evolution of liquid degree of saturation of the clay aggregates in the compacted the Czech bentonite B75. The water content corresponding to each suction applied in the ESEM chamber was calculated by interpolation from wetting path of the water retention curves. Afterwards, the volume change of aggregates for each suctions was calculated from ESEM microphotograph analysis. Despite the adopted hydraulic and geometrical assumptions, the calculation of saturation degree for aggregates (for different dry densities) gives consistent results (Figure 2-18). The air entry value increases with the dry density and their values (10 MPa and 60 MPa) are lower than the theoretical values reported above.

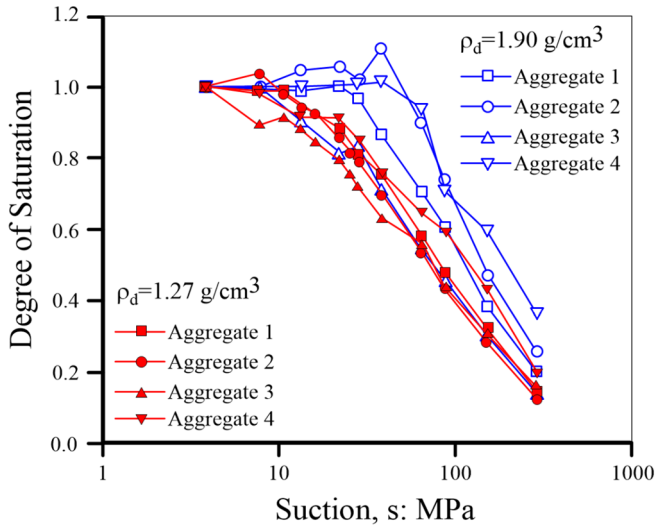

Figure 2-18. Degree of saturation of aggregates during wetting evaluated from combination of ESEM and WRC measurements (Sun et al., 2019)

Delage et al., (2006) performed a microstructure investigation about the time dependent fabric changes of MX-80 bentonite at different dry densities and water content. Statically compacted samples were kept at constant volume and water content for a several periods prior to MIP and ESEM tests. Important change in microstructure was observed,

characterised by a decrease in the inter-aggregate porosity and an increase in the very thin porosity not intruded by mercury (Figure 2-19).

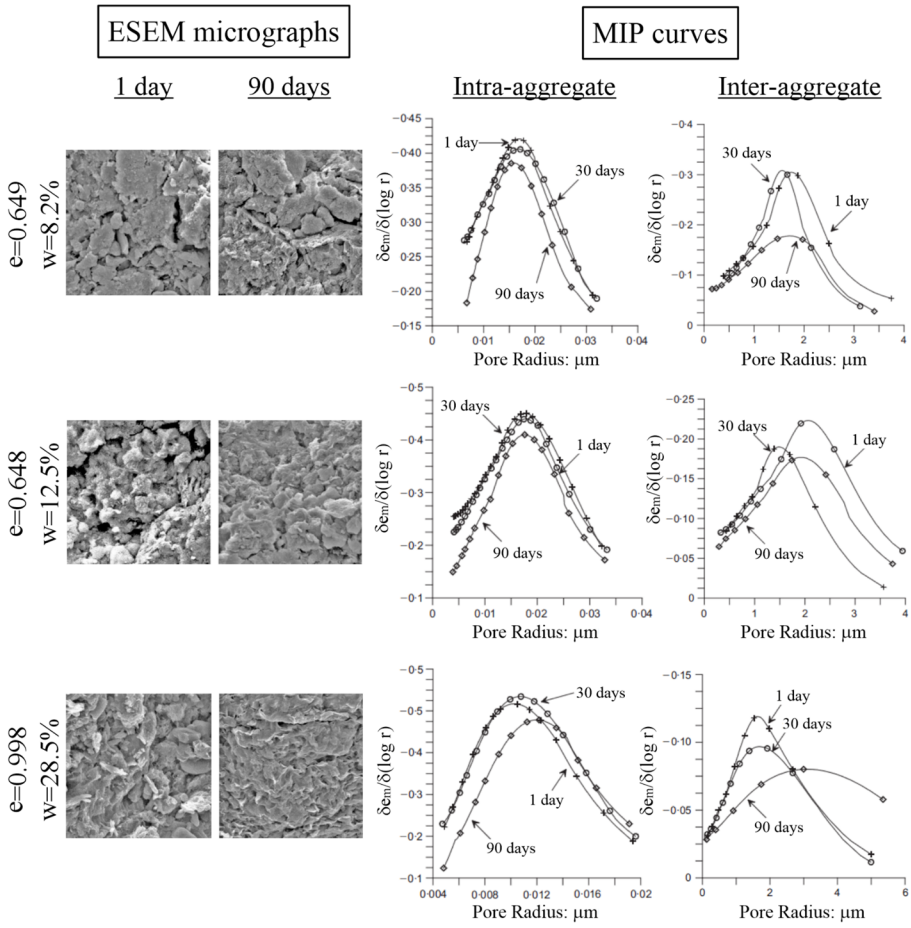

Figure 2-19. MX-80 microstructural changes due to micro-Macro water exchange (Delage et al., 2006).

The constant water content does not implies a hydraulic equilibrium between the micro and Macro structural levels. Each structural level has their own water retention properties related to their pore structure, therefore, micro and Macro structural levels may show different suction values according to the water content imposed. Finally, the water exchange phenomena leads a fabric evolution. The inter-aggregates larger pores are intruded by exfoliation, and the changes inside the aggregates are governed by progressive placement of interlayer water molecules inside the clay particle packings.

Hydration kinetics

There are important differences in the flow conditions for saturation of bentonite at laboratory and field environment. Kröhn, (2019) points out that the re-saturation of compacted bentonite, which is envisioned as buffer material for nuclear waste repositories, depends on the one hand on the ability of bentonite to take up water and on the other hand on the water supply from the host rock formation. Since one of the main requirements of the potential host rock formations for the emplacement of a repository is a low hydraulic permeability, the rate of water supply from the rock is also expected to be low. In contrast, the water uptake tests carried out in the laboratory (e.g. swelling pressure test and swelling strain test) have been mostly performed in such a way that bentonite had unimpeded access to water. Under these conditions, the initial uptake rate of bentonite is an order of magnitude higher than the typical outflow rate from a potential host rock.

Underground research laboratories (URL) has been built in order to evaluate the in-situ Chemo-Thermo-Hydro-Mechanical behaviour of the host rock formation and potential buffer materials. The pore pressure response and stresses are easy measurable responses. However, the water outflow measurements imply extreme long periods. Consequently, the hydration of the bentonite seals with water supplied from the host rock is a non-feasible experimental task. Artificial saturation systems has been used in the in-situ horizontal gallery seal structure (ANDRA, 2015) and seals of horizontal boreholes (Mokni et al., 2016). The analysis of these heavily instrumented experiments and their extrapolation to repository conditions is a challenging engineering task. A deep understanding of the expansive clays behaviour and the numerical modelling appears to be the mainstream option.

Different hydration conditions can be applied on laboratory setups; nevertheless, imposing the in-situ rate of water supply is almost impossible. Typically, the bentonite samples are hydrated under constant water pressure (full water access), in spite of the fact that controlled water flow is more related to in-situ saturation.

The European project BEACON (Bentonite Mechanical Evolution) deals with the experimental research and numerical modelling of expansive

clays for the nuclear waste repositories. As a part of the experimental work, the CIEMAT (Spanish Centre of Technology, Energy, and environmental research) performed large-scale oedometer tests on bentonite block/pellets specimens (Figure 2-20):

- MGR22: Restricted water access (controlled flow of 0.05 cm^3/h) until full saturation.
- MGR23: Full water access (water pressure of 14 kPa) until full saturation.

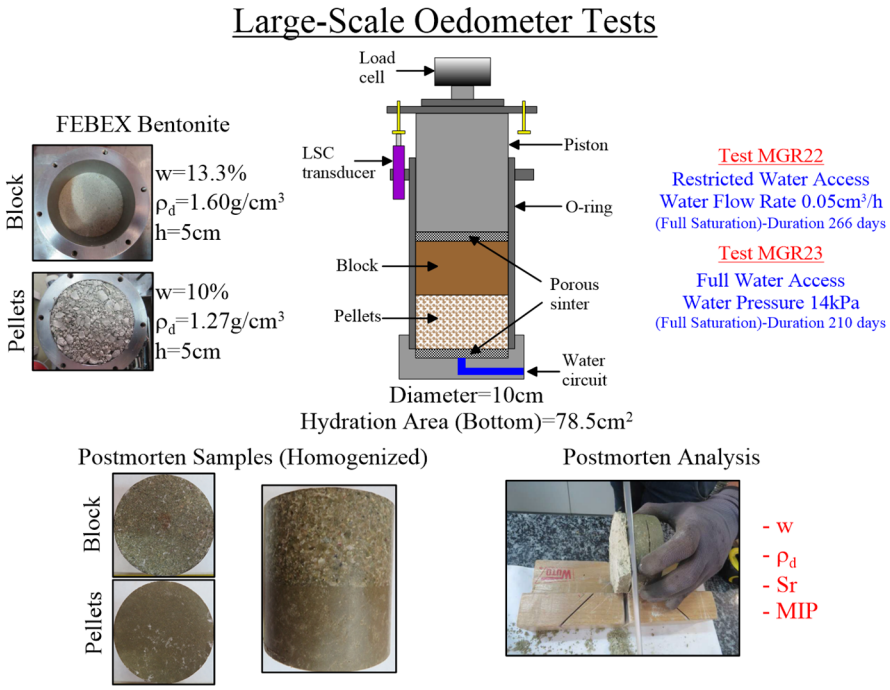

Figure 2-20. Experimental setup of CIEMAT homogenization tests: MGR22 and MGR23.

The axial pressure response and its relation with the water intake generated by the hydration condition are detailed in the Figure 2-21 and Figure 2-23. The homogenization phenomena and structural evolution are explained in the Section 2.5.2.1..

The saturation of the specimens is done through the bottom of the bentonite pellets section and this aspect implicate important differences due to flow conditions. A slow hydration process is generated by the

restricted water flow (MGR22 test), conversely, the full water access (MGR23 test) induce the fast hydration of the specimen.

There is a clear influence of hydration type on the rate of the development of swelling pressure. The full water access (MGR23 test) induce the faster pressure evolution. Expected experimental results are the same final axial pressure value (same average dry density) and the complex pattern behaviour of swelling pressure (rapid increase until a peak value – pressure drops – secondary increase until stationary value) (see Figure 2-21-Left).

The time evolution of the water intake is shown in the Figure 2-21-Right. The water intake for the specimen MGR23 evolves with the fabric evolution of the sample; it increases rapidly at the beginning of the test and the rate continuously decreases until constant value. On the contrary, the restriction on water flow (MGR22) controls the rate of water intake, because the water pressure on the hydration boundary changes in order to keep the constant flow value. As a reliable result, the final water intake value at the end of the test is similar for the two specimen. They correspond to the unsaturated pore space at constant volume condition.

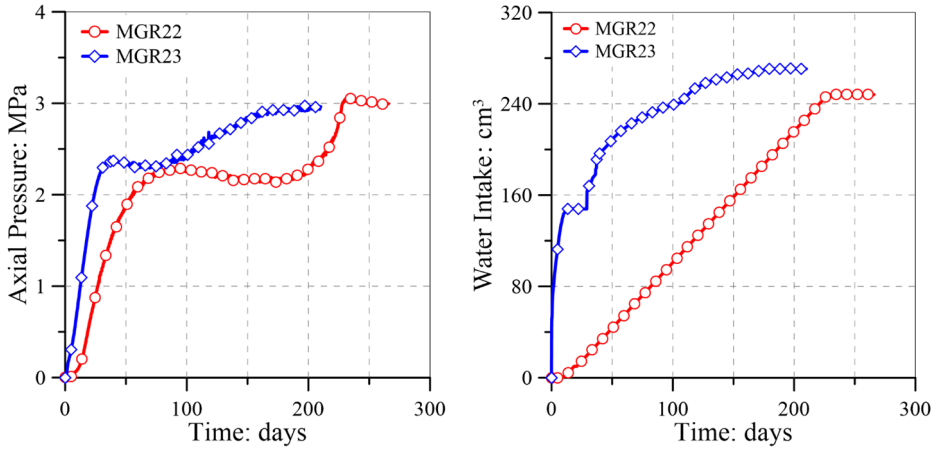

Figure 2-21. Left: axial pressure evolution; Right: water intake evolution. CIEMAT homogenization tests MGR22 and MGR23.

As stated Hoffmann et al., (2007), the pellet mixture response during a fast hydration process can be described assuming two different phases. During the initial phase, water goes into the sample through the

interconnected macro-porosity and the bentonite pellets remain almost unchanged. After this initial phase, the bentonite pellets start to hydrate exchanging water with the water stored in the macro-pores. The bentonite granules swell filling the macro-pores and reducing dramatically the permeability (see Figure 2-22).

If water inflow is controlled, the saturation of the specimen begins as a hydration front through the granular pellets mixture. The bentonite pellets, at the base of the specimen, start to swell due to water exchange, reducing the macro pore space and the permeability. The above mechanism induces a delayed hydration of the specimen (Figure 2-22).

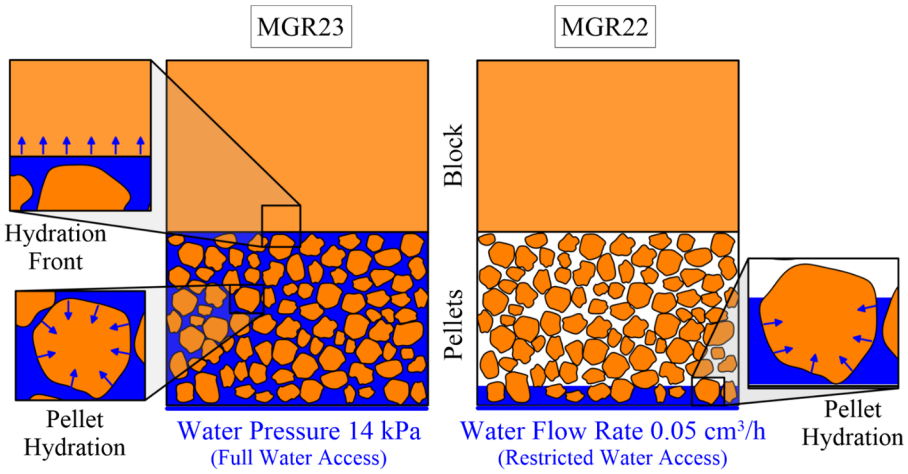

Figure 2-22. Hydration mechanism of CIEMAT homogenization tests at early stage.

Based on the hydration mechanisms, it is worthwhile to express the axial pressure evolution as a function of water intake (Figure 2-23). The MGR23 test requires important amount of water to generate axial pressure, because the filling of the macro pore space of the bentonite pellets section (see Figure 2-22). The early development of axial pressure in the MGR22 test is given by the swelling of the pellets according to the hydration front and the vertical stress equilibrium. The curves coincides at certain point and then follow the same pattern; indicating that the two hydration kinetics reach an state in which the saturation of the samples are similar and the hydration of the pellets and block progresses towards the full saturation.

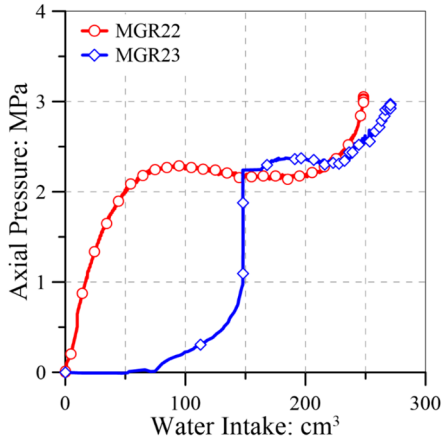

Figure 2-23. Axial pressure as function of water intake. CIEMAT homogenization tests MGR22 and MGR23

2.2.4.4. Heterogeneity and homogenization processes

According to the time evolution of a nuclear waste repository, the main sources of heterogeneity in bentonite barriers are:

- *Selected materials.*

Filling the excavations of underground nuclear waste repositories through the in-situ compaction of bentonite powder is not a straightforward task. Taking into account that the final values of swelling pressure and swelling strains rely on the dry density, a certain compaction level is required.

Several pre-compacted materials have emerged as engineering solution to reduce the compaction effort required to achieve the value of average dry density. Some of these materials are: bentonite pellets (Hoffmann et al., 2007), powder/pellets mixtures (Gens et al., 2011; Molinero-Guerra et al., 2017), compacted bentonite blocks (Lloret et al., 2003) and sand/bentonite mixtures (Saba et al., 2014; Cui, 2017). The heterogeneous fabric of these materials requires special approaches in order to describe adequately its behaviour during hydration.

- *Design and emplacement.*

The role of the bentonite in the nuclear waste repositories has been established by their final swelling pressures. For example, the preliminary

design of the seal systems considers the recovery of the initial in-situ stress of the host rock formation due to the bentonite swelling (ANDRA, 2011). However, the configuration and emplacement of the bentonite-based materials in the repository excavations are open issues.

Heterogeneities are coming from the following factors: a) the use of pellets and blocks in the same section, b) the geometrical features of the opening, c) the presence of technological gaps and voids and the non-homogeneity of bentonite emplacement (segregation of granular bentonite).

- *Behaviour during transient stage.*

The degree and distribution of heterogeneities, in water content and dry density, will vary during the transient phase involving only hydration (backfills, seals and plugs) or hydration and heating (buffers).

Although the bentonite exhibits a natural tendency towards homogenization, observations during dismantling of very long-term tests have revealed that, even at or close to saturation, a degree of heterogeneity persists (Mayor and Velasco, 2014; Villar et al., 2019). Potentially, heterogeneity may evolve beyond the end of the transient phase.

- *Saturated phase.*

The events in the saturated stage, after transient phase, can be erosion, piping, dissolution or the cracking of the seal due to the rising of the water pressure in some fracture of the host rock formation. The self-healing ability of be bentonite and its (T)HM evolution is a serious concern (Börgesson et al., 2014). Recently, Navarro et al., (2016) analysed the swelling and mechanical erosion of the MX-80 bentonite through the numerical modelling of a pinhole test. The loss of mass at the water–soil interface generates significant swelling strains and stress redistribution around the hole. A double-structure constitutive model and a Lagrangian formulation have been required to reproduce this coupled response.

It is necessary to predict the evolution and final state of the heterogeneities, nevertheless the average dry density is not sufficient to

characterize the state of the barrier or the seal. Homogenization process understanding requires a research on the effects of the initial expansive clays fabric and its evolution. The irreversibility (and stress-path dependency) during the (T)-HM actions is a core feature of the behaviour underlying final heterogeneity. Well-controlled laboratory and field tests over a range of conditions and scales are the best sources of knowledge.

Direct observations of the hydration process in a compacted 50/50 powder-pellets mixture were obtained by Van Geet et al., (2005) using X-ray computed tomography. With the initial dry density of 1.36 g/cm^3 and an average water content of 5.67%, the hydration was performed from the bottom of the sample under constant volume condition. From the computation of the linear X-ray attenuation coefficient, the density distribution through the sample could be determine. The Figure 2-24 shows the density distribution on a vertical slice through the centre of the sample at different times of the experiment. From this visualization Gens et al., (2011) concluded:

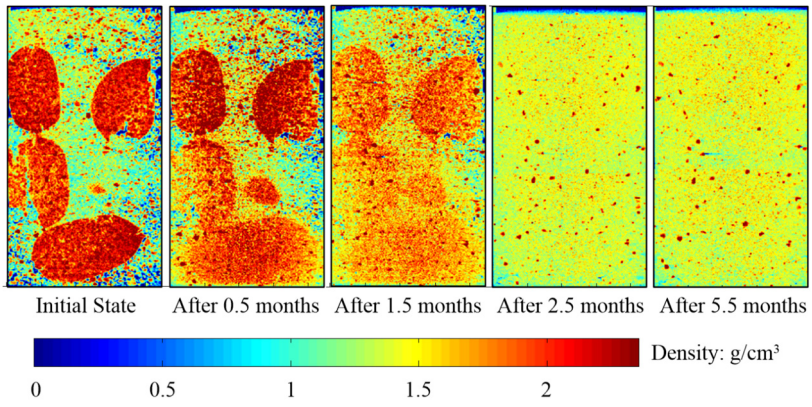

Figure 2-24. Distribution of densities on a vertical slice of a powder/pellets mixture at different stage of hydration. The specimen is 7 cm high and 3.8 cm in diameter (from Gens et al., 2011 and Van Geet et al., 2005)

- At initial state, there is a clear difference in density between pellets and powder.
- During hydration, the density of the pellets reduces (swelling) whereas the density of the powder rises because of both soil compression and water content increase; the changes move gradually from bottom to top following the progress of hydration.

- An apparently homogeneous specimen is obtained at the end of the test.

Additional information is provided in Figure 2-25 that shows the incremental density changes between the stages depicted in Figure 2-24. It can be observed how the water front rises from the bottom of the sample towards the top, causing density change due to the swelling of the pellets and to increase in saturation. Very little density change occurs after 2.5 months where the specimen has become much more homogeneous. It is interesting to note that, in the initial stages of the test, the surfaces of the pellets away from the hydration front show certain swelling due to local water exchange between powder and pellets.

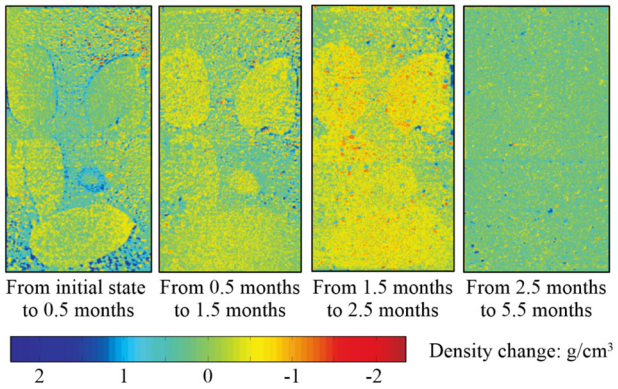

Figure 2-25. Distribution of incremental density change on a vertical slice of a powder/pellets mixture at different stage of hydration. The specimen is 7 cm high and 3.8 cm in diameter (from Gens et al., 2011 and Van Geet et al., 2005)

The postmortem examination of laboratory tests offer quantitative information of the final specimen heterogeneity. The spatial distribution of dry density, water content and pore space distribution are obtained from the saturated specimens of the CIEMAT homogenization tests (see Figure 2-20). From this spatial information, it can be noted:

- There is not important influence of the hydration kinetics on the spatial distributions of the final dry density and water content (Figure 2-26). This fact is in agreement with the close values of the final swelling pressure in both tests. The dry density evolution in the block and pellets sections are given by their behaviour in the homogenization process. The dry density of the compacted block

reduces (swelling) whereas the pellets dry density rises because soil compression and water content increase.

- Although the general trend of the evolution of the pore size distributions is similar in both tests, the final values are affected by the hydration condition (Figure 2-27 and Figure 2-28). The saturation of the compacted block induces an important increase of micro pores (<50nm) and the hydration and compression of the bentonite pellets reduces the macro pores (>50nm).

- In contrast to the saturated powder/pellets mixture presented previously, certain degree of heterogeneity persist after saturation in these pellets-block configurations.

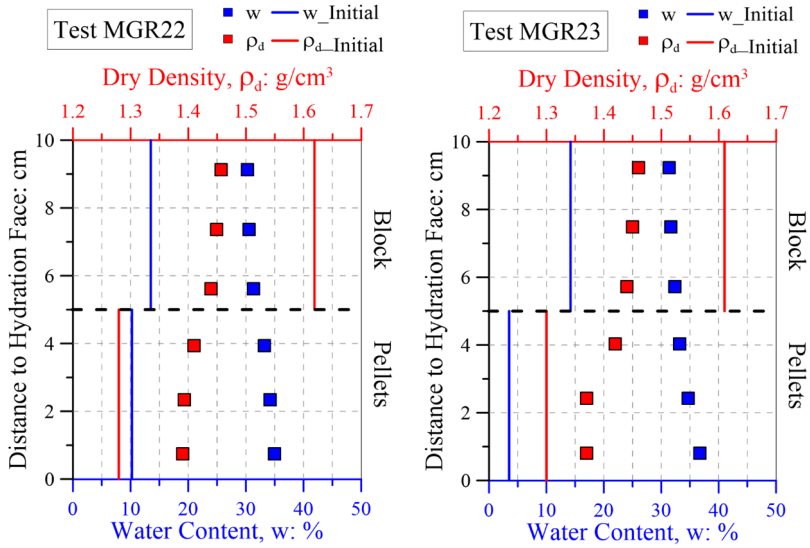

Figure 2-26. Dry density and water content distribution in the CIEMAT homogenization tests MGR22 and MGR23.

The testing of homogenization process involves additional factors to the bentonite-based materials interaction due to hydration. The Figure 2-29 shows a dismantled parallel test where preferential water paths are generated in the contact with the oedometer cell. The friction with the cell can be also produced. The in-situ bentonite homogenization will be affected also by its interaction with the excavations walls.

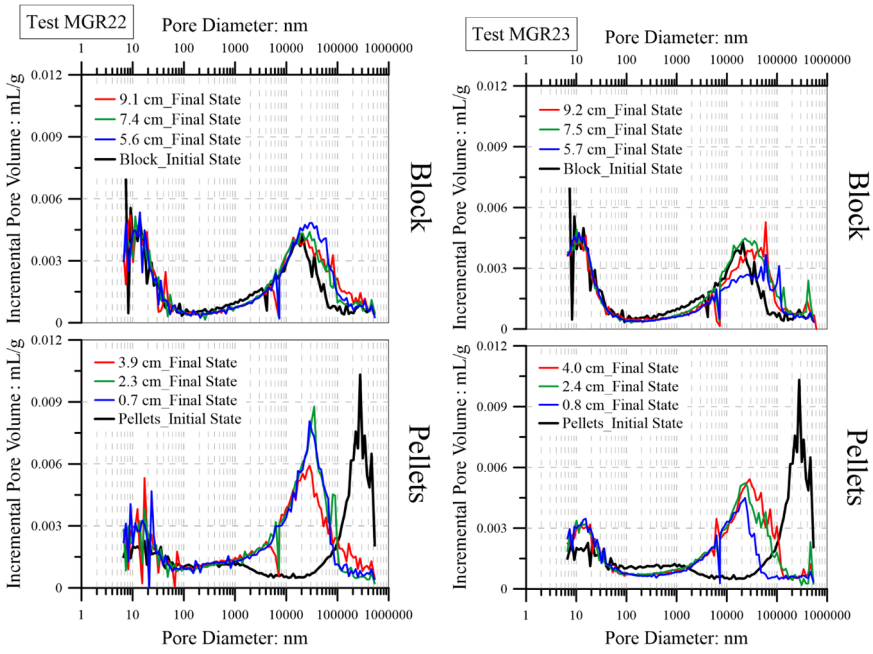

Figure 2-27 Distribution of incremental pore volume in the CIEMAT homogenization tests MGR22 and MGR23.

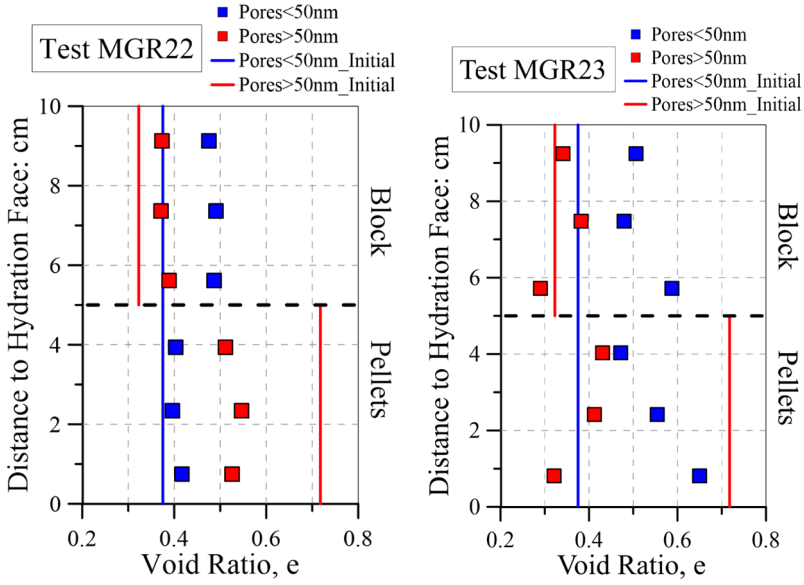

Figure 2-28. Void ratio evolution in the CIEMAT homogenization tests MGR22 and MGR23.

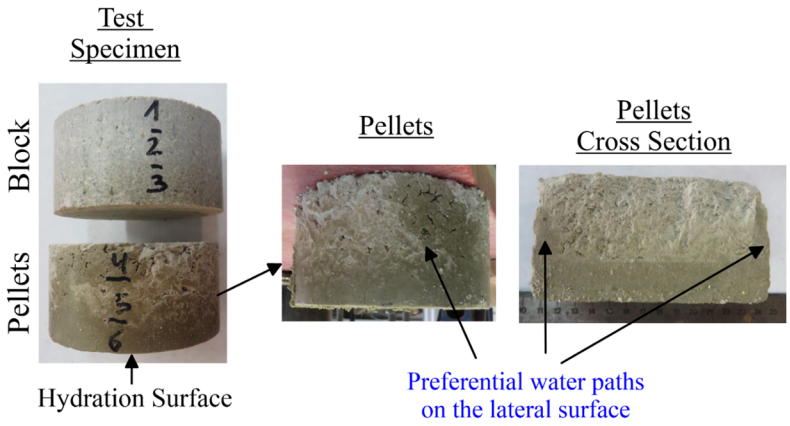

Figure 2-29. Preferential hydration paths in CIEMAT homogenization test.

2.3. Theoretical approach

The conceptual model of the porous media determines the theoretical approach for their coupled hydro-mechanical (HM) formulation. As pointed out by Schrefler, (2002), the porous material are classified as those with an internal structure. They comprise the solid phase and pores geometry. According to the physical features of the expansive clays presented above, the expansive clay was defined as double-structure material composed by the arrangement of clay aggregates and micro- and macro-pores (Figure 2-5).

Geomaterials (e.g. soil, rock, concrete) where the pores are filled with more than one fluids (i.e. water, water vapour and dry air), they are classified as multiphase media. The solid and the fluids usually have a relative velocity to each other, due to this fact and the different material properties that exist; there are interaction between the components. Besides, the pore arrangement has an extremely complicated geometry. Instead of considering this discrete nature, a continuum approach can be usefully adopted. According to this approach, the multiphase porous medium is replaced by a fictitious continuum.

The key concepts to reconcile continuum mechanics with the microscopic discontinuities inherent in porous media constituted by solid and fluid phases are twofold (Coussy, 2004):

- The first concept is to consider the porous medium as the superposition of several continua that move with distinct kinematics, while mechanically interacting and exchanging energy and matter. The continuous media that composes an unsaturated double-structure clay are shown in the Figure 2-30.

- Since the formulation of the constitutive equations of any solid requires its deformation to be referred to an initial configuration, the second concept is to transport the equations governing the physics of the superposed fluid and solid continua from their common current configuration to an initial reference configuration related to the solid skeleton.

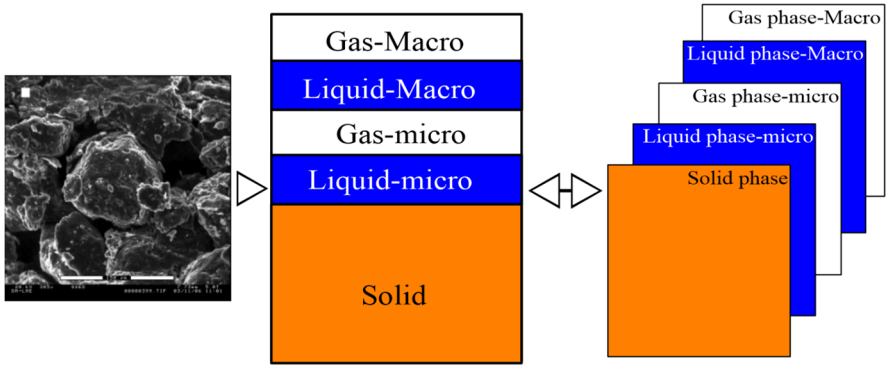

Figure 2-30. Expansive clay as the overlapping of several continuous media. (ESEM picture of the FEBEX bentonite taken from Musso et al., 2013).

There are two continuous strategies with an intensive research activity and successful applications. One starts from a micromechanics viewpoint and the other from macromechanics viewpoint. The first methodology, typically named *hybrid mixture theory*, uses the averaging theories to stablish the macroscopic behaviour from a micromechanical formulation. Since the modern statement of the mixture theory, the first formal development for multiphase systems employing averaging theory was presented by Hassanizadeh and Gray, (1979 and 1980). Afterwards, Lewis and Schrefler, (1998) applied this kind of theory to boundary value problems such as subsidence, oil reservoir and non-isothermal flows in porous media. The second strategy, defined as *phenomenological approach*, works directly with measurable macroscopic variables. There is not a clear distinction between the macroscopic and microscopic domains.

Probably the firts contribution to this kind of porous media approximation is due to Biot, (1940). Later on, several contribution and improvements have been derived in applications on transport in porous media, non-isothermal multiphase flow in deformable media, strain localization phenomena, biomechanics and others. (Bear, 1972; Olivella et al., 1994; Coussy, 2004; de Boer, 2005; Gens, 2010).

Referring to the soil in unsaturated state, the inclusion of the interfaces between the fluids filling the pores (menisci) in the balance equations can be the main difference in both approaches. The thermodynamic properties of the interfaces are disregarded in the macroscopic approach. However, this fact does not exclude the possibility of exchange of mass, momentum or energy between the components of the porous media. At the end, the adoption of the approach is a matter of convenience. Actually, de Boer et al., (1991) concluded that under appropriate assumptions, the averaging theory generates the same equations of the phenomenological theory, at least as far as balance equations are concerned.

This work uses the macroscopic approach developed by Olivella et al., (1994) and Olivella, (1995) which originally was formulated for saline media. The extension for a broad spectrum of geomaterials was a consequence of the continuous evolution and the generation of a numerical simulator (Olivella et al., 1996). Specifically for expansive clays, Sánchez, (2004) expressed the governing and constitutive equations for a double-structure porous media. In the following items, several contributions of this work to these aspects are presented.

2.4. Problem formulation

The porous media under study consist of three phases [solid (s), liquid (L) and gas (g)] and three main components [solid (s), water (w) and air (a)]. An important difference with respect to the original formulation (Olivella et al., 1994) is that each structural level contains air and water in gas and liquid state (Figure 2-31). Additionally, the possibility to have unsaturated states in the micro-structural level represents a new feature with respect to the formulation of Sánchez, (2004). This means a general state of the expansive clay, because strong drying paths or some

compaction procedures can induce this state at the micro-structural level (see Figure 2-18).

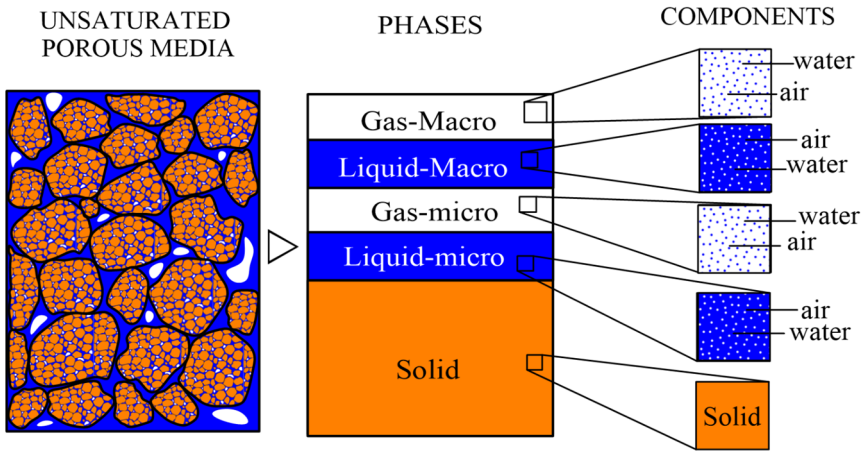

Figure 2-31. Continuum approximation of unsaturated double-structure porous media. Phases and components at each structural levels.

According to the Figure 2-31, the full description of the hydro-mechanical (HM) state of the double-structure medium is given in terms of a large number of variables. As indicated in the equation (Eq. 2-2), in the description of any entity (ψ), the subscript refers to the phase (P) and the superscript means the component (C). The overall notation is depicted in Table 2-4, before the governing equations statement.

$$\psi_{\mathrm{P}}^{\mathrm{C}} \qquad \text{(Eq. 2-2)}$$

Some imprecise definitions in previous models came from the definition of porosities for each structural level (macro and micro). Before formulating the governing equations, it is necessary a critical review of those concept for a double-structure medium.

One of the main requirements in the coupled HM formulation is the reference of the quantities respect to the whole volume. From this point, the *volume fraction concept* plays a key role. Volume fractions are given by the ratio of the volume of the constituents respect to the total volume of the control space. The macroscopic approach is intrinsically integrated by the concept of the volume fraction (Lewis and Schrefler, 1998 ; de Boer, 2005; Borja and Koliji, 2009; Salimzadeh and Khalili, 2016).

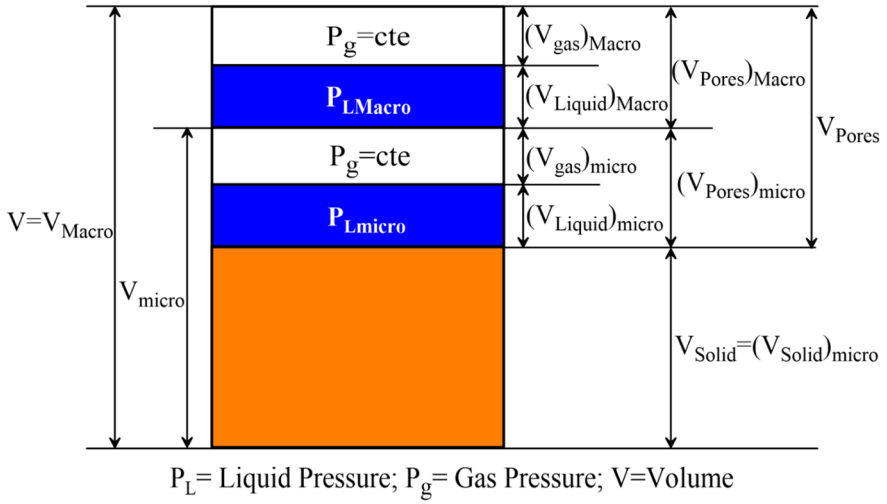

Figure 2-32. Phase diagram of an unsaturated double-structure soil—Volumes.

The Figure 2-32 shows the phase volumes distribution in a double-structure porous media. It is useful to determine the porosities and volume fractions.

Based on the structural levels of an expansive clays, it is possible to define the *micro pore volume fraction* (Eq. 2-3) and *macro pore volume fraction* (Eq. 2-4). The above expressions relate the volume of pores at the macro- and micro-structure with the total volume of the control space. They are adequate quantities to express the balance equations of this porous medium. Besides the pore volume fractions, there is also a *solid volume fraction*, which is defined in the equation (Eq. 2-5). This involves the solid particles contained in the clay aggregates (micro-structure).

$$\bar{\phi}_{micro} = \frac{(V_{Pores})_{micro}}{V} \qquad \text{(Eq. 2-3)}$$

$$\bar{\phi}_{Macro} = \frac{(V_{Pores})_{Macro}}{V} \qquad \text{(Eq. 2-4)}$$

$$\bar{\phi}_{Solid} = \frac{(V_{Solid})_{micro}}{V} \qquad \text{(Eq. 2-5)}$$

The physical constraint over the volume fraction condition is that their summation have to be equal to one (Eq. 2-6).

$$\sum \bar{\phi} = \bar{\phi}_{micro} + \bar{\phi}_{Macro} + \bar{\phi}_{Solid} = 1 \qquad \text{(Eq. 2-6)}$$

The *total porosity* of the double-structure soil is given by the summation of both pore volume fractions (Eq. 2-7).

$$\phi = \bar{\phi}_{micro} + \bar{\phi}_{Macro} \quad \text{(Eq. 2-7)}$$

A detailed revision of the pore volume fractions ($\bar{\phi}_{micro}$ and $\bar{\phi}_{Macro}$) indicates that they are not the strictly definition of the porosities at each structural levels, as they are defined in classical soil mechanics. The *micro-porosity* comes from the relation of the volume of micro-pores and the volume of the micro-structural level (Eq. 2-8).

$$\phi_{micro} = \frac{(V_{Pores})_{micro}}{V_{micro}} \quad \text{(Eq. 2-8)}$$

In this kind of porous media, the definition of *macro porosity* (ϕ_{macro}) is not clear, because the volume of the Macro-structural level coincides with the total volume. The macro-structure can be conceived as a "virtual" medium that would be found for the case in which the whole volume of the micro-structure is occupied only by solid phase.

The porosity changes are directly related to the volumetric deformation of the structural levels and the porous medium itself. From this fact, the right porosity definitions is mandatory. Certainly, there are relationships between the pore volume fractions and the porosities. In the micro-structure level, they are related by a volume relation (Eq. 2-9). The relationship for the macro-structural level is only true if we consider the clay aggregates as incompressible bodies (Eq. 2-10).

$$\phi_{micro} = \frac{V}{V_{micro}} \bar{\phi}_{micro} \quad \text{(Eq. 2-9)}$$

$$\phi_{Macro} = \bar{\phi}_{Macro} \quad \text{(Eq. 2-10)}$$

A remarkable fact is that the porosities of the micro- and macro-structural levels don't satisfy the physical constrain expressed in the equation (Eq. 2-6), therefore, they are not a good choice for the statement of the governing equations.

Previous models defined the pore volume fractions equal to the porosities of the structural levels. It does not imply a wrong consideration, however, the analysis of the evolving structure can be confusing. Probably, these

imprecise definitions come from the fact that in single-structure materials the pore volume fraction coincides to the porosity. Clearly, this is not true in the double-structure porous media.

A detailed explanation of stress-strain variables for the constitutive formulation is presented in the Chapter 3. Nevertheless, the concept of volumetric deformation (ε_v) appears in the governing equation. Statements of the continuum mechanics give the deformation of any body. Taking $\mathbf{u}$ as the tensor field displacement, the strain tensor and volumetric strain are defined as:

$$\boldsymbol{\varepsilon} = \frac{1}{2}(\nabla \mathbf{u} + (\nabla \mathbf{u})^{T}) \qquad \text{(Eq. 2-11)}$$

$$\varepsilon_v = \nabla \cdot \mathbf{u} = \mathrm{tr}(\boldsymbol{\varepsilon}) \qquad \text{(Eq. 2-12)}$$

From the volume definitions of a double-structure porous medium (Figure 2-32), it is also possible to obtain its incremental volumetric strain.

$$d\varepsilon_v = \frac{dV}{V} = \frac{d(V_{Solid})_{micro} + dV_{Pores}}{V} = \frac{d(V_{Solid})_{micro} + d(V_{Pores})_{micro}}{V} + \frac{d(V_{Pores})_{Macro}}{V} \qquad \text{(Eq. 2-13)}$$

The last expression suggest the first decomposition of the incremental volumetric strain.

$$d\varepsilon_v = d\bar{\varepsilon}_{v\_micro} + d\bar{\varepsilon}_{v\_Macro} \qquad \text{(Eq. 2-14)}$$

Both components of the incremental volumetric strain (micro and macro) are defined respect to the total volume of the porous medium. In fact, this decomposition is equivalent to the total porosity decomposition (Eq. 2-7) due to the direct relationship between the total porosity changes and the incremental volumetric strain.

The term $d\bar{\varepsilon}_{v\_Macro}$ is the strict deformation of the medium only in the case of an incompressible micro-structural level (e.g. single-structure porous medium). The real meaning of this term in a double-structure porous media (compressible micro-structural level) is explored in the

Section 2.5.1.1. Furthermore, $d\bar{\varepsilon}_{v\_micro}$ is not the volumetric deformation of the clay aggregates. The volumetric strain at this structural level is given by the ratio between the volume increments and its volume (Eq. 2-15). The factor that correlates both volumetric strain definitions is the same as the relation between the micro-porosity and micro pore volume fraction (Eq. 2-9).

$$d\varepsilon_{v\_micro} = \frac{dV_{micro}}{V_{micro}} = \frac{V}{V_{micro}} d\bar{\varepsilon}_{v\_micro} \qquad \text{(Eq. 2-15)}$$

The incremental form of the pore volume fractions also play an important role in the mathematical treatment of the governing equations. In a general way, we can proceed as follows:

$$d\bar{\phi}_{\alpha} = d\left(\frac{(V_{Pores})_{\alpha}}{V}\right) = \frac{d(V_{Pores})_{\alpha} V - (V_{Pores})_{\alpha} dV}{V^2} \qquad \text{(Eq. 2-16)}$$
$$= \frac{d(V_{Pores})_{\alpha}}{V} - \frac{(V_{Pores})_{\alpha}}{V}\frac{dV}{V}$$

where:

- α is the structural level, either Macro or micro.

Using the previous definitions ((Eq. 2-13) and (Eq. 2-14)), the incremental form of the pore volume fractions (micro and macro) and solid volume fraction are:

$$d\bar{\phi}_{Macro} = d\bar{\varepsilon}_{v\_Macro} - \bar{\phi}_{Macro} d\varepsilon_{v} \qquad \text{(Eq. 2-17)}$$

$$d\bar{\phi}_{micro} = d\bar{\varepsilon}_{v\_micro} - d\bar{\phi}_{Solid} - \bar{\phi}_{micro} d\varepsilon_{v} \qquad \text{(Eq. 2-18)}$$
$$= d\bar{\varepsilon}_{v\_micro} + (1-\phi)\frac{d\rho_s}{\rho_s} - \bar{\phi}_{micro} d\varepsilon_{v}$$

$$d\bar{\phi}_{Solid} = \frac{V_{Solid}}{V}\frac{dV_{Solid}}{V_{Solid}} = (1-\phi)\frac{1}{V_{Solid}} d\left(\frac{m_s}{\rho_s}\right) \qquad \text{(Eq. 2-19)}$$
$$= (1-\phi)\frac{1}{V_{Solid}}\left(\frac{\rho_s dm_s - m_s d\rho_s}{\rho_s^2}\right)$$
$$= -(1-\phi)\frac{1}{V_{Solid}}\frac{m_s}{\rho_s}\frac{d\rho_s}{\rho_s} = -(1-\phi)\frac{d\rho_s}{\rho_s}$$

where:

- ρ_s is the local density of the solid phase;
- m_s is the mass of the solid phase.

As for the total porosity, using the additive definitions (Eq. 2-7) and (Eq. 2-14), we have:

$$d\phi = (1-\phi)\left(\frac{d\rho_s}{\rho_s} + d\varepsilon_v\right) \qquad \text{(Eq. 2-20)}$$

This well-known expression in soil mechanics (Olivella, 1995; Gens, 2010) indicates that the porosity changes depends on the variation of the density of the solid phase and the volumetric strain increments of the medium.

2.5. Governing equations

The equations that govern this problem can be categorized into four main groups: balance equations, constitutive equations, equilibrium relationships and definitions constrains.

2.5.1. Balance equations

In this part, we derive the mass balance of different components at micro and macro structural levels and the balance of momentum for the medium as a whole that reduces to the stress equilibrium. Balance of momentum for fluid phases are reduced to constitutive equations (i.e. Fick's and Darcy's laws).

The formulation described here is based on the general approach of Olivella et al., (1994) and Olivella, (1995) applied to the specific case of isothermal problems involving double-structure unsaturated soils. The compositional approach is adopted to establish the mass balance equations. It consists of balancing the components (water and air) rather than the phases (gas and liquid): total components equations are obtained by adding over all phases the equation of balance of each components. In this way, the phase exchange terms (evaporation/condensation for water and liberation/dissolution for air) cancel out, which is particularly useful when equilibrium is assumed.

There are several descriptions of the mass balance of any thermodynamic property in a continuum (e.g. Malvern, 1969; Oliver and Agelet De Saracibar, 2016). These balance principles has been focussed mainly in non-porous materials (e.g. metals). From these early ideas, several

developments have been made concerning the continuum treatment for multiphase porous media (Bear, 1972; Hassanizadeh and Gray, 1979; Olivella, 1995; Lewis and Schrefler, 1998; de Boer, 2005; Borja, 2006). The macroscopic balance of porous media can be expressed as follow:

$$\frac{\partial}{\partial t}\begin{pmatrix}\text{Mass or energy}\\ \text{per unit volume}\\ \text{of porous media}\end{pmatrix} + \nabla\cdot\begin{pmatrix}\text{Fluxes}\\ \text{of mass}\\ \text{or energy}\end{pmatrix} = \begin{pmatrix}\text{Sources or}\\ \text{sinks of mass}\\ \text{and energy}\end{pmatrix} \qquad \text{(Eq. 2-21)}$$

The first term of the equation (Eq. 2-21) is named the storage term. With respect to the second term, the physical interpretation of the divergence ($\nabla\cdot$) of a flux can be considered as the excess of outflow over inflow of a considered quantity, per unit volume, per unit time (Figure 2-33).

Assigning entities into the equation (Eq. 2-21), the balance of a property π (per unit mass) can be expressed by:

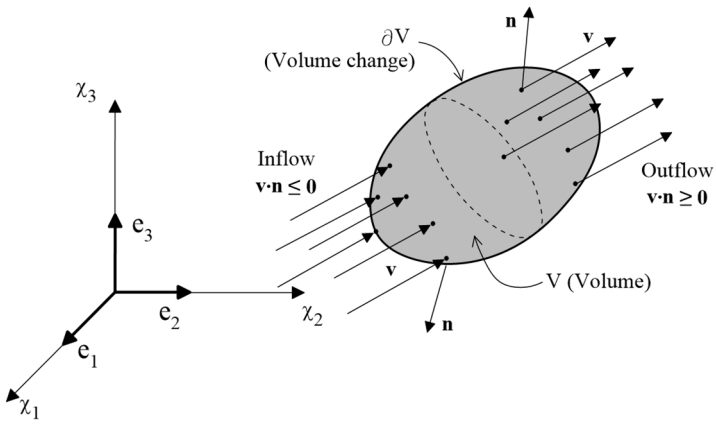

Figure 2-33. Net outflow through a closed control surface (modified from Oliver and Agelet De Saracibar, 2016).

$$\frac{\partial}{\partial t}(\rho\pi) + (j_\pi) = f^\pi \qquad \text{(Eq. 2-22)}$$

where:

- ρ is the mass of the species per unit volume containing π;
- j_π is the total flux of π with respect to a fixed reference system;
- f^π is the rate of production/removal of π per unit volume.

Considering the solid phase of the porous media as the reference system of the flux j_π, some corrections may be required if this phase moves significantly. The total flux can be decomposed into two components: and advective one (phase motion) and non-advective one (motion of the species inside the phases). That is,

$$j_\pi = \rho\pi \boldsymbol{v} + i_\pi \qquad \text{(Eq. 2-23)}$$

where:

- $\boldsymbol{v}$ is the mass weighted mean velocity.
- i_π is the non-advective flux.

Using the above decomposition, the equation (Eq. 2-22) coincides with the general equation given by Hassanizadeh and Gray, (1980).

Taking into account that the dependence of the storage term on porosity variations will be important and it does not appear explicitly, the general conservation equation for scalar quantities (i.e. the components of the porous media) can be rewritten in other useful forms. Until now, the balance equation has been expressed since a spatial or *eulerian* point of view where the focus is on a point in space and the property is described as a function of the point in space and time. On the contrary, in the material or *lagrangian* description, a given property is described by a certain function where the argument represents the material coordinates. The Figure 2-34 illustrates both description.

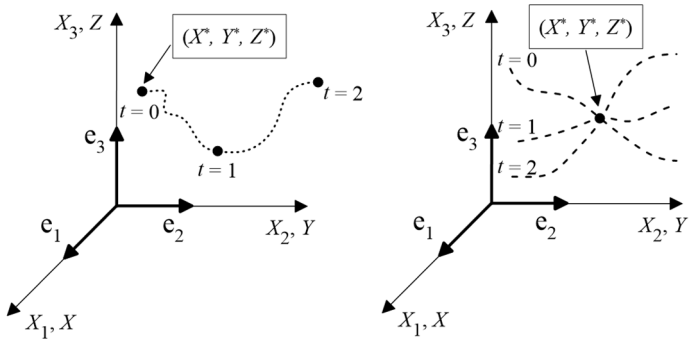

Figure 2-34. Description of a property—Material or *lagrangian* description(left) and spatial or *eulerian* description (from Oliver and Agelet De Saracibar, 2016).

Therefore, we can use a differential operator called the *material derivative* (D/Dt). It gives the rate of change of any quantity as seen by an observer moving with the porous media. Actually, it is useful for

turning the solid mass balance equation into a porosity changes and introduce it in the overall hydro-mechanical (HM) formulation (Gens, 2010).

The main tools to handle the conversion of the eulerian description of the balance equation into its lagrangian description are the mathematical definition of the material derivative (Eq. 2-24) and product property of the divergence operator (Eq. 2-25). The particular algebraic development on each case (mass of solid, water and air) will be shown in the next sections.

$$\frac{D(\bullet)}{Dt} = \frac{\partial(\bullet)}{\partial t} + \frac{d\mathbf{u}}{dt}\cdot\nabla(\bullet) \qquad \text{(Eq. 2-24)}$$

$$\nabla\cdot(f\mathbf{v}) = \nabla f\cdot\mathbf{v} + f\nabla\cdot\mathbf{v} \qquad \text{(Eq. 2-25)}$$

A detailed description of the variable notation (Table 2-4) is necessary to the right comprehension of the mathematical statement of the governing equations and the hydro-mechanical (HM) formulation. The solution requires specifying an equal number of unknown variables and equations. Thus, the state variables are as follows: solid velocity, $\dot{\mathbf{u}}$ (in three spatial directions) and the liquid and gas pressure in both structural levels, P_{L_Macro}, P_{L_micro}, P_{g_Macro} and P_{g_micro}.

The following equations present a considerable extension; therefore, it is convenient to use a compact system of variable names. From now, we refer the micro-structural level with the subscript 1, the Macro-structural level with the subscript 2 and the double-structural porous media without subscript.

Table 2-4. Equation and variable summary (modified from Olivella, 1995)

General	
$(\bullet)_\alpha$	Subscript used to identify the structural level (1=micro, 2= macro) and/or phases (s=solid, L=liquid, g=gas)
$(\bullet)^{\mathbf{i}}$	Superscript used to identify the components (s=solid, w=water, a=air)
$\bar{\phi}$	Volume fraction
ϕ	Porosity
$\rho, \tilde{\rho}$	Local and global density
$\omega, \omega_\alpha^{\mathbf{i}}$	Mass fraction and mass fraction of the

	component i in phase α
θ_α^i	Mass fraction of the component i in phase α per unit of volume of phase α
S	Saturation degree
$\mathbf{j}, \mathbf{j}_\alpha^i$	Mass flux respect to the solid skeleton and mass flux respect to the solid skeleton of the component i in phase α per unit of volume of phase α
Balance equations unknowns	
Solid mass balance	$\bar{\phi}$ — Volume fraction
Water mass balance for macro-structure	P_{L2} — Liquid pressure at Macro-structural level
Water mass balance for micro-structure	P_{L1} — Liquid pressure at micro-structural level
Air mass balance for macro-structure	P_{g2} — Gas pressure at Macro-structural level
Air mass balance for micro-structure	P_{g1} — Gas pressure at micro-structural level
Momentum balance	$\dot{\mathbf{u}} = d\mathbf{u}/dt$ — Solid Velocity

Prior of the governing equations formulation, it is necessary to define the mass of the components for the all phases (Figure 2-35) and for double-structure porous medium itself (Figure 2-36). Considering an unsaturated micro-structure level, we have to include the mass of air and water at this level in the hydro-mechanical analysis.

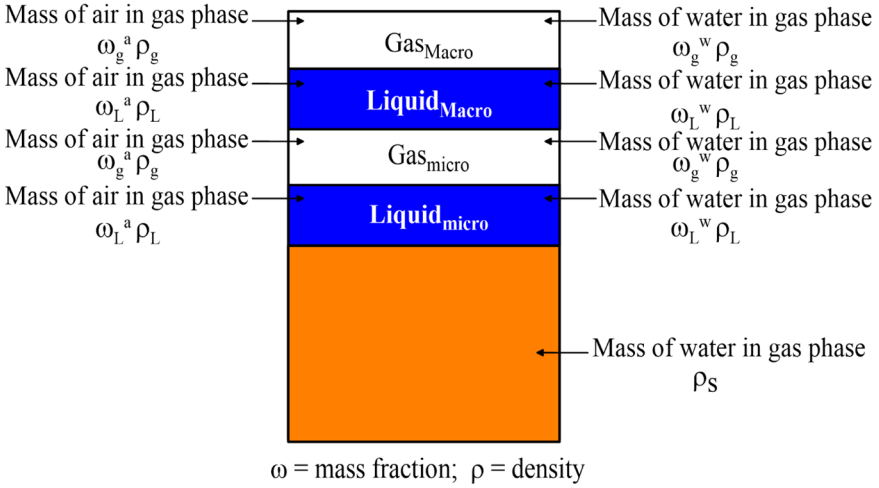

Figure 2-35. Phase diagram of an unsaturated double-structure soil—Mass in phases.

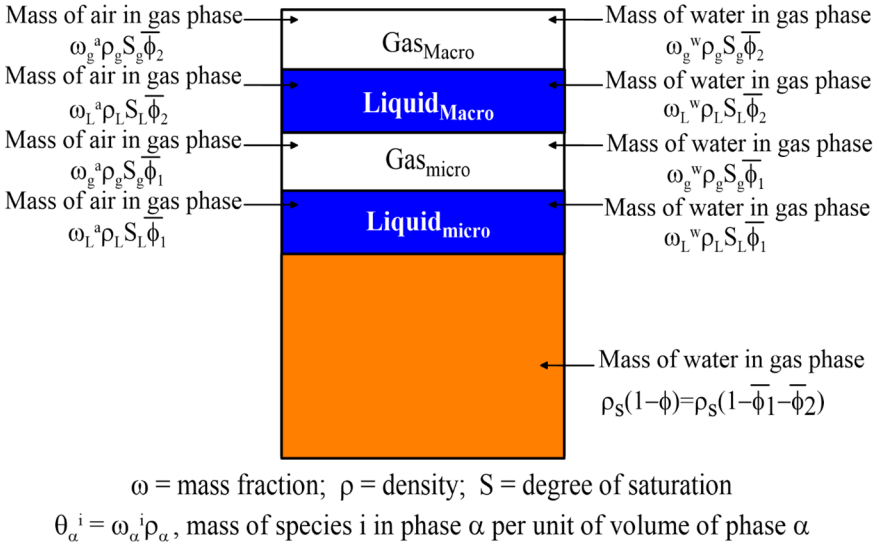

Figure 2-36. Phase diagram of an unsaturated double-structure soil—Mass in porous medium.

2.5.1.1. Solid mass balance equation

Expansive clays have been clearly observed to be double-structure porous media and the balance equations must reflect this fact. However, the definition of the solid mass balance in a single-structure porous medium can be of interest in order to highlight the components of porosity changes and the structural levels interaction in the subsequent mass balance analysis for double-structure porous media.

Single-structure porous media:

The particle arrangement of a single-structure porous media is shown in the Figure 2-37. The solid density ρ_s is associated to the mineral particles and the pore space ϕ is used to determine the solid volume fraction of the medium (Eq. 2-26). It can be noted that this expression is also valid for a double-structure media.

$$\bar{\phi}_{Solid} = \frac{V - V_{Pores}}{V} = \frac{V_{Solid}}{V} = (1 - \phi) \qquad \text{(Eq. 2-26)}$$

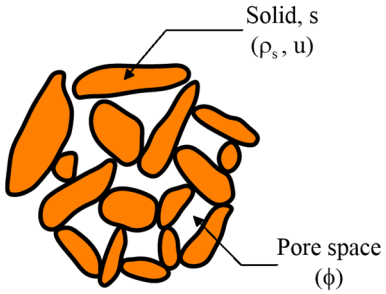

Figure 2-37. Solid particles of a single-structure soil.

Using the equations (Eq. 2-21) and (Eq. 2-22), Olivella et al., (1994) expressed the balance of the mineral (solid phase) as follow:

$$\frac{\partial}{\partial t}\left(\rho_s(1-\phi)\right) + \nabla\cdot(\mathbf{j}_s) = 0 \qquad \text{(Eq. 2-27)}$$

where:

- ρ_s is the mass of solid per unit volume of solid;
- $\mathbf{j}_s$ is the flux of solid.

The mathematical development of the above equation requires transforming the solid balance into porosity changes of the medium.

$$\frac{\partial}{\partial t}\left(\rho_s(1-\phi)\right) + \nabla\cdot\left(\rho_s(1-\phi)\frac{d\mathbf{u}}{dt}\right) = 0 \qquad \text{(Eq. 2-28)}$$

$$(1-\phi)\frac{\partial\rho_s}{\partial t} - \rho_s\frac{\partial\phi}{\partial t} + (1-\phi)\frac{d\mathbf{u}}{dt}\cdot\nabla\rho_s + (1-\phi)\rho_s\nabla\frac{d\mathbf{u}}{dt} - \rho_s\frac{d\mathbf{u}}{dt}\cdot\nabla\phi = 0 \qquad \text{(Eq. 2-29)}$$

Finally, using the time derivative definition (Eq. 2-24) and the product property of the divergence operator (Eq. 2-25), it is possible express the porosity changes according to:

$$\frac{D\phi}{Dt} = \frac{(1-\phi)}{\rho_s}\frac{D\rho_s}{Dt} + (1-\phi)\nabla\cdot\frac{d\mathbf{u}}{dt} \qquad \text{(Eq. 2-30)}$$

where the volumetric strain rate is:

$$\nabla\cdot\frac{d\mathbf{u}}{dt} = \frac{d\varepsilon_x}{dt} + \frac{d\varepsilon_y}{dt} + \frac{d\varepsilon_z}{dt} = \frac{d\varepsilon_v}{dt} \qquad \text{(Eq. 2-31)}$$

The right hand part of the equation (Eq. 2-30) is split into two terms. The first gives the porosity change associated to the solid density

variation (Figure 2-38) and the second one is the porosity change due to the volumetric strain of the porous medium (Figure 2-39). Actually, this equation is comparable with the expression (Eq. 2-20) which defines the incremental change of total porosity for a double-structure medium.

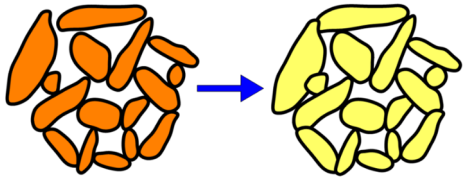

Figure 2-38. Porosity changes due to solid density variation in a single-structure soil.

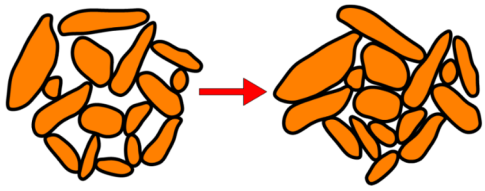

Figure 2-39. Porosity changes due to volumetric strain in a single-structure soil.

In a single-structure porous medium, the concept of volumetric strain can be easily understood. According to Figure 2-39, this concept is the change of the solid particle arrangement. If we come back to the given definition for a double-structure porous medium, probably its volumetric strain is not an intuitive idea. Thereby, it is interesting to examine the formulation of the solid mass balance for a medium composed by aggregates of clay particles in order to explore the role of structural levels on the volumetric deformation.

Double-structure porous media:

The solid volume fraction for a double-structure porous media was defined previously (Eq. 2-5) and it is practically the same as the definition for a single-structure porous media (Eq. 2-26). The only difference is that the volume of pores (V_{Pores}) is the sum of macro- and micro-pores. Now, the balance of the clay minerals (solid phase) is stated in the following way:

$$\frac{\partial}{\partial t}\left(\rho_s(1-\bar{\phi}_1-\bar{\phi}_2)\right)+\nabla\cdot\left(\rho_s(1-\bar{\phi}_1-\bar{\phi}_2)\frac{d\mathbf{u}}{dt}\right)=0 \qquad \text{(Eq. 2-32)}$$

where:

- **u** is the field displacement of the particle (clay minerals) in a double-structure porous medium (Figure 2-40).

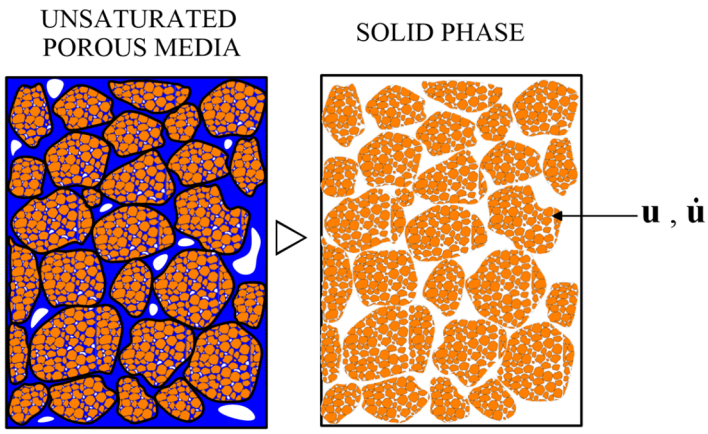

Figure 2-40. Displacement of the solid phase in a double-structure soil.

Following the same mathematical treatment of the single-structure porous media, there is a certain relation between the change of macro and micro pore volume fractions ($\bar{\phi}_2$ and $\bar{\phi}_1$) (Eq. 2-33). It is convenient to consider a different approach of the displacements (and rate of displacements) of the medium components.

$$\frac{D\bar{\phi}_2}{Dt} = \frac{(1-\bar{\phi}_1-\bar{\phi}_2)}{\rho_s}\frac{D\rho_s}{Dt} + (1-\bar{\phi}_1-\bar{\phi}_2)\nabla\cdot\frac{d\mathbf{u}}{dt} - \frac{D\bar{\phi}_1}{Dt} \qquad \text{(Eq. 2-33)}$$

Based on the approach proposed by Alonso and Vaunat, (2001), we can consider different velocities for the solid phase (clay particles) and the aggregates (Figure 2-41). It means the existence of a relative velocity between them. This theoretical idea comes from the sources of volumetric deformations in a double-structure porous medium: displacements and deformations of the clay aggregates (Figure 2-42).

An adequate description of a double-structure medium requires considering two distinct *Representative Elementary Volumes* (REV). Properties associated with micro-structure level (clay particles and micro-pores) are averaged over a microscopic REV (noted REV_1), while properties associated with Macro-structural level (clay aggregates and

macro-pores) are averaged over the macroscopic REV (REV_2). In agreement with the double-structure soil description, the REV_1 is embedded inside REV_2 (Figure 2-41).

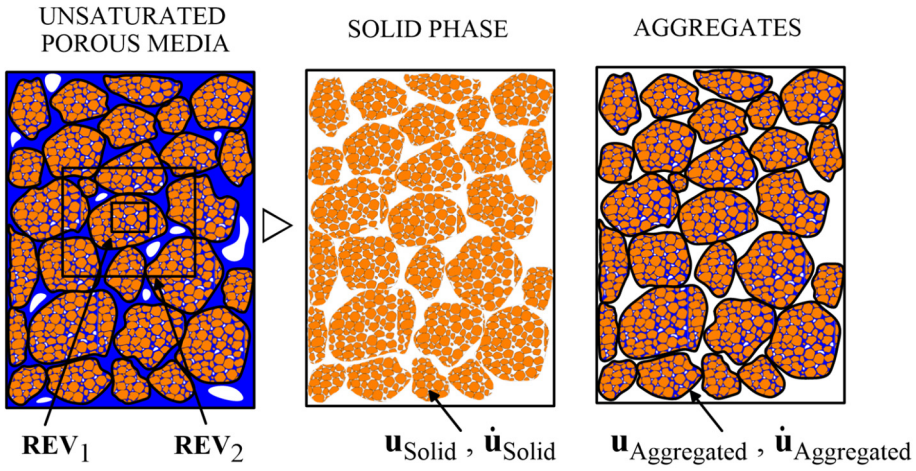

Figure 2-41. Displacement of the solid phase and the clay aggregates in a double-structure soil.

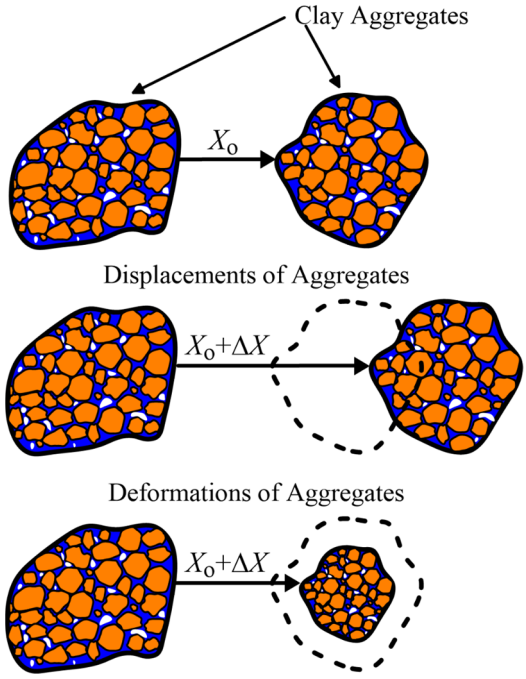

Figure 2-42. Sources of volumetric deformation in a double-structure porous medium.

The porosity at REV1 coincides with the micro-porosity (ϕ_1) defined previously (Eq. 2-8). Likewise, the pore space in the REV2 is characterized by the Macro pore volume fraction ($\bar{\phi}_2$) (Eq. 2-4). At each point of the equivalent macroscopic medium, the mass of solid per unit volume of a double-structure medium is given by the product of the density of the solid particles and the solid volume fraction (Eq. 2-5):

$$\rho_s(1-\phi_1)(1-\bar{\phi}_2) = \rho_s\bar{\phi}_{\text{Solid}} \qquad \text{(Eq. 2-34)}$$

Mass balance of solid over REV2 is then expressed by:

$$\frac{D_2}{Dt}\left[\rho_s(1-\bar{\phi}_2)(1-\phi_1)\right] + \rho_s(1-\bar{\phi}_2)(1-\phi_1)\nabla\cdot\frac{d\mathbf{u}_2}{dt} = 0 \qquad \text{(Eq. 2-35)}$$

where:

- $\mathbf{u}_2$ is the field displacement of the clay aggregates ($\mathbf{u}_{\text{Aggregate}}$) in a double-structure porous medium (Figure 2-41).

(Eq. 2-35 leads to the following expression for the volumetric strain rate at macroscopic scale:

$$\frac{d\varepsilon_{v2}}{dt} = \nabla\cdot\frac{d\mathbf{u}_2}{dt} = \frac{1}{1-\bar{\phi}_2}\frac{D_2\bar{\phi}_2}{Dt} + \frac{1}{1-\phi_1}\frac{D_2\phi_1}{Dt} \qquad \text{(Eq. 2-36)}$$

The first term of the right hand part represents the difference between macro-structural and micro-structural volume change. Vardoulakis and Sulem, (1995) call it relative volumetric strain rate.

$$\frac{d\varepsilon_v^{1\to2}}{dt} = \frac{1}{1-\bar{\phi}_2}\frac{D_2\bar{\phi}_2}{Dt} \qquad \text{(Eq. 2-37)}$$

On the other hand, the mass balance of solid over REV1 is expressed by the equation:

$$\frac{D_1}{Dt}\left[\rho_s(1-\phi_1)\right] + \rho_s(1-\phi_1)\nabla\cdot\frac{d\mathbf{u}_1}{dt} = 0 \qquad \text{(Eq. 2-38)}$$

where:

- $\mathbf{u}_1$ is the field displacement of the solid particles ($\mathbf{u}_{\text{Solid}}$) in a double-structure porous medium (Figure 2-41).

Applying the assumption that $(d\mathbf{u}_1/dt)\cdot\nabla\cdot(\phi_1)$ is constant, which means that there are not micro-porosity gradients inside the clay aggregates; it is then possible to define a volumetric micro-structural strain, expressing the change in REV_1 whose rate reads:

$$\frac{d\varepsilon_{v1}}{dt} = \nabla\cdot\frac{d\mathbf{u}_1}{dt} = \frac{1}{1-\phi_1}\frac{\partial\phi_1}{\partial t} \qquad \text{(Eq. 2-39)}$$

Since REV_1 is embedded inside REV_2, a change in volume REV_1 induce change in volume of REV_2. The substitution of (Eq. 2-39) into (Eq. 2-36) provides a relationship for this interaction:

$$\frac{d\varepsilon_{v2}}{dt} = \frac{d\varepsilon_v^{1\to2}}{dt} + \frac{d\varepsilon_{v1}}{dt}\frac{1}{1-\phi_1}\left(\frac{D_2\phi_1}{Dt} - \frac{\partial\phi_1}{\partial t}\right) \qquad \text{(Eq. 2-40)}$$

The last term of (Eq. 2-40) can be rewritten by using the expression of material derivative D_2/Dt :

$$\frac{1}{1-\phi_1}\left(\frac{D_2\phi_1}{Dt} - \frac{\partial\phi_1}{\partial t}\right) = \frac{d\mathbf{u}_2}{dt}\frac{\nabla\phi_1}{1-\phi_1} = \frac{d\mathbf{u}_2}{dt}\cdot\nabla\frac{d\varepsilon_{v1}}{dt} \qquad \text{(Eq. 2-41)}$$

Finally, the volumetric strain rate at macro-structure can be decomposed as:

$$\frac{d\varepsilon_{v2}}{dt} = \frac{d\varepsilon_v^{1\to2}}{dt} + \frac{d\mathbf{u}_2}{dt}\cdot\nabla\frac{d\varepsilon_{v1}}{dt} = \frac{d\varepsilon_v^{1\to2}}{dt} + \frac{D_2\varepsilon_{v1}}{Dt} \qquad \text{(Eq. 2-42)}$$

When the displacements are small, the material derivative is close to time derivative. (Eq. 2-42) reduces to:

$$\frac{d\varepsilon_{v2}}{dt} = \frac{d\varepsilon_v^{1\to2}}{dt} + \frac{d\varepsilon_{v1}}{dt} \qquad \text{(Eq. 2-43)}$$

The last expression is a clear theoretical explanation of the mechanical interaction of the structural levels in a double-structure porous media. This is in agreement with the experimental data reported above and with the constitutive expansive framework (Gens and Alonso, 1992; Alonso et al., 1999; Sánchez et al., 2005; Gens et al., 2011; Guimaraes et al., 2013).

This analysis can be extended for media with more than two structural levels; for example, three levels—micro, meso and macro (see Alonso and

Vaunat, 2001). They can represent fissured expansive clays. However, the mathematical statement of these interactions may be extremely complex. This work is only concentrated on the mechanical interaction of two structural levels.

2.5.1.2. Water mass balance equation for macro-structure

Similar to the solid mass, the mass balance for water can be established following the general approach for governing equations outlined previously. The Figure 2-43 is a useful scheme to determine the water mass balance over a double-structure porous medium. The change in the amount of water inside the REV must be equal to the net inflow/outflow of water (accounting also for sink or source term that may exist). The net inflow/outflow is of course equivalent to the divergence of the total flow (Figure 2-33). Because unsaturated medium is being considered (at micro- and Macro-structural level), it is necessary to account for the water in liquid and gas form, both in the storage term and in the flux term.

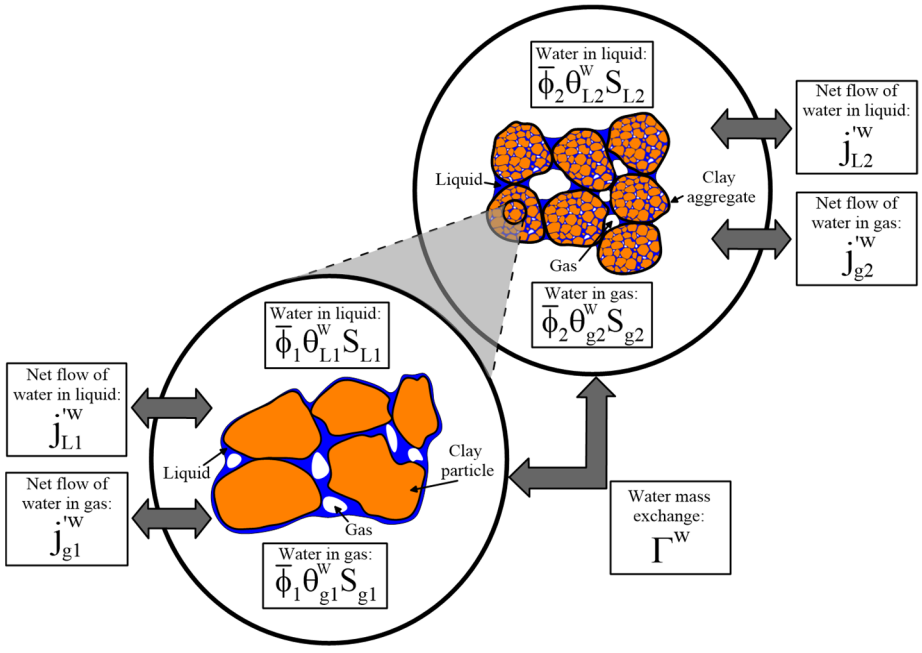

Figure 2-43. Scheme to establish the equation for the mass balance of water in a double-structure material (modified from Gens, 2010).

Based in the Figure 2-36 and Figure 2-43, the mass balance of water for the Macro-structural level reads:

$$\frac{\partial}{\partial t}((\theta^{w}_{L2}S_{L2}+\theta^{w}_{g2}S_{g2})\bar{\phi}_{2})+\nabla\cdot(\mathbf{j}^{w}_{L2}+\mathbf{j}^{w}_{g2})=-\Gamma^{w} \qquad \text{(Eq. 2-44)}$$

where:

- Γ^{w} is the term the term related to the water mass exchange between the two structural levels.

The water flux Γ^{w}can go from micro- to macro-structure or vice versa. In wetting paths, the water hydrates the macro-structure and later goes to the hydration of the micro-structure. Conversely, the drying paths in expansive clays generate a flux of water in the opposite way. The time-dependent mechanisms that controls this water exchange will be explained in Chapter 3.

In this particular case, we develop the above equation in order to obtain the material description of the macro-structural water balance. For the following balances, only the material description will be shown, because the procedure is practically the same.

Developing time time derivative of equation (Eq. 2-44) and applying again the material derivative definition (Eq. 2-24) and the divergence operator property (Eq. 2-25), we find:

$$\frac{D(\theta^{w}_{L2}S_{L2}+\theta^{w}_{g2}S_{g2})}{Dt}\bar{\phi}_{2}+(\theta^{w}_{L2}S_{L2}+\theta^{w}_{g2}S_{g2})\left(\frac{d\bar{\varepsilon}_{v2}}{dt}\right) \qquad \text{(Eq. 2-45)}$$
$$+\nabla\cdot(\mathbf{j}^{w}_{L2}+\mathbf{j}^{w}_{g2})=-\Gamma^{w}$$

where:

- $\bar{\varepsilon}_{v2}$ is the volumetric deformation of the macro-structural level respect to the total volume of the porous medium. This term imposes a hydro-mechanical coupling.

The hydraulic constitutive laws for the volumetric advective fluxes $\mathbf{j}^{w}_{L2}, \mathbf{j}^{w}_{g2}$ are described in the Section 2.5.2.1.

2.5.1.3. Water mass balance equation for micro-structure

Coussy, (2004) gives the following expression for the mass conservation in the water exchange in a double porosity network:

$$\Gamma^{w}_{1\to2}=-\Gamma^{w}_{2\to1} \qquad \text{(Eq. 2-46)}$$

Following the same mathematical procedure, the eulerian and lagrangian descriptions of the water species at micro-structural level are:

$$\frac{\partial}{\partial t}((\theta^{w}_{L1}S_{L1}+\theta^{w}_{g1}S_{g1})\bar{\phi}_1)+\nabla\cdot(\mathbf{j}^{w}_{L1}+\mathbf{j}^{w}_{g1})=-\Gamma^{w} \qquad \text{(Eq. 2-47)}$$

$$\begin{aligned}\frac{D(\theta^{w}_{L1}S_{L1}+\theta^{w}_{g1}S_{g1})}{Dt}\bar{\phi}_1+(\theta^{w}_{L1}S_{L1}+\theta^{w}_{g1}S_{g1})\left(\frac{d\bar{\varepsilon}_{v1}}{dt}\right)\\ +\nabla\cdot(\mathbf{j}^{w}_{L1}+\mathbf{j}^{w}_{g1})\\ =\Gamma^{w}-(\theta^{w}_{L1}S_{L1}+\theta^{w}_{g1}S_{g1})(1-\phi)\frac{d\rho_s}{\rho_s}\end{aligned} \qquad \text{(Eq. 2-48)}$$

where:

- $\bar{\varepsilon}_{v1}$ is the volumetric deformation of the micro-structural level respect to the total volume of the porous medium.

From the physical features of the expansive clays, the water at micro-structural level has a low mobility. Therefore, the water fluxes inside the micro-structural level (micro to micro) can be treated in two different ways:

- The choice of a lower power for the law of relative permeability (see Section 2.5.2.1.) for the micro-structure. Consequently, the volumetric advective fluxes $\mathbf{j}^{w}_{L1}, \mathbf{j}^{w}_{g1}$ are not disregarded and they are used to solve the coupled hydro-mechanical problem. Here, the water mass balance at micro-structural level plays the same role that the water balance at macro-structure.

- Alternatively, the low mobility of the water at clay aggregates is accounted for in the balance equations themselves ($\mathbf{j}^{w}_{L1}+\mathbf{j}^{w}_{g1}=0$). This simplification allows us to treat the water pressure at micro-structure as a history variable to be integrated at gauss point level during the constitutive integration. This approach is used in this hydro-mechanical (HM) formulation.

Finally, the water mass balance at this level is reduced to:

$$\begin{aligned}\frac{D(\theta^{w}_{L1}S_{L1}+\theta^{w}_{g1}S_{g1})}{Dt}\bar{\phi}_1+(\theta^{w}_{L1}S_{L1}+\theta^{w}_{g1}S_{g1})\left(\frac{d\bar{\varepsilon}_{v1}}{dt}\right)\\ =\Gamma^{w}-(\theta^{w}_{L1}S_{L1}+\theta^{w}_{g1}S_{g1})(1-\phi)\frac{d\rho_s}{\rho_s}\end{aligned} \qquad \text{(Eq. 2-49)}$$

2.5.1.4. Air mass balance equation for macro-structure

By proceeding in the same way as the balance of water species in the macro-structure, we find:

$$\frac{D\left(\theta^{a}_{L2}S_{L2}+\theta^{a}_{g2}S_{g2}\right)}{Dt}\bar{\phi}_{2}+\left(\theta^{a}_{L2}S_{L2}+\theta^{a}_{g2}S_{g2}\right)\left(\frac{d\bar{\varepsilon}_{v2}}{dt}\right)+\nabla\cdot\left(\mathbf{j}^{a}_{L2}+\mathbf{j}^{a}_{g2}\right)=-\Gamma^{a} \quad \text{(Eq. 2-50)}$$

2.5.1.5. Air mass balance equation for micro-structure

Neglecting the influence of the micro to micro flux of air ($\mathbf{j}^{a}_{L2}+\mathbf{j}^{a}_{g2}=0$), the balance at this structural level is:

$$\frac{D\left(\theta^{a}_{L1}S_{L1}+\theta^{a}_{g1}S_{g1}\right)}{Dt}\bar{\phi}_{1}-\left(\theta^{a}_{L1}S_{L1}+\theta^{a}_{g1}S_{g1}\right)\left(\frac{d\bar{\varepsilon}_{v1}}{dt}\right)=\Gamma^{a}-\left(\theta^{a}_{L1}S_{L1}+\theta^{a}_{g1}S_{g1}\right)(1-\phi)\frac{d\rho_{s}}{\rho_{s}} \quad \text{(Eq. 2-51)}$$

2.5.1.6. Momentum balance equation

The equation of equilibrium stresses of the double-structure porous media is given by Cauchy's expression.

$$\nabla.\boldsymbol{\sigma}+\mathbf{b}=0 \quad \text{(Eq. 2-52)}$$

where the body forces are given by the gravity and the global density of the medium:

$$\mathbf{b}=\tilde{\rho}\mathbf{g} \quad \text{(Eq. 2-53)}$$

$$\tilde{\rho}=\rho_{s}(1-\phi)+\left(\rho_{L1}S_{L1}+\rho_{g1}S_{g1}\right)\bar{\phi}_{1}+\left(\rho_{L2}S_{L2}+\rho_{g2}S_{g2}\right)\bar{\phi}_{2} \quad \text{(Eq. 2-54)}$$

Equations (Eq. 2-35), (Eq. 2-45), (Eq. 2-49), (Eq. 2-50), (Eq. 2-51) and (Eq. 2-52) are the set of fundamental balance equations that must be satisfied simultaneously at every instant of time and at every point of the domain.

2.5.2. Constitutive equations

Sánchez, (2004) established the role of the constitutive equations in the following manner: they establish the link between the unknowns and the dependent variables. There are several categories of dependent variables depending on the complexity with which they are related to the

unknowns. Here, some of the basic constitutive laws are presented, divided in hydraulic and mechanical. In spite of this distinction between the two basic components of the problem, the constitutive equation provides in fact the links that couple the various phenomena considered in the formulation (Gens and Olivella, 2001). The governing equations are finally written in terms of the unknowns when the constitutive equations are substituted in the balance equations.

2.5.2.1. Hydraulic constitutive equations

The volumetric advective fluxes, used in the balance equations, are defined by the product of the mass fraction of the component and the mass flow with respect to the solid phase.

$$\mathbf{j}_{\alpha}^{i} = \theta_{\alpha}^{i}\mathbf{q}_{\alpha} \qquad \text{(Eq. 2-55)}$$

where:

- i indicates the component (w=water and a=air).
- α refers to the phase (L=liquid and g=gas).

The generalized Darcy's law governs liquid and gas flow (Bear, 1972). This is only formulated for macro-structural level, due to the neglected advective fluxes in the micro-structure ($\mathbf{j}_{L1}^{w} + \mathbf{j}_{g1}^{w} = 0$).

$$\mathbf{q}_{\alpha 2} = -\frac{\mathbf{k}_2 k_{r_{\alpha 2}}}{\mu_{\alpha}} (\nabla P_{\alpha 2} - \rho_{\alpha 2}\, \mathbf{g}) \qquad \text{(Eq. 2-56)}$$

where:

- $\mathbf{k}_2$ is the intrinsic permeability tensor of the macro-structural level.
- $k_{r_{\alpha 2}}$ is the relative permeability of gas and liquid.
- μ_{α} is the fluid viscosity which is function of temperature.
- $P_{\alpha 2}$ is the gas or liquid pressure at macro-structure.
- $\rho_{\alpha 2}$ is the fluid density.
- $\mathbf{g}$ is the gravity force.

A power law defines the relative permeability, which expresses the effect of degree of saturation (or suction) on global permeability (Eq. 2-57). Intrinsic permeability depends on many factors such as pore size distribution, pore shape, tortuosity and porosity. Here a dependence of

intrinsic permeability on the macro pore volume fraction ($\bar{\phi}_2$) is adopted through two different options ((Eq. 2-58) and (Eq. 2-59).

$$(k_r)_\alpha = [(S_e)_\alpha]^c \quad \text{(Eq. 2-57)}$$

$$\mathbf{k}_2 = \mathbf{k}_{o2} \frac{\bar{\phi}_2^{\,3}}{(1-\bar{\phi}_2)^2} \frac{\left(1-(\bar{\phi}_o)_2\right)^2}{(\bar{\phi}_o)_2^{\,3}} \quad \text{(Eq. 2-58)}$$

$$\mathbf{k}_2 = \mathbf{k}_{o2} \exp\left[b\left(\bar{\phi}_2 - (\bar{\phi}_o)_2\right)\right] \quad \text{(Eq. 2-59)}$$

where:

- c is the power for relative permeability law.
- S_e is the effective saturation degree.
- $\mathbf{k}_{o2}$ is the initial intrinsic permeability tensor.
- b is a fitting parameter.

Finally, the retention curve relates suction (or matric potential) with degree of saturation at both structural levels. Chapter 3 and Appendix A explore the multimodal water retention curves for double structure porous media. A linear superposition of subcurves (Macro and micro) of Van Genuchten type is formulated.

2.5.2.2. Mechanical constitutive equations

The general form of a HM constitutive equation, showing explicitly the contributions of strains and fluid pressures can be expressed as:

$$d\boldsymbol{\sigma}_j = \mathbf{D}_j d\boldsymbol{\varepsilon}_j + \mathbf{h}_j ds_j \quad \text{(Eq. 2-60)}$$

where:

- j indicates the structural level (1=micro and 2=Macro).
- $\boldsymbol{\sigma}_j$ is the constitutive stress (net or effective stress).
- $\boldsymbol{\varepsilon}_j$ is the strain vector.
- s_j is a variable related to the fluid pressure, typically the suction.
- $\mathbf{D}_j$ is the constitutive stiffness matrix.
- $\mathbf{h}_j$ is the generic constitutive vectors relating the changes in fluid pressures.

Note that although the total stress is common for structural levels micro and Macro, the constitutive stress may be different because the fluid pressures may be different. Therefore, the two equations corresponding to

the two levels considered reduce to a single equation (in order to be introduced in the equilibrium of stresses,(Eq. 2-52) as the sum of strains is performed and the equation is solved for the total stress (Sánchez, 2004).

The constitutive formulation that describes the material behaviour and the HM coupling are presented in the Chapter 3.

2.5.2.3. Phase physical properties

The properties of the fluid phases appear in the balance equations and in the constitutive law. In general, they depend on the composition of the phases and on the state variables (temperature and fluid pressure). A complete description of the adopted laws can be found elsewhere (e.g. Olivella, 1995; Gens and Olivella, 2001; DIT-UPC, 2018).

2.5.3. Equilibrium restrictions

According to Olivella et al., 1994, it is assumed that phase changes are rapid in relation to the characteristic times typical of these types of problems. Therefore, they can be considered in local equilibrium, giving rise to a set of equilibrium restrictions that must be satisfied at all times. In addition, the adopted compositional approach has the advantage that the phase change terms do not appear explicitly and the number of equations is thereby reduced. In spite of the minor relevance in the isothermal case, the equilibrium restrictions can be established for the concentration of water vapour in gas phase, which is computed through the psychometric law; and for the concentration of dissolved air in liquid phase, which is evaluated by means of Henry's law (Olivella, 1995).

2.6. Chapter conclusions

The potential expansion of a clay relies on the physicochemical phenomena occurring at mineral structure. Nevertheless, this is not enough to describe the engineering behaviour of the active clays. The hierarchical structure of the material is a key element for the understanding of their behaviour. The double-porosity system appears to be well suited to describe them as an arrangement of clay aggregates; accordingly micro and Macro structural levels are defining, interacting in a particular way.

Strain irreversibility, stress path dependency and homogenization processes are attributed to the effects of the microstructure deformation on the macrostructure. The distinction between micro-structural and macro-structural levels has been useful to explain the development of swelling strain with time. By assuming the water exchange between structural levels, a wide variety of strain-time responses can be reproduced.

A critical reflection on the concepts of volume fractions and macro- and micro-porosities has been presented in order to overcome some imprecise definitions in previous formulations. Afterwards, the governing equations are formulated for the more general case. The consideration of an unsaturated micro-structural level (clay aggregates) implies the proper account of the phases and species in each structural level.

It should be stressed that the mechanical interaction between the structural levels emerges naturally from the solid mas balance equation of the medium. Similarly, the mass water exchange is explicitly considered in the water mass balance equations for the micro- and Macro-structure.

In this Chapter the general structure of the HM formulation has been presented. The following Chapter focus on the constitutive laws. A double structure model for expansive soil will then be presented in detail.

2.7. References

Alonso, E.E., Gens, A., Hight, D.W., 1987. Special problem soils. General report, in: Hanrahan, E.T. et Al ., Editors. Proceedings of the 9th European Conference of Soil Mechanics and Foundation Engineering. Dublin. pp. 1087–1146.

Alonso, E.E., Gens, A., Josa, A., 1990. A constitutive model for partially saturated soils. Géotechnique 40, 405–430.

Alonso, E.E., Romero, E., Hoffmann, C., García-Escudero, E., 2005. Expansive bentonite-sand mixtures in cyclic controlled-suction drying and wetting. Eng. Geol. 81, 213–226.

Alonso, E.E., Vaunat, J., 2001. An appraisal of structure level interactions in expansive soils, in: M.M. Fernandes, L. Ribeiro e Sousa, R.F. Azevedo, and E.A.V. (Ed.), 3rd Int. Workshop on Applications of Computational Mechanics in Geotechnical Engineering. Oporto, Portugal. pp. 17–30.

Alonso, E.E., Vaunat, J., Gens, A., 1999. Modelling the mechanical behaviour of expansive clays. Eng. Geol. 54, 173–183.

ANDRA, 2015. Expérimentat¡on NSC. Bilan des mesures et suivi de la phase d'hydratation. Report D.RP.AMFS.r5.0017. Châtenay-Malabry: ANDRA.

ANDRA, 2011. Evaluation du comportement THM des scellements du stockage CIGEO: ouvrages de liaison jour-fond, galeries et alvéoles MAVL. Report CCCAEAP110093. Châtenay-Malabry: ANDRA.

Bear, J., 1972. Dynamics of fluids in porous media. New York: Dover Publications, Inc.

Biot, M.A., 1940. General theory of three-dimensional consolidation. J. Appl. Phys. 12, 155–164.

Börgesson, L., Sandén, T., Dueck, A., Andersson, L., Jensen, V., Nilsson, U., Olsson, S., Åkesson, M., Kristensson, O., Svensson, U., 2014. Consequences of water inflow and early water uptake in deposition holes. Technical Report TR-14-22. SKB.

Borja, R.I., 2006. On the mechanical energy and effective stress in saturated and unsaturated porous continua. Int. J. Solids Struct. 43, 1764–1786.

Borja, R.I., Choo, J., 2016. Cam-Clay plasticity, Part VIII: A constitutive framework for porous materials with evolving internal structure. Comput. Methods Appl. Mech. Eng. 309, 653–679.

Borja, R.I., Koliji, A., 2009. On the effective stress in unsaturated porous continua with double porosity. J. Mech. Phys. Solids 57, 1182–1193.

Brackley, I.J., 1975. Swell under load., in: Proc. 6th Reg. Conf. for Africa on SMFE. DURBAN. pp. 65–70.

Brackley, I.J., 1973. Swell pressure and free swell in compacted clay., in: 3rd International Conference on Expansive Soils, Haifa. pp. 169–179.

Buzzi, O., Giacomini, A., Fityus, S., 2011. Towards a dimensionless description of soil swelling behaviour. Géotechnique 61, 271–277. https://doi.org/10.1680/geot.7.00194

Chen, F.H., 1988. Foundations on Expansive Soils. Amsterdam: Elsevier.

Collins, K., McGownn, A., 1974. The form and function of microfabric features. Géotechnique 24, 223–254.

Coussy, O., 2004. Poromechanics. West Sussex:John Wiley & Sons Ltd.

Cui, Y.-J., 2017. On the hydro-mechanical behaviour of MX80 bentonite-based materials. J. Rock Mech. Geotech. Eng. 9, 565–574.

de Boer, R., 2005. Trends in continuum mechanics of porous media. Netherlands: Springer.

de Boer, R., Ehlers, W., Kowalski, S., Plischka, J., 1991. Porous media, a survey of different approaches. Forschungsbericht aus dem Fachbereich Bauwesen. Univ. Ess. 54.

Delage, P., Marcial, D., Cui, Y.J., Ruiz, X., 2006. Ageing effects in a compacted bentonite: a microstructure approach. Géotechnique 56, 291–304.

DIT-UPC, 2018. CODE_BRIGHT, a 3-D program for Thermo-Hydro-Mechanical analysis in geological media: User's guide, CIMNE, Barcelona.

Fityus, S.G., Buzzi, O., 2009. The place of expansive clays in the framework of unsaturated soil mechanics. Appl. Clay Sci. 43, 150–155.

Fityus, S.G., Smith, D.W., 2004. The development of a residual soil profile from a mudstone in a temperate climate. Eng. Geol. 74, 39–56.

Gens, A., 2010. Soil–environment interactions in geotechnical engineering. Géotechnique 60, 3–74.

Gens, A., Alonso, E.E., 1992. A framework for the behaviour of unsaturated expansive clays. Can. Geotech. J. 29, 1013–1032.

Gens, A., Olivella, S., 2001. THM phenomena in saturated and unsaturated porous media. Rev. Française Génie Civ. 5, 693–717.

Gens, A., Valleján, B., Sánchez, M., Imbert, C., Villar, M.V., Van Geet, M., 2011. Hydromechanical behaviour of a heterogeneous compacted soil: experimental observations and modelling. Géotechnique 61, 367–386.

Guimaraes, L.D.N., Gens, A., Sanchez, M., Olivella, S., 2013. A chemo-mechanical constitutive model accounting for cation exchange in expansive clays. Geotechnique 63, 221–234.

Hassanizadeh, S., Gray, W.G., 1980. General conservation equations for multiphase systems. 3: Constitutive theory for porous media. Adv. Water Resour. 3, 25–40.

Hassanizadeh, S., Gray, W.G., 1979. General conservation equations for multiphase systems. 2: Mass, momenta, energy and entropy

equations. Adv. Water Resour. 2, 191–203.
Hoffmann, C., Alonso, E.E., Romero, E., 2007. Hydro-mechanical behaviour of bentonite pellet mixtures. Phys. Chem. Earth 32, 832–849.
Karnland, O., Nilsson, U., Weber, H.-P., Wersin, P., 2008. Sealing ability of Wyoming bentonite pellets foreseen as buffer material - Laboratory results. Phys. Chem. Earth 33, 472–475.
Kröhn, K., 2019. Re-saturation of compacted bentonite under repository-relevant flow conditions. Geomech. Energy Environ. 17, 115–122.
Lambe, T.W., Whitman, R.V., 1969. Soil mechanics. John Wiley & Sons.
Lewis, R.W., Schrefler, B.A., 1998. The finite element method in the static and dymanic deformation and consolidation of porous media. John Wiley and Sons, Ltd.
Lloret, A., Villar, M. V., Sánchez, M., Gens, A., Pintado, X., Alonso, E.E., 2003. Mechanical behaviour of heavily compacted bentonite under high suction changes. Géotechnique 53, 27–40.
Malvern, L.E., 1969. Introduction to the mechanics of a continous medium. Englewood, New Jersey: Prentice-Hall, Inc.
Martin, R.T., 1960. Adsorbed water on clay: a review. Clays Clay Miner. 9, 28–70.
Mayor, J.C., Velasco, M., 2014. Long-term performance of engineered barrier systems PEBS - EB dismantling. DELIVERABLE-N°: D2.1-8. PEBS Project.
Mazurik, A., Komornik, A., 1973. Interaction of superstructure and swelling clay, in: Proc. 3rd Int. Conf. on Expansive Soils. Haifa. pp. 309–317.
Mitchell, J.K., Soga, K., 2005. Fundamentals of Soil Behavior. 3rd ed. Hoboken, NJ: Wiley.
Mokni, N., Barnichon, J.D., Dick, P., Nguyen, T.S., 2016. Effect of technological macro voids on the performance of compacted bentonite/sand seals for deep geological repositories. Int. J. Rock Mech. Min. Sci. 88, 87–97.
Molinero-Guerra, A., Mokni, N., Delage, P., Cui, Y.-J., Tang, A.M., Aimedieu, P., Bernier, F., Bornert, M., 2017. In-depth characterisation of a mixture composed of powder/pellets MX80 bentonite. Appl. Clay Sci. 135, 538–546.
Murad, M., Cushman, J., 2000. Thermomechanical theories for swelling porous media with microstructure. Int. J. Eng. Sci. 38, 517–564.
Musso, G., Romero, E., Della Vecchia, G., 2013. Double-structure effects on the chemo-hydro-mechanical behaviour of a compacted active clay. Géotechnique 63, 206–220.
Navarro, V., Asensio, L., De la Morena, G., Pintado, X., Yustres, A., 2015. Differentiated intra-and inter-aggregate water content models of mx-80 bentonite. Appl. Clay Sci. 118, 325–336.

Navarro, V., Asensio, L., Yustres, Á., De la Morena, G., Pintado, X., 2016. Swelling and mechanical erosion of MX-80 bentonite: Pinhole test simulation. Eng. Geol. 202, 99–113. https://doi.org/10.1016/j.enggeo.2016.01.005

Nowamooz, H., Mrad, M., Abdallah, A., Masrouri, F., 2009. Experimental and numerical studies of the hydromechanical behaviour of a natural unsaturated swelling soil. Can. Geotech. J. 46, 393–410.

Olivella, S., 1995. Non-isothermal multiphase flow of brine and gas through saline media. PhD Thesis, Universitat Politecnica de Catalunya, Spain.

Olivella, S., Carrera, J., Gens, A., Alonso, E.E., 1994. Non-isothermal multiphase flow of brine and gas through saline media. Transp. Porous Media 15, 271–293.

Olivella, S., Gens, A., Carrera, J., Alonso, E.E., 1996. Numerical formulation for a simulator (CODE_BRIGHT) for the coupled analysis of saline media. Eng. Comput. 13, 87–112.

Oliver, X., Agelet De Saracibar, C., 2016. Continuum Mechanics for Engineers. Theory and Problems. Barcelone: Edicions UPC.

Pousada, E., 1984. Deformabilidad de arcillas expansivas bajo succión controlada (in spanish). PhD thesis, Universidad Politécnica de Madrid, Spain.

Romero, E., Simms, P.H., 2008. Microstructure investigation in unsaturated soils: A review with special attention to contribution of mercury intrusion porosimetry and environmental scanning electron microscopy. Geotech. Geol. Eng. 26, 705–727.

Saba, S., Delage, P., Lenoir, N., Cui, Y.-J., Tang, A.M., Barnichon, J.D., 2014. Further insight into the microstructure of compacted bentonite-sand mixture. Eng. Geol. 168, 141–148.

Salimzadeh, S., Khalili, N., 2016. Three-Dimensional Numerical Model for Double-Porosity Media with Two Miscible Fluids Including Geomechanical Response. Int. J. Geomech. 16, 04015065.

Sánchez, M., 2004. Thermo-Hydro-Mechanical coupled analysis in low permeability media. PhD Thesis, Universitat Politecnica de Catalunya, Spain.

Sánchez, M., Gens, A., do Nascimento Guimarães, L., Olivella, S., 2005. A double structure generalized plasticity model for expansive materials. Int. J. Numer. Anal. Methods Geomech. 29, 751–787. https://doi.org/10.1002/nag.434

Santamarina, J.C., Klein, K.A., Palomino, A., Guimaraes, M.S., 2001. Micro-scale aspects of chemical-mechanical coupling: Interparticle forces and fabric, in: Maio, C.D., Hueckel, T., Loret, B. (Eds.), Proc. of the Workshop on Chemo-Mechanical Coupling in Clays: From Nano-Scale to Engineering Applications. Maratea, Italy. pp. 47–64.

Santamarina, J.C., Klein, K.A., Wang, Y.H., Prencke, E., 2002. Specific surface: determination and relevance. Can. Geotech. J. 39, 233–241.

Schrefler, B., 2002. Mechanics and thermodynamics of saturated/unsaturated porous materials and quantitative solutions. Appl. Mech. Rev. 55, 351.

Seed, H.B., Woodward, R.J., Lundgren, R., 1962. Prediction of swelling potential for compacted clays. J. ASCE, Soil Mech. Found. Div 88, 53–88.

Skempton, A.W., 1953. The colloidal "activity" of clays, in: Proc. 3rd Int. Conference on Soil Mechanics and Foundation Engineering. Zurich, Switzerland. pp. 57–61.

Sun, H., Masin, D., Najser, J., Nedela, V., Navratilova, E., 2019. Bentonite microstructure and saturation evolution in wetting-drying cycles evaluated using ESEM, MIP and WRC measurements. Géotechnique 68, 713–726.

Van Geet, M., Bastiaens, W., Volckaert, G., Weetjens, E., Imbert, C., Billaud, P., Touzé, G., Fillipi, M., Plas, F., Villar, M. V., García, M., Mingarro, M., Gens, A., Vallejan, B., 2009. A large-scale in situ demonstration test for repository sealing in an argillaceous host rock. RESEAL project - Phase II. EUR 24161. Luxembourg: European Commission.

Van Geet, M., Volckaert, G., Roels, S., 2005. The use of microfocus X-ray computed tomography in characterising the hydration of a clay pellet/powder mixture. Appl. Clay Sci. 29, 73–87.

Vardoulakis, I., Sulem, J., 1995. Bifurcation analysis in geomechanics. London: Chapman & Hall.

Villar, M.V., Iglesias, R.J., García-Siñeriz, J.L., 2019. State of the in situ Febex test (GTS, Switzerland) after 18 years: a heterogeneous bentonite barrier. Environ. Geotech. Accepted, 1–13.

Villar, M.V., Martin, P., Lloret, A., Romero, E., 2004. Final Report on Thermo-Hydro-Mechanical Laboratory Test. FEBEX II. ENRESA Report: 70-IMA-L-0-97.

Wang, G., Wei, X., 2015. Modeling swelling–shrinkage behavior of compacted expansive soils during wetting–drying cycles. Can. Geotech. J. 52, 783–794.

Wang, Q., Cui, Y.-J., Tang, A.M., Li, X.-L., Ye, W.-M., 2014. Time- and density-dependent microstructure features of compacted bentonite. Soils Found. 54, 657–666.

Chapter 3

Constitutive Modelling and micro-Macro Interactions

'Models are abstractions of the reality and are, therefore, uncertain'.

J.C. Santamarina, (2001)

3.1. Introduction

A constitutive model is a series of mathematical expressions relating stresses and strains (or stress rate and strain rates) that are used to reproduce the material behaviour in an element. Unlike governing equations, these laws do not obey to physical statements.

Because the source of expansive clay behaviour lies in the physicochemical phenomena occurring in the vicinity of the clay particle, there is some merit in trying to incorporate explicitly this micro-structural level in the constitutive model. The proposed formulation contains now two structural levels: a micro-structure where the interactions at particle level occur and a Macro-structure that accounts for the overall fabric arrangement of the material comprising aggregates and macropores. The incorporation of microstructural considerations and its use as a platform for incorporating the influence of new variables are highlighted.

The chapter structure is directly related to the structural arrangement of expansive clays. The role of suction on each structural level is briefly described and, subsequently, the selection of constitutive variables is analysed. The choice of these variables impose advantages and restrictions on the capability of the formulation.

Finally, a brief summary of the double-structure formulation is depicted in the following manner:

i. The micro-structural level is modelled by a non-linear elasticity formulation. The resulting strains are assumed to be largely reversible.
ii. The Macro-structure is governed by a conventional elastoplastic model for unsaturated soil.
iii. The water retention model for a double-structure material is considered as the superposition of the retention models of the micro- and Macro-structure.
iv. The Hydro-Mechanical structural levels interactions involve the pure elastic behaviour, the plastic strains at Macro-structure due to micro-structure deformations and the local water mass exchange.

v. The stress-strain relationships for the different stress regions are indicated.

As closing remark, all constitutive models are approximations of material behaviour. Advanced models may recreate several aspects of material behaviour but none can recreate all aspects and knowing what they are not able to model is just as important as knowing what they do model.

3.2. Suction concept

To set the study of unsaturated soils on a proper course, it was essential to realize that any soil could be unsaturated and, therefore, there could be no reason why a fundamental approach, already successful in the case of saturated soils, could not be applied also to this type of materials. As a matter of principle, there is nothing special in an unsaturated soil apart from the simple fact that some part of the pore space is occupied by air (or other non-wetting fluids) (Gens et al., 2006).

Schofield, (1935) appears to be the first one to have introduced the role of suction on the behaviour of unsaturated soils and in the late 1950s and 1960s, there was intensive experimental work (e.g. Bishop and Blight, 1963) where, generally, laboratory results were interpreted in terms of newly defined effective stress for unsaturated soils. Subsequent research on unsaturated soils mechanics demonstrated that total stress path and suction paths had to be considered independently and not combined in a single expression (Section 3.3).

The concept of suction is the key for the adequate understanding of the generalized behaviour of soils. Suction is closely related to water potential that can be defined as the amount of work that must be done per unit mass of pure water in order to transport reversibly and isothermally an infinitesimal quantity of water from a reservoir of pure water at a specified elevation and gas pressure to the soil point under consideration (units: L^2T^{-2}). Although only total water potential matters concerning water flow, this arbitraries division has proved useful in the context of geotechnical engineering (Gens, 2010, 2013):

$$\psi = \psi_g + \psi_p + \psi_m + \psi_o \qquad \text{(Eq. 3-1)}$$

where ψ_g is the gravitational potential, ψ_p is the gas pressure potential, ψ_m is the matric potential and ψ_o is the osmotic potential.

Only the internal components of the potential (i.e. matric and osmotic) have noticeable effects on unsaturated soil behaviour. The osmotic potential depends on differences in solute concentrations (across a semi-permeable membrane); and the matric potential is related to the interaction between liquid and solid (Gens, 2010).

Matric (s) and osmotic (s_o) suctions are obtained expressing potential per unit volume (and changing the sign); they have unit of pressure ($ML^{-1}T^{-2}$). Total suction (s_t) is the sum of the two components and it is related to relative humidity through Kelvin's law. As pointed out by Gens, (2013), the matric suction is often linked to capillary phenomena, being the most important suction component concerning the mechanical behaviour of soil. Osmotic suction is only relevant in the case of some very active clays, in which a degree of semi-permeable membrane is naturally established.

In the light of a double-porosity configuration, it is worth to identify the role of suction in each structural level for the constitutive modelling statement.

3.2.1. The role of suction at micro-structural level

In spite of the existence of a semi-permeable membrane in a clay particles arrangement, a reasonable assumption for many porous media in a non-saline environment can be the predominance of matric suction with respect to the osmotic suction ($s >> s_o$). The role of osmotic suction due to cation exchange on micro-structural level and their implication on the expansive clay behaviour was studied by Guimaraes, (2002) and Guimaraes et al., (2013).

Baker and Frydman, (2009) divided the matric suction in the absorbed and the capillary water components. In this structural level, when conditions of high suctions prevail, it is not certain that the water is in a state of true tension. Then, the high negative pore pressures that frequently arise from the capillary equation reflect the degree of attraction of the water by the solid matrix and are often more related to

the physico-chemical effects than to some virtual capillary meniscus existing in the soil (Gens and Olivella, 2001).

3.2.2. The role of suction at Macro-structural level

Due to the coarse nature of the Macro-structural level, the water form menisci between particles. Surface tension and interface curvature give rise to a difference between water liquid pressure (P_L) and gas pressure (P_g) that is generally equated to matric suction. In addition, the presence of menisci in the particle contacts generates interparticle forces. As those forces are roughly aligned with the normal of the contact, they tend to have a stabilising influence on soil skeleton.

3.3. Discussion on stress concept, constitutive variables and models classification

Prior to this brief discussion, it is worth quoting the professor Burland, (1967), who wrote: 'the stress is a philosophical concept ... deformation is a physical reality'. Accordingly, the choice of appropriate stress variables for unsaturated soils has often been an intensively debatable issue, often in connection with the possibility of defining a single effective stress measure (Gens et al., 2006). There is a general agreement that at least two constitutive variables are generally required to represent adequately the full range of unsaturated soil behaviour, that is, including strength and deformation. As pointed out in Jommi, (2000): 'in fact, no single stress variable has ever been found which, substituted for effective stress, allows for a description of all the aspects of the mechanical behaviour of a given soil in the unsaturated range'.

As summarized Gens, (2010), the two constitutive variables used by most unsaturated constitutive models can be expressed as:

FCV (first constitutive variable):

$$(\sigma_t)_{ij} - P_g\delta_{ij} + \mu_1(s, S_L)\delta_{ij} \qquad \text{(Eq. 3-2)}$$

SCV (second constitutive variable):

$$\mu_2(s, S_L) \qquad \text{(Eq. 3-3)}$$

They are intentionally not called *constitutive stress variables*, to leave open the possibility that variable types other than stresses might be adopted. Usually, the FCV tries to account for the overall stress state of the soil, whereas the SCV tends to address mainly the effects of suction changes. Although tensor functions could be used, most constitutive models assume that μ_1 and μ_2 are scalars.

Depending on the expression for μ_1, three main classes of models can be distinguished:

I. $\mu_1 = 0$ which correspond to the use of net stresses.
II. μ_1 (s) function of suction but not of degree of saturation.
III. μ_1 (s, Sr) dependent on suction and degree of saturation (e.g. the classic Bishop's effective stress).

In Table 3-1, the main characteristics of the different model categories is listed according to their FCV.

So far, the selection of stress variables for unsaturated soils is a matter for convenience. The contribution of Houlsby, (1997) has provided much needed clarification of this issue. Houlsby, (1997) showed that, under reasonably general conditions, the rate of work input (W) per unit volume of unsaturated soil is (the work dissipated by flow of fluids has been not included):

$$W \equiv \frac{P_g \, \phi (1 - S_L) \dot{\rho}_g}{\rho_g} - (P_g - P_L) \phi \dot{S}_L + \{\boldsymbol{\sigma}_t - [S_L P_L + (1 - S_L) P_g] \mathbf{I}\} \dot{\boldsymbol{\varepsilon}} \qquad \text{(Eq. 3-4)}$$

where:

- ρ_g is the gas density.
- $\boldsymbol{\varepsilon}$ is the strain tensor.
- P_g and P_L are the gas and liquid pressure, respectively.
- ϕ is the porosity.
- S_L is the liquid saturation degree.

In this expression is assumed that, on average, the contractile skin moves with the soil skeleton—probably the most questionable assumption. If gas compressibility term is neglected, the work input rate is given by the equation (Eq. 3-5).

Table 3-1. Clasification of constitutive models for unsaturated soils according to the choice of FCV (from Gens, 2010)

Class	First constitutive variable FCV	Model features
I	Net stress $(\sigma_t)_{ij} - P_g\delta_{ij}$; $\mu_1 = 0$	-Stress paths easily represented. -Constitutive variables are independent (except for P_g). -Difficulties at saturated/unsaturated transition. -Decoupled hydraulic and mechanical components. Hydraulic hysteresis is not incorporated. -An independent function is required to model the increase of shear strength with suction.
II	$(\sigma_t)_{ij} - P_g\delta_{ij} + \mu_1(s)\delta_{ij}$	-Representation of stress paths not straightforward. -Constitutive variable is independent of material state. -Constitutive variables are linked. -Difficulties at saturated/unsaturated transition. -Decoupled hydraulic and mechanical components. Hydraulic hysteresis is not incorporated. -The increase of strength with suction is a result of the constitutive variable definition.
III	Bishop's effective stress $(\sigma_t)_{ij} - P_g\delta_{ij} + \mu_1(s, S_L)\delta_{ij}$	-Representation of stress paths not straightforward. -Constitutive variable incorporates a state parameter (S_L). -Constitutive variables are linked. -Natural transition from saturated to unsaturated states. -Coupled hydraulic and mechanical components. Hydraulic hysteresis is incorporated. -The increase of strength with suction is a result of the constitutive variable definition.

$$W \equiv -(P_g - P_L)\phi\dot{S}_L + \{\boldsymbol{\sigma}_t - [S_L P_L + (1 - S_L)P_g]\mathbf{I}\}\dot{\boldsymbol{\varepsilon}} \qquad \text{(Eq. 3-5)}$$

Based in the above formulation, Gens, (2010) defined sets of stress and strain variables that are conjugated to each other. An immediate choice is:

$$\begin{pmatrix} \boldsymbol{\sigma}_t - [S_L P_L + (1 - S_L)P_g]\mathbf{I} \\ \phi(P_g - P_L) \end{pmatrix} \leftrightarrow \begin{pmatrix} \dot{\boldsymbol{\varepsilon}} \\ -\dot{S}_L \end{pmatrix} \qquad \text{(Eq. 3-6)}$$

where Bishop's stress is conjugated to strains, and modified suction is conjugated to degree of saturation. However, (Eq. 3-5) can be rearranged to give the following conjugates stress-strain:

$$\begin{pmatrix} \boldsymbol{\sigma}_t - P_g\mathbf{I} \\ (P_g - P_L) \end{pmatrix} \leftrightarrow \begin{pmatrix} \dot{\boldsymbol{\varepsilon}} \\ \dot{\varepsilon}_w = -\phi\dot{S}_L + S_L\dot{\varepsilon}_v \end{pmatrix} \qquad \text{(Eq. 3-7)}$$

Now, net stress is conjugate to strains and suction conjugated to volumetric water content.

As concluded by Gens, (2010): from this perspective, the work input expression does not provided a criterion to select one set of constitutive variables in preference to the other. However, the choice of constitutive variables is not neutral; it has a significant influence on the nature of the constitutive law developed (see Table 3-1). Recently, Gallipoli et al., (2018) showed that the above two sets of stress variables lead to different values of the second order term of the hydro-mechanical work input. They are therefore no longer equivalent with respect to other aspects of material behaviour governed by the second-order work such as the flow rule of elasto-plastic models.

The first conceptual model for expansive clays (Gens and Alonso, 1992) conceives the micro-structural level (i.e. the clay aggregates) in a perpetual saturated state. Therefore, only one stress variable describes the behaviour (see Section 3.4.3.). Considering the possibility of unsaturated states at clay aggregates (see Chapter 2), the third type of FCV and the micro-suction as SCV have been selected (Table 3-1 and Table 3-2).

The modelling of unsaturated soils of low activity has been traditionally based on net stress and suction variables (Alonso et al., 1987, 1990). This

selection is maintained for the Macro-structural level (Table 3-1 and Table 3-2).

Table 3-2. Constitutive variables for a double-structure formulation

Structural Level	First constitutive variable FCV	Second constitutive variable FCV
micro	Bishop's effective stress $\boldsymbol{\sigma}'_1 = \boldsymbol{\sigma}_{t1} - P_{g1}\mathbf{I} + \chi(S_{L1})s_1\mathbf{I}$	micro-suction $s_1 = \max(P_{g1} - P_{L1}, 0)$
Macro	Net stress $\boldsymbol{\sigma}''_2 = \boldsymbol{\sigma}_{t2} - P_{g2}\mathbf{I}$	Macro-suction $s_2 = \max(P_{g2} - P_{L2}, 0)$

where:

- The subscripts 1 and 2 are refers to micro- and Macro structural levels, respectively. No subscript indicates the double-structural porous medium.
- $\mathbf{P_g}$ is the gas pressure.
- $\mathbf{P_L}$ is the liquid pressure.
- χ is the Bishop's parameter, which is typically dependent on the saturation degree S_L.
- $\boldsymbol{\sigma_{ti}}$ is the total stress for structural level Macro (i=2) or micro (i=1).

The total stresses of the double-structural porous medium are assumed to be also the total stresses acting at each structural level. Therefore, $\boldsymbol{\sigma_t} = \boldsymbol{\sigma_{t1}} = \boldsymbol{\sigma_{t2}}$. Moreover, the constitutive stress for the double-structural porous medium is defined as the constitutive stress of the Macro-structural level (i.e. Net stress $\boldsymbol{\sigma}'' = \boldsymbol{\sigma}''_2$).

An alternative option can be the analysis of the constitutive variables for the expansive porous medium, instead to consider the structural levels separately. Li et al., (2017) give the work input for unsaturated expansive soils considering a double-porosity system (Eq. 3-8) taking into account four phases, i.e., aggregates (ag), capillary water (c), absorbed water (ad) and air (a); a different phases definition from Olivella et al., (1994) (see Chapter 2). It is assumed that the total surface of the aggregates is covered by adsorbed water, the capillary water is concentrated in the inter-aggregate pores, and air occupies the central portion of the inter-aggregate pores. Consequently, a saturated micro-structural level (Figure 3-1).

$$
\begin{aligned}
W \equiv & -u'_{c,j} w_j^c - u'_{ad,j} w_j^{ad} - u'_{a,j} w_j^d \\
& + (\sigma_{ij} - u_c S_r^c \delta_{ij} - u_{ad} S_r^{ad} \delta_{ij} - u_a S_r^a \delta_{ij}) \dot{\varepsilon}_{ij\_2} \\
& - \bar{\phi}_2 (u_a - u_c) \dot{S}_r^c - \bar{\phi}_2 (u_a - u_{ad}) \dot{S}_r^{ad} \\
& - \left(u_c - u_{ad} \frac{\rho^c}{\rho^{ad}} \right) \frac{c^c}{\rho^c} + u_a \bar{\phi}_2 S_r^a \frac{\dot{\rho}^a}{\rho^a} \\
& + (p - u_{ad}) \dot{\varepsilon}_{v\_1}
\end{aligned}
\qquad \text{(Eq. 3-8)}
$$

where:

- The subscripts 1 and 2 refer to micro- and Macro structural levels, respectively.
- p is the total mean stress.
- u_α is the phase α pressure and $u'_{\alpha,j}$ is the excess pore pressure gradient in the phase α.
- w_j^α is the seepage velocity of the α phase. This is function of phase velocity and the average velocity of the aggregate phase.
- S_r^α is the Macro-structural degree of saturation of the α phase.
- $\bar{\phi}_2$ is the Macro pore volume fraction.
- ρ^α is the density of the α phase.
- c^α is the mass exchange rate of the α phase with the other phase.

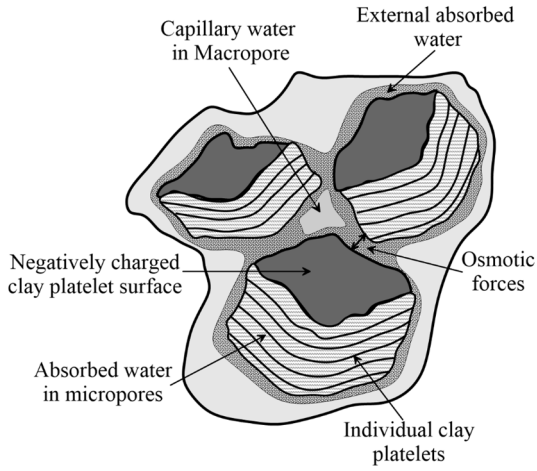

Figure 3-1. The double porosity model used in Li et al., (2017).

The first three terms on the right side of the equation (Eq. 3-8) represent the work caused by the seepage of the pore fluid relative to the aggregate phase (important difference with the Houlsby, (1997) proposal). The fourth term represents the work caused by the Macro-structural

deformation. The fifth and sixth terms represent the work caused by the change in the degree of saturation of the capillary water and adsorbed water phases in Macro-pores, respectively. The seventh term represents the work caused by the mass exchange of the capillary water phase with the adsorbed water phase. The eighth term represents the work caused by the compression of the air phase. Finally, the ninth term represents the work caused by the deformation of the micro-structure.

The interpretation of some key terms in (Eq. 3-8) is as follows (Li et al., 2017):

- The fourth term implies that the stress variable work-conjugate of the Macro-structural strain increment is $\sigma_{ij}^{*} = (\sigma_{ij} - u_a\delta_{ij}) + S_r^c(u_a - u_c)\delta_{ij} + S_r^{ad}(u_a - u_{ad})\delta_{ij}$, which is termed as the inter-aggregate stress. Different from Bishop's stress, the additional term $S_r^{ad}(u_a - u_{ad})\delta_{ij}$ in the inter-aggregate stress considers the physico-chemical effect between the absorbed water and the solid matrix

- The fifth and sixth terms imply that the stress variables work-conjugate of $\dot{S}_r^c$ and $\dot{S}_r^{ad}$ are $\bar{\phi}_2(u_a - u_c)$ and $\bar{\phi}_2(u_a - u_{ad})$, respectively. These stress variables are similar to the modified suction proposed by Houlsby, (1997) (Eq. 3-6). However, the water content change related to the adsorbed water phase has been separated from the capillary water phase in the Macro-pores.

- The ninth term implies that the stress variable work-conjugate of the microstructural volumetric deformation is $(p - u_{ad})$, which implies the effect of the external applied stresses and adsorbed water pressure on the size of the aggregates.

From the theoretical point of view, the separation of adsorbed water and capillary water offers a clear physical explanation on the water distribution in expansive clays. However, the experimental quantification of capillary and adsorbed water is uncommon and the adsorbed water pressure cannot be measured directly; limiting the application of the (Eq. 3-8). Consequently, Li et al., (2017) assumed that the adsorbed water in Macro-pores is part of clay aggregates. The following set of stress and strain conjugated variables arises from the modify work input analysis:

$$\begin{pmatrix} (\sigma_{ij} - u_a) + (u_a - u_c)S_r^M \delta_{ij} \\ \bar{\phi}_2 (u_a - u_c) \end{pmatrix} \leftrightarrow \begin{pmatrix} \dot{\varepsilon}_{ij} \\ -\dot{S}_r^M \end{pmatrix} \qquad \text{(Eq. 3-9)}$$

where S_r^M is the Macro-structural degree of saturation (water volume in Macro-pores over the Macro pore volume).

The stress variable is similar to Bishop's proposal, however, the effective stress parameter (S_r^M) is chosen as the effective degree of saturation rather than the total degree of saturation for unsaturated clays, resulting in a microstructurally based effective stress (Alonso et al., 2010).

The explicit definition of conjugated stress-strain for two structural levels (Table 3-2) seems to be suitable to stablish a double-structure constitutive model, rather than the global analysis (Eq. 3-9). The main reasons are:

- It is consistent with the conception of the expansive clays as two overlapping medium (Chapter 2).
- There are conjugated stress-strain relationships for micro- and Macro-structure. Therefore, constitutive laws for the two structural levels have to be defined.
- It does not require specific assumptions on the water at micro-structural level. Unsaturated micro-structural states and the transition to full saturation are possible.

3.4. Double-structure constitutive model for expansive clays

3.4.1. Introduction

The computation of swelling pressure and swelling strains of bentonites might be the major concern in engineering applications. The Barcelona Basic Model (Alonso et al., 1990) is not able to reproduce satisfactorily the swelling behaviour of clays. Nevertheless, some modifications in the elastic part of the model are introduced in order to reproduce the expansive behaviour of compacted bentonites. This is mainly because the description of the material behaviour inside the yield surface is particularly important.

The variation of stress-stiffness with suction and, especially, the variation of swelling potential with stress and suction have been considered (Sanchez and Gens, 2014). The resulting elastic model is the following:

$$\dot{\varepsilon}_v^e = \frac{\kappa}{(1+e)}\frac{\dot{p}}{p} + \frac{\kappa_s}{(1+e)}\frac{\dot{s}}{(s+p_{atm})} \quad \text{(Eq. 3-10)}$$

$$\dot{\varepsilon}_s^e = \frac{\dot{J}}{G} \quad \text{(Eq. 3-11)}$$

where:

- $\dot{\varepsilon}_v^e$ and $\dot{\varepsilon}_s^e$ are the volumetric and deviatoric component of the elastic strain, respectively.
- κ and κ_s are the elastic stiffness parameter for change in stress and suction.
- G is the shear modulus.

The expression (Eq. 3-12) has been proposed to evaluate the elastic stiffness parameter for changes in net mean stress. The Figure 3-2 shows the linear variation of this parameter respect to suction values for the MX-80 bentonite.

$$\kappa = \kappa_o(1 + \alpha_s s) \quad \text{(Eq. 3-12)}$$

where:

- κ_o is the elastic stiffness parameter in saturated condition.
- α_s is a model parameter.

The elastic stiffness parameter for changes in suction is computed according to:

$$\kappa_s = \kappa_{so}(1 + \alpha_{sp}\ln(p/p_{ref}))\,\exp(\alpha_{ss}s) \quad \text{(Eq. 3-13)}$$

where:

- κ_{so} is the elastic stiffness parameter in saturated condition.
- α_{sp} and α_{ss} are model parameters.

The general response of the modified elastic part is depicted in Figure 3-3. According to the suction and stress dependence of the elastic stiffness parameters, the elastic slopes (e vs p and e vs s) variate.

As an example of the constitutive law capabilities, Figure 3-4 presents the model prediction in a swelling pressure test (Sanchez and Gens, 2014). The experimental data correspond to swelling pressure tests

carried out on FEBEX bentonite samples with two different dry densities. As it can be observed, the model results can be considered satisfactory, because the stress path is reasonably well reproduced as well as the observed value of the swelling pressure. Ruiz et al., (2018, 2017) used of this modified elastic law to reproduce the swelling pressure evolution of a bentonite fill that is the main component of a seal structure for a main galleries of a nuclear waste repository.

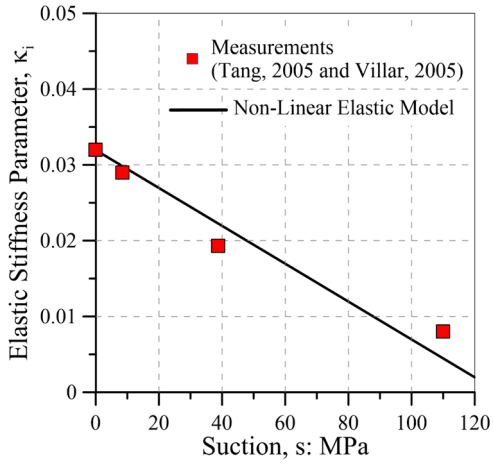

Figure 3-2. Variation of elastic stiffness parameter with suction for MX-80 bentonite (Zandarin et al., 2011).

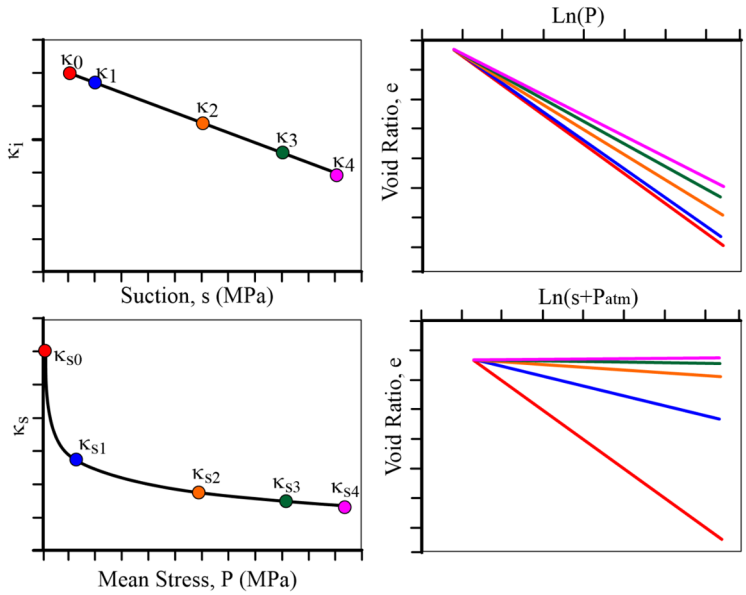

Figure 3-3. General behaviour of a modified non-linear elasticity model.

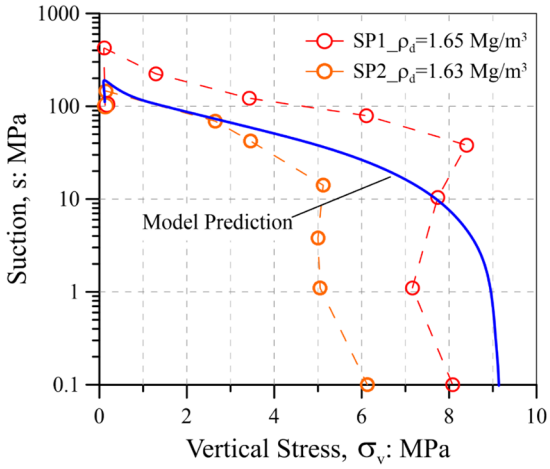

Figure 3-4. Computed stress path for swelling pressure tests using a modified BBM (Sanchez and Gens, 2014). Experimental data from Lloret et al., (2003).

In spite of the satisfactory swelling pressure reproduction, the above formulation present important drawbacks such as:

- There is not an explicit relation with the aggregated fabric of the expansive clays (see Chapter 2). Therefore, it does not account the microstructural evolution due to Hydro-Mechanical actions.
  - The response is fully reversible. Contradicting the experimental results that suggest a Macro-structural plastic response due to clay aggregates deformation. Accordingly, the stress-path dependence and the irreversible strain accumulation are not taking into account.
  - The response after Macro-structural collapse is not well reproduced. If a particular stress-path crosses the LC yield surface, the pressure drop is reproduced. However, the subsequent pressure increases is not reached because it is intrinsically related to the microstructure.

Concluding, single porosity models are not able to handle properly the role that the structure of the swelling clays play during hydration.

Therefore, in order to perform a more detailed analysis of the clay fabric effects, a double-structure Hydro-Mechanical formulation has been developed. A more suitable framework has been adopted to simulate problems in which two different pore levels (see Chapter 2) can be clearly distinguished. This approach would allow the adoption of a conceptual

model for the hydration of the swelling clays closer to the observed behaviour.

Probably the concept of double porosity system was first introduced by Barrenblatt et al., (1960) to simulate flow through rigid fissured porous media and it was later enlarged to consider the coupling between fluid flow and soil deformation. Gens and Alonso, (1992) developed a conceptual model based on this concept to describe the mechanical behaviour of unsaturated expansive clay. From clay fabric studies (e.g. SEM and MIP) that revealed the compacted expansive clays as a configuration of clay aggregates, they seated three important basis:

- The mechanisms responsible to soil expansion occurs in the clay aggregates due to physico-chemical interactions (see Chapter 2).
- The irreversible response (e.g. collapse, accumulation of plastic deformations, among other) is reflected on the large-scale structure of soil (see Chapter 2).
- There is a mechanical coupling between the two structural levels. Additional plastic response of the Macro-structure due to micro-structure deformation.

Certainly, the postulate of this mechanical coupling between the structural levels has been the keystone of the subsequent double-structure formulations for expansive clays.

Alonso et al. (1999) presented the first mathematical expression of this conceptual model established in an elasto-plasticity framework. Later, a more convenient formulation based on generalized plasticity concepts has been developed (Sánchez, 2004; Sanchez et al., 2005) while keeping the same basic features and assumptions. A similar formulation has been implemented by Mašin, (2013) in the hypoplastic formalism.

The explicit consideration of the two dominant levels of pores can also assist towards a better understanding of some key processes that take place during hydration of the expansive clay. Guimaraes et al., (2013) and Navarro et al., (2017) presented a chemo-mechanical model for expansive clays that takes into account the effects of cation content and cation exchange. Chemical effects were defined at micro-structural level, the seat of the basis physico-chemical phenomena.

In the following sections, the Hydro-Mechanical double-structure model developed in this thesis is described. A water retention formulation taking into account the two porosity levels is presented first. Then the mechanical models for the micro-structural and Macro-structural levels are introduced followed by an account of the various interactions between the two structural levels: elastic, Macro-micro mechanical and Macro-micro hydraulic. Subsequently the elastoplastic stress-strain equations are derived for all the potential plastic mechanisms. The model description closes with a summary of the constitutive input parameters.

Once again, for compact variable names, we refer the micro-structural level with the subscript 1, the Macro-structural level with the subscript 2 and the double-structural porous medium without subscript.

3.4.2. Hydraulic constitutive model — Water Retention Curve

As described in Chapter 2, Darcy's generalized law (Eq. 2-56) rules the unsaturated flow in the double-structure porous media. The intrinsic permeability of expansive clays shows a strong dependence on the porous space. The Kozeny's law (Eq. 2-58) and an exponential law (Eq. 2-59) were proposed to model the dependence of permeability on the Macro pore volume fraction, $\bar{\phi}_2$. The well-known cubic law was adopted for the relative permeability of the model (Eq. 2-56).

In order to close the hydraulic formulation, the modelling of the retention property of double-structure materials is required. The water retention curve relates the suction with the degree of saturation.

The aggregated fabric of compacted expansive clays, characterized by intra-aggregate and inter-aggregate pores see Chapter 2), play a significant role on the water retention properties. Accordingly, experimental multimodal water retention curves are commonly obtained from active clays (Lloret et al., 2003; Romero et al., 2011; Seiphoori et al., 2014). Information of the mercury intrusion porosimetry (MIP), linking the cumulative pore volume to an apparent pore size, has been useful to account for the role of clay fabric.

So far, the consideration of expansive clays as the overlapping of two interacting structural levels has been theoretically and mathematically convenient; the water retention curve model is not an exception. A

unique water retention curve, involving both structural levels, leads to a cumbersome formulation that is difficult to apply in practice.

The first water retention model was proposed by Romero and Vaunat, (2000), which account for different retention mechanism in the different structural domains, introducing a void ratio dependency only in the level dominated by capillarity phenomena. Dieudonne et al., (2017) formulates a water retention model for compacted bentonites; the micro-structural water retention domain is governed by adsorption water storage and the classical Van Genuchten retention model is used for the Macro-structure.

Here, the multimodal retention model is applied (Casini et al., 2012). The water retention curve of an expansive clay is obtained by linear superposition of the micro- and Macro-structural sub-curves:

$$S_e = \frac{Sr - Sr_{res}}{Sr_{max} - Sr_{res}} = \sum_{i=1}^{2} w_i \, [WRC]_i \qquad \text{(Eq. 3-14)}$$

where:

- S_e is the equivalent saturation degree of the double-structure material.
- Sr, Sr_{max} and Sr_{res} are the actual, the maximum and the residual saturation degree of the double-structure material, respectively.
- Subscript i is 1 for micro-structural level and 2 for Macro structural level.
- w is the weighting parameter for each structural level. It relates the pore volume fraction of each level ($\bar{\phi}_i$) with the total porosity (ϕ) of the material $w_i = \bar{\phi}_i/\phi$. Casini et al., (2012) defined them as the Macro- and micro area below the pore capillary density function.
- WRC is a Van Genuchten type water retention curve for each structural level. Can be used a classical (Eq. 3-15) or modified
- (Eq. 3-16) versions.

$$S_e = \frac{Sr - Sr_{res}}{Sr_{max} - Sr_{res}} = \left(1 + \left(\frac{P_g - P_L}{P}\right)^{\frac{1}{1-\lambda}}\right)^{-\lambda} \qquad \text{(Eq. 3-15)}$$

$$S_e = \frac{Sr - Sr_{res}}{Sr_{max} - Sr_{res}} = \left(1 + \left(\frac{P_g - P_L}{P}\right)^{\frac{1}{1-\lambda}}\right)^{-\lambda} fd \qquad \text{(Eq. 3-16)}$$

$$fd = \left(1 - \left(\frac{P_g - P_L}{P_d}\right)\right)^{\lambda_d}$$

$$P = P_o \frac{\sigma}{\sigma_o} \qquad \text{(Eq. 3-17)}$$

where:

- S_e is the equivalent saturation degree of each structural level.
- Sr, Sr_{max} and Sr_{res} are the actual, the maximum and the residual saturation degree of each structural level (i.e. micro and Macro).
- P_o is the air entry value.
- σ_o is the subsurface tension at certain temperature.
- λ is the shape function for retention curve.
- P_g and P_L are the gas and liquid pressure in each structural level.
- P_d is the pressure related with the suction at zero degree of saturation.
- λ_d is a model parameter.

The micro-structure air entry value, P_{o_1}, is associated to adsorbed phenomena and it is always higher than the Macro-structural value, P_{o_2}.

The weighting parameter, w_i, account for the role of the structural levels on the hydraulic properties of the expansive materials. The HM double structure formulation presented in this work does not update these weighting factors along the imposed stress-suction-paths. In that sense, the constitutive formulation is not fully coupled.

The effect of dry density on bentonite structure is essentially related to changes in the inter-aggregate space and the pore size distribution in this domain. Compaction efforts mainly affects the Macro-structural pore volume (see Chapter 2). As pointed in Dieudonne et al., (2017), when the density increases, not only is the total volume of the voids reduced, but also the size of the Macro pores decreases. Accordingly, Pores can sustain high suctions before emptying. From a phenomenological point of view, a reduction in dry density implies a reduction of the air entry value of the material. Experimental data can be fitted using a power law of the form:

$$P_{o\_2} = \left(\frac{A}{\bar{\phi}_2} \right)^B \qquad \text{(Eq. 3-18)}$$

where:

- A and B are materials parameters.

The nature of the above equation is basically phenomenological and related to the hydraulic response of the porous medium at the laboratory scale. However, it implicitly describes an additional role of the Macro-structure on the hydraulic properties (Dieudonne et al., 2017).

Different configurations of bentonite-based materials has been proposed for the sealing systems and engineering barriers of the nuclear waste repositories (e.g. compacted blocks, bentonite granular mixtures, powder/pellets mixtures, bentonite/sand mixtures). This implies additional complexities in the water retention description. The Appendix A shows the fitting of experimental WRC of different expansive materials whit the model proposed previously. Main assumptions and clay fabric simplifications are discussed.

3.4.3. Mechanical model for micro-structural level

Based on the former assumption proposed by Gens and Alonso, (1992), the strains of the micro-structural level are volumetric and mainly reversible. Therefore, a non-linear elasticity model describe the stress-strain-suction relations in this level.

From Chapter 2, we can recover the following description of the pore space in the micro-structure:

$$\phi_1 = \frac{(V_P)_1}{V_1} \qquad \text{(Eq. 3-19)}$$

$$\bar{\phi}_1 = \frac{(V_P)_1}{V} \qquad \text{(Eq. 3-20)}$$

$$\phi_1 = \frac{V}{V_1}\bar{\phi}_1 \qquad \text{(Eq. 3-21)}$$

The micro porosity, ϕ_1, relates the volume of micro-pores with the volume of the micro-structural level. Instead, the micro pore volume fraction, $\bar{\phi}_1$, considers the whole volume of the double-structure medium (see Figure 2-32). Both entities are linked by a simple volume ratio (Eq. 3-21). Obtaining the micro volumetric strain from the volume relations, we found the same relation.

$$d\varepsilon_{v1} = \frac{dV_1}{V_1} = \frac{V}{V_1}\frac{d(V_s)_1 + d(V_P)_1}{V} = \frac{V}{V_1} d\bar{\varepsilon}_{v1} \qquad \text{(Eq. 3-22)}$$
Also (Eq. 2-15)

The constitutive variables for this structural-level are indicated in Table 3-2. They are the Bishop-type micro-structural effective stress and the micro-structural suction.

$$\boldsymbol{\sigma'}_1 = \boldsymbol{\sigma}_t + [\chi_1(P_{g1} - P_{L1}) - P_{g1}]\mathbf{I} \qquad \text{(Eq. 3-23)}$$

$$s_1 = \max(P_{g1} - P_{L1}, 0) \qquad \text{(Eq. 3-24)}$$

where:

- P_{g1} and P_{L1} are the gas and liquid pressures at micro-structural level.
- χ_1 is the Bishop's parameter.
- $\boldsymbol{\sigma}_t$ is the total stress.

The Bishop's parameter is defined as a function of micro saturation degree, S_{L1}. The (Eq. 3-25) is a popular form when χ_1 is considered equal to degree of saturation. However, it should be noted that Bishop's proposal was more general, since χ_1 was not claimed to be equal to the saturation degree; then an exponential law is provided in (Eq. 3-26).

$$\chi_1 = S_{L1} \qquad \text{(Eq. 3-25)}$$

$$\chi_1 = \frac{1}{\ln 2 - q_k} \ln\left(e^{-q_k S_{L1}^{p_k}} + e^{-q_k (2 - S_{L1})^{p_k}}\right) \qquad \text{(Eq. 3-26)}$$

where:

- q_k and p_k are fitting parameters.

Bishop's parameter incorporates information regarding the structure of the deformable medium and can be mainly envisioned as a scaling factor that captures the weight of the contribution of each fluid pressure to the effective stress (Mainka et al., 2014; Vaunat and Casini, 2017). For instance, Mainka et al., (2014) analyzed the dependence of χ_1 on the compressibility of the clay aggregates through an upscaling formulation (see Chapter 5).

The above effective stress definition is a direct consequence of the consideration of unsaturated states in the micro-structure level of the expansive clays. Original formulations consider a permanent saturation of clay aggregates (Gens and Alonso, 1992; Alonso et al. 1999). Accordingly, the Terzaghi effective stress governs the volumetric

deformation of this level. Mašín and Khalili, (2016) discussed the applicability of the Terzagui effective stress principle to predict the behaviour of expansive clay aggregates in combination with the assumption of aggregate response reversibility. They found a relation of the aggregate dry density with the Terzaghi effective stress by a unique function under the assumption of aggregate saturation and the inter-particle distances larger than approximate 1.5 nm. At smaller distances, this relation becomes inaccurate.

As showed in the Table 3-1, Bishop`s type effective stress presents a natural transition to the Terzaghi effective when the micro-structure goes to saturated states.

The stress-strain relation for the micro-structural-level itself is given by:

$$d\boldsymbol{\varepsilon}_1 = \mathbf{D}_1{}^{-1} d\boldsymbol{\sigma}'_1 \qquad \text{(Eq. 3-27)}$$

where:

- $d\boldsymbol{\varepsilon}_1$ measures the variation of micro-pores with respect to the micro level.
- $\mathbf{D}_1$ is the elastic constitutive matrix dependant of the micro volumetric bulk modulus, K_1, and the shear modulus, G_1.

$$\mathbf{D_1} = \begin{bmatrix} K_1 + \frac{4}{3}G_1 & K_1 - \frac{2}{3}G_1 & K_1 - \frac{2}{3}G_1 & & & \\ K_1 - \frac{2}{3}G_1 & K_1 + \frac{4}{3}G_1 & K_1 - \frac{2}{3}G_1 & 0\ 0\ 0 & & \\ K_1 - \frac{2}{3}G_1 & K_1 - \frac{2}{3}G_1 & K_1 + \frac{4}{3}G_1 & 0\ 0\ 0 & & \\ & & & 0\ 0\ 0 & & \\ & 0\ 0\ 0 & & & G_1\ 0\ 0 & \\ & 0\ 0\ 0 & & & 0\ G_1\ 0 & \\ & 0\ 0\ 0 & & & 0\ 0\ G_1 \end{bmatrix} \qquad \text{(Eq. 3-28)}$$

$$K_1 = \frac{(1+e_1)p'_1}{\kappa_1} = \frac{p'_1}{(1+\phi_1)\kappa_1} \qquad \text{(Eq. 3-29)}$$

where:

- p'_1 is the mean effective stress at micro-structural level.
- κ_1 is the elastic stiffness parameter at micro-structural level for changes in the mean effective stress.

Now, the variation of the micro-pores respect to the total volume of the soil is expressed as $d\bar{\boldsymbol{\varepsilon}}_1$. In particular, as it has been shown before (Chapter 2 and (Eq. 3-21)), we have the following relationships:

$$d(\bar{\varepsilon}_v)_1 = \frac{1+e_1}{1+e} d(\varepsilon_v)_1 = \frac{1+e_1}{1+e} \frac{1}{K_1} dp'_1 = \frac{1}{\overline{K}_1} dp'_1 \quad \text{(Eq. 3-30)}$$

$$\overline{K}_1 = \frac{1+e}{1+e_1} K_1 \quad \text{(Eq. 3-31)}$$

Finally, the transformation of the stress-strain relation for the micro-structural-level is:

$$d\bar{\boldsymbol{\varepsilon}}_{\mathbf{1}} = \bar{\mathbf{D}}_{\mathbf{1}}^{-1} d\boldsymbol{\sigma}'_{\mathbf{1}} \quad \text{(Eq. 3-32)}$$

$$\bar{\mathbf{D}}_{\mathbf{1}} = \begin{bmatrix} \overline{K}_1 + \frac{4}{3}\bar{G}_1 & \overline{K}_1 - \frac{2}{3}\bar{G}_1 & \overline{K}_1 - \frac{2}{3}\bar{G}_1 & & & \\ \overline{K}_1 - \frac{2}{3}\bar{G}_1 & \overline{K}_1 + \frac{4}{3}\bar{G}_1 & \overline{K}_1 - \frac{2}{3}\bar{G}_1 & 0\ 0\ 0 & & \\ \overline{K}_1 - \frac{2}{3}\bar{G}_1 & \overline{K}_1 - \frac{2}{3}\bar{G}_1 & \overline{K}_1 + \frac{4}{3}\bar{G}_1 & & & \\ & 0\ 0\ 0 & & \bar{G}_1 & 0 & 0 \\ & 0\ 0\ 0 & & 0 & \bar{G}_1 & 0 \\ & 0\ 0\ 0 & & 0 & 0 & \bar{G}_1 \end{bmatrix} \quad \text{(Eq. 3-33)}$$

Modifying the Bishop's effective stress (Eq. 3-23) according to the assumptions on the stresses definitions (Table 3-2), we can obtain a general stress-strain-suction relation.

$$\boldsymbol{\sigma}'_1 = \boldsymbol{\sigma}'' + [\max(P_{g2}, P_{L2}) + \chi_1(P_{g1} - P_{L1}) - P_{g1}]\mathbf{m} \quad \text{(Eq. 3-34)}$$

where:

- The auxiliary vector $\mathbf{m} = [1 \quad 1 \quad 1 \quad 0 \quad 0 \quad 0]^T$ is used for Voigt notation.

Replacing the above effective stress expression into the (Eq. 3-32), the micro-structural strain becomes:

$$d\bar{\boldsymbol{\varepsilon}}_{\mathbf{1}} = \bar{\mathbf{D}}_{\mathbf{1}}^{-1} d\boldsymbol{\sigma}'' + \frac{1}{3\overline{K}_1}[d\max(P_{g2}, P_{L2}) + (P_{g1} - P_{L1})d\chi_1 + (dP_{g1} - dP_{L1})\chi_1 - dP_{g1}]\mathbf{m} \quad \text{(Eq. 3-35)}$$

The mathematical development of the derivatives and the reorganization of different terms conduct to the final hydro-mechanical stress-strain relation for an unsaturated micro-structural level and hydraulic disequilibrium with the Macro-structural level (Eq. 3-41).

$$D\bar{\boldsymbol{\varepsilon}}_{\mathbf{1}} = \overline{\mathbf{D}}_{\mathbf{1}}^{-1} d\boldsymbol{\sigma}'' + \left[\frac{\zeta_{g1}}{3\overline{\overline{K}}_1} dP_{g1} + \frac{\zeta_{L1}}{3\overline{\overline{K}}_1} dP_{L1} + \frac{1}{3\overline{\overline{K}}_1} d\max\left(P_{g2}, P_{L2}\right)\right] \mathbf{m} \quad \text{(Eq. 3-36)}$$

where:

$$\zeta_{g1} = \left(P_{g1} - P_{L1}\right) \frac{d\chi_1}{dS_{L1}} \frac{dS_{L1}}{dP_{g1}} \quad \text{(Eq. 3-37)}$$

$$\zeta_{L1} = \left(P_{g1} - P_{L1}\right) \frac{d\chi_1}{dS_{L1}} \frac{dS_{L1}}{dP_{L1}} \quad \text{(Eq. 3-38)}$$

The terms dS_{L1}/dP_{g1} and dS_{L1}/dP_{L1} arises from the water retention curve of the micro-level (Section 3.4.1.).

When the gas pressure at micro (and Macro) level is constant, the final expression is:

$$d\bar{\boldsymbol{\varepsilon}}_{\mathbf{1}} = \bar{\mathbf{D}}_{\mathbf{1}}^{-1} d\boldsymbol{\sigma}'' + \left[\frac{\zeta_{L1}}{3\overline{\overline{K}}_1} dP_{L1} + \frac{1}{3\overline{\overline{K}}_1} d\max\left(P_{g2}, P_{L2}\right)\right] \mathbf{m} \quad \text{(Eq. 3-39)}$$

In the p'-s plane the line corresponding to constant micro-structural effective stress is called *Neutral Loading* line. There are not micro-structural deformations when the stress paths moves on this line (Figure 3-5.).

$$p'_1 = \text{constant} = p_t + \left[\chi_1\left(P_{g1} - P_{L1}\right) - P_{g1}\right] = p'_{1\_NL} \quad \text{(Eq. 3-40)}$$

where:

- p'_{1_NL} is a reference micro-structural effective stress.

The Neutral Loading line divides the p'-s plane into two parts, defining two main generalized stress paths (Sánchez, 2004), which are identified as:

$dp'_1 > 0 \rightarrow$ microstructural contraction path (mC) (Eq. 3-41)

$dp'_1 < 0 \rightarrow$ microstructural swelling path (mS) (Eq. 3-42)

In previous version of the numerical model, Alonso et al. (1999), the paths (Eq. 3-41) and (Eq. 3-42) were called "suction increase" and "suction decrease", respectively, in order to highlight the role of suction on the micro-structural behaviour. Herein the names micro-structural contraction (mC) and micro-structural swelling (mS) refer to the actual response of this structural level.

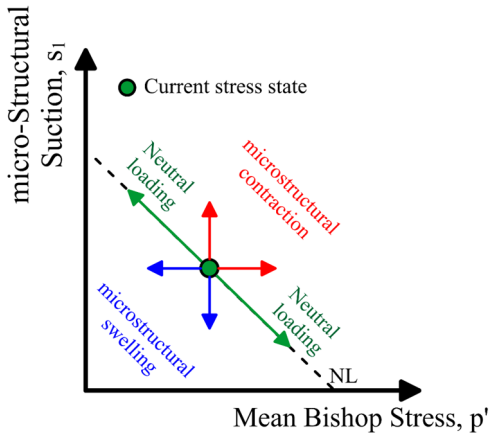

Figure 3-5. Definition of micro-structural swelling and contraction directions (from Sánchez, 2004)

3.4.4. Mechanical model for Macro-structural level

The inclusion of this structural level in the analysis allows the consideration of phenomena that affect the skeleton of the material (e.g. macro-structural collapse and strain accumulation), which have a strong influence on the macroscopic response of expansive materials (Sánchez, 2004). The Barcelona Basic Model (Alonso et al., 1990) is able to reproduce many of the basic patterns of behaviour observed in non-expansive soils. Therefore, it is a proper constitutive model for the Macro-structural behaviour.

As exposed in Section 3.3., the BBM considers two independent constitutive variables to model the unsaturated soil behaviour (Table 3-2): net stresses ($\boldsymbol{\sigma}_2'' = \boldsymbol{\sigma}''$) and suction ($s_2$). The main features of this model can be summarized as follow:

- Contribution of suction to stiffening the soil against external load (Figure 3-6).
- Development of small reversible expansion strains due to wetting (suction decrease) at low confining stress.
- Development of irreversible strains (collapse) due to wetting at high confining stress (Figure 3-7).
- Dependence of the amount of collapse with confining stress.
- Dependence of the shear strength on suction (an increase of suction implies an increment in the apparent cohesion of the material).

The stress-strain relation at this level is stated as:

$$d\bar{\boldsymbol{\varepsilon}}_2 = \bar{\mathbf{D}}_{\mathbf{2}}^{-1} d\boldsymbol{\sigma}'' + d\boldsymbol{\varepsilon}_{s_2}^{r} + d\boldsymbol{\varepsilon}_{LC}^{p} + d\boldsymbol{\varepsilon}_{\beta}^{p} \quad \text{(Eq. 3-43)}$$

where:

- $\bar{\mathbf{D}}_{\mathbf{2}}$ is the elastic constitutive matrix (Eq. 3-44) dependant of Macro volumetric bulk modulus, $\overline{\overline{K}}_2$ (Eq. 3-45), and the shear modulus, $\bar{G}_2$.
- $d\boldsymbol{\varepsilon}_{s_2}^{r}$ are the reversible deformations associated to suction changes (Eq. 3-46).
- $d\boldsymbol{\varepsilon}_{LC}^{p}$ are the plastic strains associated to loading-collapse mechanism.
- $d\boldsymbol{\varepsilon}_{\beta}^{p}$ are the plastic Macro-structural strains generated by micro-structural deformations (see Section 3.4.2.2.).

$$\bar{\mathbf{D}}_{\mathbf{2}} = \begin{bmatrix} \overline{\overline{K}}_2 + \frac{4}{3}\bar{G}_2 & \overline{\overline{K}}_2 - \frac{2}{3}\bar{G}_2 & \overline{\overline{K}}_2 - \frac{2}{3}\bar{G}_2 & & & \\ \overline{\overline{K}}_2 - \frac{2}{3}\bar{G}_2 & \overline{\overline{K}}_2 + \frac{4}{3}\bar{G}_2 & \overline{\overline{K}}_2 - \frac{2}{3}\bar{G}_2 & 0\ 0\ 0 & & \\ \overline{\overline{K}}_2 - \frac{2}{3}\bar{G}_2 & \overline{\overline{K}}_2 - \frac{2}{3}\bar{G}_2 & \overline{\overline{K}}_2 + \frac{4}{3}\bar{G}_2 & 0\ 0\ 0 & & \\ & & & 0\ 0\ 0 & \bar{G}_2\ 0\ 0 & \\ 0\ 0\ 0 & & & & 0\ \bar{G}_2\ 0 & \\ 0\ 0\ 0 & & & & 0\ 0\ \bar{G}_2 & \end{bmatrix} \quad \text{(Eq. 3-44)}$$

$$\overline{\overline{K}}_2 = \frac{(1+\bar{e}_2)p''}{\bar{\kappa}_2} = \frac{p''}{(1-\bar{\phi}_2)\bar{\kappa}_2} \quad \text{(Eq. 3-45)}$$

where:

- p'' is the mean net stress.
- $\bar{\kappa}_2$ is the elastic stiffness parameter at Macro-structural level for changes in the mean net stress.
- $\bar{\phi}_2$ is the Macro pore volume fraction.

$$D\boldsymbol{\varepsilon}_{s_2}^{r} = \frac{1}{3K_s} ds_2 \mathbf{m} \quad \text{(Eq. 3-46)}$$

$$K_s = \frac{(1+\bar{e}_2)(s_2 + P_{atm})}{\kappa_s} = \frac{s_2 + P_{atm}}{(1-\bar{\phi}_2)\kappa_s} \quad \text{(Eq. 3-47)}$$

where:

- κ_s is the elastic stiffness parameter at Macro-structural level for changes in the suction.

According to classical plasticity theory, the occurrence of $d\boldsymbol{\varepsilon}^{p}_{LC}$ arises from crossing certain yield limit that defines an elastic domain. An idealized consolidation behaviour show that the yielding points move beyond the saturated consolidation line (s_2=0) as suction increases. The physical reasons are the stabilising forces due to suction, which allow the material to sustain a higher applied stress at a given void ratio. The various yield points are plotted in isotropic space (mean net stress–suction) in Figure 3-6. By joining them together, a yield curve, denoted as LC (loading–collapse), results. In the BBM, the expression for the shape of LC yield surface is derived from the variation of the post-yield slope (in semi-logarithmic space) of the consolidation lines at different suctions:

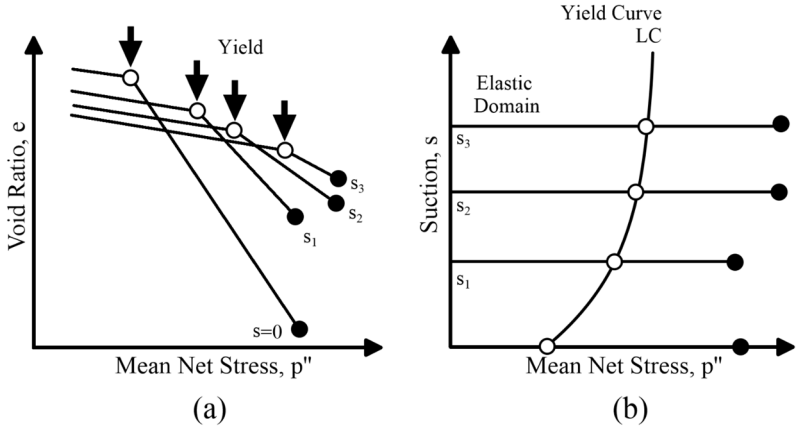

Figure 3-6. a) Idealised scheme of consolidation lines at different suction values; b) Definition of the LC (loading–collapse) yield curve in the isotropic plane (from Gens, 2010).

$$P_o = p_c \left(\frac{p_o^*}{p_c}\right)^{(\lambda_{sat}-\bar{\kappa}_2)/(\lambda_{(s_2)}-\bar{\kappa}_2)} \qquad \text{(Eq. 3-48)}$$

$$\lambda(s_2) = \lambda_{sat}[r + (1-r)e^{-\beta s_2}] \qquad \text{(Eq. 3-49)}$$

where:

- p_o is the yield mean stress.
- p_o^* is the saturated preconsolidation stress.
- p_c is a reference stress.
- λ_{sat} is the slope of the saturated virgin consolidation line.
- $\lambda(s_2)$ is the slope of the virgin consolidation line for a specific value of Macro-structural suction.
- r and β are models parameters.

The evolution of the LC yield surface is shown in Figure 3-7. Assuming an unsaturated soil specimen located on the yield curve LC_1, two suction-stress paths can be considered:

- A loading path (L) at constant Macro-structural suction. The yield curve will move from position LC_1 to LC_2 due to irreversible plastic strains.
- A wetting path (C) under constant stress. The movement of LC yield curve is the same as before, and the same irreversible plastic volumetric strain. These strains correspond to collapse deformation upon wetting.

Therefore, the LC curve links together the compressive strains due to loading with the collapse strains due to wetting.

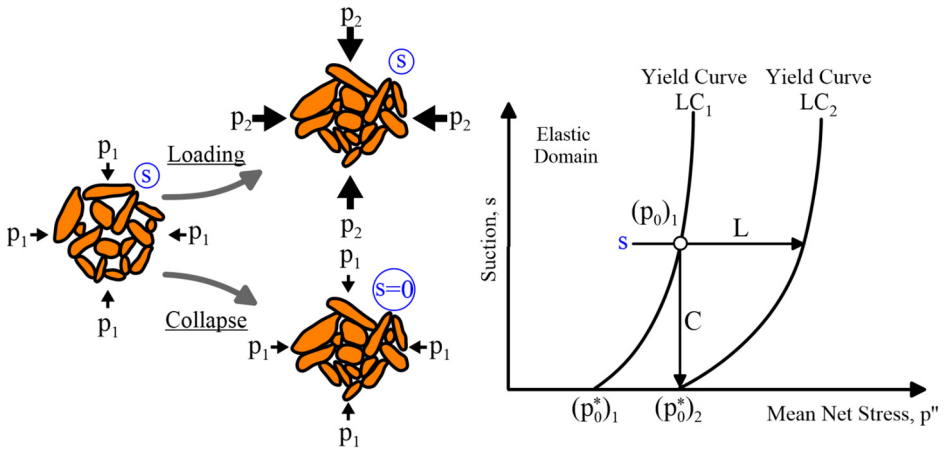

Figure 3-7. Displacement of the LC yield curve on loading at constant suction (path L) and wetting at constant applied stress (path C) (from Gens, 2010).

According to plasticity theory, the movement of the yield curve is associated with irreversible plastic volumetric strains, $d\varepsilon_v^p$. Assuming a hardening law of the Cam-Clay type, the plastic volumetric strain is expressed as:

$$d\varepsilon_v^p = \frac{\lambda_{sat} - \bar{\kappa}_2}{1 + \bar{e}_2} \frac{dP_o^*}{P_o^*} \qquad \text{(Eq. 3-50)}$$

The extension of the model to include deviatoric response and the three-dimensional view of the yield surface in space p-q-s are illustrated in

Figure 3-8. The ellipse of the Modified Cam-Clay model (MCCM) was chosen. As suction increases, the ellipse size also increases. On the right-hand side, p_o increases in accordance with the shape of the LC yield curve. On the left-hand side, p_s increases linearly with suction. The implicit assumption here is that the friction angle (or the slope of the critical state line) is not affected by suction, but the apparent cohesion increases in proportion to suction (Alonso et al., 1990; Gens, 2010).

In order to formulate the Macro-structural constitutive model in a general stress-suction-strain space the fully three-dimensional model, from triaxial space (p-q-s) formulation, is used (Gens, 1995).

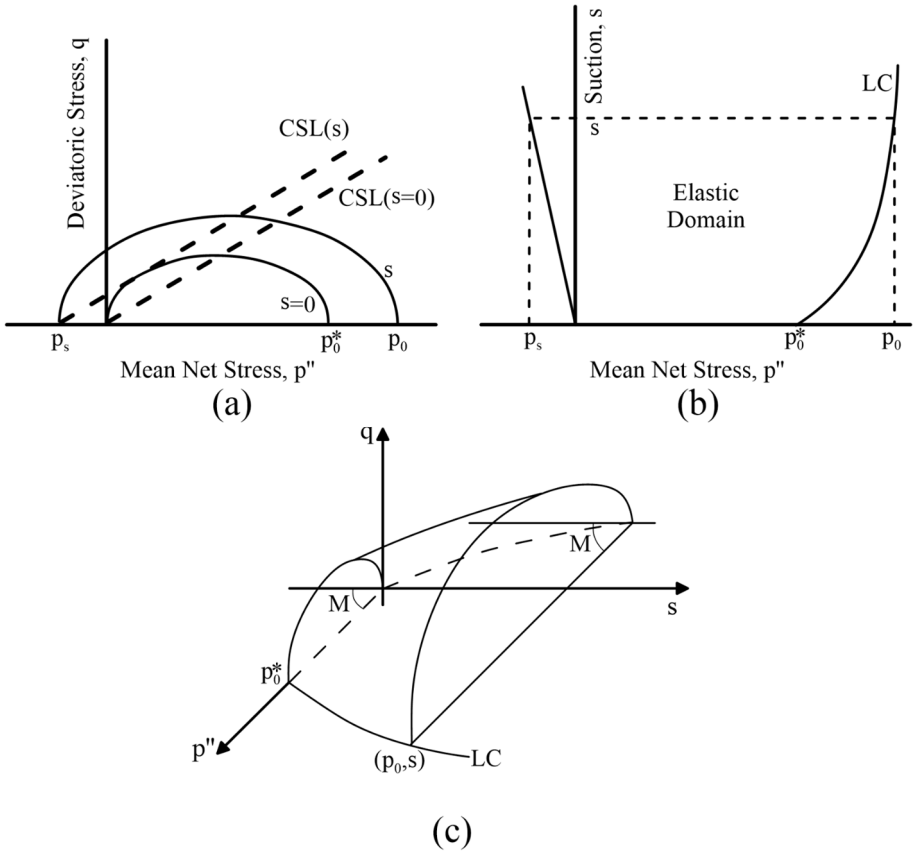

Figure 3-8. a) Yield surfaces in the q–p plane for saturated (s=0) and unsaturated conditions (s); b) Trace of the yield surface in the p–s isotropic plane and c) Three-dimensional view of the yield surface in (p, q, s) stress space (from Gens, 2010).

Now, the yield function F_{LC} determines the elastic domain:

$$F_{LC} = \frac{C_F}{g_F^2(\theta)} J^2 - (p'' + p_s)(p_o - p'') \quad \text{(Eq. 3-51)}$$

$$C_F = \frac{3g_F^2\left(-\frac{\pi}{6}\right)}{M_F^2} \quad \text{(Eq. 3-52)}$$

$$M_F = \frac{6\sin\varphi}{3 - \sin\varphi} \quad \text{(Eq. 3-53)}$$

$$p_s = (p_s)_o + k_s s_2 \quad \text{(Eq. 3-54)}$$

where:

- J is the second deviatoric stress invariant.
- $(p_s)_o$ is the tensile strength at saturated state. Typically $(p_s)_o = 0$.
- k_s is a model parameter.
- φ is the friction angle.
- The dependency on Lode`s angle $g_F(\theta)$ is treated with smoothing techniques (Gesto et al., 2011).

The plastic strains are assumed to have the form:

$$d\boldsymbol{\varepsilon}_{LC}^p = d\lambda_{LC}\mathbf{m}_{LC} = d\lambda_{LC}\frac{\partial G_{LC}}{\partial \boldsymbol{\sigma}} \quad \text{(Eq. 3-55)}$$

where:

- λ_{LC} is the plastic multiplier associated to LC mechanism.
- G_{LC} is the plastic potential function defined as:

$$G_{LC} = \alpha_{BBM}\frac{C_F}{g_G^2(\theta)} J^2 - (p'' + p_s)(p_o - p'') \quad \text{(Eq. 3-56)}$$

It is assumed the associated plasticity in octahedral planes $\left(g_F(\theta) = g_G(\theta)\right)$ and stress space ($\alpha_{BBM} = 1$).

The world-wide acceptance of the BBM model relies in the good reproduction of the main trends of unsaturated soils and the correspondence with the MCC model at saturated state. Accordingly, the natural heritage are the shortcomings of the MCC model. Although the main concerning of the expansive clays is their volumetric behaviour, they can undergo to deviatoric stresses. The Macro-structural constitutive model offers inaccurate responses at over consolidated states which are characteristic in compacted soils. Other yield surface shapes could equally use for overcome this limitation (Georgiadis et al., 2005; Tsiampousi et al., 2013).

The choice of net stresses and suction as stress variables implies that there may be a lack of continuity in the transition between saturated and unsaturated states (Sheng, 2003). Another feature of the BBM is the assumption that there is a link between the shape of the LC yield surface and the post-yield slopes of the virgin consolidation lines at different suctions. Depending on the values of parameters p_c and r computed collapse strains will either continuously increase or decrease with applied stress (Wheeler et al., 2002). However, it is not possible to predict collapse strains that increase with stresses, go through a maximum value and reduce it down to zero at very high stresses. Alonso et al., (2013) presented a modified version to reproduce this behaviour.

3.4.5. Interactions between structural levels

The modelling of expansive clays has been based on the proper recognition of two structural levels (micro and Macro) and the interactions between them. The Figure 3-9 presents in a schematic way those hydro-mechanical interactions reflecting the clay hierarchical structure.

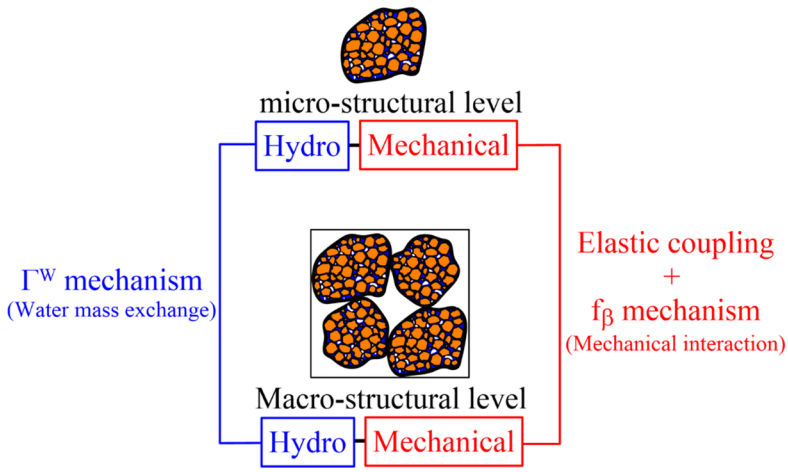

Figure 3-9. Hydro-Mechanical interactions between micro- and Macro-structural levels

These structural interactions arise in a natural manner from the physical assumptions stated in the governing equations (Chapter 2). Here, they are expressed in a constitutive formalism. This double-structure formulation consider the following couplings:

- The assumption of null fabric changes at the elastic regime seems physically reasonable. This imposes geometrical restrictions that relates the elastic modulus of the structural levels.

- In accordance with the experimental evidence depicted in Chapter 2, the micro-structural deformation is considered independent on the Macro-structure, the reverse is not true. This fact has been well established since the first formulation for expansive clays (Gens and Alonso, 1992). Here, the mathematical statement of the mechanism and its physical roots through discrete modelling are given.
- The hydraulic equilibrium between micro- and Macro-structure is not assumed. Consequently, the water mass exchange between them is expected (Figure 2-43). The tendency of the system towards equilibrium induces a coupled time-dependent mechanism.

3.4.5.1. Elastic coupling

Precedent formulations of the double-structural model for expansive clays do not account structural levels interaction at elastic regime (Alonso et al., 1999; Gens et al., 2011; Sanchez et al., 2005). This HM formulation contains an elastic coupling arising from the assumption of null fabric changes at the elastic range. It means that the slips between the clay aggregates are a main factor for the irreversibility at Macro-structural level. The other plastic component is the collapse volumetric strains, accounted by LC mechanism (Section 3.4.3.).

The Figure 3-10 shows a simple analysis of the clay fabric hypothesis considering a small system of particles that do not slip to each other. Swelling and shrinkage particle volumetric deformations are analysed. Finally, the porosity remains constant; ensuring a constant fabric associated to elastic deformation.

A global compatibility analysis taking into account the geometrical restriction from constant clay fabric generates the elastic coupling between Macro- and micro-structural levels.

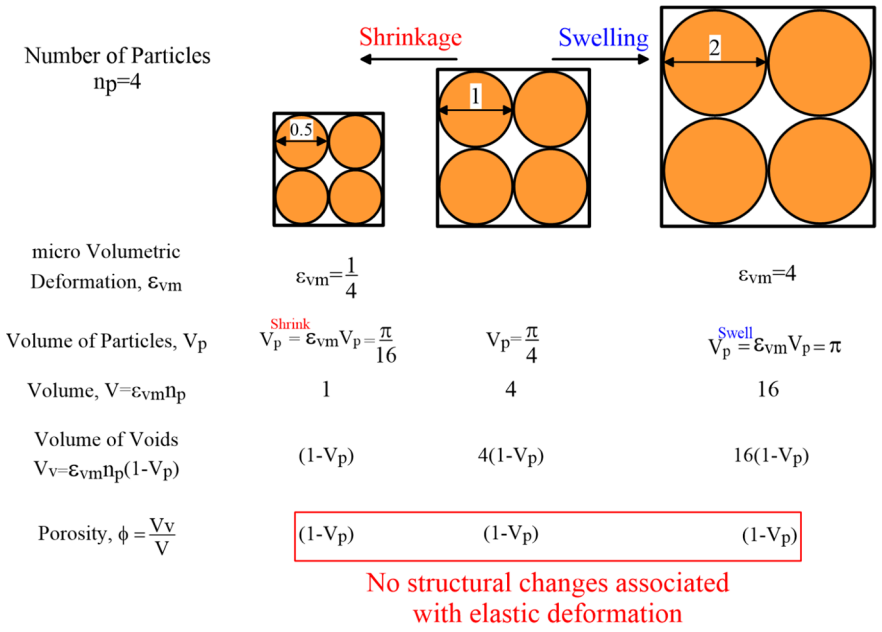

Figure 3-10. Elastic response of a particulate system under swelling and shrinkage deformation.

The total strains of the double-structure porous media is given by the addition of the micro (Eq. 3-39) and Macro (Eq. 3-43) strain components.

$$d\boldsymbol{\varepsilon} = d\bar{\boldsymbol{\varepsilon}}_1 + d\bar{\boldsymbol{\varepsilon}}_2 \qquad \text{(Eq. 3-57)}$$

The above global constitutive equation suggest the definition of a global matrix of elastic coefficient (Eq. 3-58). In the particular case of null irreversible strains ($d\boldsymbol{\varepsilon}^p_{LC}, d\boldsymbol{\varepsilon}^p_{\beta}$) and Macro-structural suction variation, it seems reasonable to assume that strain tensors of the whole soils coincides whit the strain tensor of the medium micro. Therefore, the micro elastic constitutive matrix, $\mathbf{D_1}$, determines the elastic mechanical behaviour of the expansive medium (Eq. 3-59).

$$\mathbf{D}^{-1} = \bar{\mathbf{D}}_{\mathbf{1}}{}^{-1} + \bar{\mathbf{D}}_{\mathbf{2}}{}^{-1} \qquad \text{(Eq. 3-58)}$$

$$\mathbf{D}^{-1} = \mathbf{D}_{\mathbf{1}}{}^{-1} \qquad \text{(Eq. 3-59)}$$

The pure volumetric elastic expressions are generated from the elastic constitutive definition $\mathbf{D_1}^{-1} = \bar{\mathbf{D}}_{\mathbf{1}}{}^{-1} + \bar{\mathbf{D}}_{\mathbf{2}}{}^{-1}$ and the bulks modulus relationship for the micro-structural level (Eq. 3-31). We may also assume, for the sake of simplicity, the same Poisson's ratio both

structural levels and the soil ($\nu_1 = \bar{\nu}_1 = \bar{\nu}_2 = \nu$). Finally, the overall pure elastic behaviour can be determined from the Macro bulk modulus $\overline{\overline{K}}_2$ and a Poisson's ratio ν:

$$\bar{G}_2 = \frac{3(1-2\nu)}{2(1+\nu)}\overline{\overline{K}}_2 \qquad \text{(Eq. 3-60)}$$

$$K = K_1 = \frac{e - e_1}{1+e}\overline{\overline{K}}_2 = \bar{\phi}_2\overline{\overline{K}}_2 \qquad \text{(Eq. 3-61)}$$

$$\overline{\overline{K}}_1 = \frac{e - e_1}{1+e_1}\overline{\overline{K}}_2 = \bar{e}_2\overline{\overline{K}}_2 \qquad \text{(Eq. 3-62)}$$

$$\bar{G}_1 = \frac{e - e_1}{1+e_1} = \bar{e}_2\bar{G}_2 \qquad \text{(Eq. 3-63)}$$

As pointed out in Santamarina, (2001), the small-strain elastic regime exist at constant fabric. The observed deformation and very stiff response are primarily controlled by contact-level deformation and the frictional energy losses are small. Conversely, the large-strain behaviour is determined by fabric changes where slippage at contacts and the ensuing non-elastic behaviour imply stress-history dependent behaviour (See Section 3.4.4.2. and Appendix A).

The consideration of pure elastic zone in the double structure formulation is a questionable choice. Although it was considered in former constitutive models (Alonso et al., 1999), the plastic slips between clay aggregates are required to obtain measurable strain levels. Therefore the existence of some degree of plastic micro-Macro interaction at stress space delimited by the LC yield limit seems to be in agreement with the above analysis (Sánchez, 2004; Sanchez et al., 2005). Later, the Figure 3-14 illustrates the numerical implications of considering a pure elastic zone.

Certainly, the definition of volumetric elastic modulus of micro- and Macro-structure are dependant on the elastic coupling (Table 3-3). For precedent models, there are not any restriction on them. On the contrary, the elastic moduli relationship, due to fabric restriction, is function of the constitutive variables, as follow:

- The global compatibility analysis determined that the elastic response is given by a global bulk modulus for stress changes and macro-structural bulk modulus for suction changes. The Macro-structural

bulk modulus, Ks, seems to be function of the water retention curve and global bulk modulus, but an explicit expression is not founded yet.

- A next step on the enhanced formulation can be the use of the Bishop effective stress for both structural levels. The effect of suction on volumetric elastic strains is accounted for via the variation in Bishop's stress with suction. Therefore, a global bulk modulus define the elastic response of the expansive medium considering the coupling at the elastic response.

Table 3-3. Bulk moduli for different double-structure model formulations. (Subscripts M and m are referred to the Macro and micro, respectively)

Precedent Formulations	Alonso et al., 1999 Sanchez et al., 2005 Gens et al., 2011	Macro bulk modulus K_M K_s micro bulk modulus K_m
Enhanced Formulation	This thesis **Macro-structure** Net stress **micro-structure** Bishop's effective stress	Medium bulk modulus $K=fn(K_m,K_M)$ Macro bulk modulus $K_s=fn(WRC,K)$
	Macro-structure Bishop's effective stress **micro-structure** Bishop's effective stress	Medium bulk modulus $K=fn(K_m,K_M)$

The main advantage of an enhanced formulation is an adequate theoretical analysis, however from the numerical point of view; the flexibility for choosing the model parameters could be affected.

3.4.5.2. Macro-micro mechanical interaction — f_β mechanism

Gens and Alonso, (1992) included the mechanical interaction between the two structures levels as a key point of the double-structure approach to achieve a more comprehensive description of the expansive soil behaviour. It works in unidirectional way, i.e. Macro-structural behaviour can be affected by micro-structural deformations in an irreversible manner. An assumption of the model is that the irreversible deformations of the

Macrostructure ($d\boldsymbol{\varepsilon}_\beta$) are proportional to the microstructural strains according to an interaction function f_β.

$$d\boldsymbol{\varepsilon}_\beta = f_\beta d\bar{\boldsymbol{\varepsilon}}_1 \qquad \text{(Eq. 3-64)}$$

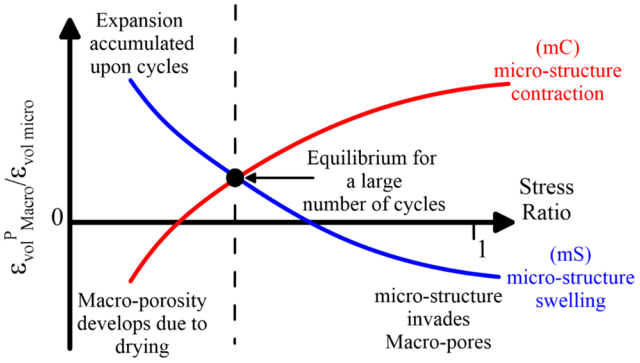

Figure 3-11. Mechanical interaction functions (modified from Alonso et al., 1999).

Two interaction functions f_β are defined: mC for micro-structural contraction paths and mS for micro-structural swelling paths (Figure 3-5). In the case of isotropic load, the interaction functions depend on the stress ratio p/p_o. Figure 3-11 shows a generic representation of the interaction functions indicating the physical phenomena underlying each branches.

The Figure 3-12 depicts the constitutive behaviour due to this structural coupling. The isotropic stress ratio p/p_o is a measure of the degree of openness of the macrostructure. When this ratio is low, it implies a dense packing of the clay aggregates. It is expected that under this condition (closed Macro-structure) the micro-structural swelling (mS path) affects strongly the global arrangements of clay aggregates, inducing large Macro-structural plastic strains. Thus, the higher values of the mS function correspond to low values of p/p_o. In this case, the microstructure effects induce a more open macrostructure, which implies a Macro-structural softening (i.e. the LC moves towards the left). On the other hand, when the micro-structure contracts (mC path) the larger induced Macro-structural plastic strains occur with open macrostructures, that is, p/p_o close to 1. Under this path, the clay tends to a more dense state, which implies a hardening of the Macro-structure due to the pushing of LC yield curve.

This mechanical coupling between both plastic mechanisms is considered at constitutive formulation assuming that:

$$d\varepsilon_v^p = d\varepsilon_{v\_LC}^p + d\varepsilon_{v\_\beta}^p \qquad \text{(Eq. 3-65)}$$

The hardening variable of the Macro-structure P_o^* (Eq. 3-50), depends on total plastic volumetric strains ($d\varepsilon_v^p$) obtained from as the sum of plastic volumetric strains induced by BBM mechanism ($d\varepsilon_{v\_LC}^p$) and the ones coming from the micro-Macro mechanical interaction mechanism ($d\varepsilon_{v\_\beta}^p$). Accordingly, the behaviour of the soil described by the double structure model can be regarded as the consequence of joint action of several mechanisms that can act simultaneously. Some concepts of multi-dissipative materials introduced by Rizzi et al., (1996) have been considered to take into account that different mechanisms can induce plastic deformations.

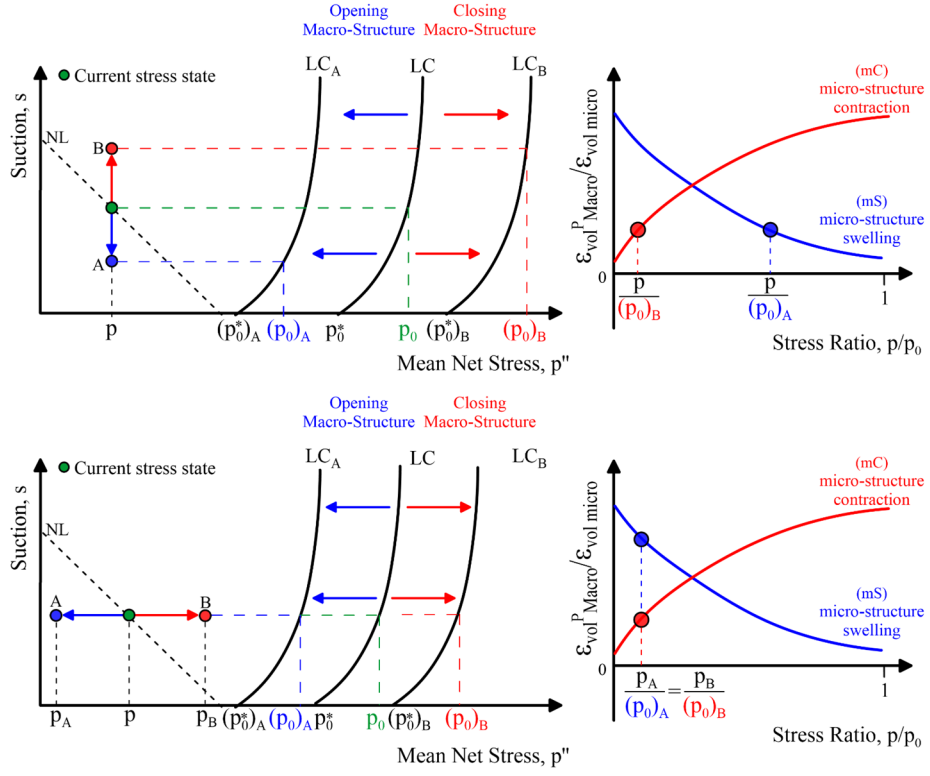

Figure 3-12. Schematic evolution of the LC yield curve due to micro-structural effects.

The material response will depend strongly on the loading and unloading micro-structural direction. Given a generalized stress state and a generalized stress increment, the criterion to identify the micro-structural stress path can be specified as:

$\mathbf{n}_c^T \cdot d\boldsymbol{\sigma}^e > 0$ as micro-Structural contraction criterion (mC) (Eq. 3-66)

$\mathbf{n}_s^T \cdot d\boldsymbol{\sigma}^e > 0$ as micro-Structural swelling criterion (mS) (Eq. 3-67)

$\mathbf{n}_s^T \cdot d\boldsymbol{\sigma}^e = 0$ as neutral loading criterion (Eq. 3-68)

where:

- $\mathbf{n}_c^T$ and $\mathbf{n}_s^T$ are auxiliary vectors to determine the loading criteria (Figure 3-13).

In precedent double-structure formulations, exponential or sigmoidal expressions have been selected for the mathematical statement of f_β. Here, the following exponential functions are chosen (Eq. 3-69).

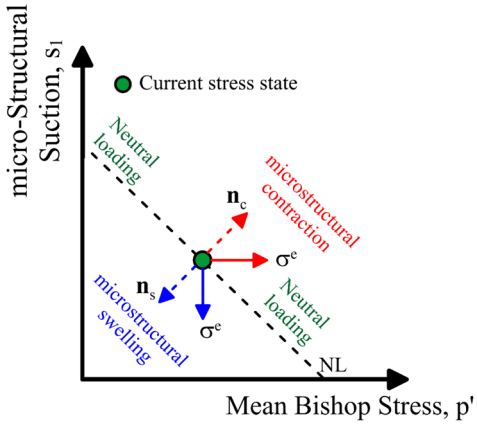

Figure 3-13. Definition of microstructural swelling and contraction directions (Sánchez, 2004).

$$f_\beta = \begin{cases} f_{mC1} + (f_{mC0} - f_{mC1})\left(1 - \mu_\beta\right)^{n_{mC}} \text{ for mC paths} \\ f_{mS1} + (f_{mS0} - f_{mS1})\left(1 - \mu_\beta\right)^{n_{mS}} \text{ for mS paths} \end{cases} \quad \text{(Eq. 3-69)}$$

where:

- μ_β is the stress ratio for generic stress states (Sanchez et al., 2005).
- f_{mS1}, f_{mS0} and n_{mS} are model parameters for the case of micro-structural swelling.
- f_{mC1}, f_{mC0} and n_{mC} are model parameters for the case of micro-structural swelling.

There are several experimental works oriented to identify the different phenomena and mechanisms included in this coupling, as well as, to determine the model parameters. In this line, it can be mentioned the work of Alonso et al, (1994), Garcia-Escudero (2001), Alonso et al, (2001) and Lloret et al, (2003). However, they are mainly based on the specimen response and some theoretical hypotheses on the micro-structural behaviour. From this perspective, the proper identification of the physical roots underlying this mechanical coupling is limited.

The Appendix A presents a discrete modelling in which the behaviour of expansive particles and global particulate system provides new insights into the physical sources of their mechanical interaction. It is found that the phenomenon responsible of the structural mechanical interactions comes from the geometrical reorganization of the spherical particles (i.e. a mimic of clay aggregates) due to hydro-mechanical actions. Also, it was demonstrate that the slippage at contacts and the ensuing plastic behaviour are stress-history dependant (Santamarina, 2001).

The analysis on the structural elastic coupling gave some physical reasons to disregard a pure elastic domain (Section 3.4.4.1.). Moreover, no clear evidence exists concerning the shapes of the internal yield surfaces corresponding to the interaction mechanisms between the two structural levels. Their experimental determination is not likely to be easy either. Therefore, generalized plasticity theory was used to deal with the consideration of two directions of different behaviour and the formulation of proper elasto-plastic laws for each region (Sánchez, 2004; Sanchez et al., 2005).

As additional benefit, the generalized plasticity is a formulation well suited for implementation in numerical codes in a simple, robust and structured manner. In Figure 3-14 is shown the different formulations of this micro-Macro mechanical interaction in stress space. Alonso et al., (1999) used three interacting yield surface: the LC curve corresponds to the Macro-structural model and the two yield surfaces (SI and SD) represent the loci of the points from which irreversible strains on the Macro-structure start to occur. If SI and SD yield surfaces occupies the same place at stress space, there is always some degree of mechanical interaction between the structural levels (Lloret et al., 2003). Although with these formulations the pure elastic domain can be minimized (or

even negligible), the numerical implementation of several intersected yield surface is a complex procedure.

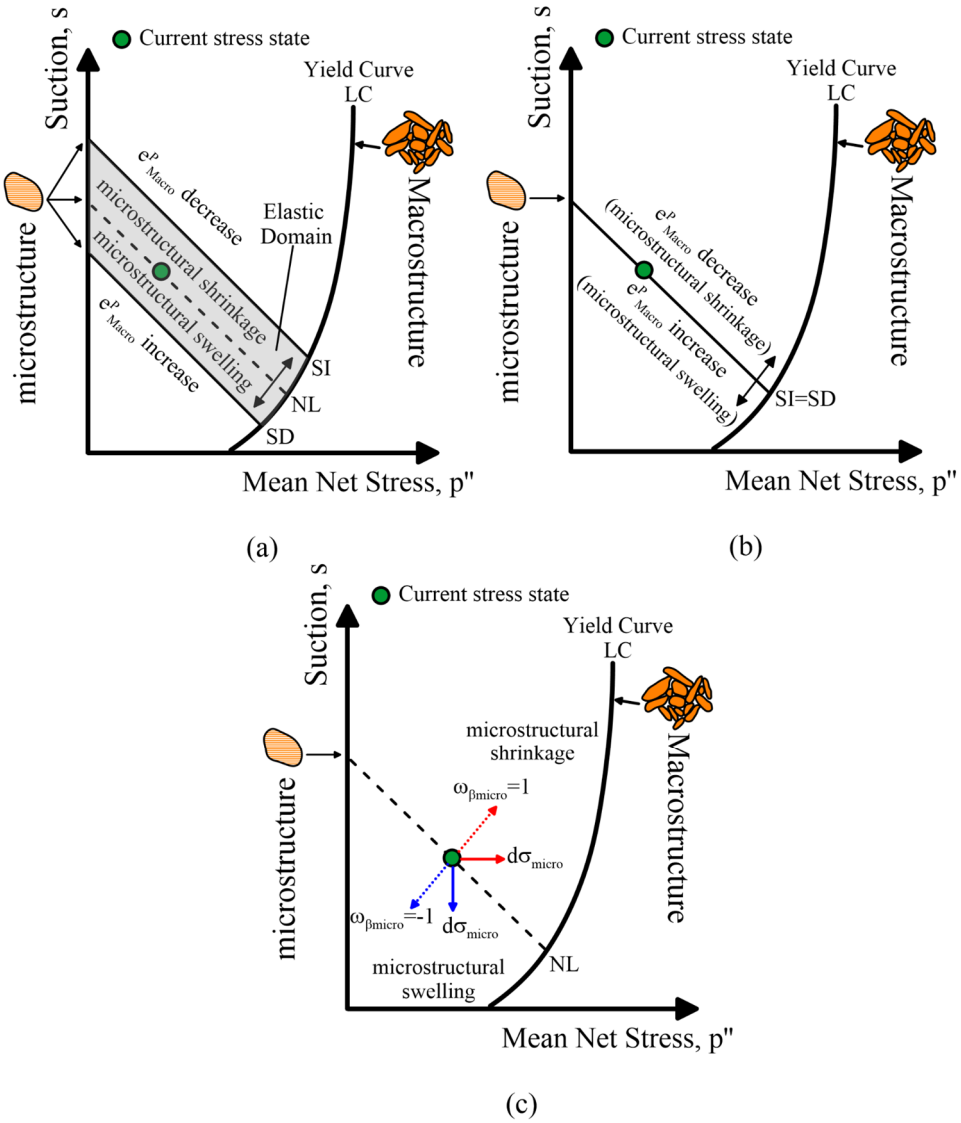

Figure 3-14. micro-Macro mechanical interaction in stress-space. a) Elastic domain defined by SI and SD (Alonso et al., 1999) , SI and SD occupying the same place (Lloret et al., 2003) and generalized plasticity (Sánchez, 2004; Sanchez et al., 2005 and this work).

3.4.5.3. Macro-micro hydraulic interaction — Γ^w mechanism

An unbalanced hydraulic potential state between structural levels explains the long-term volumetric deformations of clays. Navarro and Alonso, (2001) explains the secondary compression of clays in terms of water transfer from clay aggregates to the bulk water driven by different chemical potential. For expansive clays, the water will migrate from one structural level to the other one ensuring a time dependent expansion or shrinkage with important implications in the clay fabric evolution (see Chapter 2).

It is well accepted that the suctions difference is the thermodynamic force that generates water mass transfer (Gens et al., 2011). If a classical linear approach is used (de Groot and Mazur, 1984), the mass exchange of water may be determined as:

$$\Gamma^w = \gamma(s_1 - s_2) \qquad \text{(Eq. 3-70)}$$

where:

- Γ^w is the mass-transfer rate per unit volume from micro to Macro or vice versa.
- γ is a phenomenological leakage parameter.

Under a constant gas pressure in the double-structure porous medium, the formulation is based on the difference in water pressure at Macro and micro levels.

$$\Gamma^w = \gamma(P_{L2} - P_{L1}) \qquad \text{(Eq. 3-71)}$$

This micro-Macro water interchange affects the total deformation of the micro-structure due to the dependence of the micro liquid pressure changes on the amount of water interchanged between the two structural levels (Eq. 3-39).

The leakage parameter, γ, is sometimes associated with some geometric characteristics of the medium. For fractured clayey media the specific surface of the matrix block, the number of fractures and fracture intervals or the average size of clay blocks have been proposed. Because of lack of relevant geometric information in expansive media, it is considered a constant value of the leakage parameter that is typically calibrate it by back-analysis.

An alternative option for a geometrical characteristic of the double-structure arrangement can be the openness of the Macro-structure. The isotropic stress ratio p/p_o is a constitutive measure of local distance between the water at two structural levels (Figure 3-15). An open fabric can contribute to lower rates of water mass transfer. An exponential dependence on this stress ratio (p/p_o) is indicated in (Eq. 3-72). In spite of the lack of clear physical evidence, these relations imposes another hydro-mechanical coupling.

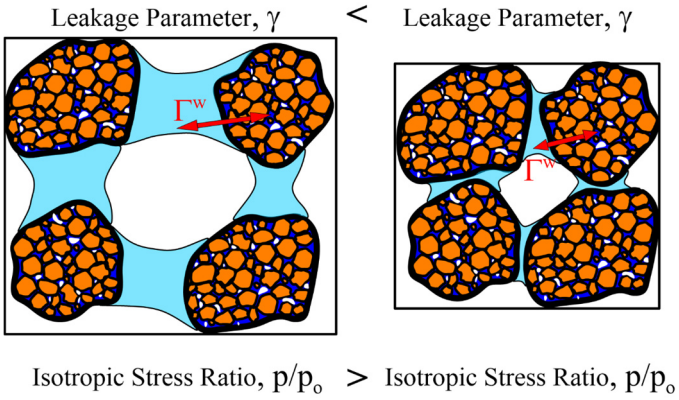

Figure 3-15. Leakage parameter as function of Macro pore volume fraction.

$$\gamma = \gamma_o \exp\left[\omega\left(\frac{p}{p_o} - \left(\frac{p}{p_o}\right)_{ref}\right)\right] \qquad \text{(Eq. 3-72)}$$

where:

- γ_o is the initial leakage parameter.
- ω is a model parameter the mass-transfer rate per unit volume from micro to Macro or vice versa.
- $(p/p_o)_{ref}$ is a reference value of the isotropic stress ratio.

3.4.6. Elasto-plastic stress-strain relations

The constitutive model described contains two plastic mechanism:

- A plastic mechanism associated with the yield of the Macro-structure defined by a classical plasticity law.
- A plastic mechanism associated with the interaction between micro- and Macro-structure described by a generalized plasticity.

Now, it is worth to define a global compatibility analysis taking into account the mentioned plastic mechanisms. For the micro level, we have established an expression for the variation of the micro-pores respect to the total volume of the soil expressed for $d\bar{\boldsymbol{\varepsilon}}_1$ (Eq. 3-39), then, it is possible to derive:

$$d\boldsymbol{\sigma}'' = \bar{\mathbf{D}}_{\mathbf{1}} d\bar{\boldsymbol{\varepsilon}}_{\mathbf{1}} - [\zeta_{L1} dP_{L1} + dmax\ (P_{g2}, P_{L2})]\mathbf{m} \quad \text{(Eq. 3-73)}$$

On the other hand, we found a constitutive expression for the expansive soil, using the stress assumption $\boldsymbol{\sigma}_2'' = \boldsymbol{\sigma}''$ (see Table 3-2):

$$\begin{aligned} d\boldsymbol{\sigma}'' = \mathbf{D}\Big(d\boldsymbol{\varepsilon} - \frac{1}{3K_1}[\zeta_{L1} dP_{L1} + dmax\ (P_{g2}, P_{L2})]\mathbf{m} - d\boldsymbol{\varepsilon}_{s_2}^{r} \\ - d\boldsymbol{\varepsilon}_{LC}^{p} - d\boldsymbol{\varepsilon}_{\beta}^{p}\Big) \end{aligned} \quad \text{(Eq. 3-74)}$$

$$\begin{aligned} d\boldsymbol{\sigma}'' = \mathbf{D}d\boldsymbol{\varepsilon} - \frac{K}{K_s} ds_2 \mathbf{m} - \frac{K}{K_1}[\zeta_{L1} dP_{L1} + dmax\ (P_{g2}, P_{L2})]\mathbf{m} \\ - d\lambda_{LC}\mathbf{D}\mathbf{m}_{LC} - f_\beta \mathbf{D} d\bar{\boldsymbol{\varepsilon}}_1 \end{aligned} \quad \text{(Eq. 3-75)}$$

So, the following compatibility condition must be permanently fulfilled:

$$\begin{aligned} \bar{\mathbf{D}}_{\mathbf{1}} d\bar{\boldsymbol{\varepsilon}}_{\mathbf{1}} - [\zeta_{L1} dP_{L1} + dmax\ (P_{g2}, P_{L2})]\mathbf{m} \\ = \mathbf{D}d\boldsymbol{\varepsilon} - \frac{K}{K_s} ds_2 \mathbf{m} \\ - \frac{K}{K_1}[\zeta_{L1} dP_{L1} + dmax\ (P_{g2}, P_{L2})]\mathbf{m} - d\lambda_{LC}\mathbf{D}\mathbf{m}_{LC} \\ - f_\beta \mathbf{D} d\bar{\boldsymbol{\varepsilon}}_1 \end{aligned} \quad \text{(Eq. 3-76)}$$

$$d\bar{\boldsymbol{\varepsilon}}_{\mathbf{1}} = (\bar{\mathbf{D}}_{\mathbf{1}} + f_\beta \mathbf{D})^{-1}\mathbf{D}(d\boldsymbol{\varepsilon} - d\lambda_{LC}\mathbf{m}_{LC}) - \frac{K}{K_s} ds_2 (\bar{\mathbf{D}}_{\mathbf{1}} + f_\beta \mathbf{D})^{-1}\mathbf{m} \quad \text{(Eq. 3-77)}$$

where:

$$\bar{\mathbf{D}}_{\mathbf{1}} = \frac{1+e}{1+e_1}\mathbf{D} \quad \text{(Eq. 3-78)}$$

$$\bar{\mathbf{D}}_{\mathbf{1}} + f_\beta \mathbf{D} = \left(\frac{1+e}{1+e_1} + f_\beta\right)\mathbf{D} \quad \text{(Eq. 3-79)}$$

Finally, we obtain a fundamental relationship:

$$d\bar{\boldsymbol{\varepsilon}}_{\mathbf{1}} = \left(\frac{1+e}{1+e_1} + f_\beta\right)^{-1}\left[d\boldsymbol{\varepsilon} - d\lambda_{LC}\mathbf{m}_{LC} - \frac{1}{3K_s} ds_2 \mathbf{m}\right] \quad \text{(Eq. 3-80)}$$

In classical plasticity theory, it is assumed that the material behaves either as an elastic or an elasto-plastic solid. The yield surface defines the

transition from elasticity to plasticity, stress states inside the yield surface are considered as elastic ($F_{LC} < 0$). In generalized plasticity theory, the state of the material is determined directly from the control variables: generalised stresses (i.e. stress and suction), strains and a finite number of internal variables. A process of loading is defined as elastic if the set of internal variables remains unchanged (Sanchez et al., 2005; Sánchez et al., 2008). Therefore, three different cases can be distinguished in relation to the current stress state and the number of plastic mechanisms active: i) Only the plastic mechanism associated with mechanical interaction (β) is active; ii) Only the plastic mechanism associated with Macro-structural yielding (LC) is active; and iii) the two plastic mechanism are active simultaneously. The ensuing items present the elasto-plastic relations for each specific case.

3.4.6.1. Case 1: only the plastic mechanism β is active

We are assuming that β mechanism is always active (i.e. null elastic zone), thus the elasto-plastic relations corresponds to the case $d\lambda_{LC} = 0$.

$$d\bar{\boldsymbol{\varepsilon}}_{\mathbf{1}} = \left(\frac{1+e}{1+e_1} + f_\beta\right)^{-1}\left[d\boldsymbol{\varepsilon} - \frac{1}{3K_s} ds_2 \mathbf{m}\right] \quad \text{(Eq. 3-81)}$$

$$dP_o^* = f_\beta \frac{(1+\bar{e}_2)P_o^*}{\lambda_{sat} - \bar{\kappa}_2} \mathbf{m}^T d\bar{\boldsymbol{\varepsilon}}_{\mathbf{1}} \quad \text{(Eq. 3-82)}$$

$$dP_{L1} = \frac{\rho_{L1} S_{L1}}{\bar{\phi}_1 \left(\frac{1+e}{1+e_1} + f_\beta\right) \frac{\partial(\rho_{L1} S_{L1})}{\partial P_{L1}}} \left[d\varepsilon_v - \frac{1}{K_s} ds_2 + \frac{\left(\frac{1+e}{1+e_1} + f_\beta\right)}{\rho_{L1} S_{L1}} \Gamma^w dt \right] \quad \text{(Eq. 3-83)}$$

The above equations lead to the fact that, if the micro-structure is saturated and the micro liquid density is constant, then it is not possible to obtain the value of dP_{L1}. Because if $d\lambda_{LC} = d\varepsilon_v = ds_2 = 0$, then $(d\bar{\varepsilon}_v)_1 = 0$ and the volume of micro-pores remains constant. Nevertheless, under this condition we may have $P_{L1} \neq P_{L2} \rightarrow \Gamma^w \neq 0$. Then, it is necessary that $S_{L1}(d\rho_{L1}/dP_{L1}) + \rho_{L1}(dS_{L1}/dP_{L1}) \neq 0$, even when the micro level is saturated. It means $(d\rho_{L1}/dP_{L1}) \neq 0$ at any time. In other

words, it is necessary to guarantee some water storage capacity even in the case of constant micro-structural volume.

Finally, the stress-strain relation is:

$$\mathrm{d}\boldsymbol{\sigma}'' = \mathbf{D}\left(\mathrm{d}\boldsymbol{\varepsilon} - \frac{1}{3\mathrm{K_s}}\mathrm{ds_2}\mathbf{m} - \frac{1}{\mathrm{K_1}}\left[\zeta_{\mathrm{L1}}\mathrm{dP_{L1}} + \mathrm{dmax}\ (\mathrm{P_{g2}}, \mathrm{P_{L2}})\right]\mathbf{m} - \mathrm{f_\beta}\mathbf{D}\mathrm{d}\bar{\boldsymbol{\varepsilon}}_1\right) \quad \text{(Eq. 3-84)}$$

3.4.6.2. Case 2: only the plastic mechanism LC is active

The unknowns are the plastic multiplier increment $\mathrm{d}\lambda_{\mathrm{LC}}$ and the micro-liquid pressure increment $\mathrm{dP_{L1}}$. Therefore, it is necessary to solve the next system of equations:

$$\begin{bmatrix}\mathrm{H_{11}} & \mathrm{H_{12}}\\ \mathrm{H_{21}} & \mathrm{H_{22}}\end{bmatrix}\begin{bmatrix}\mathrm{d}\lambda_{\mathrm{LC}}\\ \mathrm{dP_{L1}}\end{bmatrix} = \begin{bmatrix}\mathrm{C_1}\\ \mathrm{C_2}\end{bmatrix} \quad \text{(Eq. 3-85)}$$

where:

$$\mathrm{H_{11}} = (\mathrm{A}-1)\boldsymbol{\nu}^{\mathrm{T}}\mathbf{m}_{\mathrm{LC}} \quad \text{(Eq. 3-86)}$$

$$\mathrm{H_{12}} = \zeta_{\mathrm{L1}}\mathbf{n}_{\mathrm{LC}}^{\mathrm{T}}\mathbf{m} \quad \text{(Eq. 3-87)}$$

$$\mathrm{H_{21}} = \mathbf{m}^{\mathrm{T}}\mathbf{m}_{\mathrm{LC}} \quad \text{(Eq. 3-88)}$$

$$\mathrm{H_{22}} = \frac{\bar{\phi}_1}{\rho_{\mathrm{L1}}\mathrm{S_{L1}}}\left(\frac{1+\mathrm{e}}{1+\mathrm{e_1}}\right)\left[\mathrm{S_{L1}}\frac{\mathrm{d}\rho_{\mathrm{L1}}}{\mathrm{dP_{L1}}} + \rho_{\mathrm{L1}}\frac{\mathrm{dS_{L1}}}{\mathrm{dP_{L1}}}\right] \quad \text{(Eq. 3-89)}$$

$$\mathrm{C_1} = (\mathbf{n}_{\mathrm{LC}}^{\mathrm{T}}\mathbf{D})\mathrm{d}\boldsymbol{\varepsilon} + \left[l_{\mathrm{LC}} - \frac{1}{3\mathrm{K_s}}(\mathbf{n}_{\mathrm{LC}}^{\mathrm{T}}\mathbf{D})\mathbf{m}\right]\mathrm{ds_2} - \mathrm{dmax}\ (\mathrm{P_{g2}}, \mathrm{P_{L2}})\mathbf{n}_{\mathrm{LC}}^{\mathrm{T}}\mathbf{m} \quad \text{(Eq. 3-90)}$$

$$\mathrm{C_2} = \mathrm{d}\varepsilon_{\mathrm{v}} - \frac{1}{\mathrm{K_s}}\mathrm{ds_2} + \frac{\Gamma^{\mathrm{w}}}{\rho_{\mathrm{L1}}\mathrm{S_{L1}}}\left(\frac{1+\mathrm{e}}{1+\mathrm{e_1}}\right)\mathrm{dt} \quad \text{(Eq. 3-91)}$$

$$\mathbf{n}_{\mathrm{LC}} = \frac{\partial \mathrm{F_{LC}}}{\partial \boldsymbol{\sigma}} \quad \text{(Eq. 3-92)}$$

$$\mathbf{m}_{\mathrm{LC}} = \frac{\partial \mathrm{G_{LC}}}{\partial \boldsymbol{\sigma}} \quad \text{(Eq. 3-93)}$$

$$l_{\mathrm{LC}} = \frac{\partial \mathrm{F_{LC}}}{\partial \mathrm{s_2}} \quad \text{(Eq. 3-94)}$$

$$\boldsymbol{\nu} = \frac{\partial \mathrm{F_{LC}}}{\partial \mathrm{p_o}}\frac{\partial \mathrm{p_o}}{\partial \mathrm{P_o^*}}\frac{\mathrm{d}\varepsilon_{\mathrm{v}}^{\mathrm{p}}}{\partial \mathrm{P_o^*}}\mathbf{m} - \mathbf{D}\mathbf{n}_{\mathrm{LC}} \quad \text{(Eq. 3-95)}$$

$$\det = \mathrm{H_{11}H_{22}} - \mathrm{H_{12}H_{21}} \quad \text{(Eq. 3-96)}$$

The evolution of saturated pre-consolidation stress becomes:

$$\mathrm{d}P_o^* = \frac{(1+\bar{e}_2)P_o^*}{\lambda_{sat}-\bar{\kappa}_2}\mathbf{m}^T\mathbf{m}_{LC}\mathrm{d}\lambda_{LC} \quad \text{(Eq. 3-97)}$$

Finally, the stress-strain relation is defined by the follow general expression:

$$\mathrm{d}\boldsymbol{\sigma}'' = \mathbf{D}^{ep}\mathrm{d}\boldsymbol{\varepsilon} + \mathbf{h}_{s_2}\mathrm{d}s_2 + \mathbf{h}_{p_f}\mathrm{d}p_f + \mathbf{h}_{dt}\mathrm{d}t \quad \text{(Eq. 3-98)}$$

where:

$$\mathbf{D}^{ep} = \mathbf{D}(\mathbf{I} - \mathbf{m}_{LC}\mathbf{w}_1^T) - \zeta_{L1}\mathbf{m}\mathbf{w}_2^T \quad \text{(Eq. 3-99)}$$

$$\mathbf{h}_{s_2} = \left(\frac{K}{K_s} + \zeta_{L1}B_4\right)\mathbf{m} + \mathbf{D}\mathbf{m}_{LC}B_1 \quad \text{(Eq. 3-100)}$$

$$\mathbf{h}_{p_f} = -(\zeta_{L1}B_5 + 1)\mathbf{m} - \mathbf{D}\mathbf{m}_{LC}B_2 \quad \text{(Eq. 3-101)}$$

$$\mathbf{h}_{dt} = -[\zeta_{L1}B_6\mathbf{m} + \mathbf{D}\mathbf{m}_{LC}B_3]\Gamma^w \quad \text{(Eq. 3-102)}$$

$$\mathbf{w}_1^T = \frac{1}{\det}[H_{22}\mathbf{n}_{LC}^T\ \mathbf{D} - H_{12}\mathbf{m}^T] \quad \text{(Eq. 3-103)}$$

$$\mathbf{w}_2^T = \frac{1}{\det}[H_{11}\mathbf{m}^T - H_{21}\mathbf{n}_{LC}^T\ \mathbf{D}] \quad \text{(Eq. 3-104)}$$

$$B_1 = B_1 = \frac{1}{\det}\left[H_{22}\left(l_{LC} - \frac{K}{K_s}\mathbf{n}_{LC}^T\ \mathbf{m}\right) + \frac{H_{12}}{K_s}\right] \quad \text{(Eq. 3-105)}$$

$$B_2 = \frac{H_{22}}{\det}\mathbf{n}_{LC}^T\mathbf{m} \quad \text{(Eq. 3-106)}$$

$$B_3 = \frac{H_{12}}{\det}\frac{\left(\frac{1+e}{1+e_1} + f_\beta\right)}{\rho_{L1}S_{L1}} \quad \text{(Eq. 3-107)}$$

$$B_4 = \frac{1}{\det}\left[\frac{H_{11}}{K_s} + H_{21}\left(l_{LC} + \frac{K}{K_s}\mathbf{n}_{LC}^T\ \mathbf{m}\right)\right] \quad \text{(Eq. 3-108)}$$

$$B_5 = \frac{H_{21}}{\det}\mathbf{n}_{LC}^T\mathbf{m} \quad \text{(Eq. 3-109)}$$

$$B_6 = \frac{H_{11}}{\det}\frac{\left(\frac{1+e}{1+e_1}\right)}{\rho_{L1}S_{L1}} \quad \text{(Eq. 3-110)}$$

3.4.6.3. Case 3: two plastic mechanism (β+LC) are active

For this case, the system of equations reads:

$$\begin{bmatrix} H_{11} & H_{12} \\ H_{21} & H_{22} \end{bmatrix}\begin{bmatrix} \mathrm{d}\lambda_{LC} \\ \mathrm{d}P_{L1} \end{bmatrix} = \begin{bmatrix} C_1 \\ C_2 \end{bmatrix} \quad \text{(Eq. 3-111)}$$

where:

$$H_{11} = (A-1)\boldsymbol{\nu}^T\mathbf{m}_{LC} \quad \text{(Eq. 3-112)}$$

$$H_{12} = \zeta_{L1}\mathbf{n}_{LC}^{T}\mathbf{m} \quad \text{(Eq. 3-113)}$$

$$H_{21} = \mathbf{m}^{T}\mathbf{m}_{LC} \quad \text{(Eq. 3-114)}$$

$$H_{22} = \frac{\bar{\phi}_1}{\rho_{L1}S_{L1}}\left(\frac{1+e}{1+e_1}+f_\beta\right)\left[S_{L1}\frac{d\rho_{L1}}{dP_{L1}}+\rho_{L1}\frac{dS_{L1}}{dP_{L1}}\right] \quad \text{(Eq. 3-115)}$$

$$C_1 = (\mathbf{n}_{LC}^{T}\mathbf{D}+A\boldsymbol{\nu}^{T})d\boldsymbol{\varepsilon}+\left[l_{LC}-\frac{1}{3K_s}(\mathbf{n}_{LC}^{T}\mathbf{D}+A\boldsymbol{\nu}^{T})\mathbf{m}\right]ds_2 - d\max\,(P_{g2},P_{L2})\mathbf{n}_{LC}^{T}\mathbf{m} \quad \text{(Eq. 3-116)}$$

$$C_2 = d\varepsilon_v - \frac{1}{K_s}ds_2 + \frac{\left(\frac{1+e}{1+e_1}+f_\beta\right)}{\rho_{L1}S_{L1}}\Gamma^{w}dt \quad \text{(Eq. 3-117)}$$

$$A = f_\beta\left(\frac{1+e}{1+e_1}+f_\beta\right)^{-1} \quad \text{(Eq. 3-118)}$$

$$\mathbf{n}_{LC} = \frac{\partial F_{LC}}{\partial\boldsymbol{\sigma}} \quad \text{(Eq. 3-119)}$$

$$\mathbf{m}_{LC} = \frac{\partial G_{LC}}{\partial\boldsymbol{\sigma}} \quad \text{(Eq. 3-120)}$$

$$l_{LC} = \frac{\partial F_{LC}}{\partial s_2} \quad \text{(Eq. 3-121)}$$

$$\boldsymbol{\nu} = \frac{\partial F_{LC}}{\partial p_o}\frac{\partial p_o}{\partial P_o^*}\frac{d\varepsilon_v^{p}}{\partial P_o^*}\mathbf{m}-\mathbf{D}\mathbf{n}_{LC} \quad \text{(Eq. 3-122)}$$

$$\det = H_{11}H_{22}-H_{12}H_{21} \quad \text{(Eq. 3-123)}$$

The evolution of saturated pre-consolidation stress becomes:

$$dP_o^* = \frac{(1+\bar{e}_2)P_o^*}{\lambda_{sat}-\bar{\kappa}_2}(\mathbf{m}^{T}\mathbf{m}_{LC}d\lambda_{LC}+f_\beta\mathbf{m}^{T}d\bar{\boldsymbol{\varepsilon}}_{\mathbf{1}}) \quad \text{(Eq. 3-124)}$$

Here, the stress-strain relation is:

$$d\boldsymbol{\sigma}'' = \mathbf{D}^{ep}d\boldsymbol{\varepsilon}+\mathbf{h}_{s_2}ds_2+\mathbf{h}_{p_f}dp_f+\mathbf{h}_{dt}dt \quad \text{(Eq. 3-125)}$$

where:

$$\mathbf{D}^{ep} = (A-1)\mathbf{D}+(A-1)\mathbf{D}\mathbf{m}_{LC}\mathbf{w}_1^{T}-\zeta_{L1}\mathbf{m}\mathbf{w}_2^{T} \quad \text{(Eq. 3-126)}$$

$$\mathbf{h}_{s_2} = \left(\zeta_{L1}B_4+(A-1)\frac{K}{K_s}\right)\mathbf{m}+\mathbf{D}\mathbf{m}_{LC}B_1 \quad \text{(Eq. 3-127)}$$

$$\mathbf{h}_{p_f} = (\zeta_{L1}B_5-1)\mathbf{m}-(A-1)\mathbf{D}\mathbf{m}_{LC}B_2 \quad \text{(Eq. 3-128)}$$

$$\mathbf{h}_{dt} = -[\zeta_{L1}B_6\mathbf{m}+(A-1)\mathbf{D}\mathbf{m}_{LC}B_3]\Gamma^{w} \quad \text{(Eq. 3-129)}$$

$$\mathbf{w}_1^{\mathrm{T}} = \frac{1}{\det}\left[\mathrm{H}_{22}\left((1-\mathrm{A})\mathbf{n}_{\mathrm{LC}}^{\mathrm{T}}\,\mathbf{D} + \mathrm{A}\frac{\partial \mathrm{F}_{\mathrm{LC}}}{\partial \mathrm{p_o}}\frac{\partial \mathrm{p_o}}{\partial \mathrm{P_o^*}}\frac{\mathrm{d}\varepsilon_{\mathrm{v}}^{\mathrm{p}}}{\partial \mathrm{P_o^*}}\mathbf{m}^{\mathrm{T}}\right) - \mathrm{H}_{12}\mathbf{m}^{\mathrm{T}}\right] \quad \text{(Eq. 3-130)}$$

$$\mathbf{w}_2^{\mathrm{T}} = \frac{1}{\det}\left[\mathrm{H}_{11}\mathbf{m}^{\mathrm{T}} - \mathrm{H}_{21}\left((1-\mathrm{A})\mathbf{n}_{\mathrm{LC}}^{\mathrm{T}}\,\mathbf{D} + \mathrm{A}\frac{\partial \mathrm{F}_{\mathrm{LC}}}{\partial \mathrm{p_o}}\frac{\partial \mathrm{p_o}}{\partial \mathrm{P_o^*}}\frac{\mathrm{d}\varepsilon_{\mathrm{v}}^{\mathrm{p}}}{\partial \mathrm{P_o^*}}\mathbf{m}^{\mathrm{T}}\right)\right] \quad \text{(Eq. 3-131)}$$

$$\mathrm{B}_1 = \mathrm{B}_1 = \frac{1}{\det}\left[\mathrm{H}_{22}\left(l_{\mathrm{LC}} - \frac{\mathrm{A}}{\mathrm{K_s}}\frac{\partial \mathrm{F}_{\mathrm{LC}}}{\partial \mathrm{p_o}}\frac{\partial \mathrm{p_o}}{\partial \mathrm{P_o^*}}\frac{\mathrm{d}\varepsilon_{\mathrm{v}}^{\mathrm{p}}}{\partial \mathrm{P_o^*}} + (\mathrm{A}-1)\frac{\mathrm{K}}{\mathrm{K_s}}\mathbf{n}_{\mathrm{LC}}^{\mathrm{T}}\,\mathbf{m}\right) + \frac{\mathrm{H}_{12}}{\mathrm{K_s}}\right] \quad \text{(Eq. 3-132)}$$

$$\mathrm{B}_2 = \frac{\mathrm{H}_{22}}{\det}\mathbf{n}_{\mathrm{LC}}^{\mathrm{T}}\mathbf{m} \quad \text{(Eq. 3-133)}$$

$$\mathrm{B}_3 = \frac{\mathrm{H}_{12}}{\det}\frac{\left(\frac{1+\mathrm{e}}{1+\mathrm{e_1}} + \mathrm{f}_\beta\right)}{\rho_{\mathrm{L1}}\mathrm{S}_{\mathrm{L1}}} \quad \text{(Eq. 3-134)}$$

$$\mathrm{B}_4 = \frac{1}{\det}\left[\frac{\mathrm{H}_{11}}{\mathrm{K_s}} + \mathrm{H}_{21}\left(l_{\mathrm{LC}} - \frac{\mathrm{A}}{\mathrm{K_s}}\frac{\partial \mathrm{F}_{\mathrm{LC}}}{\partial \mathrm{p_o}}\frac{\partial \mathrm{p_o}}{\partial \mathrm{P_o^*}}\frac{\mathrm{d}\varepsilon_{\mathrm{v}}^{\mathrm{p}}}{\partial \mathrm{P_o^*}} + (\mathrm{A}-1)\frac{\mathrm{K}}{\mathrm{K_s}}\mathbf{n}_{\mathrm{LC}}^{\mathrm{T}}\,\mathbf{m}\right)\right] \quad \text{(Eq. 3-135)}$$

$$\mathrm{B}_5 = \frac{\mathrm{H}_{21}}{\det}\mathbf{n}_{\mathrm{LC}}^{\mathrm{T}}\mathbf{m} \quad \text{(Eq. 3-136)}$$

$$\mathrm{B}_6 = \frac{\mathrm{H}_{11}}{\det}\frac{\left(\frac{1+\mathrm{e}}{1+\mathrm{e_1}} + \mathrm{f}_\beta\right)}{\rho_{\mathrm{L1}}\mathrm{S}_{\mathrm{L1}}} \quad \text{(Eq. 3-137)}$$

3.4.7. Summary of the constitutive input parameters

The overall hydro-mechanical formulation of the expansive clays as multiphase double-structure material requires a large number of parameter (Table 3-4). It is necessary to point out the fact that most of them have physical meaning and they are easily measurable. Gens et al., (2011) proven that from a systematic experimental program all of them can be determined.

Table 3-4. Input parameters of the double structure model

Bishop parameter micro-structural level	χ	Bishop's effective stress parameter for micro-structure
Non-linear elasticity	$\bar{\kappa}$ (-)	Slope of the unloading/reloading related to the Macro-structure
	κ_s (-)	Slope of the drying/wetting related to expansive clay
	ν (-)	Poisson's ratio
Macro-micro mechanical interaction function	f_{ms0}(-)	Parameters for the case of micro-structure swelling
	f_{ms1}(-)	
	n_{ms}(-)	
	f_{mc0}(-)	Parameters for the case of micro-structure contraction
	f_{mc1}(-)	
	n_{cs}(-)	
Macro-structural level Plastic mechanism (BBM)	φ (^{o})	Friction angle
	p_c (MPa)	Reference stress
	λ_{sat}(-)	Slope of the virgin loading at saturated state
	r (-)	Parameter in LC curve
	β (MPa^{-1})	Parameter in LC curve
	k_s (-)	Coefficient setting the increase of tensile strength with suction
	p_{s0} (MPa)	Tensile strength at saturated state
	α (-)	Coefficient of non-associativity
Hydraulic interaction Macro-micro	γ ($kg.s^{-1}.m^{-3}.MPa^{-1}$)	Leakage parameter
Liquid density at micro- and Macro-structural levels	ρ_{Lo} (kg/m^3)	Reference density (1002.6)
	$\beta_{\rho Lo}$ (MPa^{-1})	Compressibility ($4.5x10^{-4}$)
	$\alpha_{\rho Lo}$ ($^oC^{-1}$)	Volumetric thermal expansion coefficient for water ($-3.4x10^{-4}$)
	$\gamma_{\rho Lo}$	Solute variation (0.6923)
	P_{Lo} (MPa)	Reference pressure (0.1)
Water retention curve for micro-structural level	$(P_o)_1$ (MPa)	Measured air entry pressure
	σ_{To} (N/m)	Surface tension at temperature in which $(P_o)_1$ was measured

		(Usually 0.072 N/m at 20°C)
	$(\lambda_o)_1$ (-)	Shape function
	$(S_r)_{L1}$ (-)	Residual saturation
	$(S_m)_{L1}$ (-)	Maximum saturation
	$(P_d)_1$ (MPa)	Pressure related with suction at zero degree of saturation
	$(\lambda_d)_1$ (-)	Model parameter
Water retention curve for Macro-structural level	$(P_o)_2$ (MPa)	Measured air entry pressure
	σ_{To} (N/m)	Surface tension at temperature in which $(P_o)_1$ was measured (Usually 0.072 N/m at 20°C)
	$(\lambda_o)_2$ (-)	Shape function
	$(S_r)_{L2}$ (-)	Residual saturation
	$(S_m)_{L2}$ (-)	Maximum saturation
	$(P_d)_2$ (MPa)	Pressure related with suction at zero degree of saturation
	$(\lambda_d)_2$ (-)	Model parameter
Intrinsic permeability	k_o (m^2)	Intrinsic permeability
	b (-)	Model parameter
	$(\phi_o)_2$	Reference porosity
Initial conditions	$\boldsymbol{\sigma}$ (MPa)	Initial stress state
	P_o^* (MPa)	Initial value of preconsolidation pressure at saturated state
	ϕ (-)	Initial value of total porosity
	$\bar{\phi}_2$(-)	Initial value of Macro pore volume fraction
	$\bar{\phi}_1$(-)	Initial value of micro pore volume fraction
	P_{L2} (MPa)	Initial value of liquid pressure at Macro-structural level
	P_{L1} (MPa)	Initial value of liquid pressure at micro-structural level
	P_g (MPa)	Initial value of gas pressure

3.5. Chapter conclusions

A double-structure constitutive model has been proposed which takes explicitly into account the two levels of structure. They are a closer representation of the typical fabric of expansive clays. The distinction between the Macro-structure and microstructure provides the opportunity to reproduce the dominant phenomena that affect the behaviour of each structure in a consistent way. The modelling of active clays using single-structure models might be require introducing parameters having a doubtful meaning to describe the hydro-mechanical micro-Macro interactions.

From a numerical modelling perspective, it is appropriate to assign a water retention model to each structural level. The hydraulic characteristics and parameters of these retention models are consequence to the water state in the structural levels. Nevertheless, the they are not independent. The linear superposition of micro- and Macro-structural sub-curve determines the water retention curve for expansive clays. The pore space at each level plays a weighting role.

The non-linear elasticity model has been used to handle the volumetric and reversible behaviour of micro-structural level. On the contrary, characteristic phenomena that affect the global arrangements of aggregates, i.e. Macro-structure, require an elasto-plastic formulation. The key elements for the proper modelling of expansive clays are the relationships between a capillary-controlled Macro-structure and a micro-structure where the physico-chemical phenomena, occurring at aggregate level, take place. They can be summarised as:

- There is an elastic structural coupling for small-strain regime, it means for constant clay fabric. The consideration of a pure elastic behaviour at measurable material behaviour is physically debatable. The slip between clay aggregates and the ensuing fabric evolution is a plastic mechanism.

- The consideration of irreversible effects in the Macro-structure induced by micro-structural strains has been considered as the crucial coupling to reproduce the mechanical behaviour of expansive clays. The phenomenological description and mathematical

formulation was exposed. Additionally, discrete modelling proved that the geometrical reorganization of clay aggregates (i.e. fabric evolution) is the main responsible of this coupled behaviour.

- This formulation consider non-equilibrium between the water potentials associated to each structural level. The mass water exchange is driven by the micro-Macro suction difference and a phenomenological leakage parameter dependant of geometrical aspects of the porous medium. Due to the lack of information, sometimes a constant value of the leakage parameter is the logical option. This time-dependent mechanism affects the hydraulic evolution of the system and the total deformation of the micro-structure.

A well-known elasto-plastic BBM model, which describes the Macro-structural behaviour, has been combined with a generalized plasticity model to reproduce the irreversible effects related to the mechanical interaction between the two structural levels. The non-consideration of pure elastic zone and the difficulty to identify clearly the yield surface of the plastic mechanisms associated to the coupling between the pores structures aims the adoption of this theory. Finally, the elasto-plastic expressions related to the increments of strains and Macro-structural suction, used in the numerical implementation of the model (Chapter 4), have been derived from the context of multi-dissipative materials.

One of the benefits of developing a theoretical model is that experimental programmes can be devised to examine the hypothesis and main predictions of the model in a systematic manner. As a consequence, it is likely that as further and more comprehensive experimental data becomes available more complex versions of the model will have to be used.

3.6. References

Alonso, E.E., Gens, A., Hight, D.W., 1987. Spetial problem soils: general report, Proc. 9th Eur. Conf. Soil Mech. Found. Engng. Dublin 3.

Alonso, E.E., Gens, A., Josa, A., 1990. A constitutive model for partially saturated soils. Géotechnique 40, 405–430.

Alonso, E.E., Pereira, J.M., Vaunat, J., Olivella, S., 2010. A microstructurally based effective stress for unsaturated soils 913–925.

Alonso, E.E., Pinyol, N.M., Gens, A., 2013. Compacted soil behaviour: initial state, structure and constitutive modelling. Géotechnique 63, 463–478.

Alonso, E.E., Vaunat, J., Gens, A., 1999. Modelling the mechanical behaviour of expansive clays. Eng. Geol. 54, 173–183.

Baker, R., Frydman, S., 2009. Unsaturated soil mechanics. Critical review of physical foundations. Eng. Geol. 106, 26–39.

Barrenblatt, G., Zeltov, I., Kochina, N., 1960. Basic concepts in the theory of seepage of homogeneous liquid in fissured rocks. Pirkl. Mater. Mekh. 24, 852–864.

Bishop, A.W., Blight, G.E., 1963. Some aspects of effective stress in saturated and partly saturated soils. Geotechnique 13, 177–197.

Burland, J.B., 1967. Deformation of soft clay. PhD Thesis, University of Cambridge, UK.

Casini, F., Vaunat, J., Romero, E., Desideri, A., 2012. Consequences on water retention properties of double-porosity features in a compacted silt. Acta Geotech. 7, 139–150.

de Groot, S.R., Mazur, P., 1984. Non-equilibrium thermodynamics. New York: Dover Publications, Inc.

Dieudonne, A.-C., Della Vecchia, G., Charlier, R., 2017. Water retention model for compacted bentonites. Can. Geotech. J. 54, 915–925.

Gallipoli, D., Grassl, P., Wheeler, S., Gens, A., 2018. On the choice of stress-strain variables for unsaturated soils and its effect on plastic flow. Geomech. Energy Environ. 15, 3–9.

Gens, A., 2013. The development of unsaturated soil mechanics, in: XIV Šuklje Lecture. Ljubljana, Slovenia. pp. 5–35.

Gens, A., 2010. Soil–environment interactions in geotechnical engineering. Géotechnique 60, 3–74.

Gens, A., 1995. Constitutive laws, in: Gens, A., Jouanna, P., Scherefler, A. (Eds.), Modern Issues in Non-Saturated Soils. pp. 129–158.

Gens, A., Alonso, E.E., 1992. A framework for the behaviour of unsaturated expansive clays. Can. Geotech. J. 29, 1013–1032.

Gens, A., Olivella, S., 2001. THM phenomena in saturated and unsaturated porous media. Rev. Française Génie Civ. 5, 693–717.

Gens, A., Sánchez, M., Sheng, D., 2006. On constitutive modelling of unsaturated soils. Acta Geotech. 1, 137–147.

Gens, A., Valleján, B., Sánchez, M., Imbert, C., Villar, M.V., Van Geet, M., 2011. Hydromechanical behaviour of a heterogeneous compacted soil: experimental observations and modelling. Géotechnique 61, 367–386.

Georgiadis, K., Potts, D.M., Zdravkovic, L., 2005. Three-dimensional constitutive model for partially and fully saturated soils. Int. J. Geomech. 5, 244–255.

Gesto, J.M., Gens, A., Vaunat, J., 2011. Smoothing of yield surfaces and a reformulation of multi-surface plasticity, in: Computational Plasticity XI - Fundamentals and Applications, COMPLAS XI. pp. 910–920.

Guimaraes, L.D.N., 2002. Analisis multi-componente no isotermo en medio poroso deformable no saturado (in spanish). PhD Thesis, Universitat Politecnica de Catalunya, Spain.

Guimaraes, L.D.N., Gens, A., Sanchez, M., Olivella, S., 2013. A chemo-mechanical constitutive model accounting for cation exchange in expansive clays. Geotechnique 63, 221–234.

Houlsby, G.T., 1997. The work input to an unsaturated granular material. Géotechnique 47, 193–196.

Jommi, C., 2000. Remarks on the constitutive modelling of unsaturated soils, in: Experimental Evidence and Theoretical Approaches in Unsaturated Soils (Eds A. Tarantino and C. Mancusso). Rotterdam:Balkema, pp. 139–153.

Li, J., Yin, Z.-Y., Cui, Y.J., Hicher, P.-Y., 2017. Work input analysis for soils with double porosity and application to the hydromechanical modeling of unsaturated expansive clays. Can. Geotech. J. 54, 173–187.

Lloret, A., Villar, M. V., Sánchez, M., Gens, A., Pintado, X., Alonso, E.E., 2003. Mechanical behaviour of heavily compacted bentonite under high suction changes. Géotechnique 53, 27–40.

Mainka, J., Murad, M.A., Moyne, C., Lima, S.A., 2014. A modified effective stress principle for unsaturated swelling clays derived from microstructure. Vadose Zo. J. 13, 1–17.

Mašin, D., 2013. Double structure hydromechanical coupling formalism and a model for unsaturated expansive clays. Eng. Geol. 165, 73–88.

Mašín, D., Khalili, N., 2016. Swelling phenomena and effective stress in compacted expansive clays. Can. Geotech. J. 53, 134–147.

Navarro, V., Yustres, A., Asensio, L., De la Morena, G., González-Arteaga, J., Laurila, T., Pintado, X., 2017. Modelling of compacted bentonite swelling accounting for salinity effects. Eng. Geol. 223, 48–58.

Olivella, S., Carrera, J., Gens, A., Alonso, E.E., 1994. Non-isothermal

multiphase flow of brine and gas through saline media. Transp. Porous Media 15, 271–293.

Rizzi, E., Maier, G., Willam, K., 1996. On failure indicators in multi-dissipative materials. Int. J. Solids Struct. 33, 3187–3214.

Romero, E., Della Vecchia, G., Jommi, C., 2011. An insight into the water retention properties of compacted clayey soils. Géotechnique 61, 313–328.

Romero, E., Vaunat, J., 2000. Retention curves of deformable clays, in: Exparimental Evidences and Theoretical Approaches in Unsaturated Soils. Eds. Tarantino, A. and Mancuso, C. Trento, Italy. pp. 91–106.

Ruiz, D.F., Vaunat, J., Gens, A., Mánica, M., 2018. Hydro-mechanical modelling of an unsaturated seal structure, in: Proceedings of the 9th European Conference on Numerical Methods in Geotechnical Engineering (NUMGE 2018) Cardoso et Al (Eds). Porto, Portugal. pp. 757-764. Volume 1.

Ruiz, D.F., Vaunat, J., Gens, A., Mánica, M., 2017. Hydro-mechanical modelling of a gallery sealing over the entire life of a deep repository, in: 6th International Conference on Coupled THMC Processes in Geosystems, GeoProc 2017. París, France. pp. 120–121.

Sánchez, M., 2004. Thermo-Hydro-Mechanical coupled analysis in low permeability media. PhD Thesis, Universitat Politecnica de Catalunya, Spain.

Sanchez, M., Gens, A., 2014. Modelling and interpretation of the FEBEX mock up test and of the long-term THM tests. Project PEBS: Long-term Performance of Engineered Barrier Systems. Deliverable D3. 3-3.

Sanchez, M., Gens, A., Guimarães, L., Olivella, S., 2005. A double structure generalized plasticity model for expansive materials. Int. J. Numer. Anal. Methods Geomech. 29, 751–787.

Sánchez, M., Gens, A., Guimarães, L., Olivella, S., 2008. Implementation algorithm of a generalised plasticity model for swelling clays. Comput. Geotech. 35, 860–871.

Santamarina, J.C., 2001. Soils and waves. John Wiley and Sons, Ltd.

Schofield, R.K., 1935. The pF of water in soil, in: Transactions of the Third International Congress on Soil Science, Oxord, UK, Vol. 2. pp. 37–48.

Seiphoori, A., Ferrari, A., Laloui, L., 2014. Water retention behaviour and microstructural evolution of MX-80 bentonite during wetting and drying cycles. Geotechnique 64, 721–734.

Sheng, D., 2003. Non-convexity of the Barcelona Basic Model - Comment on S. J. Wheeler, D. Gallipoli and M. Karstunen (2002;26:1561-1571). Int. J. Numer. Anal. Methods Geomech. 27, 879–881.

Tsiampousi, A., Zdravković, L., Potts, D.M., 2013. A new Hvorslev surface for critical state type unsaturated and saturated constitutive

models. Comput. Geotech. 48, 156–166.
Vaunat, J., Casini, F., 2017. A procedure for the direct determination of Bishop's χ parameter from changes in pore size distribution. Geotechnique 67, 631–636.
Wheeler, S.J., Gallipoli, D., Karstunen, M., 2002. Comments on use of the Barcelona Basic Model for unsaturated soils. Int. J. Numer. Anal. Methods Geomech. 26, 1561–1571.
Zandarin, M.T., Gens, A., Olivella, S., Alonso, E.., 2011. Thermo-hydro-mechanical model of the Canister Retrieval Test. Phys. Chem. Earth 36, 1806–1816.

Chapter 4

Numerical Implementation and Model Performance

'A difficulty of advanced numerical analysis is that the knowledge and skill required to perform numerical analysis is substantially greater than for the simple methods of approximate analysis to which we have become accustomed. This is a time when there is a shortage of trained engineers in general and of geotechnical engineers in particular'

P.R. Vaughan et al, (2004)

4.1. Introduction

The previous chapters have shown the physical features of the expansive clays and its constitutive formulation within the continuum-based framework. In order to generate a powerful analysis tool, it is necessary to solve the resulting system of PDEs (partial differential equations) through a consistent numerical method. Approaches based on finite difference (FD) and finite element method (FEM) are the most widely used in geotechnics.

The above process can be related with the requirements needed to perform useful numerical analysis (Potts, 2003):

- An in-depth understanding of soil mechanics and theory behind numerical analysis (see Chapter 2).
- An appreciation of the limitation of the constitutive models (see Chapter 3).
- Familiarization with the numerical implementation and software used to perform the analysis (this Chapter)

This chapter is composed by two main parts:

The first one is devoted to the implementation of the hydro-mechanical formulation for expansive clays into an in-house finite-element code CODE_BRIGHT (DIT-UPC, 2018). Besides the matrix formulation of the balance equations, important insights about the numerical treatment of water transfer between structural levels are given. In this scheme, it is necessary to update stresses and internal variables once for each iteration, for each time increment and for each gauss point of the spatial discretization. The highly non-linearity of the double-structure model and the final goal of solving complex HM boundary value problem imposes the necessity to develop a competent algorithm to integrate this model.

The second part deals with the verification of the model performance through simple constitutive models. These verifications essentially means checking that the model (implemented code) works correctly (Lees, 2016). They address the micro-Macro interaction mechanisms and the responses of the model under well-defined stress and suction paths.

4.2. Numerical approach

The selection of a numerical approach, to handle a system of PDEs that describes a certain formulation, is a matter of convenience. Within the context of continuum mechanics, the Arbitrary Lagrangian-Eulerian methods (e.g. PFEM, MPM, SPH, among others) are used to solve the balance equations and linear momentum at large strains; whereas in the small-strains regime in which the geometrical non-linearity has a minor relevance, the Lagrangian formulation of the finite element method (FEM) and the finite diference (FD) are suitable.

The formulation has been implemented in the finite element program CODE_BRIGHT, which is a tool designed to analyse numerically coupled Thermo-Hydro-Mechanical (THM) problems in geological media (DIT-UPC, 2018; Olivella et al., 1996).

In spite of the important deformation of the expansive clays upon wetting or drying, they are essentially volumetric. Then, inaccuracies due to strong mesh distortion are not expected. Likewise, one of the main concern is the Hydro-Mechanical response of the bentonite at confined spaces (i.e. laboratory cell, boreholes or galleries), thus limiting the swelling strains. However, the use of bentonite to fill irregular cavities, the HM analysis in non-confined states or events in the saturated stage (e.g. piping or erosion) should imply the migration to the first type of numerical approach.

4.2.1. Numerical implementation in CODE_BRIGHT

As regarded in the Chapter 2, the fundamental balance equations compose a resulting system of PDE's (partial differential equations) which has to be solved numerically. Olivella, (1995) and Olivella et al., (1996) present a detail procedure to solve the THM formulation of porous media. Here, only the main aspects of the Hydro-Mechanical formulation of double-structure porous media are presented.

The main idea can be described as follow: one unknown (state variable) is associated with each of the balance equations presented. The unknowns are obtained by solving the system of PDE's in a coupled way. The standard approach in non-linear finite element analysis is to consider a piecewise linear approximation of the problem. In a general scheme, for

any given global iteration of any discrete increment considered in the linearization, the main variables of the problem are evaluated for each node of the mesh. In a general HM problem these main variables are: the displacement field and the fluids pressures. Another main step, in non-linear analyses, is the updating of the stresses and the internal variables at each quadrature point of the finite element discretization (see Section 4.2.3.).

The starting point for discretization of the problem is the approximation of the material derivate with respect to the solid as an eulerian derivative, considering the assumption of small strain rate. Herein, the water mass balance equation for Macro-structure (Eq. 2-45), is presented as an example:

$$\bar{\phi}_2 \frac{\partial}{\partial t}\left(\theta^w_{L2} S_{L2} + \theta^w_{g2} S_{g2}\right) + \left(\theta^w_{L2} S_{L2} + \theta^w_{g2} S_{g2}\right)\left(\frac{d\bar{\varepsilon}_{v2}}{dt}\right) + \nabla\cdot\left(\mathbf{j}^w_{L2} + \mathbf{j}^w_{g2}\right) = -\Gamma^w \qquad \text{(Eq. 4-1)}$$

In a similar way, the other balance equations have been considered. The numerical approach can be viewed as divided into two parts: spatial and temporal discretizations. Galerkin finite element method (FEM) is used for the spatial discretization while finite differences are used for temporal discretization. The discretization in time is linear and the explicit schemes uses two intermediate points $t^{k+\varepsilon}$ and $t^{k+\theta}$ between the initial t^k and final t^{k+1} times. Finally, since the problem presented here is non-linear, the Newton-Raphson method was adopted as iterative scheme.

Once the solid balance is substituted in other balance equations, computation of porosity at intermediate point is not necessary because its variation is expected to occur at slow rates. For this reason, porosity is integrated explicitly, that is the values at t^k are used. Since the variation of porosity is expressed by solid mass balance equation, this assumption leads to some advantages for the iterative scheme.

As mentioned (Sheng et al., 2003), the FEM discretization of the set of the governing equations for an unsaturated soil leads to a system of first order differential equations. The residuals that are obtained from the double-structure formulation can be written (for one finite element) as:

$$\begin{pmatrix} \mathbf{r}_{u} \\ \mathbf{r}_{P_{L2}} \\ \mathbf{r}_{P_{L1}} \\ \mathbf{r}_{P_{g2}} \\ \mathbf{r}_{P_{g1}} \end{pmatrix} = \frac{d}{dt} \begin{pmatrix} \mathbf{d}_{u} \\ \mathbf{d}_{P_{L2}} \\ \mathbf{d}_{P_{L1}} \\ \mathbf{d}_{P_{g2}} \\ \mathbf{d}_{P_{g1}} \end{pmatrix} + \begin{pmatrix} \mathbf{a}_{u} \\ \mathbf{a}_{P_{L2}} \\ \mathbf{a}_{P_{L1}} \\ \mathbf{a}_{P_{g2}} \\ \mathbf{a}_{P_{g1}} \end{pmatrix} + \begin{pmatrix} \mathbf{b}_{u} \\ \mathbf{b}_{P_{L2}} \\ \mathbf{b}_{P_{L1}} \\ \mathbf{b}_{P_{g2}} \\ \mathbf{b}_{P_{g1}} \end{pmatrix} = \begin{pmatrix} \mathbf{0} \\ \mathbf{0} \\ \mathbf{0} \\ \mathbf{0} \\ \mathbf{0} \end{pmatrix} \qquad \text{(Eq. 4-2)}$$

where:
- $\mathbf{r}$ are the residuals.
- $d\mathbf{d}/dt$ are storage or accumulation terms.
- $\mathbf{a}$ are the conductance terms.
- $\mathbf{b}$ are the sink/source terms and boundary conditions.

Now, we will explain briefly how each term is handled in the program CODE_BRIGHT. For the mechanical problem, selective integration is used for quadrilateral elements and quadrilateral prisms (this means that the volumetric part is integrated with a reduced quadrature of 1 point). Finally, for all elements the flow equations are solved using element-wise and cell-wise approximations. More details are contained in Olivella et al., (1996).

- *Storage terms:*

These terms represent the variation of mass content, they are calculated from variables such as degree of saturation, density, porosity and mass fraction. They are computed in a mass conservative approach.

A typical storage term is the variation of water in the liquid phase:

$$\phi \frac{\partial}{\partial t}(\theta_L^w S_L) \qquad \text{(Eq. 4-3)}$$

The weighted residual method is applied to the governing equations and, for node *i*, (Eq. 4-3) is transformed into:

$$\int_v N_i \phi \frac{\partial}{\partial t}(\theta_L^w S_L) dv = \int_{e_1} N_i \phi \frac{\partial}{\partial t}(\theta_L^w S_L) dv + \ldots + \int_{e_m} N_i \phi \frac{\partial}{\partial t}(\theta_L^w S_L) dv \qquad \text{(Eq. 4-4)}$$

where:
- N_i is the shape function for node *i*.
- e_1, e_2,..., e_m are the elements that contain node *i*.

At this point of the development we assume that the porosity, ϕ, is defined through element-wise approximation. An elementwise variable is space constant over every element, but different from element to element.

Finally, it should be pointed out that this formulation gives rise to a concentrated scheme, which means that the storage term in node *i* is only a function of unknowns in node *i*. This is a clearly advantageous from computational point of view.

- *Advective fluxes:*

These kind of fluxes caused by motion of fluids are computed using Darcy's law and, except for the coefficients, they are explicit in terms of pressure gradients.

After applying the weighted residual method in each balance equation, the Green's theorem allows one to reduce the order of the derivatives and the divergence of flow is transformed into two terms, one of them with the gradient of shape function. Hence, after that, in the water balance equation of node *i* we find, the following advective term:

$$
\begin{aligned}
-\int_{v}(\nabla^{t}N_{i})\mathbf{j}_{L}^{w}dv &= -\left(\int_{v}(\nabla^{t}N_{i})\theta_{L}^{w}\mathbf{q}_{L}dv\right) \\
&= \left(\int_{v}(\nabla^{t}N_{i})\theta_{L}^{w}\frac{\mathbf{k}k_{r_L}}{\mu_{L}}(\nabla N_{j})dv\right)(P_{L})_{j} \\
&\quad -\left(\int_{v}(\nabla^{t}N_{i})\theta_{L}^{w}\frac{\mathbf{k}k_{r_L}}{\mu_{L}}\rho_{L}\mathbf{g}dv\right)
\end{aligned}
\qquad \text{(Eq. 4-5)}
$$

where:

- j indicates the summation over element nodes.
- P_L is a nodewise variable which means that it is defined by its nodal values and interpolated on the elements using the shape functions.

- *Non-advective fluxes:*

Having a minor relevance in the HM formulation, they are computed through Fick's law using the proportionality to gradients of mass fractions, which do not belong to the set of unknowns. Fourier's law is used for the conductive heat flux and it expresses proportionality to temperature gradients. The spatial treatment for the advective fluxes is applied here.

- *Volumetric strain fluxes:*

In fact, these terms are also storage terms. If the equation of balance of solid is substituted in all other balance equations, the variations of porosity is not explicit in them. In this way porosity only appears as parameter or coefficient and term of volumetric strain remain in the balance equations.

They are proportional to $\nabla\cdot\dot{\mathbf{u}}$ which is equivalent to the volumetric strain rate.

$$\int_{e_m} N_i \alpha \nabla . \frac{d\mathbf{u}}{dt} dv = \int_{e_m} N_i \alpha \mathbf{m}^t \mathbf{B} \frac{d\mathbf{u}}{dt} dv \qquad \text{(Eq. 4-6)}$$

where:
- α is defined from the equations.
- $\mathbf{m}^t$=(1,1,1,0,0,0) is an auxiliary vector
- $\mathbf{B}$ is the matrix used in the finite element approach for the mechanical problem. Its coefficients are gradients of the shape functions.

- *Mechanical stress equillibrium:*

The weighted residual method is also applied to the stress equilibrium equation, followed by the Green's theorem. This lead to the equation:

$$\mathbf{r}(\boldsymbol{\sigma}^{k+1}) = \int_v \mathbf{B}^t \boldsymbol{\sigma}^{k+1} dv - \mathbf{f}^{k+1} \qquad \text{(Eq. 4-7)}$$

where:
- $\mathbf{r}(\boldsymbol{\sigma}^{k+1})$ represents the residual corresponding to the mechanical problem.
- $\mathbf{f}^{k+1}$ are the body form terms.

The constitutive model relates stresses with strains, with fluid pressures (and temperatures) at a point in the medium. In general:

$$\frac{d\boldsymbol{\varepsilon}}{dt} = \frac{d\boldsymbol{\varepsilon}^e(\dot{\boldsymbol{\sigma}}, \dot{s})}{dt} + \frac{d\boldsymbol{\varepsilon}^p(\boldsymbol{\sigma}, s, \dot{\boldsymbol{\sigma}}, \dot{s})}{dt} \qquad \text{(Eq. 4-8)}$$

- *Sink/source terms:*

Application of Green's theorem to divergence terms (in balance or stress equations) produces terms which represent fluxes or stress across or on the boundaries, these terms are substituted by nodal flow rates or forces in the discretized forms of the equations (Cauchy type boundary conditions).

The final configuration of the resulting system of first order differential equations for the double-structure formulation, (Eq. 4-2), depends on the numerical treatment of the water mass balance equation for micro-structural level and the Macro-micro water exchange. The following section described the different manners to handle these aspects.

4.2.2. Numerical treatment of the Macro-micro water exchange

The physical assumption on water movement inside the micro-structural level determines the numerical strategy to account for its balance and the mass exchange with Macro-structure (see Chapter 2).

In spite of the low water mobility in micro-structure, a lower power for the relative permeability law at this level can be considered. Therefore, the advective fluxes $\mathbf{j}^{w}_{L1}, \mathbf{j}^{w}_{g1}$ are not omitted and the micro water mass balance has to be solved in the nodes.

Alternatively, the fluxes of water micro to micro can be considered negligible ($\mathbf{j}^{w}_{L1} + \mathbf{j}^{w}_{g1} = 0$). Under this conditions, the micro liquid pressure (P_{L1}) is updated as a history variable integrated al gauss point level.

4.2.2.1. Micro water liquid pressure as nodal variable

Having a constant gas pressure on the porous medium, the system of first order differential equations (Eq. 4-2) changes to:

$$\begin{pmatrix} \mathbf{r}_{u} \\ \mathbf{r}_{P_{L2}} \\ \mathbf{r}_{P_{L1}} \\ \mathbf{r}_{P_{g}} \end{pmatrix} = \frac{d}{dt} \begin{pmatrix} \mathbf{d}_{u} \\ \mathbf{d}_{P_{L2}} \\ \mathbf{d}_{P_{L1}} \\ \mathbf{d}_{P_{g}} \end{pmatrix} + \begin{pmatrix} \mathbf{a}_{u} \\ \mathbf{a}_{P_{L2}} \\ \mathbf{a}_{P_{L1}} \\ \mathbf{a}_{P_{g}} \end{pmatrix} + \begin{pmatrix} \mathbf{b}_{u} \\ \mathbf{b}_{P_{L2}} \\ \mathbf{b}_{P_{L1}} \\ \mathbf{b}_{P_{g}} \end{pmatrix} = \begin{pmatrix} \mathbf{0} \\ \mathbf{0} \\ \mathbf{0} \\ \mathbf{0} \end{pmatrix} \qquad \text{(Eq. 4-9)}$$

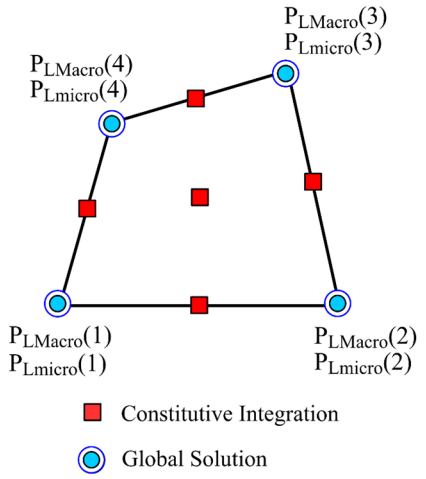

Figure 4-1. Macro and micro water mass balance on nodes.

Mixed finite elements that interpolate the solid displacement and pore pressures in the Macropores and micropores are used for this purpose (Figure 4-1). The constitutive integration points (Gauss quadrature) deals with the stresses updating. From the numerical point of view, the water exchange between structural levels is given by nodal sink/source term at both differential equations (Sánchez et al., 2016).

Borja and Choo, (2016) explored this formulation in the limit of undrained deformation. The incompressibility constraint causes unstable behaviour in the form of spurious pressure oscillation at the two pore scales. To circumvent this instability they develop a variant of the polynomial pressure projection technique for a twofold saddle point problem. The proposed stabilization allows the use of equal-order (linear) interpolations of the displacement and two pore pressure variables throughout the entire range of drainage condition (Choo and Borja, 2015).

4.2.2.2. Micro water liquid pressure as history variable

In this case the system of first order differential equations reads:

$$\begin{pmatrix} \mathbf{r}_{\mathrm{u}} \\ \mathbf{r}_{\mathrm{P_{L2}}} \\ \mathbf{r}_{\mathrm{P_g}} \end{pmatrix} = \frac{\mathrm{d}}{\mathrm{dt}} \begin{pmatrix} \mathbf{d}_{\mathrm{u}} \\ \mathbf{d}_{\mathrm{P_{L2}}} \\ \mathbf{d}_{\mathrm{P_g}} \end{pmatrix} + \begin{pmatrix} \mathbf{a}_{\mathrm{u}} \\ \mathbf{a}_{\mathrm{P_{L2}}} \\ \mathbf{a}_{\mathrm{P_g}} \end{pmatrix} + \begin{pmatrix} \mathbf{b}_{\mathrm{u}} \\ \mathbf{b}_{\mathrm{P_{L2}}} \\ \mathbf{b}_{\mathrm{P_g}} \end{pmatrix} = \begin{pmatrix} \mathbf{0} \\ \mathbf{0} \\ \mathbf{0} \end{pmatrix} \qquad \text{(Eq. 4-10)}$$

The balance of water for the medium is addressed by the Macro level equation (Eq. 2-45). Splitting the Macro-structural volumetric deformation into total and micro-structural deformation modifies this balance equation:

$$\bar{\phi}_2 \frac{\partial}{\partial t}(\theta^w_{L2} S_{L2} + \theta^w_{g2} S_{g2}) + (\theta^w_{L2} S_{L2} + \theta^w_{g2} S_{g2}) \left(\frac{d\varepsilon_v}{dt} - \frac{d\bar{\varepsilon}_{v1}}{dt}\right) + \nabla \cdot (\mathbf{j}^w_{L2} + \mathbf{j}^w_{g2}) = -\Gamma^w \quad \text{(Eq. 4-11)}$$

From the water mass balance equation for micro-structure and assuming null advective fluxes (Eq. 2-49), it is possible to expresses the micro volumetric deformation as a function of their storage and sink/source terms:

$$\left(\frac{d\bar{\varepsilon}_{v1}}{dt}\right) = \frac{1}{\theta^w_{L1} S_{L1} + \theta^w_{g1} S_{g1}} \left(\Gamma^w - \bar{\phi}_1 \frac{\partial}{\partial t}(\theta^w_{L1} S_{L1} + \theta^w_{g1} S_{g1})\right) \quad \text{(Eq. 4-12)}$$

Finally, the substitution of (Eq. 4-11) into (Eq. 4-12) provides the balance equation used in the system (Eq. 4-10):

$$\begin{aligned} &\bar{\phi}_2 \frac{\partial}{\partial t}(\theta^w_{L2} S_{L2} + \theta^w_{g2} S_{g2}) \left(\frac{d\varepsilon_v}{dt}\right) + \nabla \cdot (\mathbf{j}^w_{L2} + \mathbf{j}^w_{g2}) \\ &\quad + \left(1 - \frac{\theta^w_{L2} S_{L2} + \theta^w_{g2} S_{g2}}{\theta^w_{L1} S_{L1} + \theta^w_{g1} S_{g1}}\right) \Gamma^w \\ &\quad + \left(\bar{\phi}_1 \frac{\theta^w_{L2} S_{L2} + \theta^w_{g2} S_{g2}}{\theta^w_{L1} S_{L1} + \theta^w_{g1} S_{g1}}\right) \frac{\partial}{\partial t}(\theta^w_{L1} S_{L1} + \theta^w_{g1} S_{g1}) = 0 \end{aligned} \quad \text{(Eq. 4-13)}$$

The computation of mass water exchange is an open issue in this numerical scheme. Unlike the previous proposal, the micro and Macro liquid pressure are not located on the same node. As Figure 4-2 shows, micro liquid pressure is obtained in the integration points, which are function (quantity and location) of the element type. An averaging methodology is suitable to obtain an element value after the constitutive integration process. The mass "lumping" is used (Zienkiewicz et al., 2013b). Finally, the correspondent value of P_{L1} on node *i* is calculated through the shape function N_i.

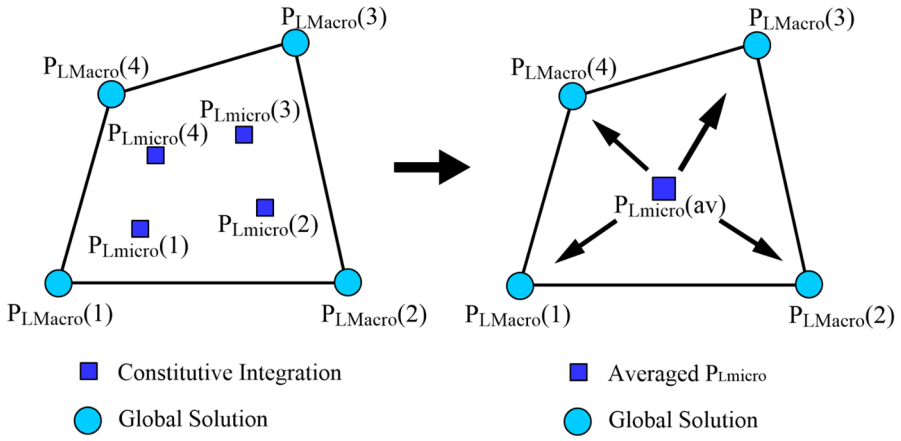

Figure 4-2. Left: micro liquid pressure on Gauss points; Right: water exchange from averaged gauss value to nodal values.

4.2.3. Stress-Strain integration

As indicated above, the CODE_BRIGHT uses the Newton-Raphson method for the global solution of the problem (at mesh level). In this scheme, it is necessary to update stresses and internal variables once for each iteration, for each time increment and for each gauss point of the discretization. In addition, there are other two strong constrains:

- The high non-linearity of the double structure constitutive model.
- The solution of complex HM coupled boundary value problems.

The strain-stress rate equations (used in the updating of stresses) are formulated as a system of ordinary differential equation (as the one presented in the Chapter 3). This system should be solved using a competent and tested integration procedure. The stresses are updated by integrating the stress–strain relations with a known strain increment.

Several numerical integration schemes have been proposed in order to implement an elastoplastic model in finite elements codes. Two main families of algorithms can be distinguished: the ones based on the explicit forward Euler scheme and the algorithms based on the implicit backward Euler method.

Generally speaking, the implicit integration of the elastoplastic problem is split in two parts: an ‘elastic predictor problem’ and a ‘plastic corrector problem’. Therefore, these methods solve the non-linear

constitutive equations by iteration; they are generally accurate but are difficult to implement since they require the second derivate of the plastic potential to be evaluated at a range of stress state. Moreover, they are not especially robust and require special procedures to be used when the iteration process fails to converge. Regarding their application to soil mechanics, the works of Borja and Lee, (1990), Borja, (1991), Potts and Ganendra, (1994), Abbo, (1997) and Vaunat et al., (2000) can be highlighted.

Zienkiewicz et al., (2013a) gives some important remarks on this kind of integration procedure:

- For associative plasticity the normality principle is valid, requiring a convex yield surface. In this case, the iteration process always converges for hardening material.
- Convergence of the finite element equations may not always occur if more than one quadrature point changes from elastic to plastic or from plastic to elastic in subsequent iterations.
- For non-associative plasticity the return direction is *not* normal to the yield surface. In this case no solution may exist for some strain increments and the iteration process will not converge.

Schemes based on the explicit method have been extensively used for the stress integration of elastoplastic models (Sloan, 1987; Abbo, 1997; Potts and Zdravkovic, 1999, Sloan et al., 2001; Sheng et al., 2003). In their simplest form, these procedures use the gradients (i.e. only the first derivative) of the yield surface and plastic potential at the start of the strain increment, and their accuracy can only be controlled by breaking up the strain increment into subincrements. Explicit methods are generally robust but, depending on their method of implementation, can be very inaccurate. The more refined versions of these algorithms combine sub-stepping techniques with automatic sub-stepping control, error control and yield surface drift correction. An advantage of this kind of schemes is that they are not iterative, which have a particular benefit when high non-linear models are considered. Zienkiewicz et al., (2013a) pointed out this kind of approach as particularly useful for the integration of non-associative models or models without yield function where “tangent” matrices are simply evaluated (e.g. generalized plasticity).

In order to implement an unsaturated soil model (i.e. the double-structure model) in a finite-element code, the stresses has to be updated by integrating the stress-strain-suction relations with a known strain and suction increment. In many constitutive models for unsaturated soils, the suction is treated as a stress variable even though it can be obtained directly from the global equations in the same way as the displacements or strains. This feature can cause computational difficulties in traditional stress integration schemes.

One special feature of the constitutive equations for unsaturated soils is the dependence of the yield surface on the suction variable.

For example, the Barcelona Basic Model (Alonso et al., 1990) treats the suction as an additional stress variable and add an extra strain variable to match it (Vaunat et al., 2000). The constitutive equations in this case are not purely driven by strain but, rather, are of a mixed form with six known strain increments and one known stress increment. This causes problems in stress integration, as the suction is a stress variable in the yield function/plastic potential and the final stress state must lie on the known suction plane. According to Sheng et al., (2003), implicit stress integration scheme result in convergence problems once an elastic trial stress path crosses a non-convex yield surface from outside. For unsaturated soils, the loading collapse curve, LC, is not guaranteed to be convex. Alternatively, if an explicit scheme is used, then the strain sub-incrementation may have to be carried out at a different rate compared to the suction (stress) sub-incrementation for sufficient accuracy to be obtained. This causes difficulties in the integration process, as it requires two separate integration steps to be performed. The suction can be treated as an additional strain component, even though it affects the yield function in a similar manner to the two stress-variable models. The advantage of this approach is that the constitutive equations are then similar to those for saturated soils and are purely strain driven. This leads to a formulation which is consistent with the conventional displacement finite-element method, where the displacements/pore pressures are found first and then the strains and finally the stresses.

González, (2011) evaluated the performance of implicit and explicit methods, integrating unsaturated soil models (BBM type) which use two options of the constitutive stress variables: net stress and Bishop's or

average stress. An explicit stress integration scheme with automatic sub-stepping and error control techniques and a fully implicit stress integration scheme based on the Backward-Euler algorithm with sub-stepping were used. The relative performance of implicit and explicit methods was strongly dependent on the precise form of the constitutive model. In terms of the efficiency of numerical algorithms, the explicit scheme is likely to be more robust than implicit scheme to solve the kind of complex stress paths involved in unsaturation behaviour. The use of explicit scheme, however, does not yield quadratic convergence of the full problem.

Based on the previous discussion, it is evident that there is not universal method that can be used with the many alternatives which can occur in geotechnical modelling practice.

Following the numerical work proposed by Sánchez et al., (2008), the double-structure constitutive formulation have been implemented through a refined Euler scheme with automatic sub-stepping and error control based on Sloan's scheme (Sloan, 1987; Sloan et al., 2001)(Figure 4-3). A feature of the double-structure formulations is that the soil behaviour can be regarded as a result of the joint action of several mechanisms that can act simultaneously (see Section 3.4.5.). Therefore, the scheme is a multi-mechanism generalization of the Sloan's one for the particular conditions of the double-structure model. As pointed out by Sánchez et al., (2008), a great advantage of Sloan's scheme is that it has been widely tested in a number of geotechnical problems proving its accuracy, robustness and efficiency.

4.2.3.1. Explicit integration scheme

The BExM model (Alonso et al., 1999) considers an elastic region where the micro-structural volumetric strains do not generate irreversible macro-structural response and the numerical integration in this region is explained in Sánchez, (2004).

The implemented algorithm has been developed for the case in which an elastic domain is neglected. For this assumption, the following three different situation can be distinguish in relation to the current stress state and the irreversible mechanism active (Section 3.4.5.):

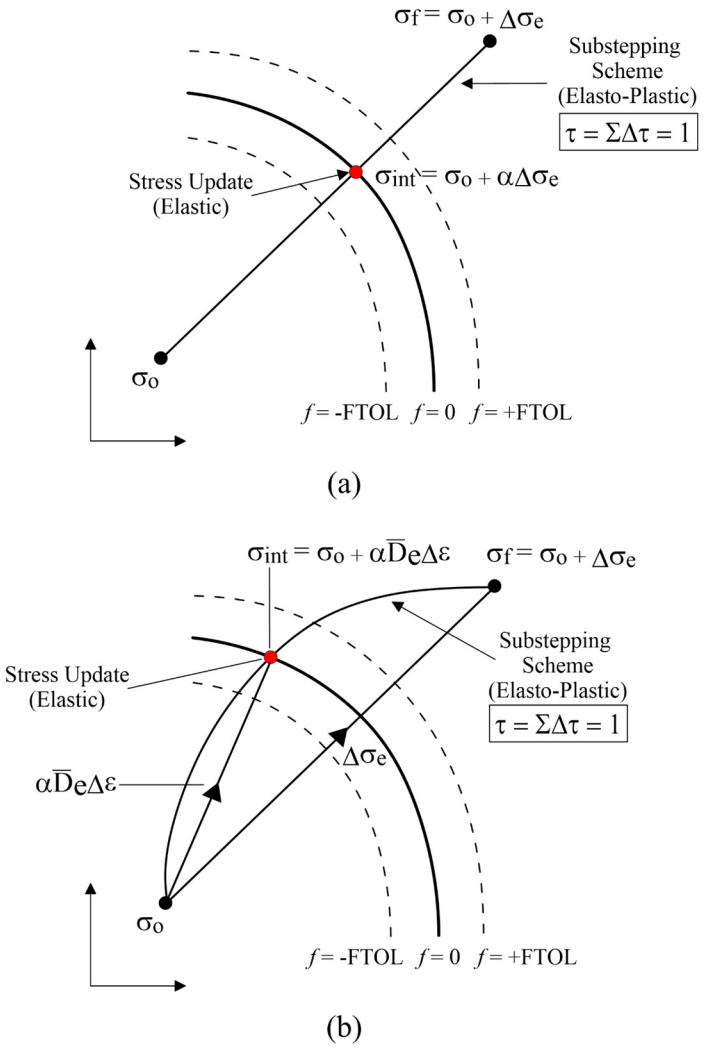

Figure 4-3. Yield surface intersection: elastic to plastic transition. a) Linear elasticity (from Sloan, 1987) and b) Non-Linear elasticity (from Sloan et al., 2001)

Case 1: the active mechanical interaction mechanism (β) at stress states inside the LC yield curve (Figure 4-4).

Case 2: it is related to the plastic response of the material due to LC yielding (BBM model). Now the stress state is on the LC yield surface and the mechanism β is not active (Figure 4-4).

Case 3: the plastic behaviour of the material is generated by the plastic mechanisms LC and β, which are working simultaneously.

The pure elastic stress increments are not very common and they are limited to stress path that move along the neutral line (Figure 4-4).

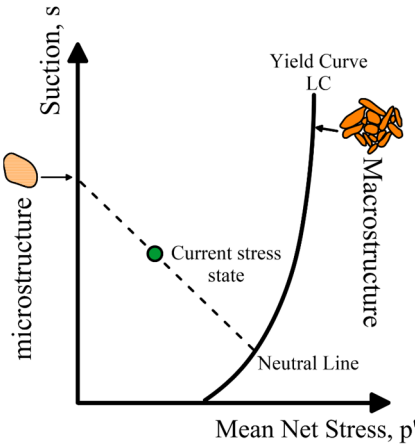

Figure 4-4. Graphical summary of double-structure elastoplastic model.

Given an increment of the control variables of the problem, $\Delta\boldsymbol{\varepsilon}$ and Δs_2, the goal of the numerical integration is the updating of the stresses and history variables ($\mathbf{hv}$) from the time t^k to the time t^{k+1} ((Eq. 4-14) to (Eq. 4-16)).

$$\boldsymbol{\sigma}^k \rightarrow \boldsymbol{\sigma}^{k+1} \qquad \text{(Eq. 4-14)}$$

$$s_2^k \rightarrow s_2^{k+1} \qquad \text{(Eq. 4-15)}$$

$$\mathbf{hv}^k = \begin{pmatrix} P_o^* \\ \omega_\beta \\ s_1 \\ \phi \\ \bar{\phi}_1 \\ \bar{\phi}_2 \end{pmatrix}^k \rightarrow \mathbf{hv}^{k+1} = \begin{pmatrix} P_o^* \\ \omega_\beta \\ s_1 \\ \phi \\ \bar{\phi}_1 \\ \bar{\phi}_2 \end{pmatrix}^{k+1} \qquad \text{(Eq. 4-16)}$$

where:

- $\boldsymbol{\sigma}$ is the stress tensor.
- s_2 is the suction at Macro-structural level.
- P_o^* is the saturated preconsolidation stress.
- ω_β is the index which determines if we have micro-structural swelling (mS) or micro-structural compression (mC).
- s_1 is the suction at Macro-structural level.
- ϕ, $\bar{\phi}_1$ and $\bar{\phi}_2$ are the porosity and the pore volume fractions for micro and Macro structural levels.

The first stage in the procedure is the division of given generalized strain increments ($\Delta\boldsymbol{\varepsilon}$ and Δs_2) into a number of sub-steps given by the standard approach of Sloan's algorithm, that is, defining a pseudo time τ:

$$\tau = \frac{t^{k+1} - t^k}{\Delta t} \quad ; \; 0 \leq \tau \leq 1 \qquad \text{(Eq. 4-17)}$$

where:

- t^k is the time at the start of the considered increment (global system) and $(t^k + \Delta t)$ is the time at the end of the increment,

The main difference between this integration strategy and the Sloan's schemes (Sloan, 1987; Sloan et al., 2001) is the application of the sub-stepping on the generalized strain increment ($\Delta\boldsymbol{\varepsilon}$ and Δs_2). The Sloan's algorithms divides the plastic portion of a given strain increment after finding the intersection with the yield surface (Figure 4-3), instead, the multi-mechanism double-structure formulation and the occurrence of plastic deformations inside the yield surface imply the sub-stepping of the entire generalized strain increment (Figure 4-5).

A number of different procedures must be used in the constitutive law integration process. Initially, a generalized strain subincrement inside the LC is assumed (Item a). After the stress integration, it must be verified whether the stress increment still remains inside the main LC yield locus and if this is not the case the yield surface contact point must be determined (Item b). The integration of the strain subincrement going outside the main yield surface must distinguish between the case where only one mechanism is active (Item c) or two mechanism are acting simultaneously (Item d).

a. Integration of generalised elasto-plastic law (irreversible mechanism associated with the micro-Macro mechanical coupling)

Here, the stress state remains inside the LC yield curve is examined (Case 1). In this case, the generalized plasticity model applies. As explained in Sanchez et al., (2005), the generalized plasticity theory offers different alternatives to model elasto-plastic behaviour. It has been assumed that there is no specific elastic response related to this mechanism.

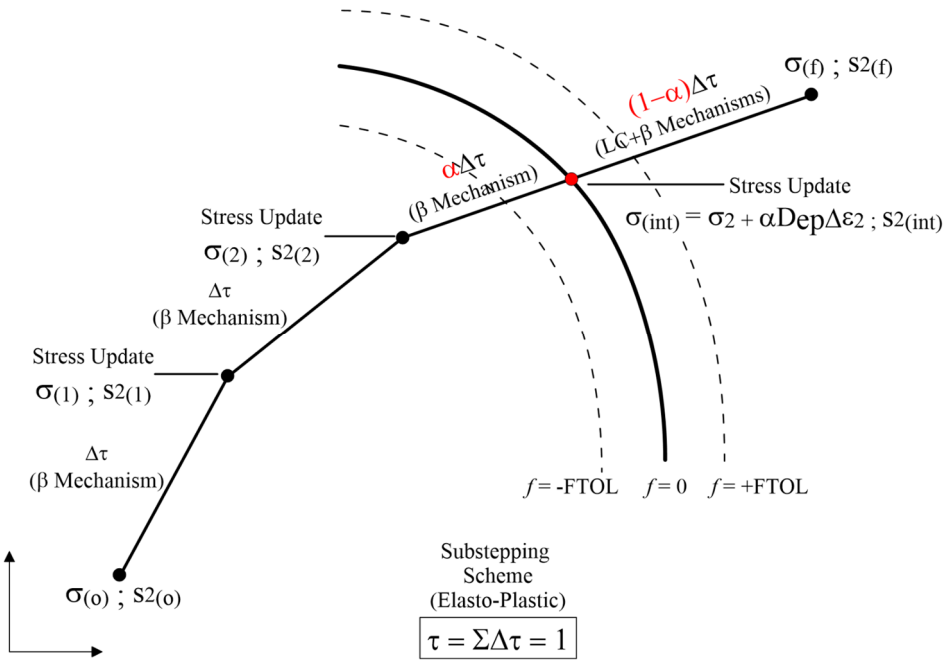

Figure 4-5. Explicit stress integration and yield surface (LC) intersection: transition from β mechanism to β+LC mechanisms.

Therefore, to determine which one of the microstructural stress paths is active, the loading/unloading criteria (see Chapter 3) is expressed in terms of tolerances, (as required by numerical implementation) as follows:

$\mathbf{n}_c^T \cdot d\boldsymbol{\sigma}^e > \text{CTOL} \rightarrow$ micro-structural contraction path (mC) (Eq. 4-18)

$\mathbf{n}_s^T \cdot d\boldsymbol{\sigma}^e > \text{CTOL} \rightarrow$ micro-structural swelling path (mS) (Eq. 4-19)

$\left.\begin{matrix}\mathbf{n}_c^T \cdot d\boldsymbol{\sigma}^e < \text{CTOL} \\ \mathbf{n}_s^T \cdot d\boldsymbol{\sigma}^e < \text{CTOL}\end{matrix}\right\} \rightarrow$ Neutral Loading (NL) (Eq. 4-20)

where:

- CTOL is a tolerance associated with the loading criteria of the mechanical coupling mechanism between structural levels.

The Euler's scheme with error control and sub-stepping (Sloan et al., 2001) has been adopted to update the stresses for the generalised plasticity model. In Sloan's algorithm, the size of each sub-increment may vary through the integration process, depending on the degree of non-linearity of the constitutive relations. Considering a pseudo time sub-increment in the range $0 \leq \Delta\tau_n \leq 1$, and using the subscript n-1 and n to

denote quantities computed at the pseudo times τ_{n-1} and $\tau_n = \tau_{n-1} + \Delta\tau_n$, the generalized strains for this sub-increment are given by:

$$\Delta\boldsymbol{\varepsilon}_n = \Delta\tau_n \Delta\boldsymbol{\varepsilon} \;\; ; \;\; \Delta s_{2_n} = \Delta\tau_n \Delta s_2 \qquad \text{(Eq. 4-21)}$$

With the explicit Euler method, the increments of the stresses ($\Delta\boldsymbol{\sigma}_1$) and history variables ($\Delta\mathbf{hv}_1$) are evaluated through the elasto-plastic relations expressed in the Section 3.4.5.1. at the end of the pseudo time step $\Delta\tau_n$. The estimated value of stress and history variables are obtained from:

$$\boldsymbol{\sigma}_n = \boldsymbol{\sigma}_{n-1} + \Delta\boldsymbol{\sigma}_1 \;\; ; \;\; \mathbf{hv}_n = \mathbf{hv}_{n-1} + \Delta\mathbf{hv}_1 \qquad \text{(Eq. 4-22)}$$

A more accurate estimation of the increments ($\Delta\boldsymbol{\sigma}_2$ and $\Delta\mathbf{hv}_2$) at the end of the interval $\Delta\tau_n$ can be found with the modified Euler procedure which uses the elasto-plastic matrices evaluated at $\boldsymbol{\sigma}_n$ and $\mathbf{hv}_n$.

The following estimations of the stresses and history variables can be made using:

$$\tilde{\boldsymbol{\sigma}}_n = \boldsymbol{\sigma}_{n-1} + \frac{1}{2}(\Delta\boldsymbol{\sigma}_1 + \Delta\boldsymbol{\sigma}_2) \qquad \text{(Eq. 4-23)}$$

$$\widetilde{\mathbf{hv}}_n = \mathbf{hv}_{n-1} + \frac{1}{2}(\Delta\mathbf{hv}_1 + \Delta\mathbf{hv}_2) \qquad \text{(Eq. 4-24)}$$

The relative error (R_n) can be obtained as Sloan, (1987):

$$R_n = \frac{1}{2}\max\left(\frac{\|\Delta\boldsymbol{\sigma}_2 - \Delta\boldsymbol{\sigma}_1\|}{\|\tilde{\boldsymbol{\sigma}}_n\|}; \frac{\|\Delta\mathbf{hv}_2 - \Delta\mathbf{hv}_1\|}{\left\|\widetilde{\mathbf{hv}}_n\right\|}\right) \qquad \text{(Eq. 4-25)}$$

The updating of the current sub-increment is accepted if R_n is not greater than the prescribed tolerance, STOL, and it is rejected otherwise. If it is rejected, a reduction of the size of the sub-increment is made and the integration process is repeated considering the new (reduced) generalised strain sub-increment (more details are given in *Item e*). This loop is repeated until the prescribed value of error tolerance is satisfied. When the acceptance condition is met, and before updating the stresses, it is necessary to check whether the new stress state remains inside the LC yield surface as described in *Item b*. If the stress state still remains in the yield surface LC, stresses and internal variables are updated according to

$$\boldsymbol{\sigma}_n = \tilde{\boldsymbol{\sigma}}_n \; ; \; \mathbf{hv}_n = \widetilde{\mathbf{hv}}_n \qquad \text{(Eq. 4-26)}$$

Then, the size of pseudo time sub-interval is automatically adjusted (as described in *Item e*) and a new sub-step can be started.

b. Intersection with the LC yield surface

At the end of each elasto-plastic sub-increment corresponding to Case 1 (i.e. only the plastic mechanism associated with the micro-Macro mechanical interaction is active, *Item a*), a check is performed to verify whether the stress state still lies inside the LC yield surface. The activation of the plastic mechanism associated with Macro-structural yielding occurs if

$$F_{n-1} = F_{|\boldsymbol{\sigma}_{n-1}, \mathbf{hv}_{n-1}|} < 0 \;\text{ and }\; F_n = F_{|\boldsymbol{\sigma}_n, \mathbf{hv}_n|} > 0 \qquad \text{(Eq. 4-27)}$$

In this case, to determine the portion of the stress increment that lies within the yield surface, it is necessary to find a scalar α such as (Sloan, 1987):

$$\boldsymbol{\sigma}_{int} = \boldsymbol{\sigma}_{n-1} + \Delta\boldsymbol{\sigma}^e(\alpha\Delta\varepsilon) \;\; ; \; F_{int} = 0 \qquad \text{(Eq. 4-28)}$$

The scalar α lies within the range $0 < \alpha < 1$. Value of α equal to zero implies a purely elasto-plastic deformation during the sub-step, whereas when it is equal to one it indicates a response inside the LC yield surface during the sub-step. In general, α gives the portion of the generalised strains sub-increment that moves the stresses from $\boldsymbol{\sigma}_{n-1}$ to the intersection with the yield surface $\boldsymbol{\sigma}_{int}$. The exact condition $F_{int} = 0$ is replaced by $\|F_{int}\| < FTOL$, were FTOL is a small positive tolerance. The value of α is obtained solving a non-linear system. The Newton–Rapshon scheme proposed by Sloan, (1987) has been extended for this model:

$$\boldsymbol{\sigma}_k = \boldsymbol{\sigma}_{k-1} + \alpha_k \mathbf{D}_e \Delta\boldsymbol{\varepsilon} \qquad \text{(Eq. 4-29)}$$

$$\alpha_{k+1} = \alpha_k + \Delta\alpha_{k+1} \qquad \text{(Eq. 4-30)}$$

$$\Delta\alpha_{k+1} = \frac{F_k}{(\partial F/\partial\boldsymbol{\sigma})_k^T \Delta\boldsymbol{\sigma} + (\partial F/\partial s_2)_k \Delta s_2} \qquad \text{(Eq. 4-31)}$$

The iterative procedure is started by assuming $\boldsymbol{\sigma}_o = \boldsymbol{\sigma}_{n-1}$ and a seed value for α_1, and continues until a relative error in the norm of stresses,

defined by the following Equation, is less than some specified tolerance ITOL.

$$\frac{\|\Delta\boldsymbol{\sigma}_{k+1} - \Delta\boldsymbol{\sigma}_{k}\|}{\|\boldsymbol{\sigma}_{k}\|} < \text{ITOL} \qquad \text{(Eq. 4-32)}$$

Once (Eq. 4-32) is satisfied the stresses and internal variables are updated using (Eq. 4-33); and the plastic part of the generalised strains increments (1-α) is integrated according to *Item c*, if only the LC plastic mechanism is active, or *Item d*, if both plastic mechanisms are active.

$$\boldsymbol{\sigma}_{n} = \boldsymbol{\sigma}_{k} \;;\; \mathbf{hv}_{n} = \mathbf{hv}_{k} \qquad \text{(Eq. 4-33)}$$

c. Integration of Macro-structural elasto-plastic law, BBM (irreversible mechanism associated with yielding of the Macro-structure)

The Macrostructure yielding alone is now considered (Case 2). The procedure to integrate the elasto-plastic law is analogous to that described in *Item a*, but now the corresponding elasto-plastic relations (Section 3.4.5.2.) are used to compute the increments of the stresses and history variables. Once the error criterion for the elasto-plastic integration is fulfilled (i.e. $R_n \leq$STOL, with R_n according to (Eq. 4-25)), stresses and history variables are updated ((Eq. 4-23) and (Eq. 4-24)). Depending on whether the sub-increment stress integration is accepted or rejected, the pseudo time is automatically adjusted for the next sub-step. Details of the sub-stepping strategy are presented in *Item e.*

At the end of each elasto-plastic sub-step it is necessary to check whether the stress state lies on the yield surface. In this scheme it is possible that the accepted updated stresses (at the end of the sub-increment) do not satisfy the yield criterion, i.e. $\|F_n\| <$ FTOL. As such departures are cumulative during the integration process, it is necessary to ensure that the stresses are corrected at the end of each sub-increment in order to satisfy the yield condition and, consequently, update accurately the stresses.

This step is known as 'yield surface drift correction'. The method proposed in Potts and Gens, (1985) has been adopted. The basic assumption is the consideration of a constant total strain during the correction process. In this model, it is also assumed that during the

correction process, Macro-suction remains constant. This implies that an elastic strain change must be balanced by an equal and opposite change in the plastic strains.

Following Potts and Gens, (1985) and Sloan, (1987), the required correction can be obtained as:

$$d\boldsymbol{\varepsilon}^{e} = [\mathbf{D}_{e}]^{-1}(\boldsymbol{\sigma}_{c} - \boldsymbol{\sigma}_{n}) \; ; \; d\boldsymbol{\varepsilon}^{e} = \mu_{c}\frac{\partial G}{\partial \boldsymbol{\sigma}} \qquad \text{(Eq. 4-34)}$$

Combining the above equations and considering the changes in hardening parameters (P_{o}^{*}), the following set of equations is obtained:

$$\boldsymbol{\sigma}_{c} = \boldsymbol{\sigma}_{n} - \mu_{c}\mathbf{D}_{e}\frac{\partial G}{\partial \boldsymbol{\sigma}} \;\; ; \; hv_{c}^{h} = hv_{b}^{h} + \mu_{c}dhv^{h}\frac{\partial G}{\partial \boldsymbol{\sigma}} \qquad \text{(Eq. 4-35)}$$

where μ_{c} is a scalar computed as

$$\mu_{c} = \frac{F_{|\boldsymbol{\sigma}_{n}, hv_{n}^{h}|}}{(\partial F/\partial \boldsymbol{\sigma})^{T}\mathbf{D}_{e}(\partial G/\partial \boldsymbol{\sigma}) + (\partial F/\partial hv^{h})^{T}hv^{h}(\partial G/\partial \boldsymbol{\sigma})} \qquad \text{(Eq. 4-36)}$$

As the change in total volumetric strain is null during the drift process, the total porosity remains constant, however the micro pore volume fraction $\bar{\phi}_{1}$ and micro-suction (s_{1}) are also corrected.

This scheme has to be applied repeatedly until the yield condition ($\|F_{c}\| < FTOL$) is satisfied.

d. Integration of elasto-plastic law when two plastic mechanism are active (β+LC)

When two irreversible mechanisms are active simultaneously, LC and β (Case 3), the integration process used is the same as indicated in the *Item a*, but now the elasto-plastic matrix and vectors correspond to those indicated in the Section 3.4.5.3. If the step is accepted, stresses and internal variables are updated. If not, the sub-increment is re-started (see *Item e*). Finally, at the end of each successful sub-increment, the correction of stresses and history variables due to the 'yield surface drift' is performed according to a procedure similar to that described previously.

e. Sub-stepping strategy

As a main feature of this strategy, it can be mentioned that once the local error has been computed for a given step, the size of the next step is evaluated considering the result of this error estimation. Therefore, the size of each sub-interval is adjusted according to the information of the previous step. This error control allows the automatic variation of the size of the interval over the course of the integration, depending on the degree of non-linearity of the model (Sánchez et al., 2008).

The sub-increment strategy and the main stages of integration can be summarized in the following stages:

1. The integration scheme is started with known initial state (stresses and history variables) and generalized strain increments ($\Delta\varepsilon$ and Δs_2) coming from the global solution.
2. An initial pseudo time step is assumed, $\Delta\tau_1$ (a value of 0.25 is adopted)
3. Generalized strains sub-increment is obtained from (Eq. 4-21).
4. The integration procedure indicated in the *Items a, b* and *c* are performed in the case of elasto-plastic integration.
5. After successful elasto-plastic sub-increment and before checking the pseudo time, it is necessary to verify the following points:
   - If the sub-increment corresponds to a Case 1 (i.e. only the interaction mechanism is active), it is necessary to check if the updated stress remains inside the LC yield surface (Item b):
     - If the stress remains inside the LC curve, stresses and history variables are updated according to (*Item a*). Then the pseudo time is checked according to stage 9.
     - If the stress sub-increment crosses the LC yield surface, stresses and internal variables are updated with the elastic-plastic portion corresponding to Case 1 (*Item a*). The other portion of the elasto-plastic sub-increment, which corresponds to Case 3 (i.e. two elato-plastic mechanisms active), is integrated according to *Item b*.
   - If the sub-increment corresponds to a Case 2 or 3, it is necessary to correct for the drift of the yield surface according to *Item c*. Then the pseudo time is checked according to stage 9.

6. The relative error measure (R_n) is computed (Eq. 4-25) and q is evaluated as:

$$q = 0.9\sqrt{STOL/R_n} \text{ with the constrain } 0.1 \leq q \leq 1.1 \qquad \text{(Eq. 4-37)}$$

7. Regardless of whether the sub-increment is accepted or not, the next pseudo time step is automatically adjusted as

$$\Delta\tau_{n+1} = q\Delta\tau_n \qquad \text{(Eq. 4-38)}$$

8. After a refused sub-increment, a new sub-increment is re-started with a smaller step-size (Eq. 4-38) and with reduced generalized strains sub-increments according to (Eq. 4-21). This loop is repeated until a successful sub-increment size is obtained. Here, an additional control is imposed in order to avoid an excessive number of iterations. The user can establish a maximum number of iterations to reach a successful integration. On reaching that number, the integration process is aborted and a reduction of the time increment is imposed over the global system. This strategy yields good results, especially when complex highly non-linear problems are modelled.
9. The sub-stepping integration continues until the entire increment of the generalized strains is applied, this is verified through:

$$\sum \Delta\tau = \tau = 1 \qquad \text{(Eq. 4-39)}$$

As pointed out by Sánchez et al., (2008), the generalized plasticity model is integrated with the same degree of accuracy and efficiency that the conventional BBM elasto-plastic law. From the algorithm point of view, the main difference is that the 'yield surface drift correction' is omitted in a generalized plasticity model, as no yield surface is explicitly define.

The graphical description and the algorithm structure of the explicit integration of the double-structure model are presented in the Figure 4-5 and Figure 4-6, respectively.

Initialize

Initial State → $\sigma_{(o)}$; $s2_{(o)}$; $f_{(o)}$
$hv_{(o)} = \{P_o^*; \omega\beta ; s1 ; \phi ; \bar{\phi}1 ; \bar{\phi}2\}_{(o)}$

Strain and Suction increment → $\Delta\varepsilon$; $\Delta s2$

$\tau = 0$; $\Delta\tau = 0.25$

DO WHILE ($\tau < 1$)

  DO WHILE ($R_n \geqslant$ STOL)

    $\Delta\varepsilon = \Delta\tau\Delta\varepsilon$; $\Delta s2 = \Delta\tau\Delta s2$; STOL

    Explicit Euler Method (β mechanism)→ $\Delta\sigma$; Δhv

    $\sigma_{(i)} = \sigma_{(o)} + \Delta\sigma$; $hv_{(i)} = hv_{(o)} + \Delta hv$; $s2_{(i)} = s2_{(o)} + \Delta s2$; R_n ; $f_{(i)}$

    $q = \max\{0.9\ (STOL/R_n)^{1/2}, 0.1\}$ New time step

    $\Delta\tau = q \cdot \Delta\tau$

  END DO

  IF (($f_{(o)} <$ -FTOL) and ($f_{(i)} \leq$ +FTOL)) **THEN**

    Update (succesful substep)

    $\sigma_{(f)} = \sigma_{(i)}$; $hv_{(f)} = hv_{(i)}$; $s2_{(f)} = s2_{(i)}$

  ELSE IF (($f_{(o)} >$ -FTOL) and ($f_{(i)} \leq$ +FTOL)) **THEN**

    Neutral Loading

    $\sigma_{(f)} = \sigma_{(o)}$; $hv_{(f)} = hv_{(o)}$; $s2_{(f)} = s2_{(o)}$

  ELSE IF (($f_{(o)} <$ -FTOL) and ($f_{(i)} >$ +FTOL)) **THEN**

    $\Delta\varepsilon = \Delta\tau\Delta\varepsilon$; $\Delta s2 = \Delta\tau\Delta s2$

    Iterative procedure - find α such that $f_{(int)} <$ ||FTOL|| (LC intersection)

    Update at LC intersection

    $\sigma_{(f)} = \sigma_{(int)} + \alpha D_{ep}\Delta\varepsilon$; $s2_{(f)} = s2_{(int)} + \alpha\Delta s2$; $hv_{(f)} = hv_{(int)}$

  ELSE IF (($f_{(o)} <$ ||FTOL||) and ($f_{(i)} >$ +FTOL)) **THEN**

    $\tau_p = 0$; $\Delta\tau_p = 1$

    DO WHILE ($\tau_p < 1$)

      DO WHILE ($R_n \geqslant$ STOL)

        $\Delta\varepsilon = \Delta\tau_p((1-\alpha)\Delta\tau\Delta\varepsilon)$; $\Delta s2 = \Delta\tau_p((1-\alpha)\Delta\tau\Delta s2)$; STOL

        Explicit Euler Method (β and LC mechanisms)→ $\Delta\sigma$; Δhv

        $\sigma_{(i)} = \sigma_{(o)} + \Delta\sigma$; $hv_{(i)} = hv_{(o)} + \Delta hv$; $s2_{(i)} = s2_{(o)} + \Delta s2$; R_n ; $f_{(i)}$

        $q = \max\{0.9\ (STOL/R_n)^{1/2}, 0.1\}$ New time step

        $\Delta\tau_p = q \cdot \Delta\tau_p$

      END DO

      IF ($f_{(i)} >$ +FTOL) **Drift correction procedure**

      Update (succesful elastoplastic substep)

      $\sigma_{(f)} = \sigma_{(i)}$; $hv_{(f)} = hv_{(i)}$; $s2_{(f)} = s2_{(i)}$

      $q = \min\{0.9\ (STOL/R_n)^{1/2}, 1.1\}$ Next substep

      $\Delta\tau_p = q \cdot \Delta\tau_p$

      $\tau_p = \tau_p + \Delta\tau_p \rightarrow \Delta\tau_p = 1 - \tau_p$

    $\sigma_{(f)} = \sigma_{(i)}$; $hv_{(f)} = hv_{(i)}$; $s2_{(f)} = s2_{(i)}$ at $\tau_p = 1$

    END DO

  ELSE

    Inadmissible Stress State Zone

  END IF

  $q = \min\{0.9\ (STOL/Rn)^{1/2}, 1.1\}$ Next substep

  $\Delta\tau = q \cdot \Delta\tau$

  $\tau = \tau + \Delta\tau \rightarrow \Delta\tau = 1 - \tau$

END DO

Exit

Final State at $\tau = 1.0$ → $\sigma_{(f)}$; $s2_{(f)}$
$hv_{(f)} = \{P_o^*; \omega\beta ; s1 ; \phi ; \bar{\phi}1 ; \bar{\phi}2\}_{(f)}$

Figure 4-6. Explicit integration algorithm of the double-structure constitutive model.

4.3. Model performance

To illustrate the performance of the formulation and the numerical implementation, a series of simple modelling cases will be presented. The description of qualitative features is the main goal, in this way, the capabilities and limitations of this formulation can be readily assessed. Herein, the constitutive responses will be obtained through small 3D geometries where the boundary conditions are applied simultaneously to all nodes in the domain. Therefore, the same response is obtained for all integration points. In this way, the constitutive behaviour and the performance of the implementation algorithm can be directly assessed.

This verification task is focused on the model response to the following micro-Macro interaction mechanisms and well-defined stress and suction paths:

- Macro-micro water exchange — Γ^w mechanism.
- Macro-micro water exchange — f_β mechanism.
- Dependence of swelling pressure on dry density.
- Dependence of swelling strains on applied stresses.
- Strain irreversibility in wetting/drying cycles.
- Homogenization process.

The performance of numerical integration algorithm, evaluated in terms of CPU time and the number of sub-increments, is not included in this analysis.

The set of input parameters for the model performance is reported in Table 4-1. They were obtained from the modelling of a compacted mixture of bentonite powder and bentonite pellets (see Chapter 5).

Table 4-1. Input parameters for the performance modelling.

Bishop parameter micro-structural level	p_k (-)	0.7
	q_k (-)	100
Non-linear elasticity	$\bar{\kappa}$ (-)	0.0001
	κ_s (-)	0.028
	ν (-)	0.3
Macro-micro mechanical interaction functions	f_{ms0}(-)	1
	f_{ms1}(-)	0

	n_{ms}(-)	2
	f_{mc0}(-)	0
	f_{mc1}(-)	1
	n_{mc}(-)	2
Macro-structural level Plastic mechanism (BBM)	φ (°)	25
	p_c (MPa)	0.035
	λ_{sat}(-)	0.13
	r (-)	0.62
	β (MPa^{-1})	0.028
	k_s (-)	0.01
	α (-)	1
Leakage parameter	γ ($kg.s^{-1}.m^{-3}.MPa^{-1}$)	1.e-5
Water retention curve for micro-structural level	$(P_o)_1$ (MPa)	379
	σ_o	0.072
	$(\lambda_o)_1$ (-)	0.899
	$(S_r)_{L1}$ (-)	0.3
	$(S_m)_{L1}$ (-)	1
	$(P_d)_1$ (MPa)	800
	$(\lambda_d)_1$ (-)	2.243
Water retention curve for Macro-structural level	$(P_o)_2$ (MPa)	15
	σ_{To}	0.072
	$(\lambda_o)_2$ (-)	0.064
	$(S_r)_{L2}$ (-)	0
	$(S_m)_{L2}$ (-)	1
	$(P_d)_2$ (MPa)	850
	$(\lambda_d)_2$ (-)	3.899
Intrinsic permeability	k_o (m^2)	2.e-20
	b (-)	7
	$(\phi_o)_2$	0.46
Initial conditions	P_o^* (MPa)	0.4
	ϕ (-)	0.40
	$\bar{\phi}_1$(-)	0.22
	P_{L1}(MPa)	-300
	P_g (MPa)	0.1

4.3.1. Macro-micro water exchange — Γ^w mechanism

According to the formulation, in a general state of the expansive clays, the water potential at both structural level are not assumed equal. The time dependent mechanism of mass water exchange, Γ^w, is evaluated in this section.

An appropriate manner to evaluate the water potential equilibration between the Macro- and micro- structural levels is through loading paths at constant Macro-structural suction (Figure 4-7). Hence, the micro-structural suction evolves according to the liquid pressure differences and the leakage parameter, γ. The classical linear approach, with constant values of γ, is used.

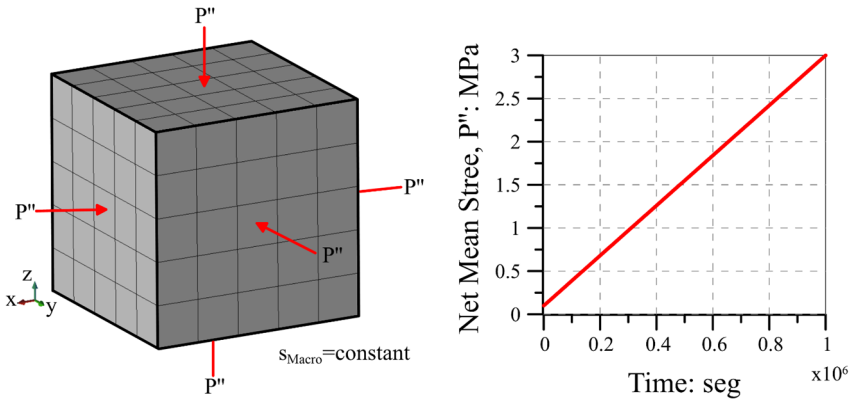

Figure 4-7. Left: FE mesh for loading stress paths at constant Macro-structural suction; Right: Applied loading rate.

The evolution of the loading-collapse (LC) curve due to the loading paths at different values of Macro suction is shown in the Figure 4-8. It behaves as in the BBM formulation (Alonso et al., 1990 and Chapter 3), in which the hardening/softening of this yield limit is suction dependent. The variation of the saturated preconsolidation isotropic stress, p_0^*, is related to the plastic volumetric strains (see Figure 4-9). The Macro-micro mechanical interaction mechanism, f_β, is always active; therefore, these irreversible strains occurs inside the LC curve as well.

The hydraulic response is analysed with the time evolution of the suction and saturation degree of both structural levels (Figure 4-10). For the constant leakage parameter γ=1.e-5 kg/s.m^3, the hydraulic equilibrium is

reached in all loading paths. At these states, the Macro and micro saturation degrees are not the same, because each structural level follows a different water retention curve.

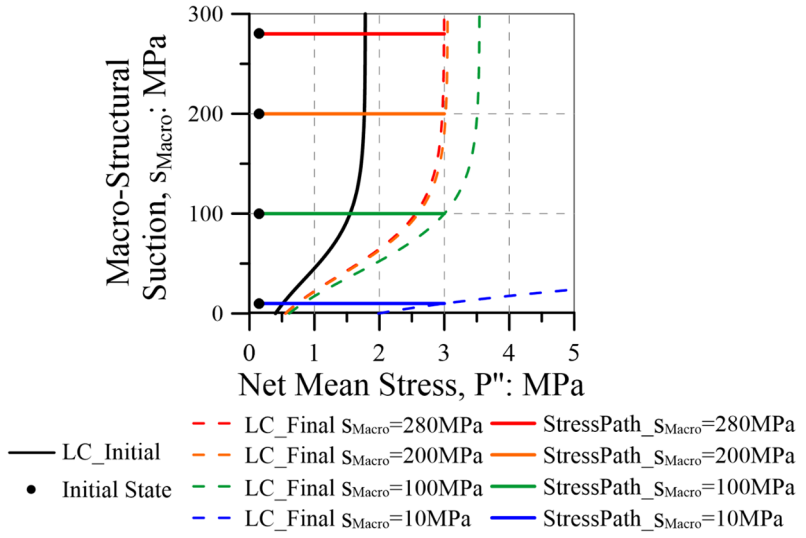

Figure 4-8. Loading stress paths at constant Macro-structural suctions and Loading-Collapse curve (LC) evolution.

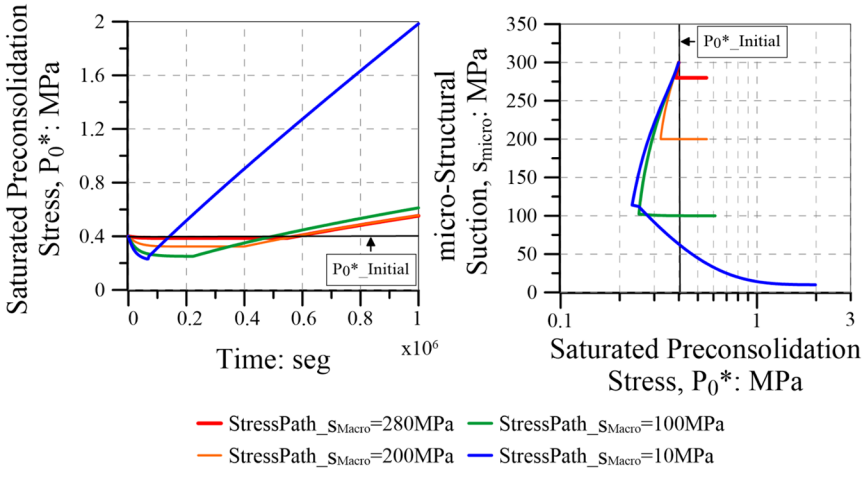

Figure 4-9. Left: time evolution of the saturated preconsolidation stress P_0*; Right: variation of the saturated preconsolidation stress P_0* with micro-structural suction.

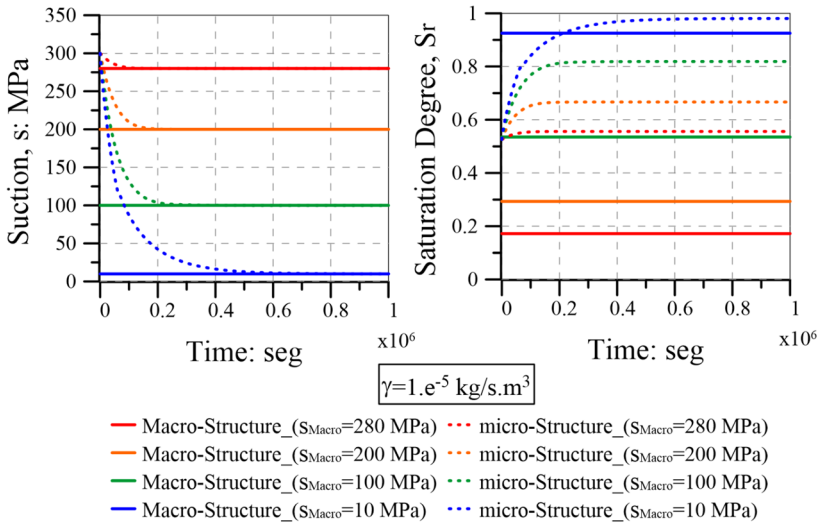

Figure 4-10. Left: time evolution of the suction in the Macro- and micro-structure; Right: time evolution of the saturation degree in the Macro- and micro-structure. Leakage parameter γ=1.e-5 kg/s.m^3.

The pore space evolution is plotted in the Figure 4-11. The Macro pore volume fraction, $\bar{\phi}_2$, increases due to micro-structural swelling and the yielding point establishes a marked volume reducing trend. The magnitude increase of the $\bar{\phi}_2$ prior to the yield point is related to the structural suction differences; resulting from the amount of mass water exchanged from Macro to micro.

The tracking of the total porosity, ϕ, is computed from the addition of the pore volume fractions ($\bar{\phi}_1$ and $\bar{\phi}_2$). However, the micro pore volume fraction, $\bar{\phi}_1$, is not the best indicator of the pore space evolution at clay aggregates. Based on its definition ($(V_{Pores})_{micro}/V$), the total volume reduction due to the Macro collapse deformation produces an increase of this pore volume fraction. Conversely, the micro-porosity ($\phi_1 = (V_{Pores})_{micro}/V_1$) reflects the actual behaviour of aggregates; they swell until hydraulic equilibrium. In conclusion, the pore volume fractions and the micro-porosity are the necessary indicators to describe the fabric evolution of the expansive clays; their proper identification is fundamental.

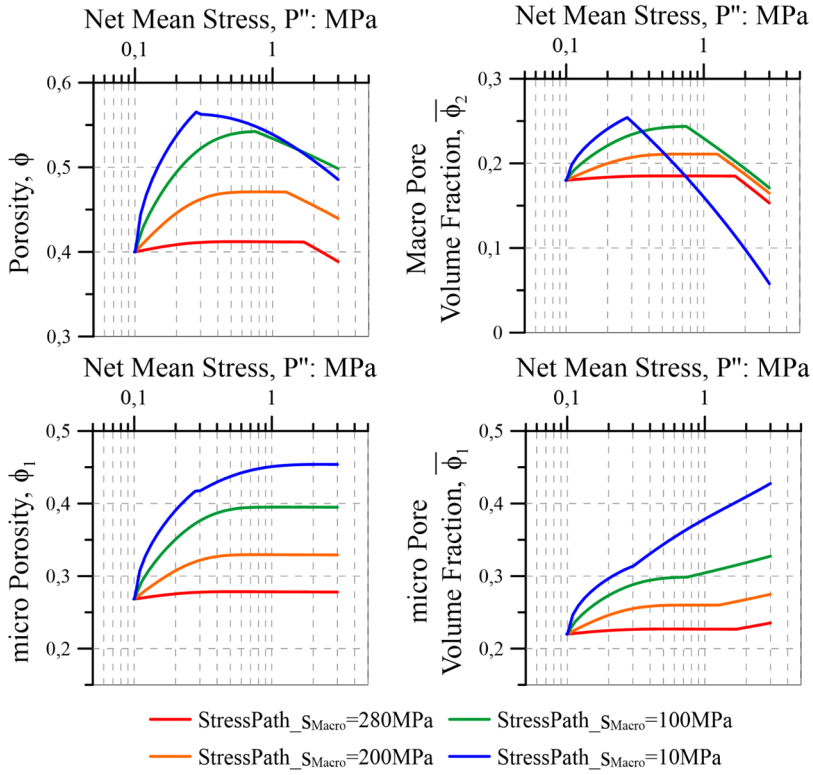

Figure 4-11. Variation of the total porosity (ϕ), pore volume fractions ($\bar{\phi}_1$ and $\bar{\phi}_2$) and micro porosity (ϕ_1) with mean net stress. Leakage parameter γ=1.e-5 kg/s.m^3.

A reduction of the leakage parameter modifies the kinematic of the water exchange. The same loading paths have been calculated for γ=1.e-6 kg/s.m^3. The hydraulic response (Figure 4-12) shows that the suction equilibrium is only reached for the Macro-structural suctions of 280 MPa and 200 MPa. The evolution of pore space presents a similar trend of the previous case, however the swelling deformations are lower due to the reduced amount of water exchanged (Figure 4-13).

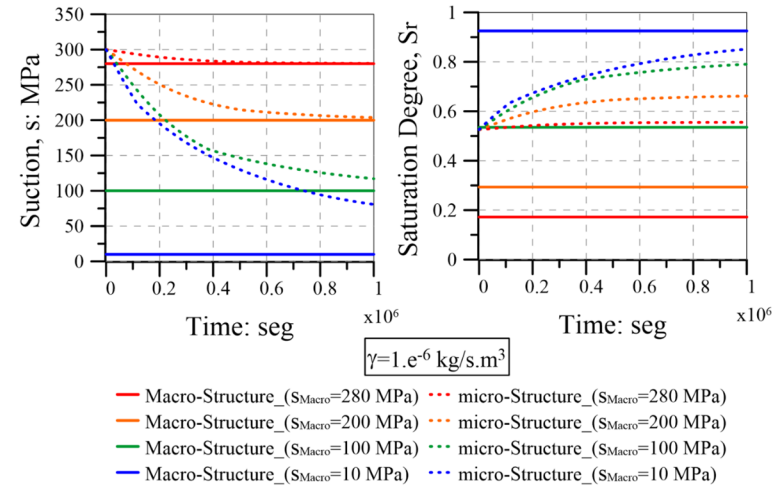

Figure 4-12. Left: time evolution of the suction in the Macro- and micro-structure; Right: time evolution of the saturation degree in the Macro- and micro-structure. Leakage parameter γ=1.e-6 kg/s.m³.

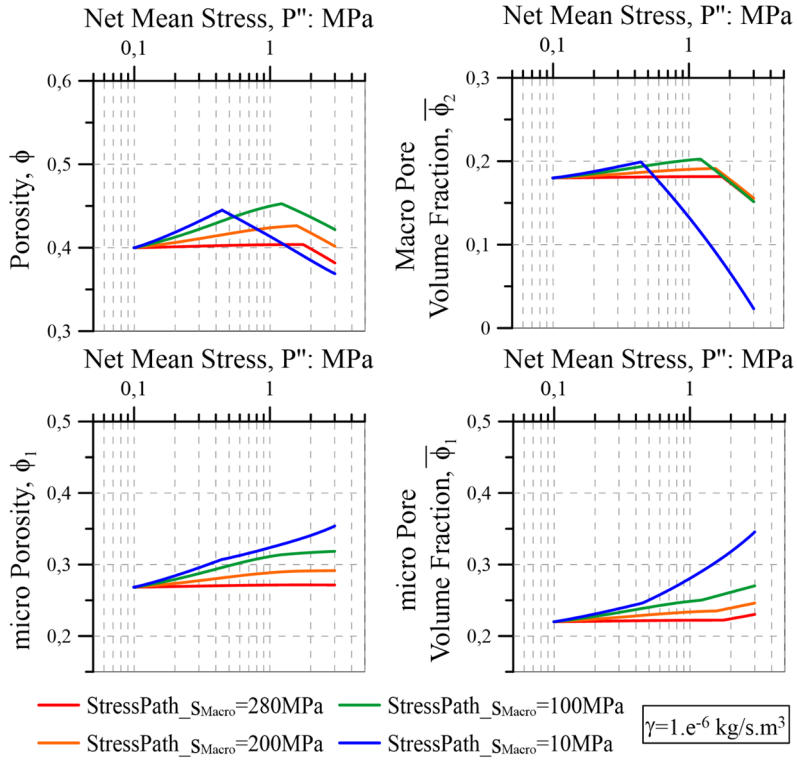

Figure 4-13. Variation of the total porosity (ϕ), pore volume fractions ($\bar{\phi}_1$ and $\bar{\phi}_2$) and micro porosity (ϕ_1) with mean net stress. Leakage parameter γ=1.e-6 kg/s.m³.

4.3.2. Macro-micro mechanical interaction — fβ mechanism

The mechanical interaction between the Macro- and micro-structural levels has been the core of the double structure formulation for expansive clays. As explained in Chapter 3, this stress dependent mechanism accounts for the plastic volumetric deformations at Macro level due to swelling or shrinkage of the micro-structure. The relevance of these deformations on the expansive clays behaviour is explored by neglecting the mechanical interaction parameters (Table 4-1) for the loading stress paths of the precedent section (Figure 4-7 and Figure 4-8).

The saturated preconsolidation isotropic stress, p_0^*, which is function of the Macro plastic volumetric strains, evolves only when the LC curve is crossed (Figure 4-14). This is a natural consequence of the deactivation of the interaction mechanism.

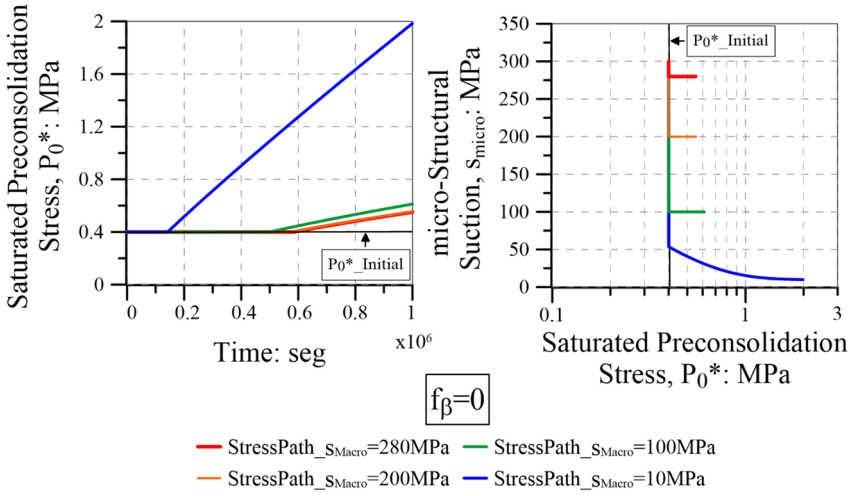

Figure 4-14. Left: time evolution of the saturated preconsolidation stress P_0^*; Right: variation of the saturated preconsolidation stress P_0^* with micro-structural suction. β mechanism deactivated.

The water exchange mechanism, Γ^w, is independent of the mechanical interaction, therefore, the hydraulic equilibration is not modified (Figure 4-15). The pore space evolution shows this particular condition (Figure 4-16). The structural levels are mechanically decoupled. On the one hand, the micro-structure swells due to the hydration coming from the Macro-structure (Γ^wmechanism). On the other hand, the macro-structure

behaves according to the Barcelona Basic Model (Alonso et al., 1990 and Chapter 3) along the loading stress paths. The physical sense of this response is truly debatable; nevertheless, this is not the goal of these computations. They provide a satisfactory check on the numerical implementation of the constitutive formulation.

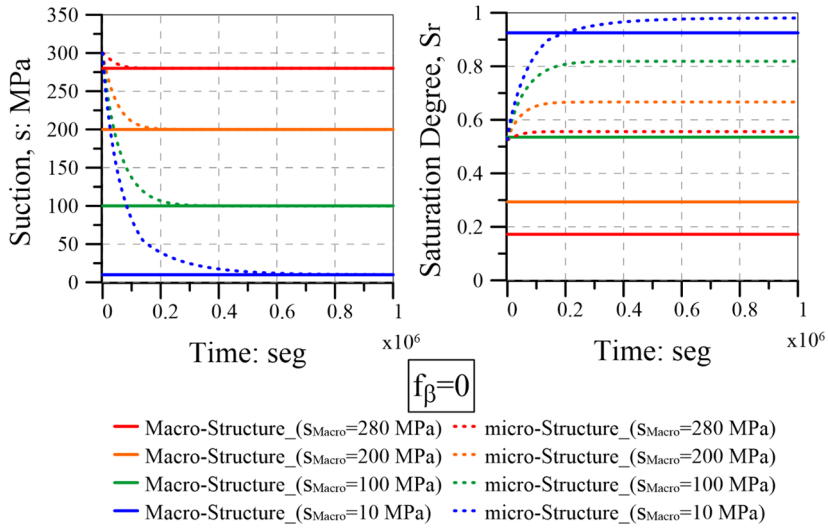

Figure 4-15. Left: time evolution of the suction in the Macro- and micro-structure; Right: time evolution of the saturation degree in the Macro- and micro-structure. Leakage parameter γ=1.e-5 kg/s.m^3 and β mechanism deactivated.

An extreme condition is to cancel both mechanisms ($\Gamma^w$and β). Applying the loading stress paths at equal Macro- and micro-suction (Figure 4-17), the BBM behaviour is recovered for the double-structure material (Figure 4-18).

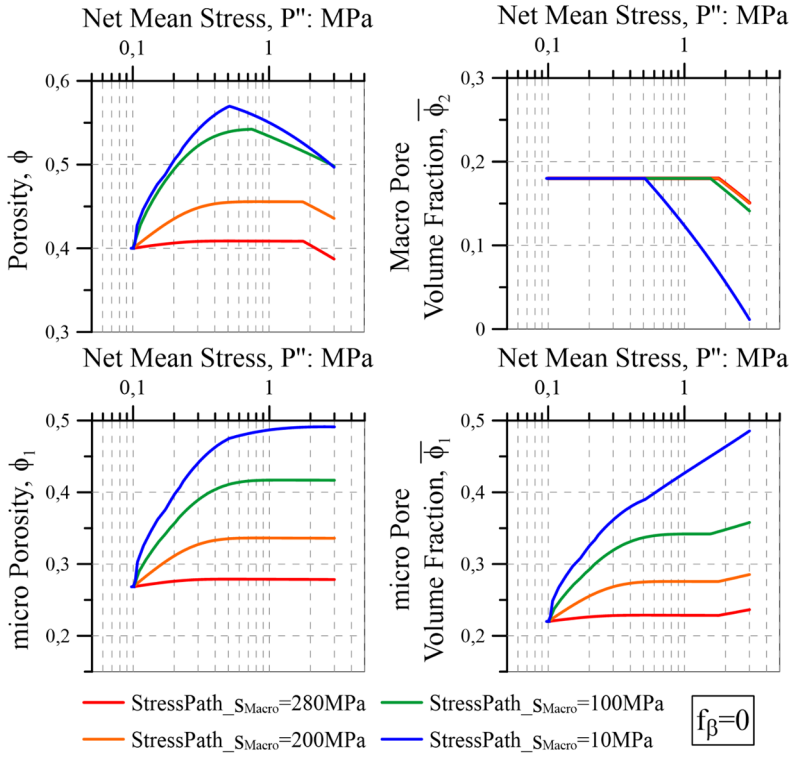

Figure 4-16. Variation of the total porosity (ϕ), pore volume fractions ($\bar{\phi}_1$ and $\bar{\phi}_2$) and micro porosity (ϕ_1) with mean net stress. β mechanism deactivated.

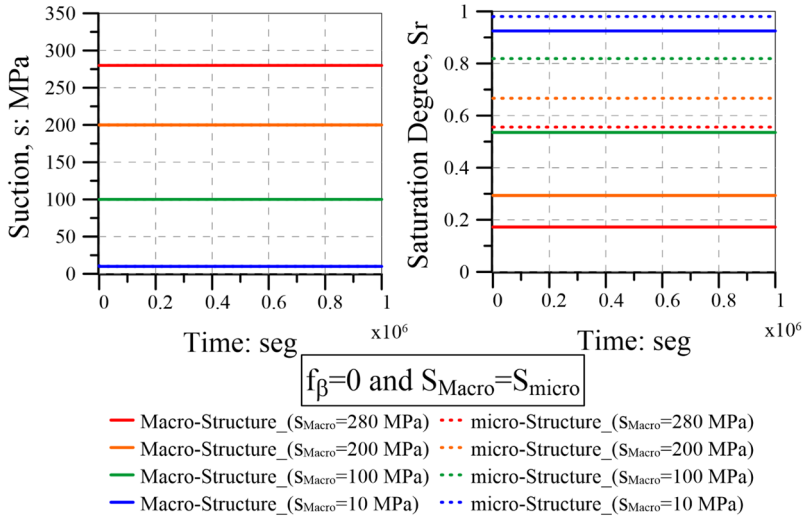

Figure 4-17. Left: time evolution of the suction in the Macro- and micro-structure; Right: time evolution of the saturation degree in the Macro- and micro-structure. . Γ^w and β mechanisms deactivated.

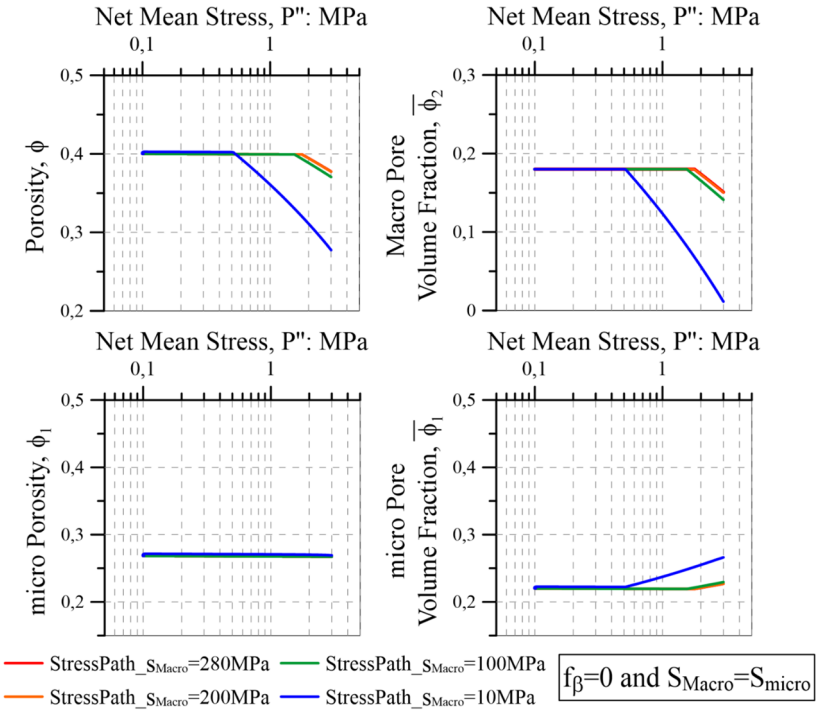

Figure 4-18. Variation of the total porosity (ϕ), pore volume fractions ($\bar{\phi}_1$ and $\bar{\phi}_2$) and micro porosity (ϕ_1) with mean net stress. Γ^w and β mechanisms deactivated.

4.3.3. Dependence of swelling pressure on dry density

The compaction plane (in terms of dry density, ρ_d, against water content, w) is a very convenient procedure to represent the compaction states of a given soil. This plane remains the basic representation for investigating the properties of compacted soils. As pointed in Alonso et al., (2013), the development of elastoplastic models provides an alternative way to characterise the initial state compacted soils by associating model parameters and variables with the pair (ρ_d, w). For instance, the dry density archived by compaction can be related to the position of the yield surface after compaction. Water content, on the other hand, is controlled mainly by the current suction, s. In the context of the elastoplastic BBM model, the yield surface is essentially defined by the isotropic yield stress for saturated conditions p_0^* (see Chapter 3). Therefore as a starting point, the pair (p_0^*, s) provide equivalent information to (ρ_d, w), with one added

advantage: they supply fundamental information for the constitutive model.

Accordingly, the variation of the dry density generates different location of loading-collapse curves (LC). Values of 0.40, 1.0 and 1.5 MPa are selected for p_0^*. The swelling pressure tests are conducted starting from the same initial stress state (p'', s), preventing any boundaries displacements and imposing a hydration rate until saturation (Figure 4-19).

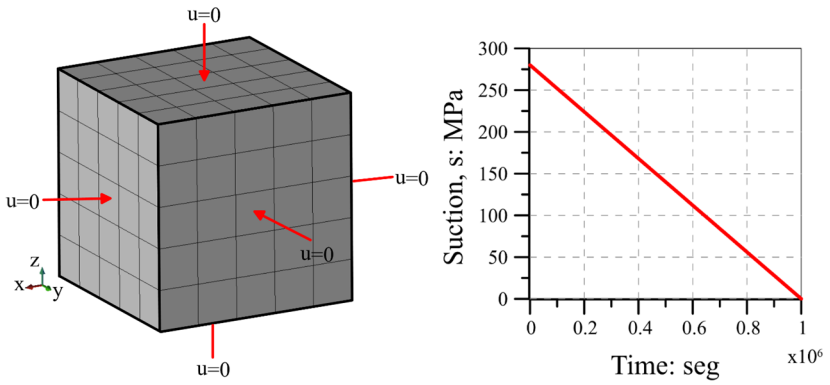

Figure 4-19. Left: FE mesh for swelling pressure test at constant volume; Right: Applied hydration rate.

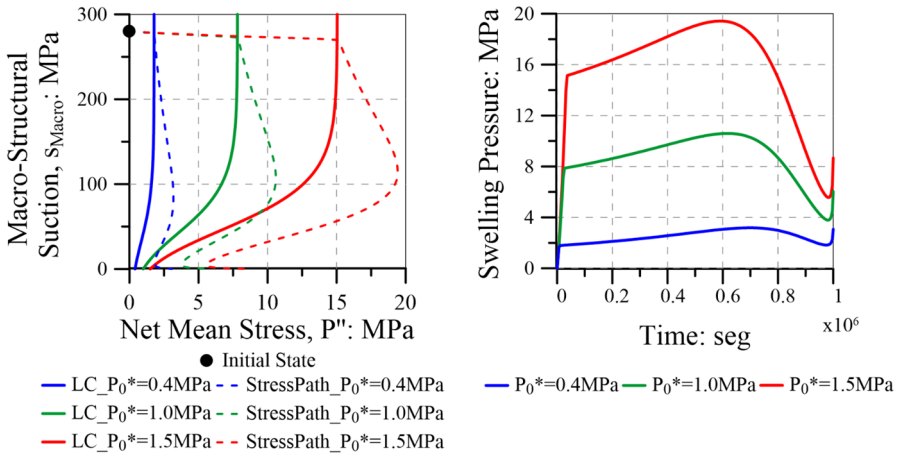

Figure 4-20. Left: stress paths at constant volume for different P_0*; Right: swelling pressure generated by suction changes.

The stress paths and the kinetic evolution of swelling pressure are shown in the Figure 4-20. The initial phase of swelling pressure is followed by the macro-structural collapse. The evolution of the micro-structural level continues after Macro-structural rearrangement, which result in an increase of the swelling pressure. The increase of swelling pressure values due to the increase of dry density (or p_0^*) is in aggreement with the experimental evidence (see Chapter 2, Figure 2-17).

4.3.4. Dependence of swelling strains on applied stress

Three swelling test are performed under constant isotropic net stress (0.5, 1.0 and 1.5 MPa), applying the same hydration of the above model (Figure 4-21). The water exchange between macro- and micro-structural levels is always activated. The initial loading-collapse curve LC is given by parameters and initial conditions (p_0^*) reported in the Table 4-1.

A clear dependence of swelling strains on applied stress at the same dry density is proven (Figure 4-22). The location of the stress path respect to the initial LC curve is the main responsible of this behaviour. The key point is the Macro-structural collapse generated at the intersection with the yield limit. Before this intersection, the f_β mechanism produces Macro-structural irreversible strains due to micro-structural swelling. After the collapse, the strains indicate a progressive swelling due to the subsequent micro-structural evolution. The evolving of the LC curve indicates denser states after the wetting paths.

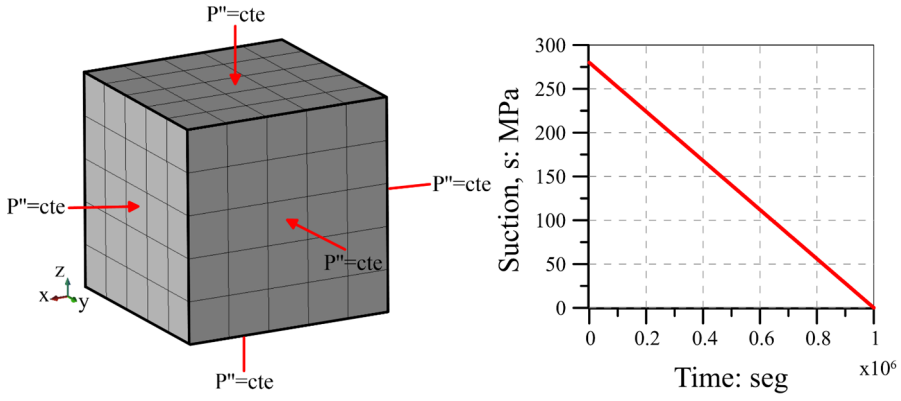

Figure 4-21. Left: FE mesh for wetting paths at constant net mean stress; Right: Applied hydration rate.

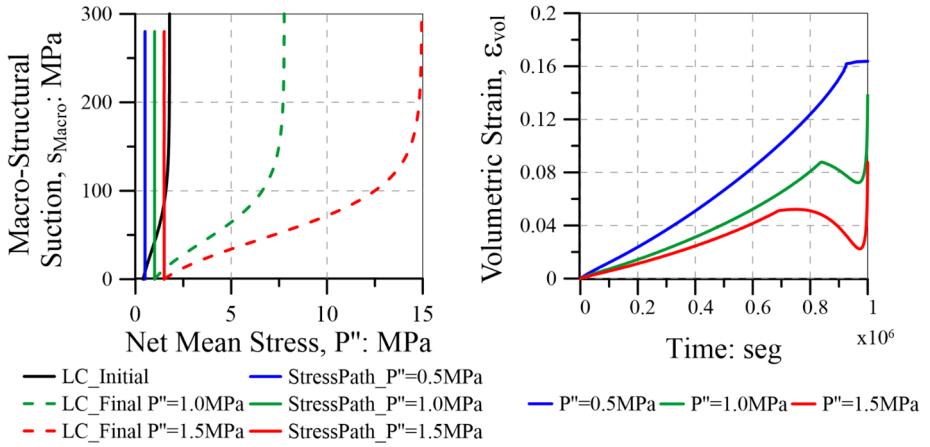

Figure 4-22. Left: wetting paths under constant isotropic net stress at the same P_0* and Loading-Collapse curve (LC) evolution; Right: volumetric strains generated by the wetting paths.

4.3.5. Strain irreversibility in wetting/drying cycles

The strain irreversibly after a wetting/drying cycle is evaluated through stress paths with constant isotropic net stress (Figure 4-23 and Figure 4-24). It is interesting to note that the stress level respect to the LC location (p_0^*) indicates the type of mechanism responsible of the plastic strains.

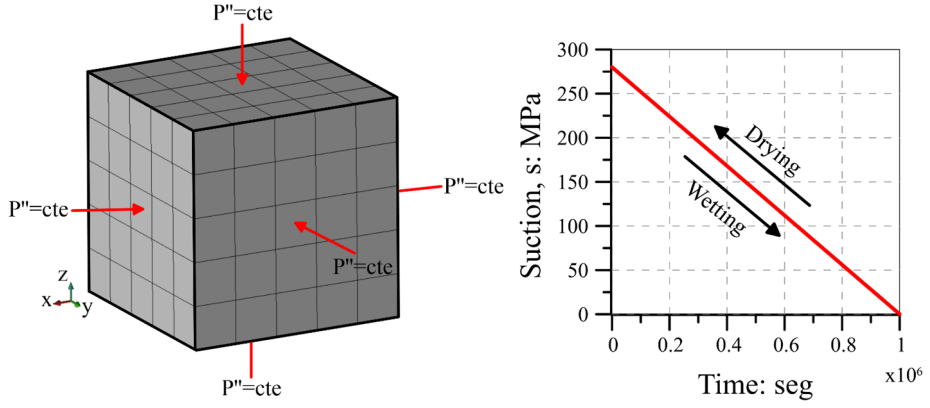

Figure 4-23. Left: FE mesh for wetting-drying cycles at constant net mean stress; Right: Applied hydration rate.

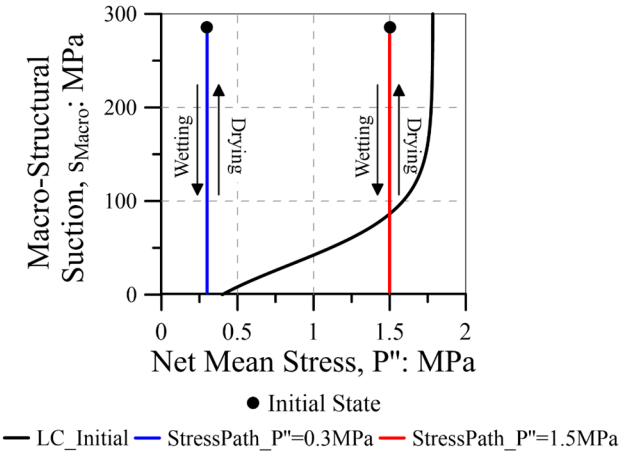

Figure 4-24. Wetting/Drying paths at constant isotropic net stress.

The Figure 4-25 shows the volumetric strain as function of time and macro-structural suction. The suction path at P''=0.3 MPa shows an interesting response; plastic deformation occurs despite it does not cross the initial LC curve; the structural mechanical interaction mechanism, f_β, is the responsible for this. In contrast, the volumetric behaviour of the path at P''=1.5 MPa involves the f_β mechanism inside the yield limit and, after crossing it, the response is accounted for the combination of f_β mechanism and the Macro-structural re-arrangement (LC). In Figure 4-24, only the initial LC yield surface is shown for clarity. However, it is not fixed during the suction changes. The LC curve evolves with the macro-structural plastic deformation induced by the mechanisms described previously.

The elastic strains due to Macro-structural suction change is in agreement with the constitutive formulation. They are stress and suction dependent, therefore the swelling or shrinkage are higher at low stress states. This is observable at the beginning of the wetting stage (before collapse of the P''=1.5 MPa) and during the complete drying stage (Figure 4-25).

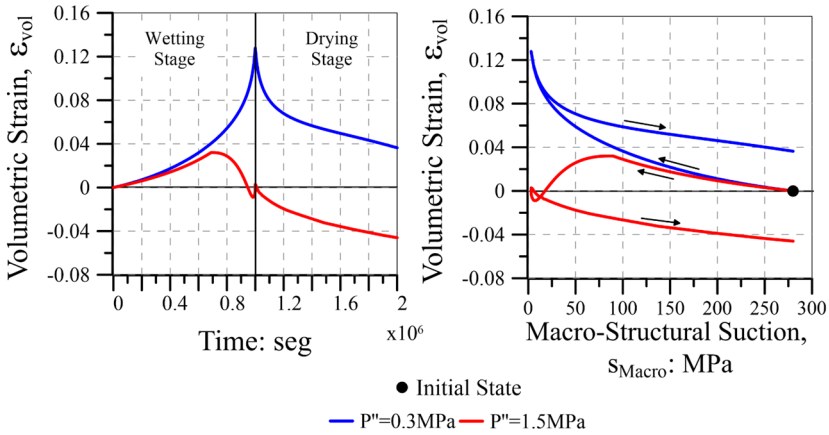

Figure 4-25. Strain irreversibility after one wetting-drying cycle.

4.3.6. Homogenization process

The bentonite homogenization is a complex phenomenon that depends on material emplacement and transient periods of hydraulic and/or thermal actions (see Chapter 2). The deep understanding of these processes is essential for the design of seals, backfills and bentonite barriers.

The numerical modelling of the homogenization should be conceived in a progressive manner. A simple homogenization case is presented (Figure 4-26). The idea is that the suction in both domains decrease linearly to zero from its initial value simultaneously in the entire domain. Therefore, this is not an infiltration test and no flow condition is enforced. The hydration of a domain using volumetric flows implies the same behaviour for all nodes and gauss points (Figure 4-27). Therefore, the constitutive response of the model is clearly evaluated. The displacements are restricted in all external boundaries; the x-displacements of boundary between the domains are not fixed along the mesh.

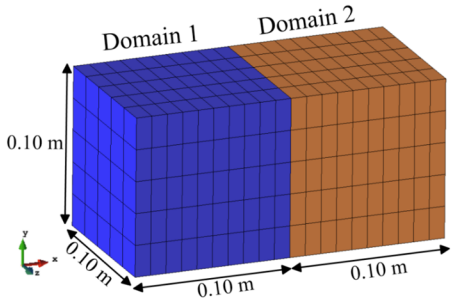

Figure 4-26. Geometry and FE mesh for homogenization test (HT-M)

Model	Suction Change Domain 1 (D1)	Suction Change Domain 2 (D2)	Flow D1 ⟶ D2
HT-M	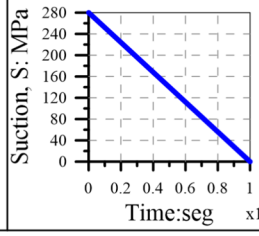	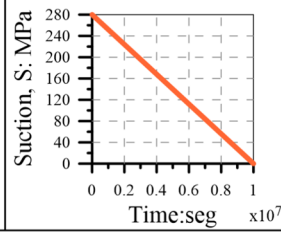	No flow conditions between domains

Figure 4-27. Volumetric flows for the HT-M model.

The Table 4-2 shows the input parameters of the materials at Domain 1 and Domain 2. The expansive material of the Domain 2 is more compressible ($\bar{\kappa}$_Domain1 < $\bar{\kappa}$_Domain2) and less compacted (P_0^*_Domain1 > P_0^*_Domain2) than the material of the Domain 1.

The hydraulic parameters are the same for both domains. Probably, this is an unrealistic condition; however, it is a simple manner to analyse a homogenization process only generated by mechanical response. When different permeability and different water mass transfer rate are taken into account, the homogenization process become a more complex phenomenon. The Chapter 5 presents the modelling of well instrumented laboratory tests, involving the mechanical and hydraulic conditions mentioned above.

Table 4-2. Input parameters for the homogenization test HT-M.

Parameter		Domain 1	Domain 2
Bishop parameter micro-structural level	p_k (-)	0.7	0.7
	q_k (-)	100	100
Non-linear elasticity	$\bar{\kappa}$ (-)	0.00018	0.00022
	κ_s (-)	0.037	0.028
	ν (-)	0.3	0.3
Macro-micro mechanical interaction functions	f_{ms0}(-)	5	5
	f_{ms1}(-)	0	0
	n_{ms}(-)	2	2
	f_{mc0}(-)	0	0
	f_{mc1}(-)	5	5
	n_{mc}(-)	2	2
Macro-structural level	φ (°)	25	25

Plastic mechanism (BBM)	p_c (MPa)	0.035	0.035
	λ_{sat}(-)	0.16	0.28
	r (-)	0.62	0.53
	β (MPa^{-1})	0.03	0.026
	k_s (-)	0.01	0.01
	α (-)	1	1
Leakage parameter	γ ($kg.s^{-1}.m^{-3}.MPa^{-1}$)	1.e-5	1.e-5
Water retention curve for micro-structural level	$(P_o)_1$ (MPa)	379	379
	σ_o	0.072	0.072
	$(\lambda_o)_1$ (-)	0.899	0.899
	$(S_r)_{L1}$ (-)	0.3	0.3
	$(S_m)_{L1}$ (-)	1	1
	$(P_d)_1$ (MPa)	800	800
	$(\lambda_d)_1$ (-)	2.243	2.243
Water retention curve for Macro-structural level	$(P_o)_2$ (MPa)	15	15
	σ_{To}	0.072	0.072
	$(\lambda_o)_2$ (-)	0.064	0.064
	$(S_r)_{L2}$ (-)	0	0
	$(S_m)_{L2}$ (-)	1	1
	$(P_d)_2$ (MPa)	850	850
	$(\lambda_d)_2$ (-)	3.899	3.899
Intrinsic permeability	k_o (m^2)	2.e-20	1.e-20
	b (-)	7	7
	$(\phi_{min})_2$	0.46	0.46
Initial conditions	P_o^* (MPa)	0.4	0.16
	ϕ (-)	0.4	0.46
	$\bar{\phi}_1$(-)	0.22	0.13
	P_{L1}(MPa)	-300	-300
	P_g (MPa)	0.1	0.1

Before computing the homogenization test HT-M, it is worthwhile, to examine the swelling behaviour of both domains separately. The Figure 4-28 shows the time evolution of the swelling pressure (mean stress) and the pore volume fractions ($\bar{\phi}_1$ and $\bar{\phi}_2$). There are important differences in the swelling pressure; the Domain 1 generates higher values of swelling pressure and volumetric collapse than the Domain 2. In contrast, the structural evolution presents a similar trend. Due to the null volume

change restriction, the Macro pore volume fractions decreases and the micro pore volume fractions increases.

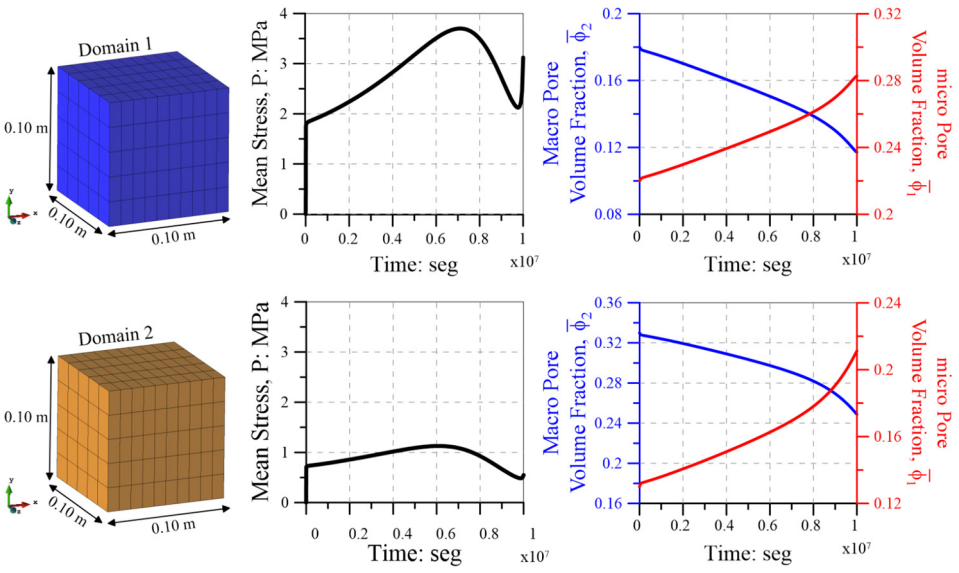

Figure 4-28. Swelling pressure test in the Domain 1 and Domain 2.

In the HT-M model, the null volume change restriction applies to the global configurations (see Figure 4-26). The horizontal displacement of the contact between the domains is allowed. The magnitude and direction of this displacement depends on the swelling behaviour of the domains. According to the individual domains analysis presented above (Figure 4-28), the compression of the domain 2 due to the swelling of domain 1 was expected. The Figure 4-29 shows the horizontal displacement of the contacts between the two domains.

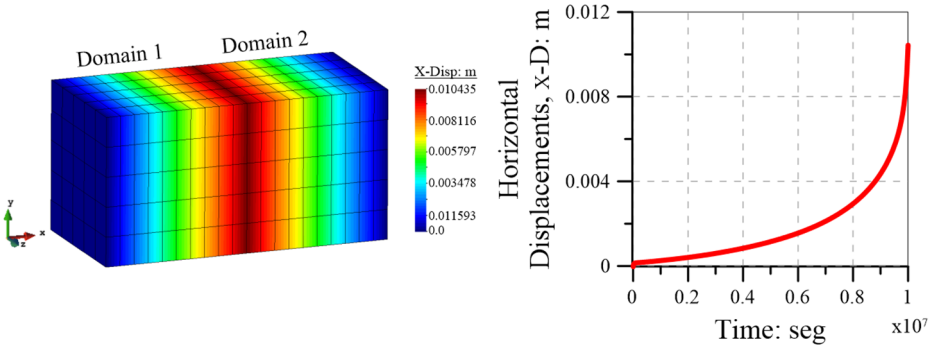

Figure 4-29. Horizontal displacement of the contact between domains.

The time evolution of the swelling pressure and the pore volume fractions for the model HT-M is presented in the Figure 4-30. The results of the individual domains computations are added (dotted lines), in order to demonstrate the effects of a homogenization process.

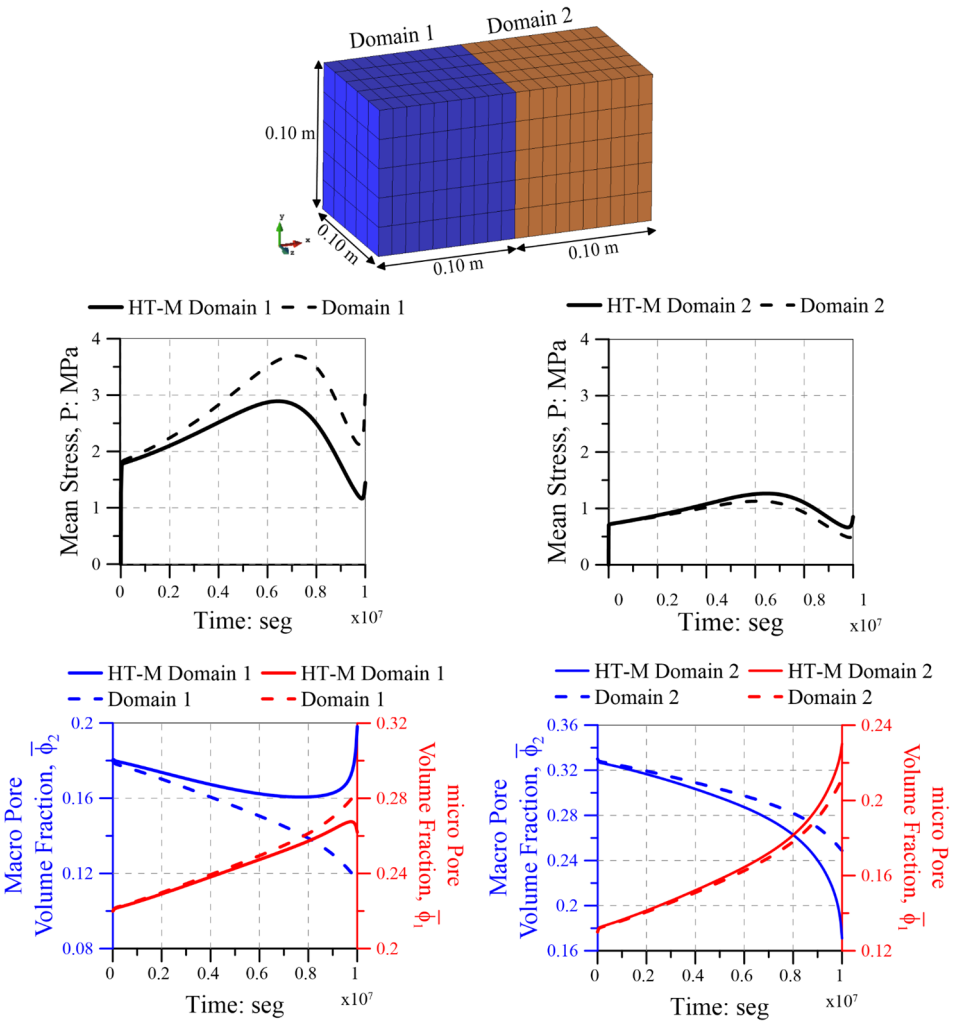

Figure 4-30. Homogenization test HT-M.

Regarding the stress state, the mean stress of the Domain 1 in the HT_M model is lower than the individual computation due to its horizontal deformation (Figure 4-29). Thus, the compression on the Domain 2 generates a higher value of swelling pressure, in contrast with the individual results.

The new stress state and deformation of the domains modify the trend of the pore volumetric fractions (Figure 4-30). The most remarkable changes are:

- The increase of the Macro pore volume fraction ($\bar{\phi}_2$) at the Domain 1 due to the horizontal expansion.
- The compressed Domain 2 presents a pronounced reduction of the Macro pore volume fraction ($\bar{\phi}_2$) and increase of the micro pore volume fraction ($\bar{\phi}_1$).

The final values of the pore volume fractions ($\bar{\phi}_1$ and $\bar{\phi}_2$) after a homogenization process should not be the same in both domains. However, they become similar, taking into the account the important initial difference (see Table 4-2). The Figure 4-31 shows the initial and final values of the Macro and micro pore volume fractions in the model HT-M.

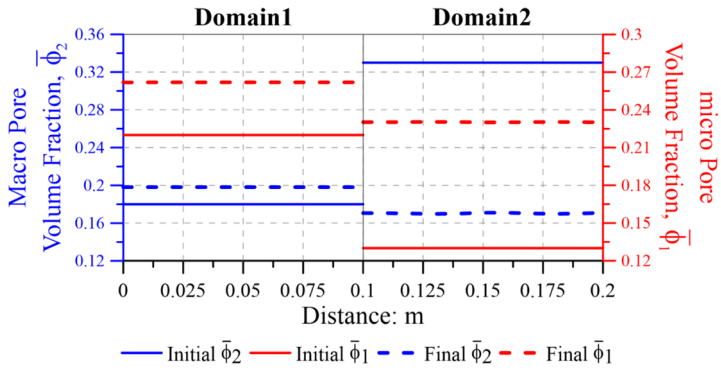

Figure 4-31. Macro and micro pore volume fractions in the model HT-M

An essential requirement is the horizontal stress equilibrium between both domains. The Figure 4-32 proves the stress equilibrium during the computation. Under experimental conditions (e.g. oedometric cells) and field conditions (e.g. gallery seals), friction between the bentonite and the walls will occur. This additional mechanism modifies the homogenization process at stress states and structural levels.

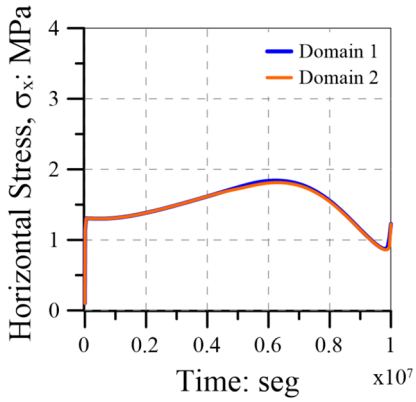

Figure 4-32. Horizontal stress evolution at the Domain 1 and Domain 2.

4.4. Chapter conclusions

The Hydro-Mechanical double-structure formulation has been implemented in the finite element program CODE_BRIGHT, which is a tool designed to analyse numerically coupled THM problems in geological media.

After FEM (space) discretization, the set of governing equations (PDE's system)that describe a double-structure materials results in a system of first order differential equations. The numerical treatments of the different terms (i.e. storage, advective fluxes, volumetric strains, mechanical equilibrium and sink/source) are designed to allow implementation procedures that are more suitable for reducing the computational cost. The finite differences are used for temporal discretization. As the problem presented here is non-linear, the Newton-Raphson method was adopted as iterative scheme.

Numerical treatment of Macro-micro mass water exchange is mainly influenced by the physical assumption on the water mobility at micro-structural levels. Certainly, there is a low water mobility in clay aggregates. Keeping the micro advective fluxes in the formulation, the liquid pressure of the microstructural level is solved as nodal variable. In contrast, if this kind of fluxes are neglected, the micro liquid pressure has to be integrated at gauss points. The latter option has been selected in this work, therefore a numerical procedure is needed for the water exchange between Macro (nodal variable) and micro (gauss point variable).

The stresses should be integrated many times on the course of a typical non-linear simulation. Therefore, the selection of the algorithm has been based on the accuracy of the solution but also on its robustness and efficiency. The stress-strain integration of the model has been performed using a refined Euler scheme with automatic sub-stepping and error control (Sánchez et al., 2008).

The numerical performance of the model has been focussed on the evaluation of the interaction mechanisms between the two structural levels and the qualitative response under well-controlled stress paths. The model (and its numerical implementation) is able to reproduce and explain some typical response of expansive materials.

4.5. References

Abbo, A., 1997. Finite element algorithms for elastoplasticity and consolidation. PhD Thesis, University of Newcastle, Australia.

Alonso, E.E., Gens, A., Josa, A., 1990. A constitutive model for partially saturated soils. Géotechnique 40, 405–430.

Alonso, E.E., Pinyol, N.M., Gens, A., 2013. Compacted soil behaviour: Initial state, structure and constitutive modelling. Geotechnique 63, 3–18.

Alonso, E.E., Vaunat, J., Gens, A., 1999. Modelling the mechanical behaviour of expansive clays. Eng. Geol. 54, 173–183.

Borja, R.I., 1991. Cam-clay plasticity, Part II: Implicit integration of constitutive equations based on a nonlinear elastic stress predictor. Comput. Methods Appl. Mech. Eng. 88, 225–240.

Borja, R.I., Choo, J., 2016. Cam-Clay plasticity, Part VIII: A constitutive framework for porous materials with evolving internal structure. Comput. Methods Appl. Mech. Eng. 309, 653–679.

Borja, R.I., Lee, S., 1990. Cam-clay plasticity, Part I: Implicit integration of elasto-plastic constitutive relations. Comput. Methods Appl. Mech. Eng. 78, 49–72.

Choo, J., Borja, R.I., 2015. Stabilized mixed finite elements for deformable porous media with double porosity. Comput. Methods Appl. Mech. Eng. 293, 131–154.

DIT-UPC, 2018. CODE_BRIGHT, a 3-D program for Thermo-Hydro-Mechanical analysis in geological media: User's guide, CIMNE, Barcelona.

Gens, A., 2010. Soil–environment interactions in geotechnical engineering. Géotechnique 60, 3–74.

González, N.A., 2011. Development of a family of constitutive models for geotechnical applications. PhD Thesis, Universitat Politecnica de Catalunya, Spain.

Lees, A., 2016. Geotechnical finite elemeny analysis. A practical guide. ICE Publising: London.

Olivella, S., 1995. Non-isothermal multiphase flow of brine and gas through saline media. PhD Thesis, Universitat Politecnica de Catalunya, Spain.

Olivella, S., Gens, A., Carrera, J., Alonso, E.E., 1996. Numerical formulation for a simulator (CODE_BRIGHT) for the coupled analysis of saline media. Eng. Comput. 13, 87–112.

Potts, D., Ganendra, D., 1994. An evaluation of substepping and implicit stress point algorithm. Comput. Methods Appl. Mech. Eng. 166, 341–354.

Potts, D.M., 2003. Numerical analysis: A virtual dream or practical reality? Geotechnique 53, 535–573.

Potts, D.M., Gens, A., 1985. A critical assessment of methods of correcting for drift from the yield surface in elastoplastic finite element analysis. Int. J. Numer. Anal. Methods Geomech. 9, 149–159.

Potts, D.M., Zdravkovic, L., 1999. Finite Element analysis in geotechnical engineering. Theory.

Sánchez, M., 2004. Thermo-Hydro-Mechanical coupled analysis in low permeability media. PhD Thesis, Universitat Politecnica de Catalunya, Spain.

Sanchez, M., Gens, A., Guimarães, L., Olivella, S., 2005. A double structure generalized plasticity model for expansive materials. Int. J. Numer. Anal. Methods Geomech. 29, 751–787.

Sánchez, M., Gens, A., Guimarães, L., Olivella, S., 2008. Implementation algorithm of a generalised plasticity model for swelling clays. Comput. Geotech. 35, 860–871.

Sánchez, M., Gens, A., Villar, M.V., Olivella, S., 2016. Fully Coupled Thermo-Hydro-Mechanical Double-Porosity Formulation for Unsaturated Soils. Int. J. Geomech. 16, D4016015.

Sheng, D., Sloan, S.W., Gens, A., Smith, D.W., 2003. Finite element formulation and algorithms for unsaturated soils. Part I: Theory. Int. J. Numer. Anal. Methods Geomech. 27, 745–765.

Sloan, S.W., 1987. Substepping schemes for the numerical integration of elastoplastic stress–strain relations. Int. J. Numer. Methods Eng. 24, 893–911.

Sloan, S.W., Abbo, A.J., Sheng, D., 2001. Refined explicit integration of elastoplastic models with automatic error control. Eng. Comput. 18, 121–154.

Vaunat, J., Cante, J., Ledesma, A., Gens, A., 2000. A stress point algorithm for an elastoplastic model in unsaturated soils. Int. J. Plast. 16, 121–141.

Zienkiewicz, O.C., Taylor, R.L., Fox, D.D., 2013a. The finite element method for soild and structural mechanics. Elsevier.Butterworth-Heinemann.

Zienkiewicz, O.C., Taylor, R.L., Zhu, J.Z., 2013b. The finite element method. Its basis and fundamentals (7th Ed.). Elsevier.Butterworth-Heinemann.

Chapter 5

Numerical Modelling

'A prediction is a forecast; typically, a prediction is obtained by manipulating data according to some method .... Predicting is a key step in the process of creating and maintaining a constructed facility, i.e. the practice of civil engineering.'

T.W. Lambe, 1973

5.1. Introduction

Realistic results of a numerical simulation usually means to predict a certain event. A prediction process is composed by six steps (Lambe, 1973).In first place a certain field situation has to be simplified in order to model a system. Then, main mechanisms of this system are identified. With respect to these findings, a suitable method and parameters are chosen and the prediction is carried out. Finally, the prediction is compared with field or experimental data. The Figure 5-1 shows the prediction process for the behaviour of expansive clays. It summarizes the observations, hypothesis and numerical method proposed in previous chapters. In spite to simplify the expansive clays as a double-structure porous media, the prediction of their hydro-mechanical behaviour is not a straightforward task. Coupled mechanisms, model parameters and initial conditions have to be taken into account.

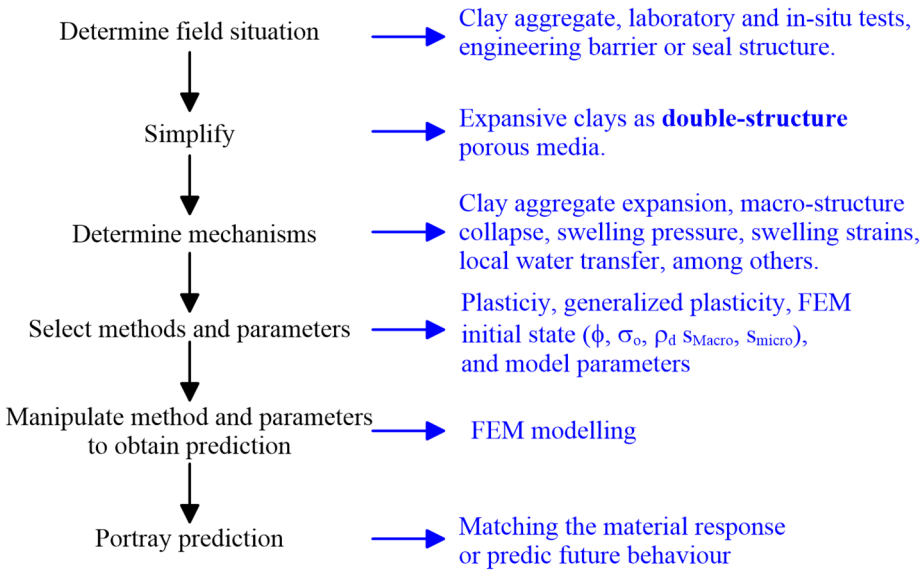

Figure 5-1. Prediction process for the expansive clays (modified from Lambe, 1973).

Three different prediction types exist (Lambe, 1973). The Class-A prediction give a forecast of the event before it takes place. A prediction during the event is classified as Class-B prediction. The outcome of the event being predicted will be known along time. The most often used prediction is the Class-C, where the calculation takes place after the event.

Better suited to proof the capabilities of a new simulation method are predictions Class-B or even better Class-A. However, difficulties in the determination of the exact field situations, relevant mechanisms and soil properties limit the accuracy of those type of predictions. On the other hand, Class-C predictions are autopsies and sort of inverse analyses. They can of course be very helpful in contributing to better understanding of the rather complex hydro-mechanical behaviour of expansive clays and provide information required to feed the previous class predictions.

The general scheme of the numerical modelling works is depicted in Figure 5-2. The modelling has been performed in a progressive manner; it goes from the clay aggregate response until homogenization phenomena. All cases come from the deep geological disposal of nuclear waste; the field of most intensive and advanced research activity at present (Gens, 2004).

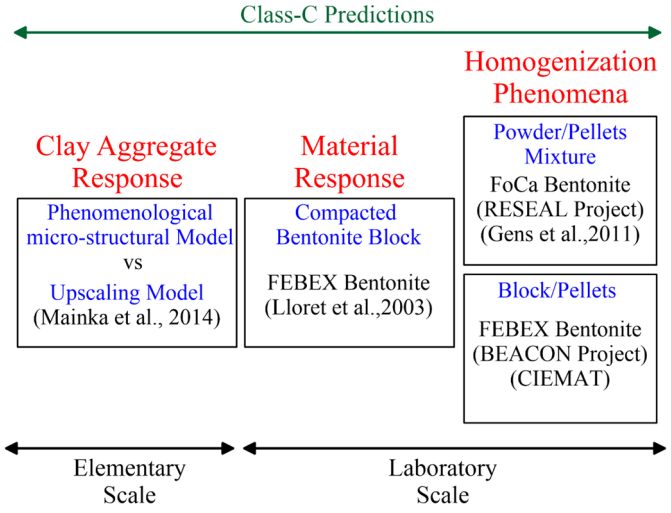

Figure 5-2. General scheme of numerical modelling works.

The clay aggregates response is a fundamental part to build consistent numerical simulations of the expansive clays. The phenomenological micro-structural model, presented in Chapter 3, is compare with a multi-scale model. Both are based on effective stress principle at unsaturated state.

Compacted bentonite is often considered as the basic material for constructing isolating barriers and backfilling galleries and shafts of deep repositories. The numerical modelling of controlled stress-suction-paths on compacted FEBEX bentonite specimens is performed.

There are a number of sources of heterogeneity in bentonite barriers, backfills, seals and plugs. Emplacement activities could imply the use of mixture of bentonite powder and highly compacted pellets as sealing material or the combination of pellets and bentonite blocks in the same gallery section. In-depth insights of homogenization processes are obtained through the numerical modelling of well-controlled laboratory test.

5.2. Clay aggregate response

As pointed in the Chapter 2, the compacted expansive clays present a hierarchical fabric. Clay clusters are made by the aggregation of platy clay particles. Group of clusters form aggregates, which in turn form the porous medium with macroscale implications. The Figure 5-3 shows the fabric of two well-known expansive clays through the ESEM technique.

The experimental hydro-mechanical characterization of an individual clay aggregate as the micro-structural level of an expansive clay is not yet possible. Nevertheless, the ESEM technique allows the tracking of strain evolution of clay aggregates due to suction changes (see Chapter 2). Mašín and Khalili, (2016) proposed the analysis of high compacted bentonites to infer the micro-level response. On the other hand, under the assumption that a single pellet represents the micro-structural level of a bentonite granular mixture, experimental programs on them can be devised to examine this hypothesis and main predictions of the model in a systematic manner (Molinero-Guerra et al., 2017; Darde et al., 2018; Molinero-Guerra et al., 2019). Therefore, the comparison of the micro-structural constitutive formulation with experimental data is not straightforward task.

Another possibility is to compare the capabilities of the proposed phenomenological model at micro-structural scale against an upscaling formulation that considers physical mechanisms through several scales.

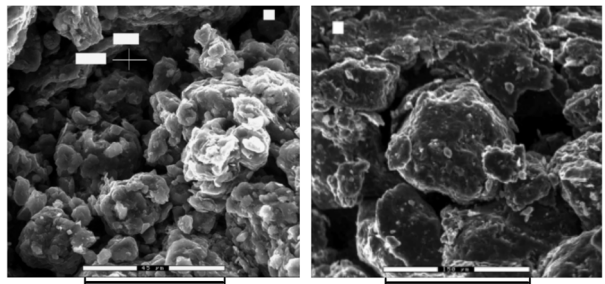

Figure 5-3. ESEM microphotographs on compacted expansive clays. a) Boom clay (Romero et al., 2011); b) FEBEX clay (Musso et al., 2013).

5.2.1. Phenomenological model

Clay aggregates are considered as a non-linear elastic swelling porous medium. A detailed description of the micro-structural constitutive model and its contribution in the double-structure formulation are presented in the Chapter 3. The main equations of the micro-structural level are presented here again in order to facilitate the models comparison. Following the convention used in precedent chapters, the micro-structural level is referred with the subscript 1.

The micro-structural or clay aggregate pore space is quantified by the micro porosity and micro void ratio:

$$\phi_1 = \frac{(V_{Pores})_1}{V_1} \qquad \text{(Eq. 5-1)}$$
Also (Eq. 3-19)

$$e_1 = \frac{(V_{Pores})_1}{(V_{Solid})_1} = \frac{\phi_1}{1-\phi_1} \qquad \text{(Eq. 5-2)}$$

The Bishop-type effective stress is defined as:

$$\boldsymbol{\sigma'}_1 = \boldsymbol{\sigma}_t + [\chi_1(P_{g1} - P_{L1}) - P_{g1}]\mathbf{I} \qquad \text{(Eq. 5-3)}$$
Also (Eq. 3-23)

where:
- P_{g1} and P_{L1} are the gas and liquid pressures at micro-structural level.
- χ_1 is the Bishop's parameter.
- $\boldsymbol{\sigma}_t$ is the total stress.

The Bishop's parameter can be defined as a function of micro saturation degree. The (Eq. 5-4 is a popular form when χ_1 is considered equal to

degree of saturation. However, it should be noted that Bishop's proposal was more general, since χ_1 was not claimed to be equal to the saturation degree (Eq. 5-5).

$$\chi_1 = S_{L1} \qquad \text{(Eq. 5-4)}$$
Also (Eq. 3-25)

$$\chi_1 = \frac{1}{\ln 2 - q_k} \ln\left(e^{-q_k S_{L1}^{p_k}} + e^{-q_k (2 - S_{L1})^{p_k}}\right) \qquad \text{(Eq. 5-5)}$$
Also (Eq. 3-26)

where:
- q_k and p_k are fitting parameters.

For the micro-structural bulk modulus the following law has been implemented:

$$K_1 = \frac{(1 + e_{o1}) p'_1}{\kappa_1} = \frac{p'_1}{(1 + \phi_{o1}) \kappa_1} \qquad \text{(Eq. 5-6)}$$
Also (Eq. 3-29)

where:
- p'_1 is the mean effective stress at micro-structural level.
- κ_1 is the elastic stiffness parameter at micro-structural level for changes in the mean effective stress.

5.2.2. Upscaling model

Mainka et al., (2014) proposed an upscaling model in order to describe the electro-chemical-mechanical couplings in unsaturated swelling clays, considering two porosity levels and three separate length scales: the nano, micro and macro (Figure 5-4).

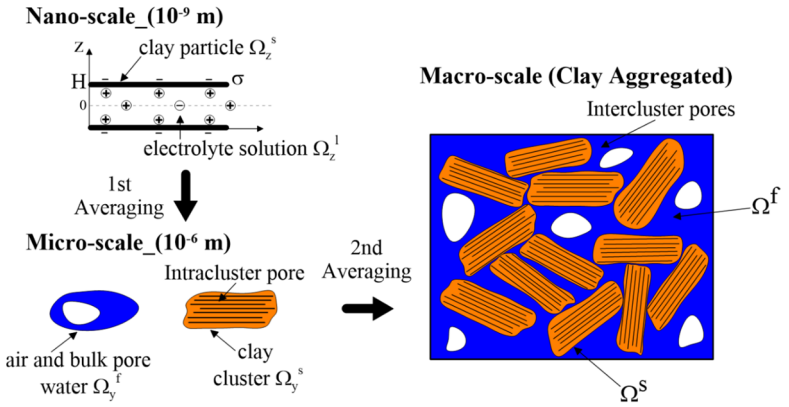

Figure 5-4. Three-scale representation of the upscaling model (modified from Mainka and Moyne, 2017)

The nano-scale portrait consist of charged clay particles separated by a nanoporous network saturated by a binary monovalent aqueous electrolyte solution with ion distribution governed by the Poisson-Boltzman equation; at this scale, the effective thickness of the electrical-double layer (EDL) is evaluated.

The microscale considers the highly heterogeneous solid-fluid interaction represented in an average fashion, where the mixture electrolyte solution, clay particles is view as overlying continua forming swollen clay clusters that are separated from each other by a network of pores (intercluster) filled with bulk water and air. At this scale, the homogenized swelling pressure stress tensor is given by:

$$\boldsymbol{\Pi} = \phi\langle\boldsymbol{\Pi}_{d}\rangle^{l} + (1-\phi)\langle\boldsymbol{\sigma}_{\Pi}\rangle^{s} \qquad \text{(Eq. 5-7)}$$

where:

- l and s defined the subdomain considered, s for clay particles and l for the electrolyte solution.
- ϕ is the intracluster porosity.

The contribution of the electrolyte solution to the swelling tensor, $\boldsymbol{\Pi}_{d}$, is defined as the average across the fluid phase of the disjoining pressure (Π_{d}=$\boldsymbol{\Pi}_{d}\mathbf{n}.\mathbf{n}$), that can be simplified as:

$$\Pi_{d} = 2RTC(\cosh\overline{\varphi}_{o} - 1) \qquad \text{(Eq. 5-8)}$$

where:

- R is the ideal gas constant, T the temperature and C the ion concentration.
- $\overline{\varphi}_{o}$ denotes the dimensionless electric potential in the middle of interlayer spacing thickness 2H, given by $\overline{\varphi}_{o} = \overline{\varphi}_{o}(C, \phi)$.

Assuming the clay particle thickness as 2δ, the intercluster porosity is defined in the following manner:

$$\phi = \frac{H}{H+\delta} \qquad \text{(Eq. 5-9)}$$

Finally, the contribution of the solid phase to the swelling tensor $\boldsymbol{\Pi}_{d}$, consists on the average of the stress tensor $\boldsymbol{\sigma}_{\Pi}$, that satisfies the local elasticity problem in the periodic solid phase, it must be in equilibrium with the disjoining pressure,

$$\boldsymbol{\sigma}_{\Pi}\mathbf{n} = -\boldsymbol{\Pi}_{d}\mathbf{n} \qquad \text{(Eq. 5-10)}$$

The upscaling of the microscopic problem to the macroscale is accomplished using the periodic structures homogenization method.

Defining n_f as the intercluster porosity (Figure 5-4), the relationship between intra (ϕ) and intercluster (n_f) porosities is defined by:

$$(1-n_f)(1-\langle\phi^0\rangle^s) = (1-n_f)(1-\langle\bar{\phi}\rangle^s)\exp(-\nabla_x.\,\mathbf{u}^0) \qquad \text{(Eq. 5-11)}$$

where:

- $\mathbf{u}^0$ is the solid motion vector.

The three-scale version for the Bishop parameter is defined as:

$$\boldsymbol{\chi}^{eff} = \mathbf{I} - (1-\chi^0)\boldsymbol{\alpha} \qquad \text{(Eq. 5-12)}$$

where:

- χ^0 is the Bishop parameter for the microscale.

An important feature is the deviation from the classical Bishop parameter induced by the cluster compressibility governed by the parameter $\boldsymbol{\alpha}$. In fact by denoting $\widetilde{K}$ as the effective macroscopic bulk modulus and K_s the cluster bulk modulus, recalling the classical definition of the Biot-Willis, (1957) coefficient:

$$\alpha = \frac{1}{3}\mathrm{tr}(\boldsymbol{\alpha}) = 1 - \frac{\widetilde{K}}{K_s} \qquad \text{(Eq. 5-13)}$$

The role of α is the scaling factor accounting for the transmissibility of stresses of various nature (disjoining pressure, capillary and contact stress) between adjacent clay clusters.

In order to obtain straightforward simplified constitutive laws for the effective parameters for a particular spherical isotropic microstructure, tools of periodic and self-consistent homogenization are combined. Considering the macroscopic system subjected to a an external pressure $P_{ext} = -\mathrm{tr}(\boldsymbol{\sigma}_T)/3$, it is possible to provide a constitutive response for some effective scalar coefficients, more precisely the bulk modulus of the solid matrix along with volumetric parts of the swelling stress tensor, effective Bishop parameter and equivalent pore pressure.

The effective modulus $\widetilde{K}$ can be represented in terms of the intercluster porosity n_f and the bulk and shear moduli (K_s, μ_s) of the clay cluster.

$$\frac{\widetilde{K}}{K_s} = 1 - \frac{n_f}{1-(1-n_f)/\{1+[2(1-2\nu_s)/1+\nu_s]\}} \quad \text{(Eq. 5-14)}$$

where:

- ν_s is the Poisson coefficient of the clay cluster which is assuming constant $K_s/\mu_s = 2/3(1+\nu_s)/(1-2\nu_s)$

Using the above result, the Biot-Willis coefficient α can be estimated as:

$$\alpha = \frac{n_f}{1-(1-n_f)/\{1+[2(1-2\nu_s)/1+\nu_s]\}} \quad \text{(Eq. 5-15)}$$

For the effective swelling pressure defined as the volumetric part of the swelling stress tensor $\Pi_{eff} = \frac{1}{3}\mathrm{tr}\,(\boldsymbol{\Pi}_{eff})$, we have:

$$\Pi_{eff} = \frac{\widetilde{K}}{K_s}\Pi_d = (1-\alpha)\Pi_d \quad \text{(Eq. 5-16)}$$

where:

- Π_d is the disjoining pressure at the clay particle scale

The upper and lower bounds for effective swelling pressure are controlled by the arrangement of the clay clusters. The estimation provided by the self-consistent method satisfies $0 \leq \Pi_{eff}/\Pi_d \leq (1-n_f)$.

The self-consistent estimation for the bishop parameter:

$$\chi^{eff} = (1-\alpha)(1-\chi) + \chi \quad \text{(Eq. 5-17)}$$

where:

- χ is the bishop parameter at cluster scale, $\chi = \chi^0(S_w)$.

5.2.3. Models comparison

Prior to the numerical results of both constitutive formulations, the qualitative comparison is a worthwhile exercise.

A graphical comparison of the models is presented in Figure 5-5. The phenomenological double-structure formulation does not consider any

structural level below the clay aggregates, on the contrary, in the upscaling model the aggregated is assumed as a dual porosity medium.

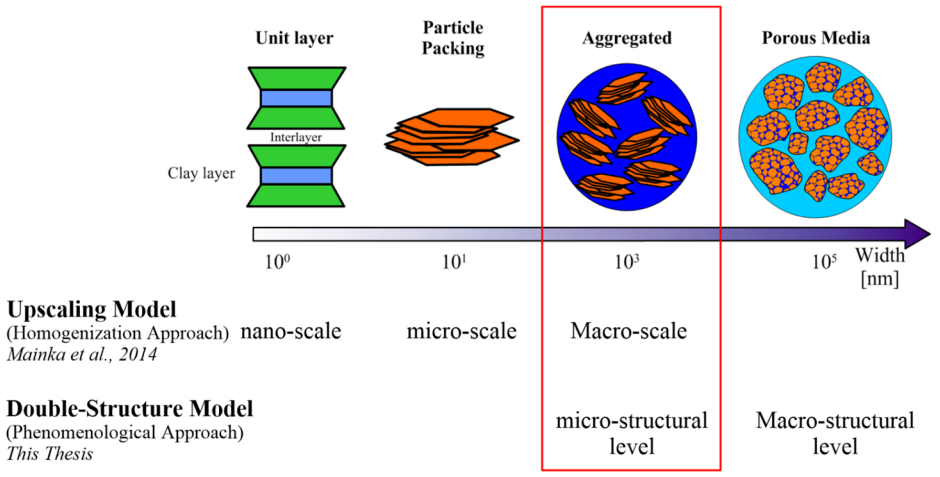

Figure 5-5. Structural levels involved in the upscaling and double-structure models.

The macroscale of the upscaling formulation is more related to a clay aggregate than a coarse arrangement of aggregates (see Figure 5-3 and Figure 5-4). Although the upscaling formulation involves periodic averaging of air/bulk water and clay clusters, it does not add an upper pore level between them. At engineering scale, this formulation can reproduce highly compacted bentonites where the pores between aggregates are negligible. Therefore, the phenomenon of volumetric collapse is not taking into account and high swelling pressures are expected.

The overall behaviour of the upscaling model depends on disjoining pressure between clay platelets, which is a function of the interlayer spacing thickness (H=0.5 nm) and the salinity of the electrolyte solution C. The Figure 5-6 depicts the effective swelling pressure as a function of salinity for different values of the Biot-Willis parameter α.

As explain Mainka et al., (2014), for incompressible clay clusters α=1.0 the electrochemical effects from nanopore level cannot be transmitted between adjacent cluster, leading Π_{eff}=0. As the cluster compressibility increases ($\alpha \rightarrow 0$), electrochemical swelling becomes more pronounced.

The phenomenological model does not include the salinity effects; therefore, the selection of low salt concentration is convenient for the models comparison. As shows the Figure 5-6, the selected ion concentration of C=10^{-2} mol/l does not affect the values of swelling pressure.

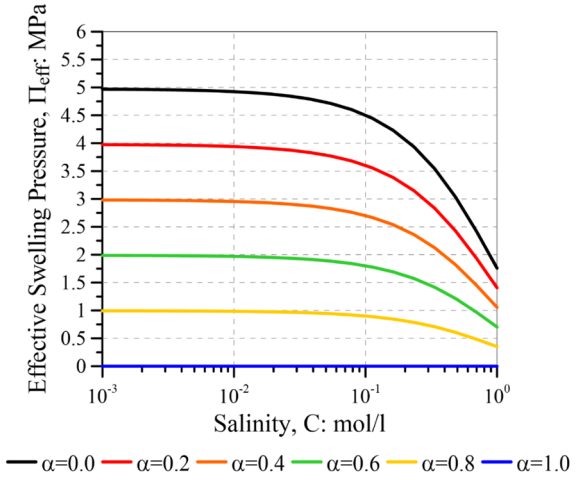

Figure 5-6. Effective swelling pressure as a function of salinity

Phenomenological models that account chemical concentrations effects at micro-structural level can be found in Guimaraes, (2002), Guimaraes et al., (2013) and Navarro et al., (2013).

The Bishop parameter as a function of the degree of saturation for both formulation is presented in Figure 5-7. According to the models description, the effective Bishop parameter in upscaling model depends on the Bishop parameter (χ) and compressibility (α) of the clay clusters (Eq. 5-17). On the other hand, the phenomenological model uses an exponential law governed by fitting parameters (Eq. 5-5).

According to Mainka et al., (2014), for the case of incompressible clusters (α=1.0), χ^{eff} is identical to its two-scale counterpart χ associated with a single-porosity medium. The gradual decrease in α leads to the appearance of the cluster compressibility and adsorbed water, which tends to increase $\chi^{eff} \geq \chi$. It should be noted that unlike the transition to the fully saturated regime where $\chi^{eff}=\chi=1$, contrary to χ, the effective parameter χ^{eff} does not vanish as Sr$\rightarrow$0 but tends to a residual

asymptotic value 1-α= $\widetilde{K}/K_s$ owing the presence of the absorbed water in the clay cluster (Figure 5-7).

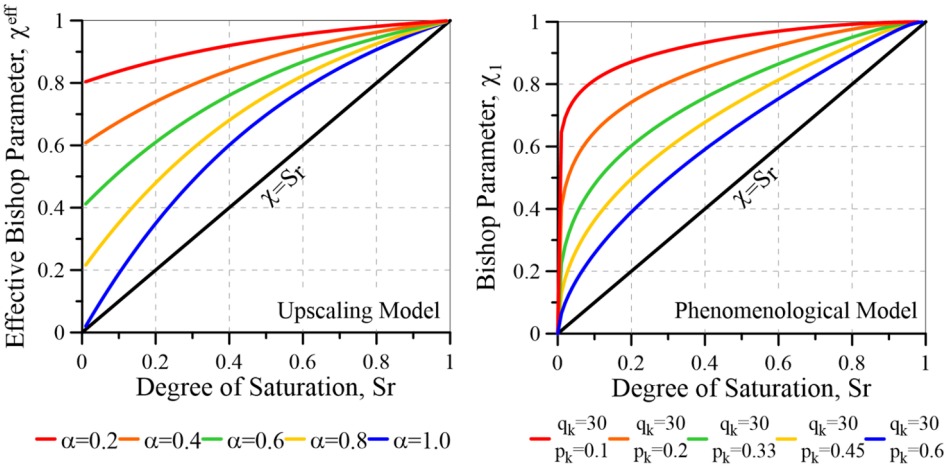

Figure 5-7. Left: effective Bishop parameter as a function of the degree of saturation in the upscaling formulation; Right: Bishop parameter as a function of the degree of saturation in the phenomenological approach.

The phenomenological model conceives the clay aggregates as a single-porosity medium. Hence, there is not asymptotic values of the Bishop parameter at Sr=0. The effect of clusters compressibility can be obtained through different values of the fitting parameters p_k and q_k (Figure 5-7).

The location of Bishop parameter at the left side of the classical definition χ=Sr is a remarkable issue (Figure 5-7). Khalili, (2019) proposes the derivation of effective stress expression for unsaturated soils on energetic equations of the system. The deviation of the Bishop parameter from the degree of saturation is due to the rate of change on the specific area of air-water interface with degree of saturation. The values of Bishop parameter (χ>Sr) in clay aggregates is attributed to the dominated effects of the air-water interface (menisci).

Figure 5-8 show the bulk modulus as a function of effective swelling pressure and micro-structural mean effective stress for the upscaling and phenomenological formulations, respectively. Agreeing with models description, the intercluster porosity (n_f) and micro porosity (ϕ_1) are equivalent. A general trend indicates higher moduli for low porosity

values. This trending at phenomenological model is achieved using different values of the elastic stiffness parameter κ_1 for changes in the mean effective stress (Eq. 5-6). Finally, there are some discrepancies at low stress values (< 2MPa) where the upscaling approach present a non-linear response.

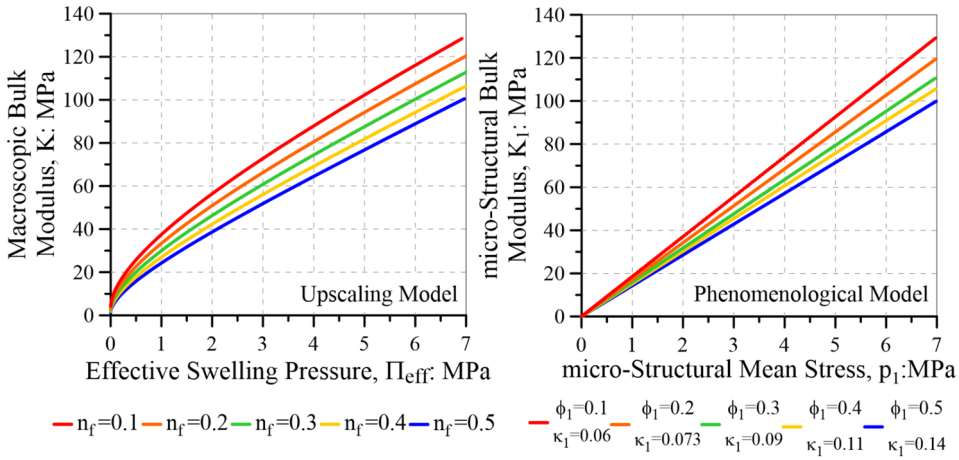

Figure 5-8. Left: macroscopic bulk modulus as a function of the effective swelling pressure in the upscaling formulation; Right: micro-structural bulk modulus as a function of the micro-structural effective mean stress in the phenomenological approach.

5.3. Material response

A comprehensive modelling of unsaturated expansive clays is a quite complex problem. The swelling behaviour of these clays has often been reproduced through relative simple and empirical laws, which relates the material response to suction changes and applied stress (see Chapter 2 and Chapter 3). The weakness of this kind of ad-hoc laws is that it can be generally used only for the stress-paths and conditions from which they are derived.

Prior to the modelling of swelling pressure evolution in bentonite-based materials (Section 5.4.1. and Section 5.4.2), it is worthy the understanding of the mechanisms behind the strain irreversibly, stress-path dependence and clay fabric evolution; for this purpose the double-structure constitutive model is a useful tool.

5.3.1. Compacted bentonite block

Lloret et al., (2003) carried out a testing program based on oedometer tests in which a combination of loading paths and at constant suction and drying/wetting paths at constant load were applied. They found significant features of mechanical behaviour, such as yield phenomena, dependence of swelling strain on applied stress, stress-path dependence of strains and a clear influence of the aggregated fabric (see Chapter 2). It was decided to model the Test A and Test B because they share the same initial and final generalised stress state but their trajectories are completely different (Table 5-1 and Figure 5-9).

Table 5-1. Stress path followed by TestA and TestB. Suction, s and vertical stress, σ_v in MPa. (from Lloret et al., 2003)

Tests	Initial conditions		Path			
	ρ_d: Mg/m^3	*w*: %	I Initial state	II	III	IV Final state
SP_TestA	1.72	13.0	σ_v:0.1 s:138	σ_v:0.1 s:550	σ_v:5.1 s:460	σ_v:5.1 s:0.1
SP_TestB	1.72	13.2	σ_v:0.1 s:138	σ_v:0.1 s:520	σ_v:0.1 s:0.1	σ_v:5.0 s:0.1

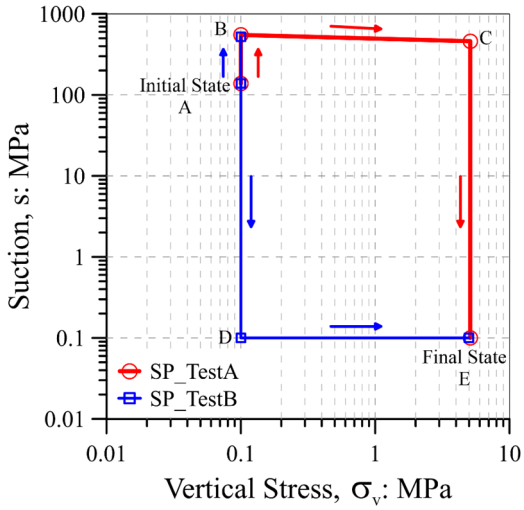

Figure 5-9. Generalized stress path followed by TestA and TestB (from Lloret et al., 2003)

Accordingly to the null lateral deformation in oedometer tests, one-dimensional modelling is suitable. Therefore, mean net stress substitutes

the net vertical stress. The material parameters and initial conditions are reported in Table 5-2. They are mainly obtained from the experimental program (Lloret et al., 2003). The initial Macro and micro pore volume fractions are determined in accordance with the MIP observations of bentonite fabric, and the initial saturated preconsolidation stress P_o^* (i.e. the initial position of LC curve) reflects the static compaction stress.

Due to the lack of information of hydraulic micro-structural state, the hydraulic equilibrium between the structural levels is assumed. The leakage parameter is higher enough to maintain this state during the stress-suction paths.

Table 5-2. Input parameters for compacted bentonite FEBEX.

Bishop parameter micro-structural level	p_k (-)	0.7
	q_k (-)	100
Non-linear elasticity	$\bar{\kappa}$ (-)	0.05
	κ_s (-)	0.001
	ν (-)	0.3
Macro-micro mechanical interaction function	f_{ms0}(-)	2
	f_{ms1}(-)	0
	n_{ms}(-)	7
	f_{mc0}(-)	0
	f_{mc1}(-)	2
	n_{mc}(-)	5
Macro-structural level Plastic mechanism (BBM)	φ (^{o})	26
	p_c (MPa)	0.5
	λ_{sat}(-)	0.15
	r (-)	0.9
	β (MPa^{-1})	1.0
	k_s (-)	0.01
	p_{s0} (MPa)	0.1
Constant leakage parameter	γ ($kg.s^{-1}.m^{-3}.MPa^{-1}$)	1.e-2
Water retention curve for micro-structural level	$(P_o)_1$ (MPa)	180
	σ_o	0.072
	$(\lambda_o)_1$ (-)	0.8
	$(S_r)_{L1}$ (-)	0.35
	$(S_m)_{L1}$ (-)	1.0
	$(P_d)_1$ (MPa)	700

	$(\lambda_d)_1$ (-)	1.5
Water retention curve for Macro-structural level	$(P_o)_2$ (MPa)	15
	σ_{To}	0.072
	$(\lambda_o)_2$ (-)	0.35
	$(S_r)_{L2}$ (-)	0
	$(S_m)_{L2}$ (-)	1
	$(P_d)_2$ (MPa)	2000
	$(\lambda_d)_2$ (-)	2
Intrinsic permeability	k_o (m^2)	1.3e-21
	b (-)	12
	$(\phi_{min})_2$	0.10
Initial conditions	P_o^* (MPa)	12
	ϕ (-)	0.41
	$\bar{\phi}_1$(-)	0.31
	P_{L1}(MPa)	-138
	P_g (MPa)	0.1

Figure 5-10 compares the numerical predictions with the experimental results for the stress-paths imposed in the two test. A good agreement is obtained in terms of void ratio against vertical stress and suction.

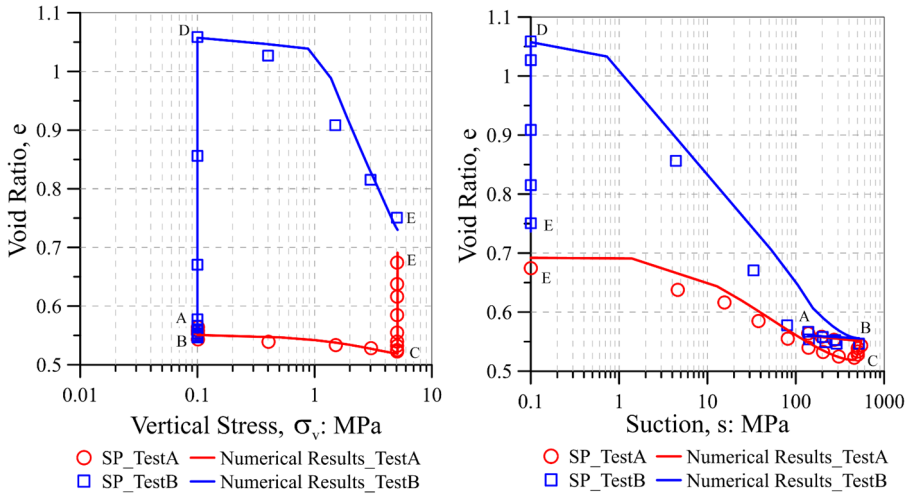

Figure 5-10. Computed evolution of void ratio, e, for TestA and TestB. Left: Variation over the vertical stress; Right: Variation over suction. (experimental data from Lloret et al., 2003).

The following major features (correctly reproduced here) have been highlight by Lloret et al., (2003) the major features:

- There are a large swelling strains when the material is wetted at low stresses (path B-D, Test B).
- There are smaller, but still significant, swelling strains when the soil is wetted under a 5.1 MPa vertical stress (path C-E, Test A).
- The slope of compression line changes during the loading, indicating yield in Test B (path D-E). No yield is apparent during the loading at high suction of Test A (path B-C).
- The final point (E) is different in two samples. There is a measure of stress path dependence.

Summarizing, the double-structure model is capable to offering a good simulation of the observed results. Therefore, further modelling information can be interesting to explain the mechanisms underlying the mechanical bentonite response. The rigorous pore space definition in this formulation (Chapter 2 and Charter 3) allows a good clay fabric description.

In the light of hydraulic equilibrium between structural levels, the acting mechanism are the micro-Macro mechanical interaction (f_β) and the loading-collapse (LC) of the Macro-structural level. As pointed out in Chapter 3 both mechanism generates irreversible Macro-structural deformations that are reflected in the hardening parameter evolution (P_o^*). Figure 5-11 shows the parts of interaction function involved in the various stages of the tests. Continuous information on the change of the LC yield limit can be obtained plotting the evolution of P_o^* (Figure 5-12). The reduction of P_o^* during swelling and subsequent increases upon loading are the general trending. Additionally, the Figure 5-12 indicates the acting mechanism (f_β or LC) at each path. The path D-E, of the Test B, is the only governed by the two mechanisms.

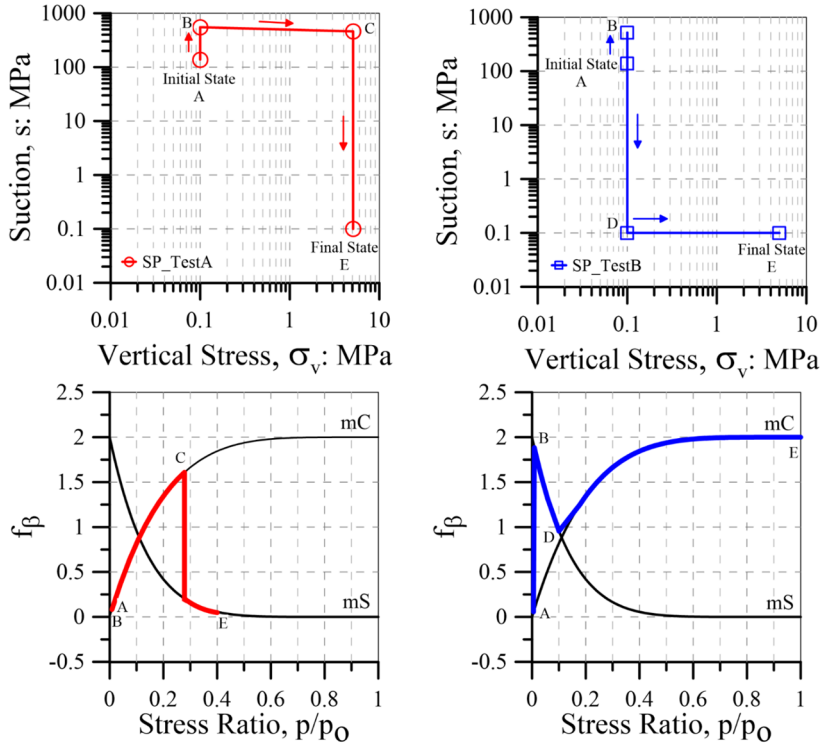

Figure 5-11. Macro-micro mechanical interactions involved in the stages of TestA (Left) and TestB (Right). mC and mS refer to micro-structural contraction and swelling, respectively.

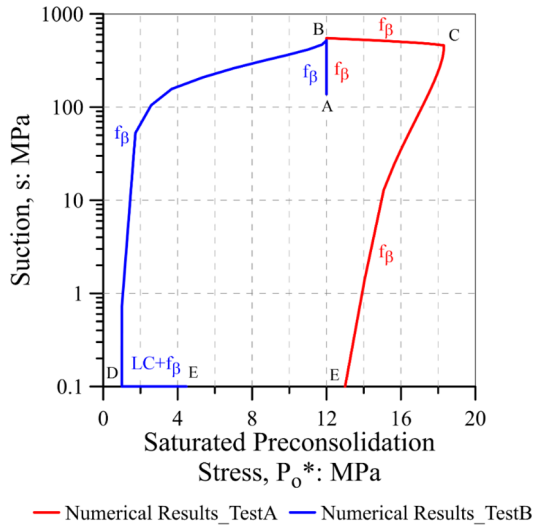

Figure 5-12. Evolution of P_o^* for TestA and TestB. fβ and LC refer to mechanical interaction mechanism and the loading-collapse mechanism, respectively.

The pore space evolution is shown in Figure 5-13 and Figure 5-14. The void ratio can be decomposed as follow:

$$e = \bar{e}_{Macro} + \bar{e}_{micro} \quad \text{(Eq. 5-18)}$$

$$\bar{e}_{micro} = \frac{\bar{\phi}_{micro}}{1 - \bar{\phi}_{micro}} \quad \text{(Eq. 5-19)}$$

$$\bar{e}_{Macro} = \frac{\bar{\phi}_{Macro}}{1 - \bar{\phi}_{Macro}} \quad \text{(Eq. 5-20)}$$

where:

- $\bar{e}_{micro}$ is the void ratio related to the micro pore volume fraction.
- $\bar{e}_{Macro}$ is the void ratio related to the Macro pore volume fraction.

As indicated in the model performance description (Chapter 4), $\bar{e}_{micro}$ is not the best indicator of pore space evolution at clay aggregates. As it is referred to the total volume, a total volume reduction due to Macro collapse deformations produces and increases of $\bar{e}_{micro}$ when the micro pores reduce or remain constant (Figure 5-13). The micro void ratio (Figure 5-14) is computed according to a simple relation:

$$e_{micro} = \frac{\bar{\phi}_{micro}}{1 - \bar{\phi}_{Macro} - \bar{\phi}_{micro}} \quad \text{(Eq. 5-21)}$$

In the Test B:

The swelling stage (path B-D) generate large micro-structural strains and they cause even larger plastic macro-structural strains explained by the large micro-Macro coupling (mS) at low stress state (Figure 5-11). The subsequent loading at saturated state (path D-E) implies a significant Macro-structure deformation that is controlled by the loading-collapse mechanism activated when LC yield curve is crossed.

In the Test A:

The stage of drying (path A-B) and subsequent loading (path B-C) generate very small micro-structural deformations. The Macro-structural strains are also small due to the stiffer behaviour at high suction values. In the final stage (path C-E), the wetting at 5.1 MPa vertical load result in important micro-structural strains although smaller than for Test B because the higher stress level.

Concluding, the basic reason for stress-path dependence of volumetric strains is the swelling stages at different stress levels. In Test B, large swelling strains take place at low stress and the f_β interaction mechanism is very strong, resulting in large plastic strains that are not fully recovered in the loading stage. In contrast, the development of irrecoverable Macro-structural strains in Test A are small, because when the swelling take place the structural mechanical interaction is small.

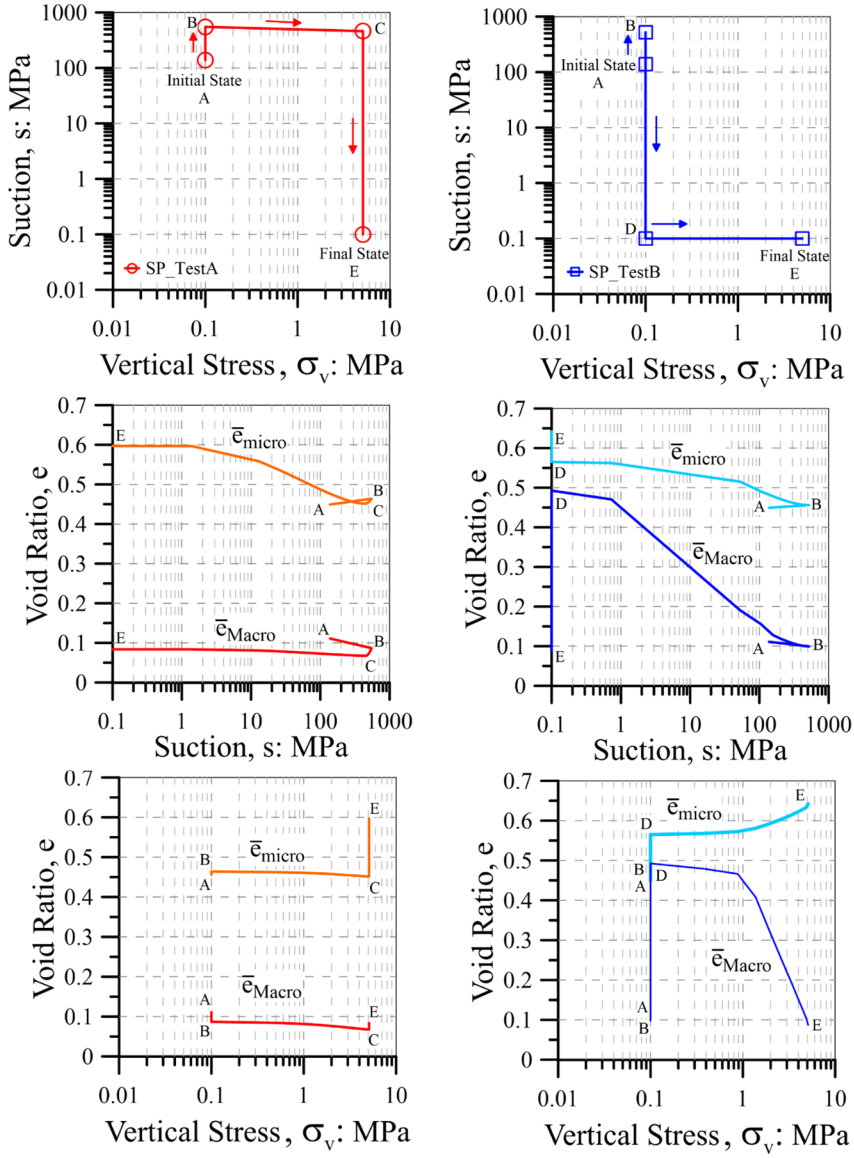

Figure 5-13. Pore space evolution for TestA (Left) and TestB (Right).

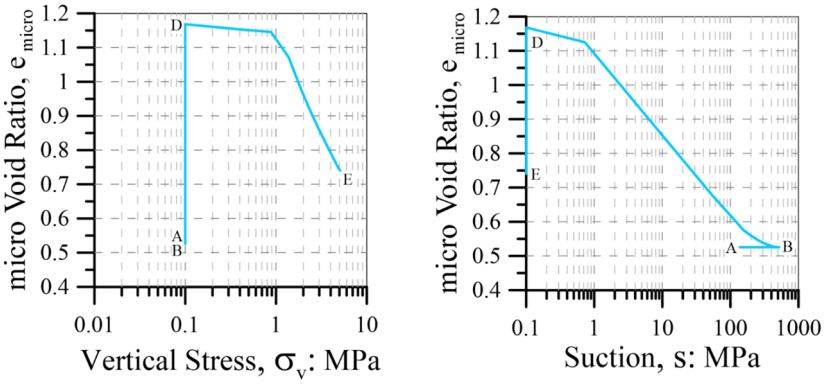

Figure 5-14. Computed evolution of micro-structural void ratio for TestB. Left: Variation over the vertical stress; Right: Variation over suction.

5.4. Homogenization phenomena

The sources of heterogeneity in bentonite barriers and the phenomena underlying the homogenization due to hydro-mechanical actions have been explained in detail in Chapter 2.

The numerical modelling of bentonite homogenization has a higher degree of complexity. Therefore, in this work, it has be conceived in a progressive manner. Chapter 4 contains a simple homogenization case in which the constitutive response is analysed. Now, the following laboratory test are reproduced:

- Swelling pressure tests on compacted heterogeneous mixtures made by bentonite powder and bentonite pellets. Two bentonite mixtures with different compacted levels are evaluated.
- Large-scale oedometer tests on bentonite block/pellets specimens. Attention is paid here to the modelling of fabric and swelling pressure evolution due to different hydration conditions.

5.4.1. Compacted mixtures of bentonite powder and pellets

The mixtures of bentonite powder and highly compacted bentonite pellets are an interesting option for sealing material in the galleries and shafts of the nuclear waste repositories (Volckaert et al., 2000; Gens et al., 2011; Molinero-Guerra et al., 2017). The main reasons to use this kind of heterogeneous material are the emplacement works and a quite high dry density due to the contribution of high-density pellets. In spite

of their high dry density value, the compacted bentonite blocks (Lloret et al., 2003) leave gaps between them and they are so difficult to accommodate when shaft and drift have non-uniform surfaces.

The resulting material is obviously highly heterogeneous, consisting of a mixture of relatively low-density bentonite powder with high-density bentonite pellets. The behaviour of such material upon hydration is likely to be complex and must be properly understood if a sufficient degree of confidence in the design and performance of the seal is to be achieved (Gens et al., 2011).

In this section, the double-structure formulation is applied on the modelling of swelling pressure tests performed in the laboratory. Imbert and Villar, (2006) analysed the swelling pressure behaviour of the powder-pellets mixture during hydration. Note that the hydration of a shaft or tunnel seal due to the inflow of host rock water is analogous to a swelling pressure test due to confined provided by excavation walls (e.g. the Reseal project reported in Volckaert et al., 2000).

Mixtures of 50% bentonite powder and 50% bentonite pellets by dry weight were tested. The FoCa clay have been selected. The dimension of the pellets are 25x25x15 mm (Figure 5-15) and their average dry density is 1.89 g/cm^3. Compaction water content lies in the range 4-5%. The Figure 5-15 shows the bentonite mixture disposed in an experimental shaft.

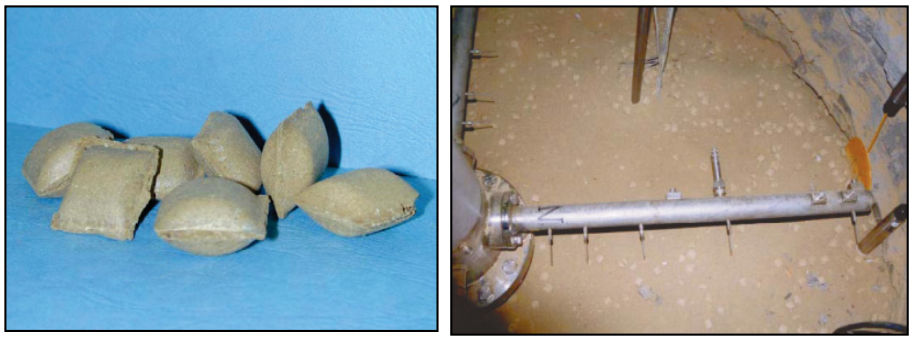

Figure 5-15. Left: Pellets of FoCa Clay; Right: Powder-pellets mixture used as sealing material in an experimental shaft (Gens et al., 2011).

The samples for the swelling pressure tests were statically compacted to the desired density and were subsequently tested in oedometers equipped

with load cells. The specimens were hydrated from the bottom, sample deformation was prevented and the evolution of the swelling pressure and water intake was recorded (Imbert and Villar, 2006).

Direct observations of the homogenization process due to hydration were depicted in the Chapter 2 (Figure 2-24 and Figure 2-25). They reveal a tendency to achieve homogeneous states and the local water exchange between powder and pellets.

From the series of infiltration tests performed by Imbert and Villar, (2006), we select the tests MGR9 and RS2E to reproduce the hydro-mechanical response according to the double-structure formulation. The specimens, with the same height, differs on their dry densities. The main characteristic of the tests are given in Table 5-3. The pellets always have the same density; the variation in the density of the samples arises from the different initial powder densities.

Table 5-3. Main characracteristics of the swelling pressure tests. (from Imbert and Villar, 2006 and Gens et al; 2011)

		Test MGR9	Test RS2E
Dimensions	**Height: mm**	100	100
	Diameter: mm	100	120
Sample	**e**	0.84	0.67
	ρ_d: g/cm^3	1.45	1.60
	Initial w: %	5.25	4.78
Pellets	**ρ_d: g/cm^3**	1.89	1.89
	Initial w: %	5.00	4.49
Powder	**ρ_d: g/cm^3**	1.182	1.390
	Initial w: %	5.80	5.07

As the main assumption, the overall medium is assumed to consist of two structural levels. According to Gens et al., (2011), the Macro-structure refers to the large-scale arrangement of soil particle aggregates and the relatively large pores between them. It is expected that, initially, most of the Macro-structural pores belong to the bentonite powder. The microstructure refers to the clay particles and the micropores and interparticle spaces associated with them. A large proportion of the micropores lie initially in the high-density pellets but there will also be micropores in the clay particle aggregates present in the powder. Ideally,

the microporosity of the powder aggregates should be distinguished from that in the pellets but, in that case, the number of interactions and parameters multiply leading to a cumbersome formulation that is difficult to apply in practice. Consequently, the pore space of the specimens and the initial suctions are listed in Table 5-4.

A 2D axisymmetric geometry is used for the modelling tasks (Figure 5-16). In accordance with the null volumetric, the behaviour is essentially one-dimensional. Therefore, the analysis at different vertical points is interesting.

Table 5-4. Initial conditions of the swelling presure test. (from Gens et al; 2011)

		Test MGR9	Test RS2E
Pore space	Total porosity, ϕ	0.46	0.40
	Macro pore volume fraction, $\bar{\phi}_2$	0.33	0.16
	Micro pore volume fraction, $\bar{\phi}_1$	0.13	0.24
Suction	Macro suction: MPa	284	284
	micro suction: MPa	321	314

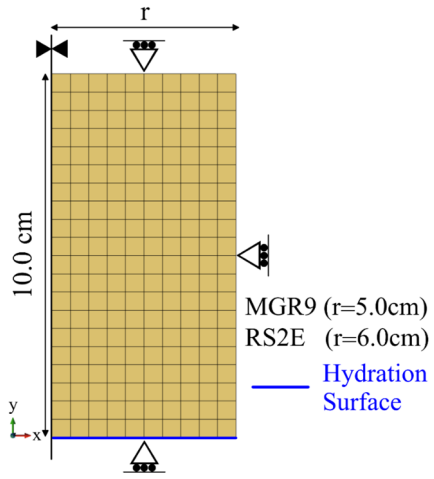

Figure 5-16. 2D axisymmetric FEM model for powder/pellets homogenization tests.

Table 5-5 contains the hydraulic and mechanic input parameters. The retention parameters are estimated from experimental curves of FoCa clay at different densities. The water retention curve for micro- and

Macro-structural levels have been estimated from the results of the higher and lower density samples, respectively (Gens et al., 2011). The double retention curves of the compacted specimens are given by the superposition of the micro and Macro van Genuchten curves (Figure 5-17). The weighting parameters are consequence of the compaction level (see Chapter 3 and Appendix A).

Table 5-5. Input parameters for the homogenization test MGR9 and RS2E.

Parameters		MGR9 Test	RS2E Test
Bishop parameter micro-structural level	p_k (-)	0.5	0.5
	q_k (-)	100	100
Non-linear elasticity	$\bar{\kappa}$ (-)	0.00015	0.00012
	κ_s (-)	0.028	0.032
	ν (-)	0.3	0.3
Macro-micro mechanical interaction function	f_{ms0}(-)	1	1
	f_{ms1}(-)	0	0
	n_{ms}(-)	2	2
Macro-structural level Plastic mechanism (BBM)	φ (^{o})	25	25
	p_c (MPa)	0.022	0.022
	λ_{sat}(-)	0.215	0.16
	r (-)	0.50	0.70
	β (MPa^{-1})	0.026	0.03
	k_s (-)	0.01	0.01
	p_{s0} (MPa)	0.1	0.1
Constant leakage parameter	γ ($kg.s^{-1}.m^{-3}.MPa^{-1}$)	1.e-5	1.e-5
Variable leakage parameter	γ_o ($kg.s^{-1}.m^{-3}.MPa^{-1}$)	1.e-8	-
	ω(-)	160	-
	$(p/p_o)_{ref}$	0.14	-
Water retention curve for micro-structural level	$(P_o)_1$ (MPa)	379	379
	σ_o	0.072	0.072
	$(\lambda_o)_1$ (-)	0.899	0.899
	$(S_r)_{L1}$ (-)	0.3	0.3
	$(S_m)_{L1}$ (-)	1	1
	$(P_d)_1$ (MPa)	800	800
	$(\lambda_d)_1$ (-)	2.243	2.243
Water retention curve for Macro-structural level	$(P_o)_2$ (MPa)	12	15
	σ_{To}	0.072	0.072

	$(\lambda_o)_2$ (-)	0.064	0.064
	$(S_r)_{L2}$ (-)	0	0
	$(S_m)_{L2}$ (-)	1	1
	$(P_d)_2$ (MPa)	750	750
	$(\lambda_d)_2$ (-)	3.899	3.899
Intrinsic permeability	k_o (m^2)	1.5e-20	1.5e-20
	b (-)	11	6
	$(\phi_{min})_2$	0.4	0.4
Initial conditions	P_o^* (MPa)	0.14	0.38
	ϕ (-)	0.46	0.4
	$\bar{\phi}_1$(-)	0.13	0.24
	P_{L1}(MPa)	-321	-314

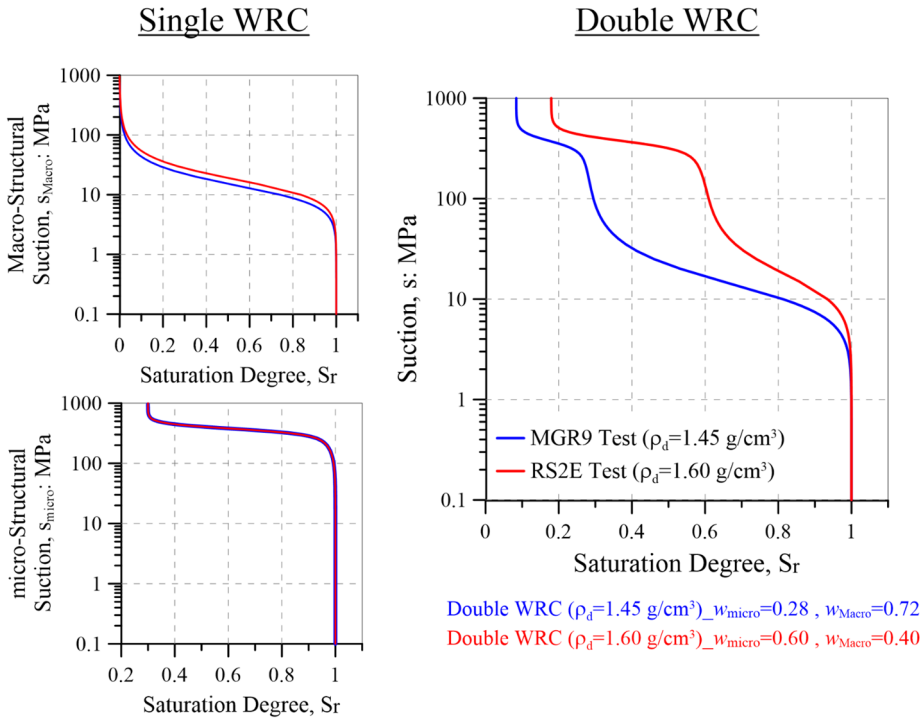

Figure 5-17. Water retention curves for compacted mixtures of bentonite powder and bentonite pellets.

The leakage parameter was obtained from back-analysis. Constant and variable values has been used. The leakage parameter is sometimes associated with some geometric characteristic of the medium. For double-

structure materials, an exponential dependence on stress ratio p/p_o was proposed (Chapter 3).

The mechanical parameters of the constitutive model are also collected in the Table 5-5. It should be noted that only one interaction function is required as only the microstructural swelling mechanism is involved in the swelling pressure test. Although some BBM parameters of the Macro-structure depend on the initial density of the powder (e.g. saturated presconsolidation stress, P_o^*), the parameters characterising the behaviour of the microstructure remain unchanged throughout all the analyses performed.

Figure 5-18 shows the computed evolutions of swelling pressure and water intake compare with measured values. The experimental swelling stress pattern is well modelled. The first swelling pressure peak and time required to reach it are adequately reproduced by the calculation. The subsequent reduction of swelling pressure due to Macro-structural collapse and the final steady-state value are also well modelled. The numerical model with the variable leakage parameter present a smaller peak value, indicating that at this specific time the micro-structural level has not hydrated enough. Later, the behaviour of both models are similar. The variation of the water mass transfer parameter, γ, was selected to be equilibrated with the constant value option at an early stage of the hydro-mechanical process. The water intake of the test is also well reproduced, but the observed rate of water inflow is a slightly larger than the computed values at the initial stages of the tests (<1 day).

Due to the satisfactory numerical results, additional output information can be obtained in order to analysis in more detail the hydro-mechanical evolution of the system. The time evolution of the micro- and Macro-structural suctions is plotted in Figure 5-19. Three different points on the model are selected: near to hydration boundary (y=0.0 m), at the middle of the sample (y=0.05 m) and near the top of the sample (y=0.095 m). It can observed that, at the bottom boundary, the structural suctions reduce rapidly, but they differ at the beginning because of the delay in micro-Macro water transfer. Similarly to the results obtained by Gens et al., (2011), the other two points the two porosities come into equilibrium before they are reached by the hydration front, that is before they exhibit

any suction reduction. They also maintain this equilibrium condition throughout the rest of the test. The numerical analysis suggests, therefore, that non-equilibrium between the two structural levels is only likely to affect the early stages of the test. The case with the variable leakage parameter modifies this equilibration period.

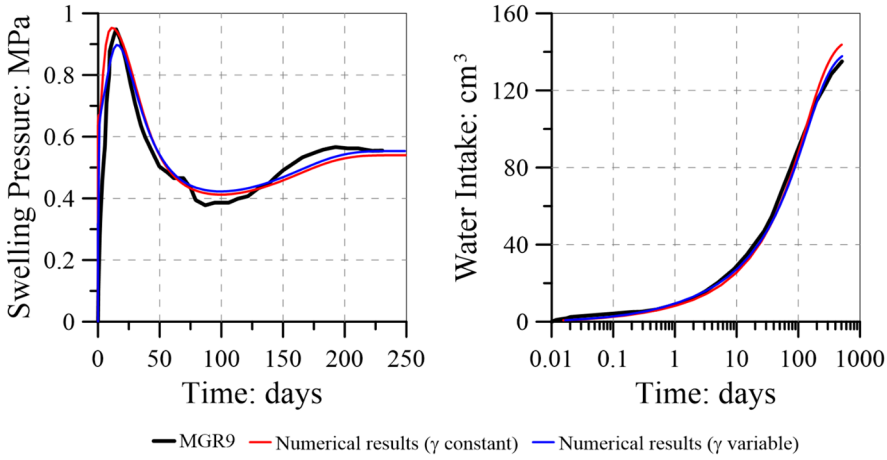

Figure 5-18. Experimental data compare with modelling results for tests MGR9 (ρ_d=1.45 gr/cm^3). Left: Swelling pressure test; Right: Accumulated water intake.

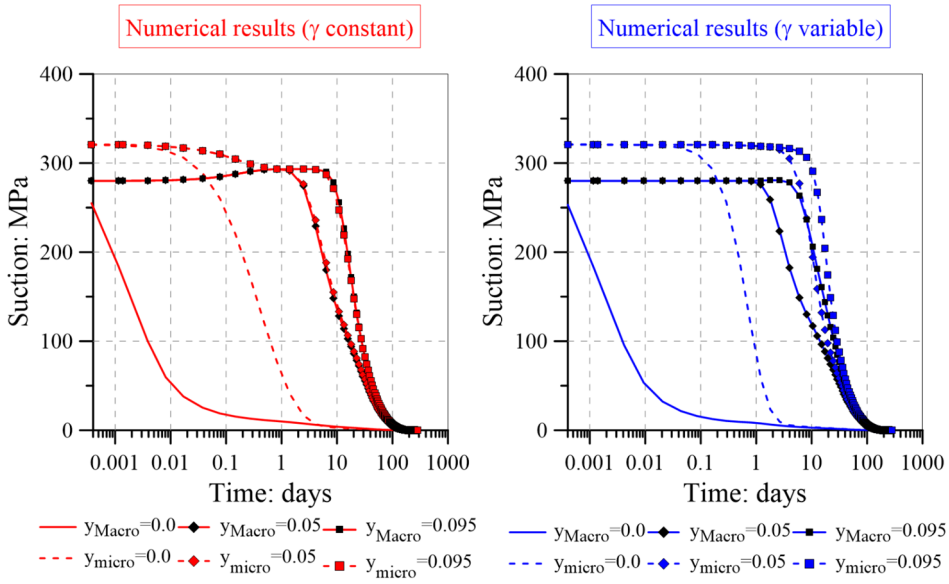

Figure 5-19. Computed evolution of Macro- and Micro-structural suctions at three different point of the modelling MGR9. Left: Constant leakage parameter; Right: Variable leakage parameter.

The swelling pressure drop is a direct consequence of the Macro-structural collapse that, in the double-structure model, correspond to the LC yield surface in the BBM formulation. The stress paths (Macro-structural suction vs vertical net stress) for the same three points illustrate the collapse mechanism (Figure 5-20). The initial location of the LC curve is also presented. Initially, the stress increases is more significant than suction reduction. Once the LC yield surface is reached, the vertical stress drops to compensate the tendency of the macrostructure to collapse so that the sample length is kept constant (Gens et al., 2011). The final stage of reduction of the Macro pore volume fraction is related with the progressive increasing of vertical stress caused by the swelling of the micro-structural level. The variable leakage parameter modifies slightly the early stages of the stress-paths evolution, but the general trend is the same for both computations.

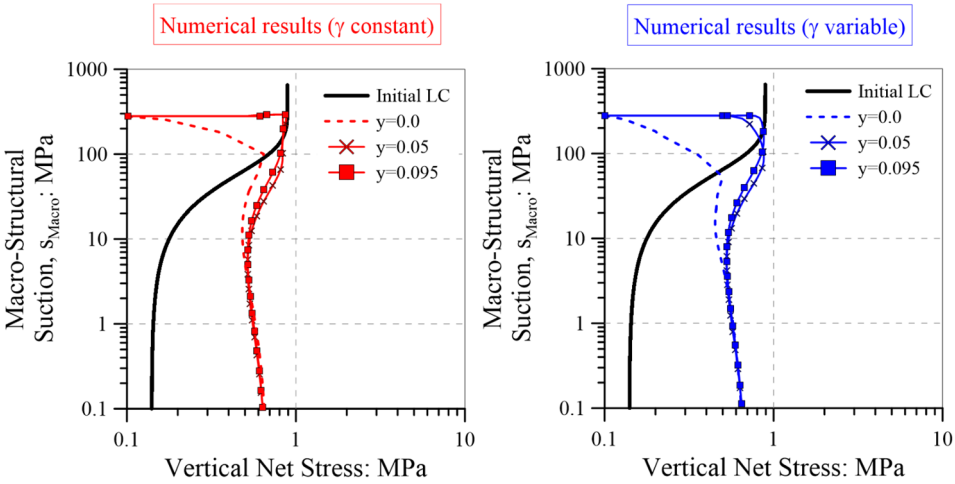

Figure 5-20. Computed stress path (Macro-structural suctions vs vertical net stress) for three different point of the modelling MGR9. Left: Constant leakage parameter; Right: Variable leakage parameter. Only the initial LC yield surface is shown for clarity.

The test performed on a denser sample is now considered (ρ_d=1.60 g/cm^3) (Table 5-3). Computed evolutions of swelling pressure and water intake compared with the experimental values are shown in Figure 5-21. Constant value of the leakage parameter for micro-Macro water transfer is only considered. The overall behaviour of this test is similar to that of the looser sample MGR9 but, in this case, the final swelling pressures are

much higher and the swelling pressure drop after the first peak is comparatively smaller. The rate of swelling pressure developed at start of the test is overestimated by the numerical analysis, but the magnitude of the first peak is adequately reproduced. The evolution of water intake is also well matched, nevertheless some discrepancies at the end of the test have been attributed to small water leakage in the experimental device at very long term test.

The time evolution of micro- and Macro-structural suction at three vertical points are shown in Figure 5-22. They are similar to those of looser sample MGR9. The stress paths for the same points are presented in Figure 5-23. The initial LC is now further to the right to account for a denser Macro-structure (P^*_{o}_RS2E > P^*_{o}_MGR9). The drop in vertical stress after reaching the LC is now smaller if compare with the looser specimen.

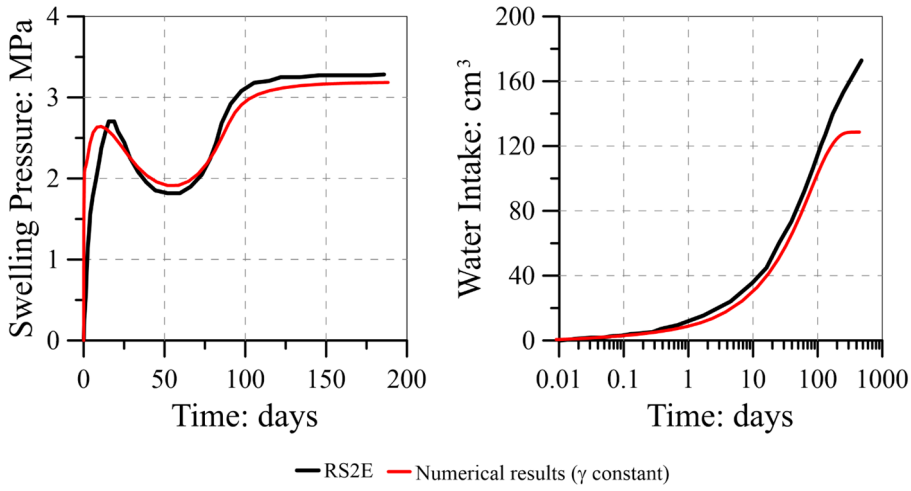

Figure 5-21. Experimental data compare with modelling results for tests RS2E (ρ_d=1.60 gr/cm^3). Left: Swelling pressure test; Right: Accumulated water intake.

Some concluding remarks about these computations are:

- The assumption of a double porosity arrangement could be an oversimplification of the complex fabric of the powder-pellets mixture. However, it appears to be sufficient to describe the pore space.
- The double-structure formulation, presented in previous Chapters, has been capable to reproduce describe the hydro-mechanical behaviour of this heterogeneous material.

- Gens et al., 2011 also presented a satisfactory reproduction of the HM behaviour of these bentonite mixtures using a former double-structure approach. The modelling presented in this section proves the consistency of the formulation presented in this thesis. Moreover, the new features (e.g. Bishop's micro-structural stress, elastic structural coupling, variable leakage parameter, micro liquid pressure as quadrature variable) are successfully tested.

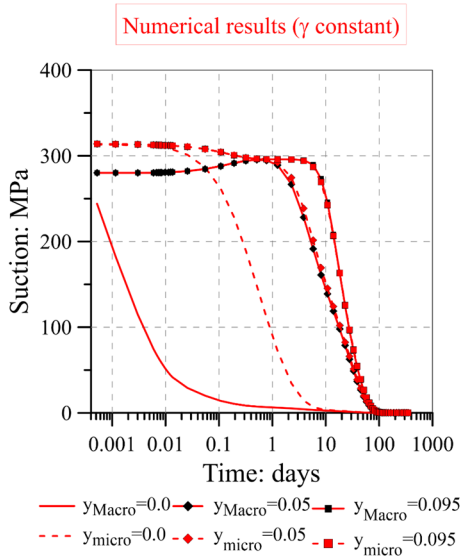

Figure 5-22. Computed evolution of Macro- and Micro-structural suctions at three different point of the modelling RS2E.

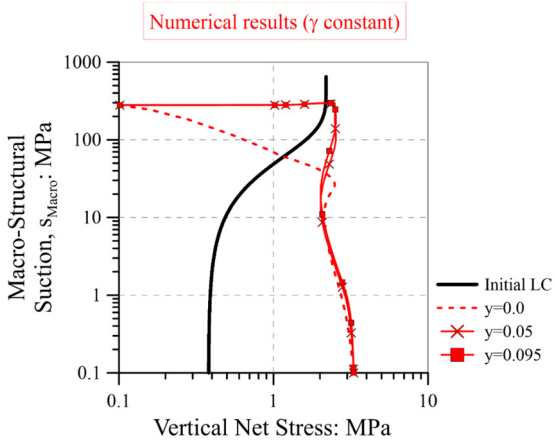

Figure 5-23. Computed stress path (Macro-structural suctions vs vertical net stress) for three different point of the modelling RS2E. Only the initial LC yield surface is shown for clarity.

5.4.2. Bentonite block-pellets specimens_CIEMAT tests

The main pitfall of a buffer or seal design based on compacted bentonite blocks is the generation of technological gaps between blocks and the gallery wall. In order to overcome this problem, several repository designs include the use of bentonite pellets to fill these voids.

The heterogeneity evolution in bentonite block-pellets arrangement and their hydro-mechanical response have been assessed by laboratory tests. Chapter 2 presented in detail two large-scale oedometer tests on FEBEX bentonite block/pellets specimens (Figure 5-24).

- MGR22: Restricted water access (controlled flow of 0.05 cm^3/h) until full saturation.
- MGR23: Full water access (water pressure of 14 kPa) until full saturation.

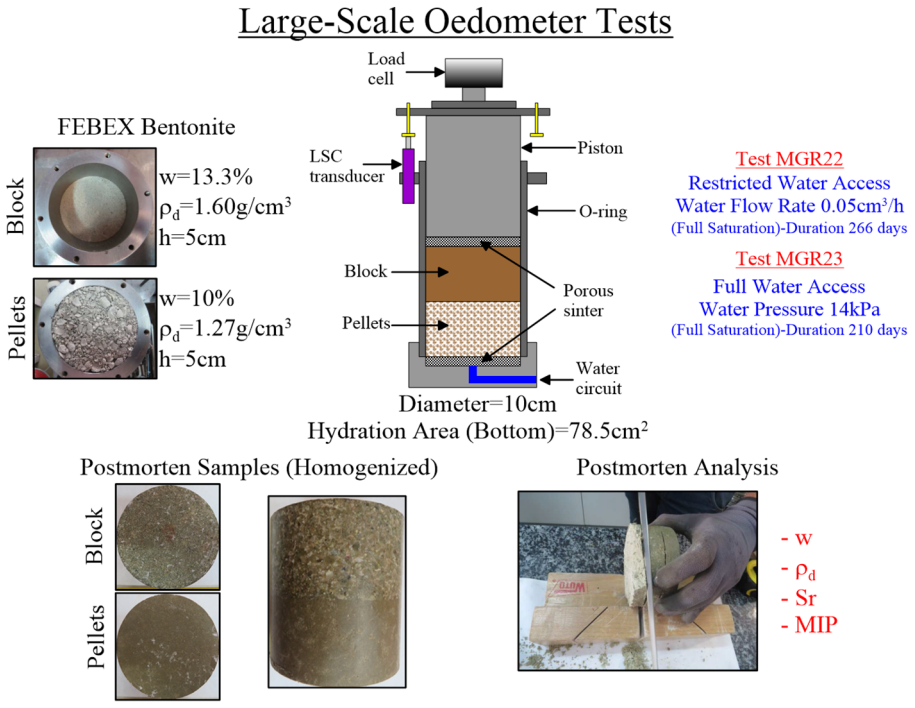

Figure 5-24. (Also Figure 2-20) Experimental setup of CIEMAT homogenization tests: MGR22 and MGR23.

The experimental results can be summarised as:

- The final value of axial pressure is the same for both tests (same average dry density). It is independent of the hydration condition (Figure 5-25).
- There is a clear influence of hydration condition on the rate of the development of axial pressure. The full water access (MGR23 test) induce a faster pressure evolution (Figure 5-25). The fabric evolution of the bentonite pellets mixture due to the hydration conditions play a central role in the pressure kinetics (Figure 2-22).
- The spatial distribution of dry density, water content and pore space distribution (MIP) show certain heterogeneous state after saturation (Chapter 2).
- The oedometer tests present the same deformation trend. The pellet mixture is compressed by the blocks expansion (see Table 5-6).

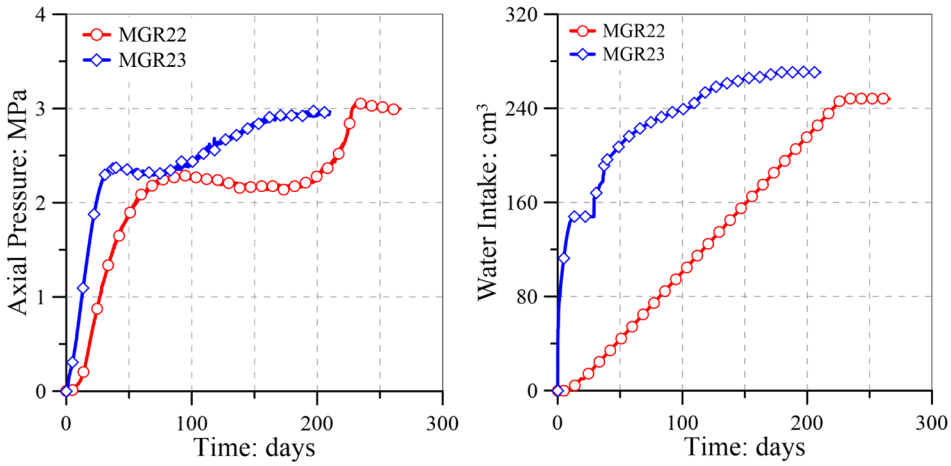

Figure 5-25. (Also Figure 2-21) Left: axial pressure evolution; Right: water intake evolution. CIEMAT homogenization tests MGR22 and MGR23.

Table 5-6. Final heights of CIEMAT homogenization test (in centimeters).

	MGR22	MGR23
Block	5.27	5.29
Pellets	4.73	4.71

The main goal of the numerical modelling of these tests is a deeper interpretation of the bentonite homogenization phenomena, and the basic mechanisms controlling them, using a double-structure formulation.

Based on the modelling cases presented in Chapter 4, a rational modelling procedure for this kind of homogenization tests consist in the analysis of swelling behaviour of compacted bentonite block and compacted mixture of pellets, separately. After that, the intricate response of the bentonite block/pellets specimens can be tackled.

The THM behaviour of the bentonite FEBEX has been intensively studied. Lloret et al., (2003) presented the stress-paths observed in the swelling pressure tests of compacted bentonite. Moreover, the hydro-mechanical behaviour of bentonite pellets mixtures is reported in Hoffmann et al., (2007).

Expected values of swelling pressure for both compacted materials are obtained from exponential trends with the dry densities values (Figure 5-26). It is interesting to note that the axial pressure obtained in MGR22 and MGR23 test are close to the average of the individual swelling pressure values.

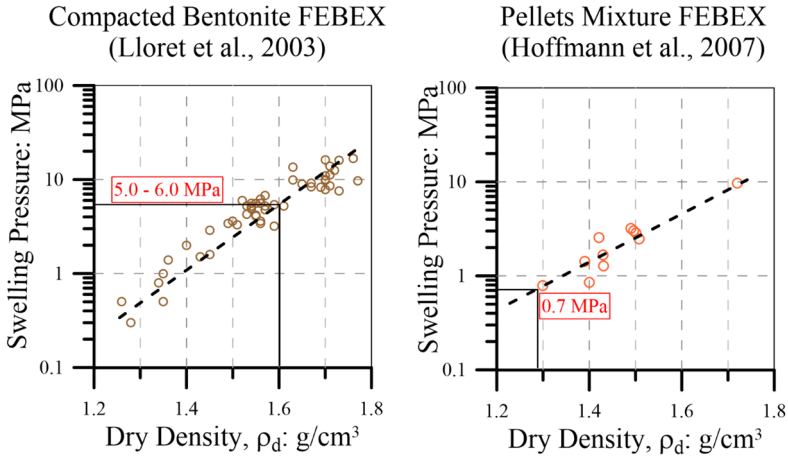

Figure 5-26. Swelling pressure as a function of dry density for compacted bentonite FEBEX (Lloret et al., 2003) and pellets mixture FEBEX (Hoffmann et al., 2007).

2D axisymmetric geometries are used for the modelling of swelling behaviour of the bentonite block and pellets mixture (Figure 5-27). The dimensions used in the homogenization tests are maintained.

Materials parameters and initial conditions are given in Table 5-7. The initial values of the micro and Macro pore volume fractions are obtained

in accordance with the mercury intrusion porosimetry (MIP) tests (Chapter 2). The water retention parameters for bentonite block has been presented in the Section 5.3.1. and the experimental water retention curve of the pellets mixture is reproduced in the Appendix A (Figure A-3). From these multimodal WRC models and the initial saturation state, the micro- and Macro liquid pressure have been estimated. Finally, Figure 5-28 shows the micro-Macro mechanical interaction functions.

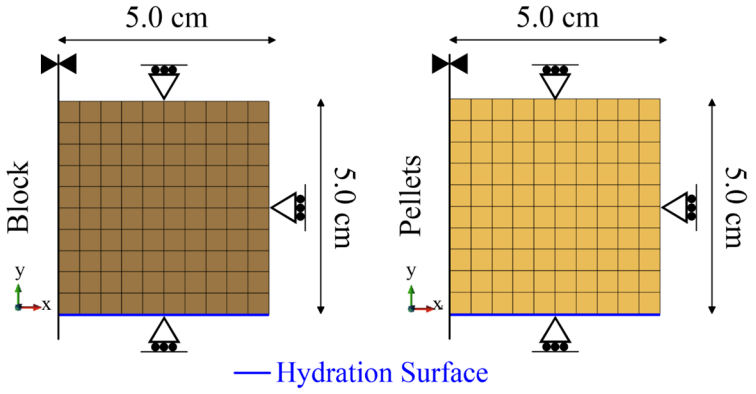

Figure 5-27. 2D axisymmetric FEM model for swelling pressure tests.

Table 5-7. Input parameters for compacted bentonite block and pellets mixtures.

Parameters		Bentonite Block	Pellets Mixture
Bishop parameter micro-structural level	p_k (-)	0.7	0.7
	q_k (-)	100	100
Non-linear elasticity	$\bar{\kappa}$ (-)	0.0009	0.0003
	κ_s (-)	0.02	0.03
	ν (-)	0.3	0.3
Macro-micro mechanical interaction function	f_{ms0}(-)	2	1
	f_{ms1}(-)	0	0
	n_{ms}(-)	7	2
	f_{mc0}(-)	0	0
	f_{mc1}(-)	2	1
	n_{mc}(-)	5	2
Macro-structural level Plastic mechanism (BBM)	φ (°)	25	27
	p_c (MPa)	0.5	0.097
	λ_{sat}(-)	0.23	0.20
	r (-)	0.65	0.6

	β (MPa^{-1})	0.010	0.03
	k_s (-)	0.01	0.01
	p_{s0} (MPa)	0.1	0.1
Constant leakage parameter	γ ($kg.s^{-1}.m^{-3}.MPa^{-1}$)	7e-7	4e-5
Water retention curve for micro-structural level	$(P_o)_1$ (MPa)	180	150
	σ_o	0.072	0.072
	$(\lambda_o)_1$ (-)	0.65	0.8
	$(S_r)_{L1}$ (-)	0.3	0.3
	$(S_m)_{L1}$ (-)	1	1
	$(P_d)_1$ (MPa)	700	700
	$(\lambda_d)_1$ (-)	1.5	1.5
Water retention curve for Macro-structural level	$(P_o)_2$ (MPa)	12	0.4
	σ_{To}	0.072	0.072
	$(\lambda_o)_2$ (-)	0.27	0.28
	$(S_r)_{L2}$ (-)	0	0
	$(S_m)_{L2}$ (-)	1	1
	$(P_d)_2$ (MPa)	2000	2000
	$(\lambda_d)_2$ (-)	2	2
Intrinsic permeability	k_o (m^2)	4.e-21	6e-19
	b (-)	12	18
	$(\phi_{min})_2$	0.25	0.42
Initial conditions	P_o^* (MPa)	3.0	0.65
	ϕ (-)	0.52	0.69
	$\bar{\phi}_1$(-)	0.27	0.27
	$\bar{\phi}_2$(-)	0.25	0.42
	P_{L1}(MPa)	-185	-190
	P_{L2}(MPa)	-180	-180
	P_g (MPa)	0.1	0.1

The computed stress-paths and time evolution for swelling pressure tests on compacted bentonite block and granular mixture are plotted in Figure 5-29. The agreement with experimental data is quite satisfactory. In accordance with the compaction levels and the initial pore space distributions, the compacted bentonite block exhibits a swelling tendency and, conversely, the bentonite pellets mixture is prone to collapse. Both tendencies are well captured by the double-structure formulation.

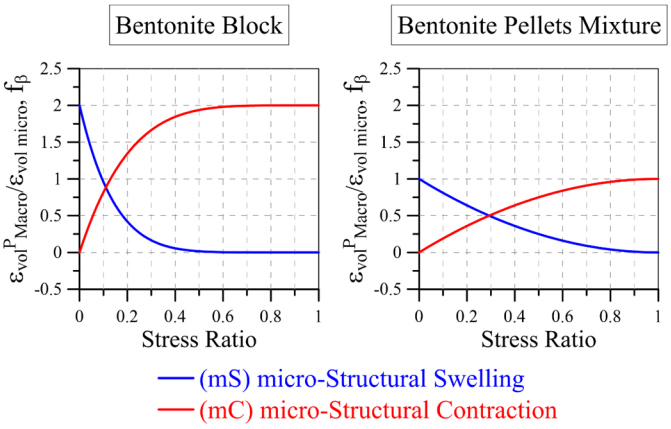

Figure 5-28. Mechanical interaction functions for compacted bentonite block and pellets mixtures.

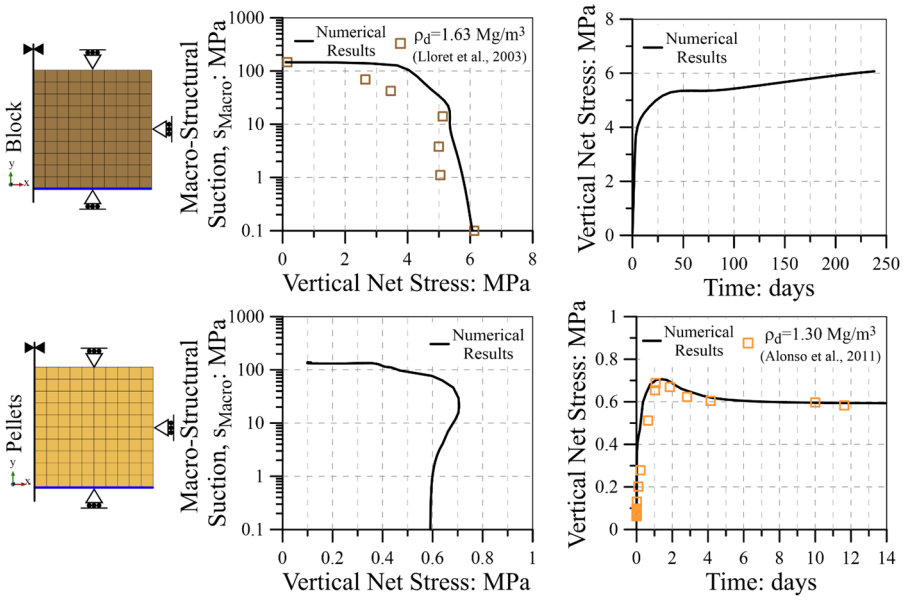

Figure 5-29. Swelling pressure tests in compacted bentonite block and pellets mixtures.

The compacted bentonite block underwent a certain swell deformation in the homogenization tests MGR22 and MGR23. Therefore, its fabric evolution can be encountered in between of constant volume condition (i.e. swelling pressure test) and the free swelling deformation. The evolution of the micro and Macro pore volume fractions for both conditions is shown in Figure 5-30. An interesting fact is the role of

micro-Macro interaction fractions in the fabric evolution. This mechanism only affects the early part of Macro-structural deformation, because the unit value of stress ratio (in which the mS function is null) is reached rapidly due to the lateral stress development. After this point, the volume fractions evolve as a function of structural levels stiffness and volume constrain.

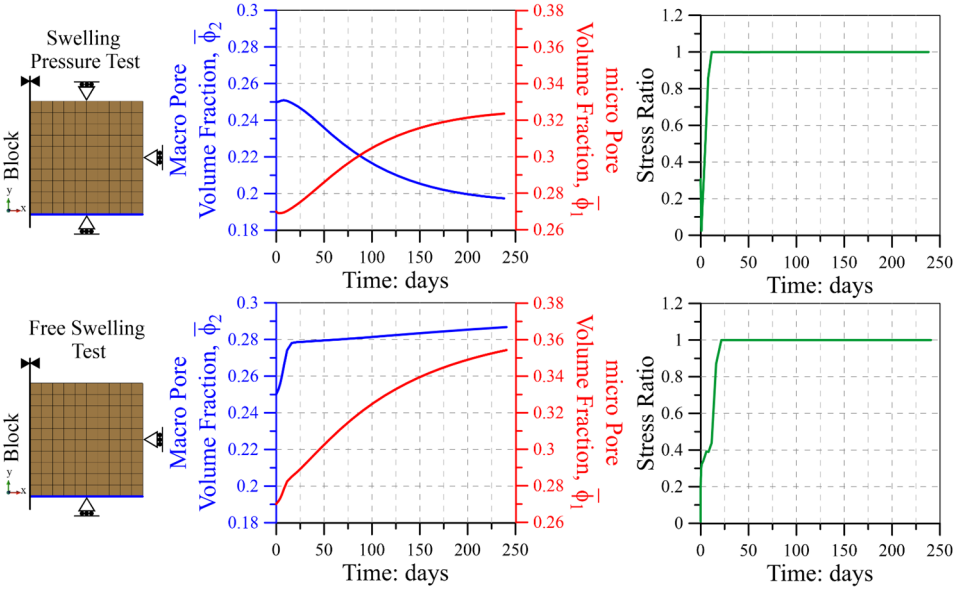

Figure 5-30. Computed pore space evolution of the compacted bentonite block due to hydration under constant volume and free swelling conditions.

The fabric evolution in the compacted pellets mixture is not bounded by the constant volume and free swelling conditions. Actually, a compression due to bentonite block swelling is expected. Figure 5-31 presents the pore volume fractions for the swelling pressure test.

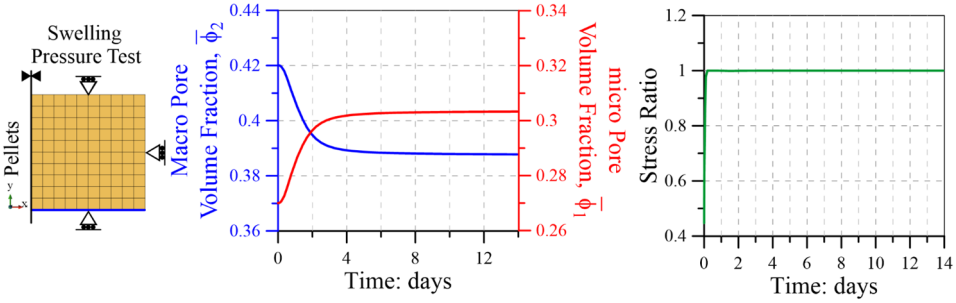

Figure 5-31. Computed pore space evolution of the compacted pellets mixture due to hydration under constant volume condition.

The modelling of the homogenization tests considers an axisymmetric geometry around the axis of the oedometer cell (Figure 5-32).

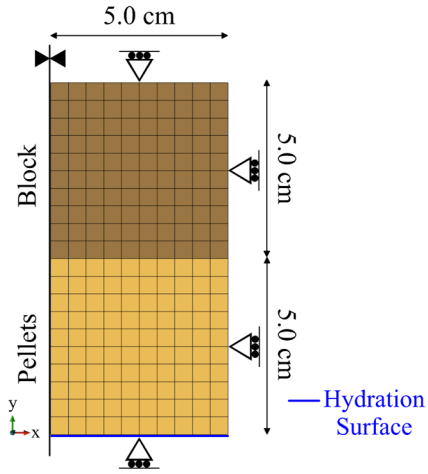

Figure 5-32. 2D axisymmetric FEM model for CIEMAT homogenization tests.

Before going to numerical reproduction of both tests, it is worthwhile to re-examine the hydration mechanism (see Chapter 2), because there are important implications on the modelling approaches. Figure 5-33 shows the development of axial pressure as a function of water intake. In test MGR22 the axial pressure starts to increase at low water intake. In contrasts, the tests MGR23 requires important amount of water to generate axial pressures.

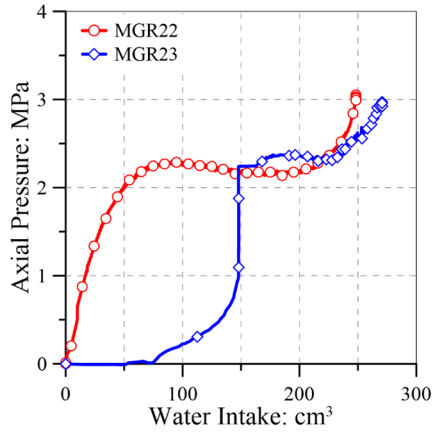

Figure 5-33. (Also Figure 2-23) Axial pressure as function of water intake. CIEMAT homogenization tests MGR22 and MGR23

The above hydro-mechanical behaviours allows to classified the homogenization tests MGR22 and MGR23 as slow and fast infiltration tests, respectively. The Figure 2-22 has depicted the hydration mechanism of the tests at early stage.

Experimental data of intrinsic permeability evolution during fast infiltration tests in FEBEX bentonite pellets (Hoffmann et al., 2007) and the exponential law adopted for the modelling are shown in Figure 5-34. The distinctive evolution of permeability (and Macro pores) arises from the fast saturation of Macro pore space, the subsequent Macro-structural collapse and the swelling of bentonite pellets due to the mass water transfer towards micro pores of the pellets.

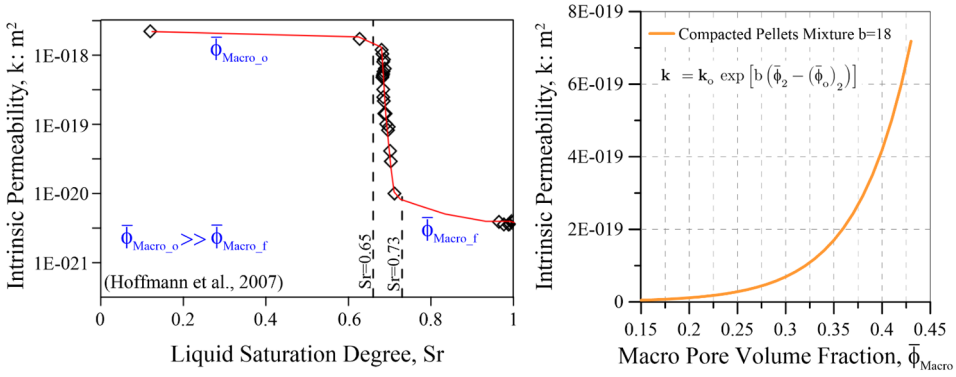

Figure 5-34. Left: Evolution of the permeability during fast infiltration tests in bentonite pellets mixture (Hoffmann et al., 2007); Right: Exponential intrinsic permeability evolution for modelling bentonite pellets mixture.

The appropriate reproduction of the intrinsic permeability evolution of the pellets mixture with the proposed exponential law require the consideration of different values of parameter b for the cases of slow and fast water infiltration. For the sake of modelling consistency, an alternative option can be start the modelling of MGR23 from an early stage of the saturation process and maintain the same constitutive parameters for both cases. The capability of the HM double-structure formulation to deal with non-equilibrated hydraulic state between micro- and Macro-structural levels is useful to emulate the water distribution generated by a fast water infiltration. Table 5-8 contains the initial micro and Macro liquid pressures considered for the bentonite block and the compacted pellets mixture.

Table 5-8. Initial values of liquid pressure for tests MGR22 and MGR23.

		MGR22	MGR23
Block	P_{LMacro}	-180	-180
	P_{Lmicro}	-185	-185
Pellets	P_{LMacro}	-180	-5
	P_{Lmicro}	-190	-190

The vectors of liquid flow, at 10 days, in the FE models are compare with the conceptual hydration mechanism at early stage (Figure 5-35 and Figure 5-36). A good agreement between them are clearly observable. The controlled water inflow in the test MGR22 generate a hydration front through the granular pellets mixture (Figure 5-35) the bentonite pellets, at the base of the specimen, start to swell due to water exchange, reducing the macro pore space and the permeability. In the MGR23 the water goes into the sample through the interconnected macro pores. After this first stage the bentonite pellets start to hydrate exchanging water with the water stored at the macro-pores and the bentonite block is hydrated through water front (Figure 5-36).

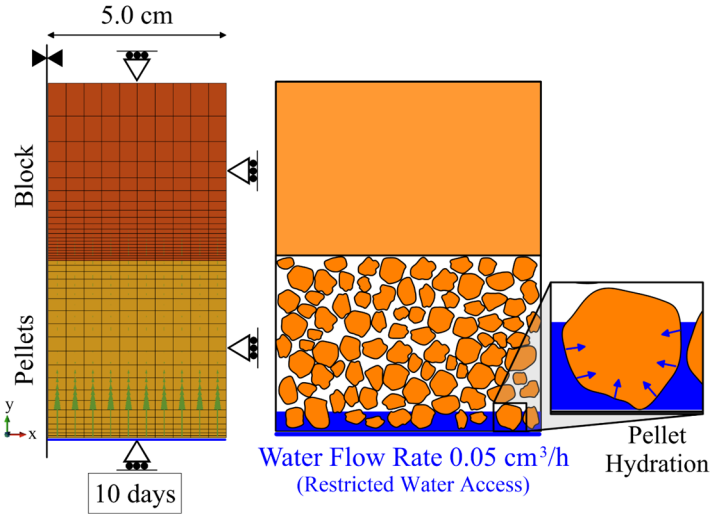

Figure 5-35. Left: Vectors of liquid flow in the modelling MGR22 at 10 days; Right: Hydration mechanism of the homogenization test MGR23 at early stage.

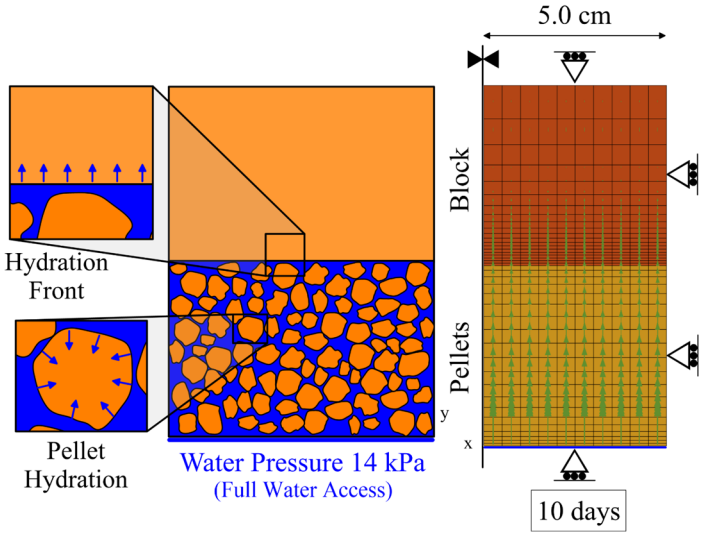

Figure 5-36. Left: Hydration mechanism of the homogenization test MGR23 at early stage; Right: Vectors of liquid flow in the modelling MGR23 at 10 days.

Figure 5-37 shows the computed evolutions of axial pressure for both homogenization tests. The rate of axial pressure developed at start of the test is slightly overestimated by the numerical analyses, but the magnitude of the final value is adequately reproduced. The initial peak of the MGR23 tests is underestimated by the numerical modelling, presumably by the assumed initial state.

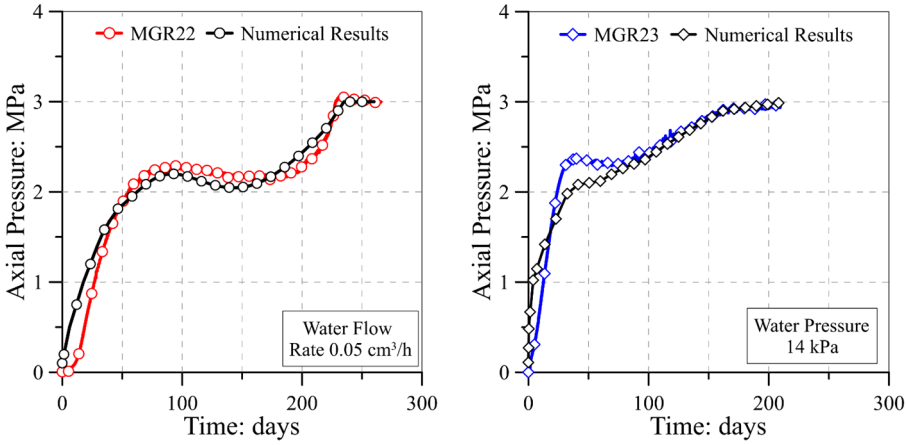

Figure 5-37. Swelling pressure experimental data compare with modelling results. Left: MGR22 test; Right: MGR23 test.

Comparisons between computed and experimental final distributions of micro and macro pore volume fractions are illustrated in Figure 5-38 and Figure 5-39. The general trends are adequately capture by the numerical analyses:

- In the bentonite block, $\bar{\phi}_{micro}$ and $\bar{\phi}_{Macro}$ increases due to hydration and swelling deformations.
- In the pellets mixture, $\bar{\phi}_{micro}$ increases due to hydration and $\bar{\phi}_{Macro}$ reduces by the swelling of the micro-structural level and compression generated by the swelling deformation of the bentonite block.

Some specific discrepancies can be mentioned:

- The final micro pore volume fraction, $\bar{\phi}_{micro}$, in the pellets mixture is overestimated by the modelling MGR22.
- The experimental data of MGR23 shows an unexpected local phenomena: a strong reduction of Macro pore volume fraction in the bentonite block, close to the material contact-pellets. This is not in accordance with the final distribution of dry density (Chapter 2 and Figure 5-42) and it is not reproduced by the MGR23 model.

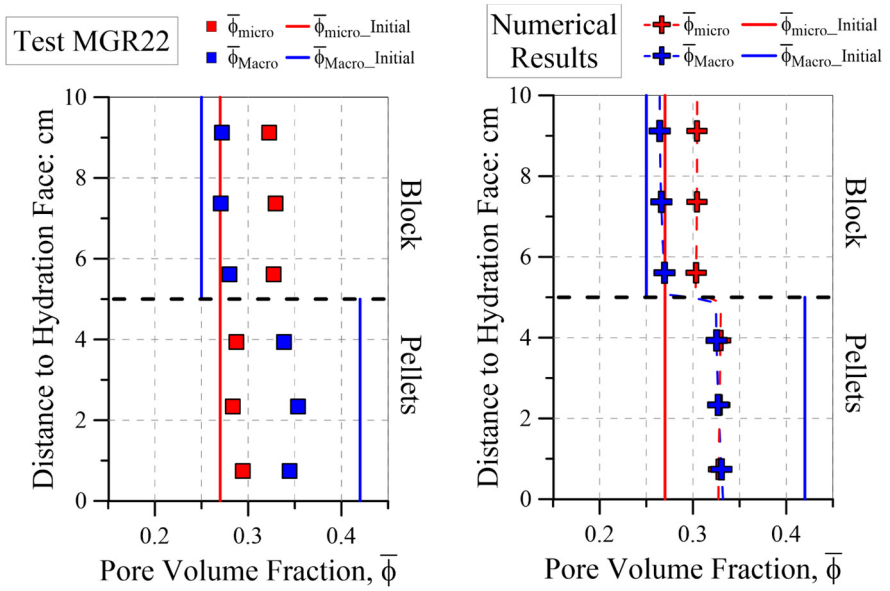

Figure 5-38. Pore volume fractions distribution in the homogenization test MGR22. Left: Experimental data test; Right: Numerical results.

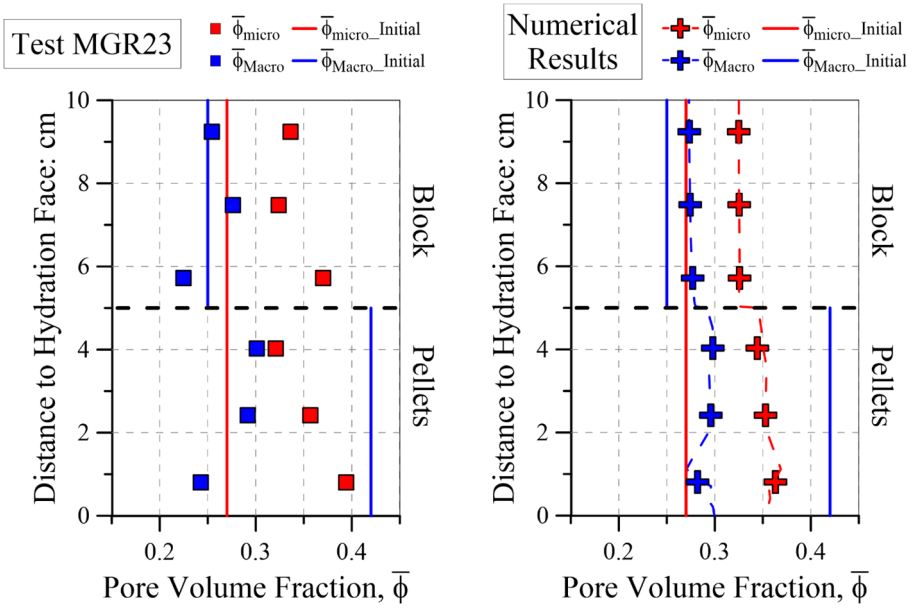

Figure 5-39. Pore volume fractions distribution in the homogenization test MGR23. Left: Experimental data test; Right: Numerical results.

The computed time evolution of micro and Macro pore volume fractions at two vertical points are shown in Figure 5-41 and Figure 5-42 for MGR22 and MGR23 models, respectively. Some remarks about these results are:

- The kinematic of pore volume fraction evolution obeys to the imposed hydration condition. The $\bar{\phi}_{micro}$ and $\bar{\phi}_{Macro}$ of the pellets mixture in the MGR23 modelling evolve faster than their counterparts in the MGR22 modelling, because the larger amount of water generated by the fast water infiltration at early stage.

- The Macro pore volume fraction, $\bar{\phi}_{Macro}$, of the bentonite block presents a similar trend in both homogenization tests. There is a small Macro-structural collapse followed by a macro pores increasing corresponding to the swelling deformation (i.e. pellets compression).

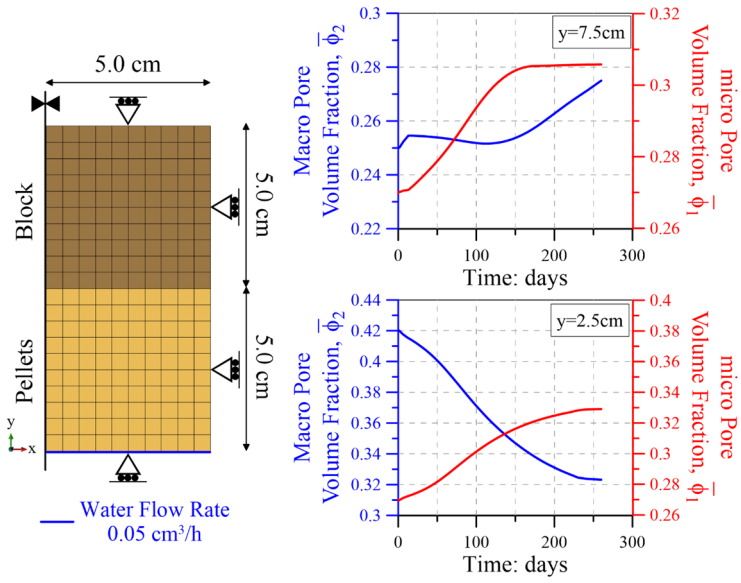

Figure 5-40. Computed evolution of Macro- and micro pore volume fractions two different points of the modelling MGR22.

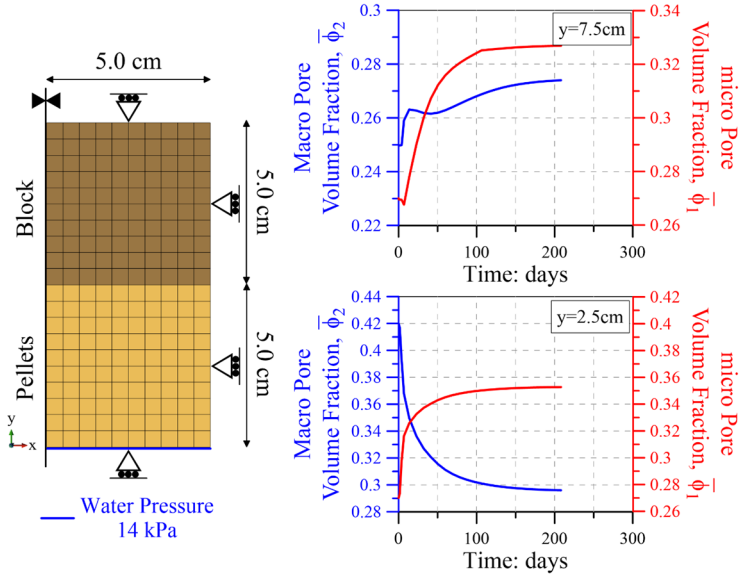

Figure 5-41. Computed evolution of Macro- and micro pore volume fractions two different points of the modelling MGR23.

The distribution and evolution of intrinsic permeability can be an additional measure of the homogenization of block-pellets specimens. Figure 5-42 shows the computed intrinsic permeability and the experimental dry density values. The computed permeability increase in the bentonite block is related with the lower dry density values. In contrast, strong permeability reduction in the pellets mixtures is in accordance with final denser states.

The permeability changes are larger in MGR23 than MGR22 modelling. Because, the vertical displacement of the contact between block and pellets is higher in MGR23 (Figure 5-43 and Figure 5-44). This differs to the measured final specimens heights (see Table 5-6).

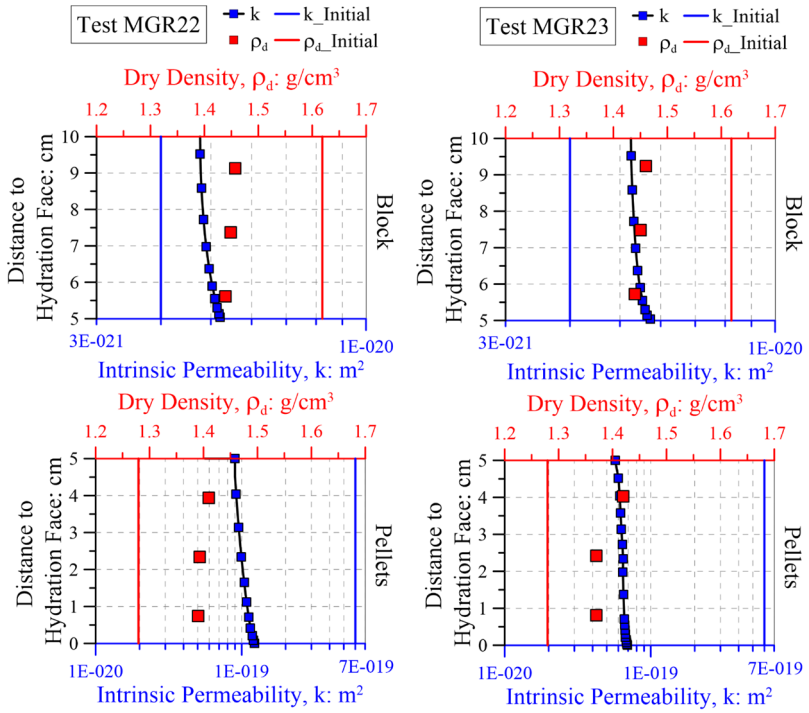

Figure 5-42. Distribution of dry density (experimental) and intrinsic permeability (computed) in homogenization tests. Left: MGR22 test; Right: MGR23 test.

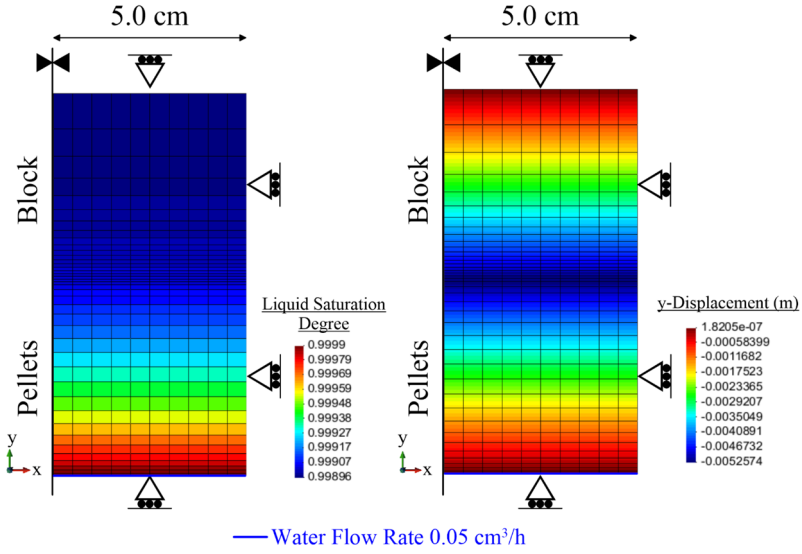

Figure 5-43. Final contours of liquid saturation degree (Left) and vertical displacement (Right) in the modelling MGR22.

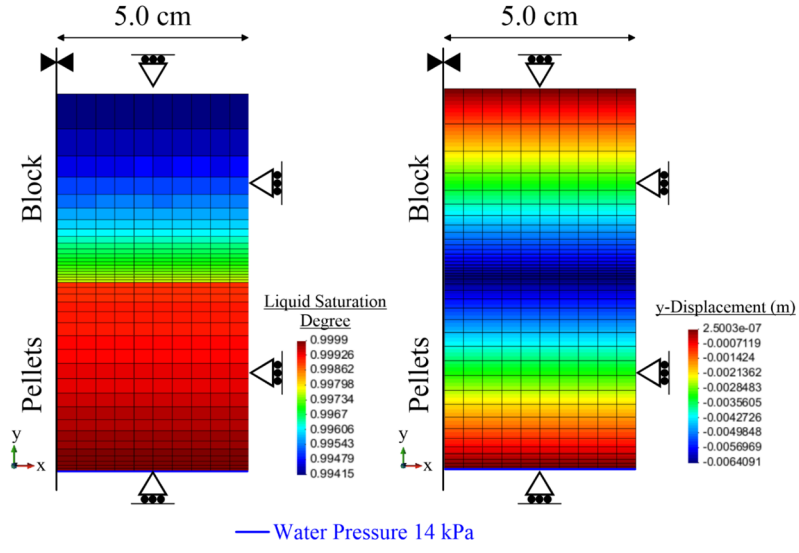

Figure 5-44. Final contours of liquid saturation degree (Left) and vertical displacement (Right) in the modelling MGR23.

5.5. Chapter conclusions

The validation of the hydro-mechanical double-structure formulation through numerical modelling has been tackled in a progressive manner. The increasing of problem scale and complexity allows a deeper understanding of HM response of bentonite based-materials.

Due to the lack of experimental evidence on the hydro-mechanical response of expansive clay aggregates, the comparison between the proposed phenomenological micro-structural model and a multiscale approach appears to be appropriated. The phenomenological model is composed by constitutive laws based on expected engineering behaviour (Chapter 3). In contrast, the upscaling formulation considers physical mechanisms through several scales (e.g. clay particle, clay clusters and clay aggregate). In spite of clear differences on model assumptions, they present similar capabilities to reproduce the fundamental features of clay aggregates.

The numerical modelling of generalized stress-paths (i.e. suction and loading) on compacted FEBEX bentonite provides interesting insights into the mechanisms underlying the clay response. Strain irreversibility, strain stress-path dependence and fabric evolution has been well reproduced by the double-structure model. The loading-collapse mechanism (LC) and the micro-Macro mechanical interaction plays a key role to reproduce them. The evolution of the Macro pore volume and micro-porosity (i.e. aggregates pore space) are obtained due to the rigorous pore space definition of this hydro-mechanical formulation.

Different configurations of bentonite-based materials for engineering barriers and seals have generated heterogeneous arrangements with complex fabric. The modelling of these materials with the double-structure approach is a quite challenging task.

- Assumptions on the fabric of compacted mixtures of bentonite powder and pellets have been required to reproduce their hydro-mechanical behaviour under a double-structure approach. The different model mechanisms (i.e. micro-Macro mass water transfer, structural mechanical interaction and loading-collapse) are required to reproduce the complex pattern of swelling pressure evolution.

- The hydro-mechanical analysis of the heterogeneity evolution of bentonite block-pellets specimens has been performed. The individual modelling of swelling pressure tests on bentonite block and pellets mixture gave important insights about material parameters and fabric changes to tackled the modelling of block-pellets samples. Two types of hydration condition were tested: restricted water access (slow infiltration test) and full water access (fast infiltration test). The numerical models reproduce the influence of hydration condition on the rate of the development of axial pressure and pore space evolution. The numerical simulation of fast infiltration tests on granular bentonite is not straightforward. Therefore, a non-equilibrated hydraulic state between micro- and Macro-structural levels was used to replicate the water distribution generated in early stage by this type of water infiltration.

5.6. References

Biot, M.A., Willis, D.G., 1957. The elastic coefficients of the theory of consolidation. J. Appl. Mech. 594–601.

Darde, B., Tang, A.M., Pereira, J.-M., Roux, J.-N., Dangla, P., Talandier, J., Vu, M.N., 2018. Hydro-mechanical behaviour of high-density bentonite pellet on partial hydration. Géotechnique Lett. 8, 330–335.

Gens, A., 2004. The role of geotechnical engineering for nuclear energy utilisation, in: Vanicek I. et Al., Editors. Proc. 13th European Conference on Soil Mechanics and Geotechnical Engineering, Vol. 3. Prague: CGtS. pp. 25–67.

Gens, A., Valleján, B., Sánchez, M., Imbert, C., Villar, M.V., Van Geet, M., 2011. Hydromechanical behaviour of a heterogeneous compacted soil: experimental observations and modelling. Géotechnique 61, 367–386.

Guimaraes, L.D.N., 2002. Analisis multi-componente no isotermo en medio poroso deformable no saturado (in spanish). PhD Thesis, Universitat Politecnica de Catalunya, Spain.

Guimaraes, L.D.N., Gens, A., Sanchez, M., Olivella, S., 2013. A chemo-mechanical constitutive model accounting for cation exchange in expansive clays. Geotechnique 63, 221–234.

Hoffmann, C., Alonso, E.E., Romero, E., 2007. Hydro-mechanical behaviour of bentonite pellet mixtures. Phys. Chem. Earth 32, 832–849.

Imbert, C., Villar, M.V., 2006. Hydro-mechanical response of a bentonite pellets/powder mixture upon infiltration. Appl. Clay Sci. 32, 197–209.

Khalili, N., 2019. Effective stress and energetics of unsaturated soils, in: InterPore2019. p. 329.

Lambe, T.. W., 1973. Predictions in soil engineering. Geotechnique 23, 149–202.

Lloret, A., Villar, M. V., Sánchez, M., Gens, A., Pintado, X., Alonso, E.E., 2003. Mechanical behaviour of heavily compacted bentonite under high suction changes. Géotechnique 53, 27–40.

Mainka, J., Moyne, C., 2017. A multi-scale approach to analyze the role of the disjoining pressure in the overall stiffness of expansive clays, in: Sixth Biot Conference on Poromechanics. pp. 1–10.

Mainka, J., Murad, M.A., Moyne, C., Lima, S.A., 2014. A modified effective stress principle for unsaturated swelling clays derived from microstructure. Vadose Zo. J. 13, 1–17.

Mašín, D., Khalili, N., 2016. Swelling phenomena and effective stress in compacted expansive clays. Can. Geotech. J. 53, 134–147.

Molinero-Guerra, A., Delage, P., Cui, Y.-J., Mokni, N., Tang, A.M.,

Aimedieu, P., Bernier, F., Bornert, M., 2019. Water-retention properties and microstructure changes of a bentonite pellet upon wetting/drying; application to radioactive waste disposal. Géotechnique 1-11 Submitted.

Molinero-Guerra, A., Mokni, N., Delage, P., Cui, Y.-J., Tang, A.M., Aimedieu, P., Bernier, F., Bornert, M., 2017. In-depth characterisation of a mixture composed of powder/pellets MX80 bentonite. Appl. Clay Sci. 135, 538–546.

Musso, G., Romero, E., Della Vecchia, G., 2013. Double-structure effects on the chemo-hydro-mechanical behaviour of a compacted active clay. Géotechnique 63, 206–220.

Navarro, V., Asensio, L., Yustres, A., Pintado, X., Alonso, J., 2013. Volumetric deformability and water mass exchange of bentonite aggregates. Eng. Geol. 166, 152–159.

Romero, E., Della Vecchia, G., Jommi, C., 2011. An insight into the water retention properties of compacted clayey soils. Géotechnique 61, 313–328.

Volckaert, G., Dereeper, B., Put, M., Ortiz, L., Gens, A., Vaunat, J., Villar, M.V., Martin, P.L., Imbert, C., Lassabatère, T., Mouche, E., Cany, F., 2000. A large-scale in situ demonstration test for repository sealing in an argillaceous host rock. RESEAL project - Phase I. EUR 19612 EN, European Commission, Brussels.

6. Chapter 6

General Conclusions and Future Developments

6.1. Concluding remarks

All chapters of the thesis have their own conclusions. Therefore, only the essential insights extracted from each chapter are presented here.

- **Chapter 2**

The hydro-mechanical responses of compacted bentonite-based materials result from the physicochemical phenomena occurring at mineral structure and their hierarchical structure. The governing equations obey these physical features.

- **Chapter 3**

A double-structure constitutive model has been proposed; it takes explicitly into account the two structural levels. Which is a closer representation of the fabric of compacted expansive clays. The distinction between the Macro-structure and micro-structure provides the opportunity to reproduce the dominant phenomena that affect the behaviour of each structure in a consistent way.

- **Chapter 4**

Both mechanical and hydraulic constitutive models were implemented in CODE_BRIGHT. The evaluation of the interaction mechanisms between the two structural levels and the qualitative response under well-controlled stress paths highlight a good performance of the model.

- **Chapter 5**

The hydro-mechanical double-structure was used to analyse laboratory and in-situ experimental tests. The increasing of problem scale and complexity allows a deeper understanding of HM response of bentonite based-materials.

6.2. Original contribution

The numerical modelling of expansive clays has been an enduring research activity in the geomechanics research group of the Polytechnic University of Catalonia (UPC). The double-structure framework developed by Gens and Alonso, (1992) has been an strong foundation for developing of a series of constitutive models (Alonso et al., 1999; Lloret

et al., 2003; Sanchez et al., 2005; Gens et al., 2011; Guimaraes et al., 2013). Thus, the aim of this research is a consequence of constant revision of these formulations and of the intensive research on bentonite-based materials. It has resulted in a hydro-mechanical double-structure formulation with a clear definition of the porous space and in further insights on the micro-Macro structural levels interactions.

The main original contributions of this PhD work include:

- A literature review of the hydro-mechanical behaviour of expansive clays. Micro-structural analysis (MIP and ESEM) shows an aggregated fabric. The interpretation of experimental responses according to the double-structure framework explains typical phenomena such as strain irreversibility, strain/stress-path dependency, a characteristic time evolution of the swelling pressure, among others. In-depth analysis of ESEM observations suggests the existence of unsaturated states in clay aggregates and time dependent mass water exchange between micro- and Macro-structural levels.

- The statement of the governing equations using the concepts of volume fractions. They are formulated for a more general case. The consideration of an unsaturated micro-structural level (clay aggregates) implies the proper account of the phases and species in each structural level. In-depth analysis of the balance equations reveals some structural levels interaction. The solid mass balance equation for a double-structure porous media shows that Macro-structural volumetric deformation is the result of micro-structural deformation and a relative volumetric strain generated by the interaction between both structural levels. Water mass balance equation is given for micro- and Macro-structural levels and the mass conservation in the water exchange entails a time-dependent mechanism towards a hydraulic equilibrium.

- A new Hydro-Mechanical double-structure model was developed including a multimodal water retention formulation taking into account the two porosity levels. The mechanical behaviour of the micro-structural and Macro-structural levels are described by a non-linear elasticity model and the Barcelona Basic Model, respectively.

The formulation is completed with the interaction between the two structural levels involving elastic coupling, Macro-micro mechanical interaction and Macro-micro hydraulic interaction.

- 3D discrete modelling is used to evaluate the global response under the swelling and shrinkage of the particles at different stress state. The mechanical interaction functions between the sphere particles and global arrangement can be properly reproduced by the continuum-based micro-Macro mechanical interactions. Accordingly, the slip between sphere particles, as the driving factor for geometrical reorganization, is comparable with the clay aggregates reorganization during hydro-mechanical processes.

- The implementation of the double-structural model in CODE-BRIGHT using a sub-stepping algorithm dealing with the different mechanisms. The micro water liquid pressure is updated as history variable (i.e. at the gauss points) and an averaging methodology is required to compute the water mass transfer with Macro water liquid pressure in the nodes.

- The numerical modelling and analysis of clay aggregate response, suction and loading paths on compacted FEBEX bentonite and oedometric swelling pressure tests on heterogeneous bentonite specimens.

6.3. Future developments

The model formulation and numerical modelling carried out in this thesis have enable a better understanding of the hydro-mechanical processes of bentonite-based materials under laboratory and field conditions. Nevertheless, several aspects require additional developments in order to solve open questions and expand knowledge. They are mainly related to additional model features and the ongoing large-scale simulations.

- The model formulation in terms of Bishop's effective stress and suction for both structural levels appears to be the next step. A priori, it is not a complex task. In fact, González, (2011) presented a Barcelona Basic Model using this constitutive stress. However, some theoretical aspects remains unsolved. Are the χ_{micro} and χ_{Macro}

independent? Are they equal? Do they evolve in the same way?. The work presented by Vaunat and Casini, (2017) can comtribute to clarify these questions.

- Further insights on micro-Macro mechanical interaction functions can be obtained from cycling deformation of spheres in 3D discrete modelling. The accumulation of swelling-shrinking cycles should converges to an elastic-like behaviour. In contrast to the continuum-based model, in which the evolution of preconsolidation stress (p_o) is easily assessed, the evolution of the stress ratio in discrete modelling is not totally clear.

- The multimodal WRC does not account explicitly for the water retention behaviour of bentonite-based materials under free swelling condition. The water content at a given suction is overestimated due to disregarding the void ratio increase. In this regard, the approach proposed by Dieudonne et al., (2017) can be followed.

- The double-structure approach has to evolve towards a coupled THMC formulation. The thermal (T) and chemical (C) are unquestionably relevant to the bentonite response in the nuclear waste disposal. The effect of temperature on this double-structure formulation is an ongoing research (Vasconcelos et al., 2019). In the other hand, Guimaraes et al., (2013) and Navarro et al., (2017) have established strong basis for adding chemical effects.

- The knowledge obtained from the numerical modelling of elementary- and laboratory-scale cases is the main basis to evaluate the hydro-mechanical bentonite response at field conditions. The sealing of access shafts and drifts prior to closure of a nuclear waste repository is a major concern. Therefore, the bentonite has been selected as a central component of seal structures (Figure 6-1).

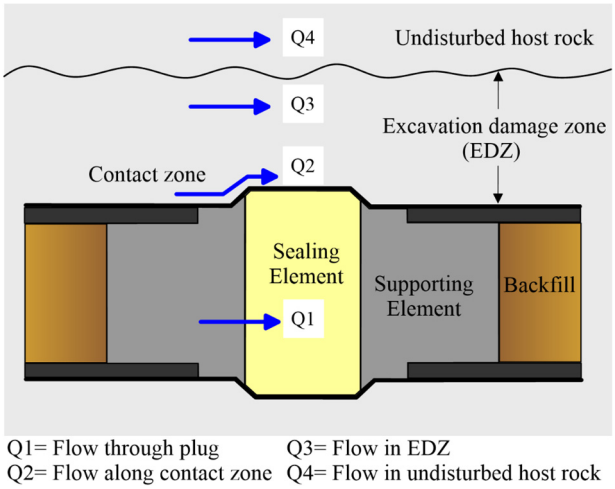

Figure 6-1. Scheme of a typical conceptual design of a seal of a horizontal access drift (modified from Gens, 2004).

The short- and long-term performance of these systems depends on the hydration condition and the interaction between the different components (i.e. host rock formation, concrete structures, bentonite core, filling materials, among others). Taking into account that CODE_BRIGHT include suitable constitutive models for the additional components of these structures, the numerical modelling of the following seal cases can be tackled with the formulation developed in this work:

- The in-situ NSC experiment that consist in the artificial hydration of a bentonite seal placed in an underground laboratory drift. The goal of this intensively instrumented test is evaluate the hydro-mechanical evolution of the expansive core and its interaction with the concrete retaining plugs and gallery walls (Figure 6-2).

- The numerical analysis of a sealing system design for a horizontal main gallery. The mimic of entire life of a deep repository impose modelling challenges in order to predict the long-term seal evolution. Here, the hydration source is the host rock formation (Figure 6-3).

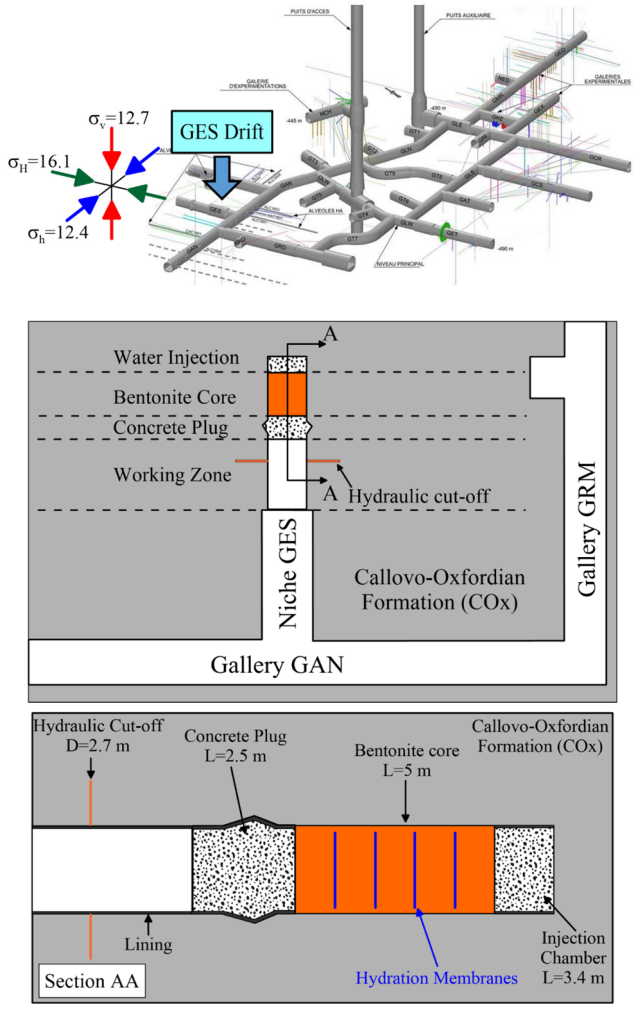

Figure 6-2. Location and configuration of the in-situ NSC experiment (ANDRA, 2015).

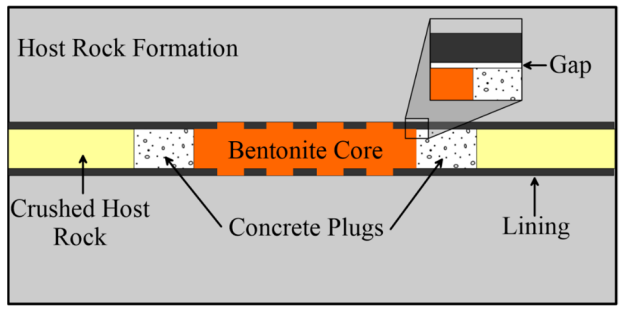

Figure 6-3. Configuration of a seal structure in a main horizontal gallery (ANDRA, 2011).

- According to their configuration, the seal structures can be modelled with an axisymmetric geometry around the axis of the drifts (Ruiz et al., 2018, 2017a, 2017b). However, an anisotropic pattern of Excavation Damage Zone (EDZ) in sedimentary argillaceous rock has been observed. In the Callovo-Oxfordian argillite, it depends on the drift orientation with respect to the horizontal stresses. Mánica et al., (2017) presented a constitutive model for argillaceous formation with the capability to reproduce asymmetrical plastic zone configurations, which is not able to reproduce through axisymmetric seal structure modelling. Taking into account the permeability increase in the damaged zones, anisotropic saturation and compression are expected in the bentonite core, retaining concrete plugs and fill. Therefore 3D modelling is required to reproduce precisely the radial and longitudinal response of the seal structure (Figure 6-4). This is a demanding computational task and the available parallel version of CODE-BRIGHT (DIT-UPC, 2018) should be used.

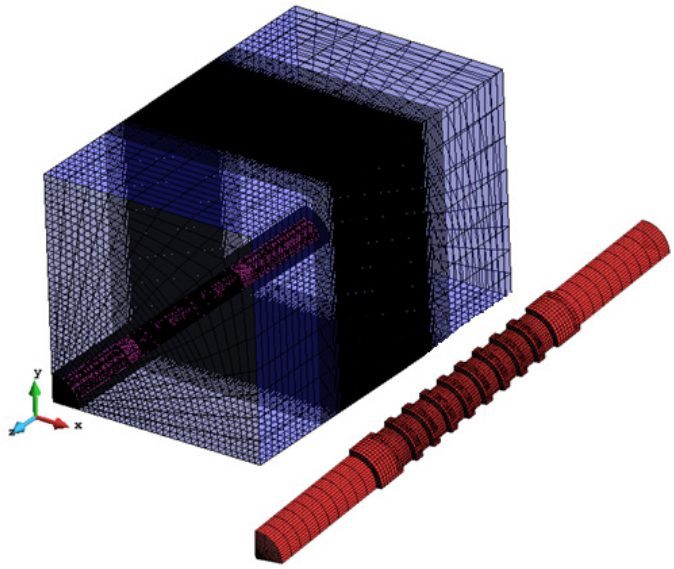

Figure 6-4. 3D finite element model of seal structure. More than 400.000 elements.

6.4. References

Alonso, E.E., Vaunat, J., Gens, A., 1999. Modelling the mechanical behaviour of expansive clays. Eng. Geol. 54, 173–183.

ANDRA, 2015. Expérimentat¡on NSC. Bilan des mesures et suivi de la phase d'hydratation. Report D.RP.AMFS.r5.0017. Châtenay-Malabry: ANDRA.

ANDRA, 2011. Evaluation du comportement THM des scellements du stockage CIGEO: ouvrages de liaison jour-fond, galeries et alvéoles MAVL. Report CCCAEAP110093. Châtenay-Malabry: ANDRA.

Dieudonne, A.-C., Della Vecchia, G., Charlier, R., 2017. Water retention model for compacted bentonites. Can. Geotech. J. 54, 915–925.

DIT-UPC, 2018. CODE_BRIGHT, a 3-D program for Thermo-Hydro-Mechanical analysis in geological media: User's guide, CIMNE, Barcelona.

Gens, A., 2004. The role of geotechnical engineering for nuclear energy utilisation, in: Vanicek I. et Al., Editors. Proc. 13th European Conference on Soil Mechanics and Geotechnical Engineering, Vol. 3. Prague: CGtS. pp. 25–67.

Gens, A., Alonso, E.E., 1992. A framework for the behaviour of unsaturated expansive clays. Can. Geotech. J. 29, 1013–1032.

Gens, A., Valleján, B., Sánchez, M., Imbert, C., Villar, M.V., Van Geet, M., 2011. Hydromechanical behaviour of a heterogeneous compacted soil: experimental observations and modelling. Géotechnique 61, 367–386.

González, N.A., 2011. Development of a family of constitutive models for geotechnical applications. PhD Thesis, Universitat Politecnica de Catalunya, Spain.

Guimaraes, L.D.N., Gens, A., Sanchez, M., Olivella, S., 2013. A chemo-mechanical constitutive model accounting for cation exchange in expansive clays. Geotechnique 63, 221–234.

Lloret, A., Villar, M. V., Sánchez, M., Gens, A., Pintado, X., Alonso, E.E., 2003. Mechanical behaviour of heavily compacted bentonite under high suction changes. Géotechnique 53, 27–40.

Mánica, M., Gens, A., Vaunat, J., Ruiz, D.F., 2017. A time-dependent anisotropic model for argillaceous rocks. Application to an underground excavation in Callovo-Oxfordian claystone. Comput. Geotech. 85, 341–350.

Navarro, V., Yustres, A., Asensio, L., De la Morena, G., González-Arteaga, J., Laurila, T., Pintado, X., 2017. Modelling of compacted bentonite swelling accounting for salinity effects. Eng. Geol. 223, 48–58.

Ruiz, D.F., Vaunat, J., Gens, A., Mánica, M., 2018. Hydro-mechanical modelling of an unsaturated seal structure, in: Proceedings of the

9th European Conference on Numerical Methods in Geotechnical Engineering (NUMGE 2018) Cardoso et Al (Eds). Porto, Portugal. pp. 757-764. Volume 1.

Ruiz, D.F., Vaunat, J., Gens, A., Mánica, M., 2017a. Analysis of the hydration of an unsaturated seal, in: Second Pan-American Conference on Unsaturated Soils, PanAm-UNSAT 2017. Dallas, USA. pp. 1–11.

Ruiz, D.F., Vaunat, J., Gens, A., Mánica, M., 2017b. Hydro-mechanical modelling of a gallery sealing over the entire life of a deep repository, in: 6th International Conference on Coupled THMC Processes in Geosystems, GeoProc 2017. París, France. pp. 120–121.

Sanchez, M., Gens, A., Guimarães, L., Olivella, S., 2005. A double structure generalized plasticity model for expansive materials. Int. J. Numer. Anal. Methods Geomech. 29, 751–787.

Vasconcelos, R.B., Gens, A., Ruiz, D.F., Villar, M.V., 2019. Modelling a heating-hydration bentonite-based column test using a double porosity approach, in: XV International Conference on Computational Plasticity Fundamentals and Applications (Eds E. Oñate, D.R.J. Owen, D. Peric, M. Chiumenti and E. de Souza Neto). Barcelona, Spain.

Vaunat, J., Casini, F., 2017. A procedure for the direct determination of Bishop's χ parameter from changes in pore size distribution. Geotechnique 67, 631–636.

Appendix A

Water Retention Curves for Compacted Expansive Clays

A.1. Introduction

The use of expansive clays for engineering purposes has led to different configurations of these kind of materials like: compacted bentonite powder, granular mixtures made of high-density pellets of bentonite, compacted mixtures of bentonite powder and pellets, compacted mixtures of sand and bentonite, among others. Generating a variety of clay structural arrangement with important implications on their hydraulic properties. The adoption of a double-porosity model appears to be suited to describe the heterogeneous nature of these materials.

This appendix presents the application of a multimodal water retention model, proposed in the Chapter 3, to reproduce experimental data from well-known expansive clays. Additional assumptions on the treatment of the structural arrangements are discussed.

A.2. Water retention curves for compacted expansive clays

As pointed out in Chapter 3, the multimodal water retention model for a double-structure material is given by:

$$S_e = \frac{Sr - Sr_{res}}{Sr_{max} - Sr_{res}} = w_1[WRC]_1 + w_2[WRC]_2 \qquad \text{(Eq. A-1)} \quad \text{Also (Eq. 3-14)}$$

where:

- S_e is the equivalent saturation degree of the double-structure material.
- Sr, Sr_{max} and Sr_{res} are the actual, the maximum and the residual saturation degree of the double-structure material, respectively.
- The subscripts 1 and 2 refer to the micro-structural level and the

Macro structural level, respectively.
- WRC is a Van Genuchten type water retention curve for each structural level. Can be used either a classical or modified versions (Eq. 3-15 and Eq. 3-16).
- w is the weighting parameter for each structural level. It relates the pore volume fraction of each level ($\bar{\phi}_1$ and $\bar{\phi}_2$) with the total porosity (ϕ) of the material ($w_1 = \bar{\phi}_1/\phi$ and $w_2 = \bar{\phi}_2/\phi$)

This hydraulic constitutive formulation is used to reproduce the water retention behaviour of the following expansive materials:

- Compacted Boom clay powder (Romero et al., 2011).
- Compacted MX-80 bentonite powder (Seiphoori et al., 2014).
- Granular mixtures of FEBEX bentonite. (Alonso et al., 2011; Hoffmann et al., 2007).
- Compacted mixture of MX-80 bentonite powder and pellets (Molinero-Guerra et al., 2019b, 2019a, 2017).

Compacted specimens of Boom clay powder and MX-80 bentonite powder present a dominant aggregated fabric (i.e. two basic pore levels). On the other hand, the pore size density function of the bentonite mixtures contains more than two characteristic pore sizes. Although the proposed multimodal water retention curve can handle several pore families, the hydro-mechanical double-structure formulation only considers the interactions between the two representative structural levels. Therefore, it is required additional assumptions on the fabric of bentonite mixtures.

Different compaction states of these expansive clays offer the opportunity to evaluate the effect of initial dry density on the water retention behaviour. As pointed out in Chapter 2, the compaction efforts are essentially related to changes in the inter-aggregate pore volume ($\bar{\phi}_2$) and the pore-size distribution at this level.

In Table A-1, the pore space descriptors and the constitutive parameters for the double WRC of the expansive materials evaluated are listed.

Table A-1. Input data for water retention curves.

Material	ρ_d: Mg/m^3	ρ_{d_Pellet}: Mg/m^3	e	ϕ	$\bar{\phi}_1$	$\bar{\phi}_2$	w_1	w_2	Po_1	Po_2	λ_1	λ_2	Sr_1	Sr_2
Boom clay			0.65	0.49	0.28	0.21	0.56	0.44	8	0.2	0.4	0.4	0	0
			0.93	0.63		0.35	0.44	0.56		0.07				
MX-80	1.55		0.83	0.58	0.23	0.35	0.4	0.6	70	8	0.8	0.6	0.3	0
	1.65		0.66	0.5		0.27	0.47	0.53		15				
	1.79		0.53	0.42		0.19	0.55	0.45		40				
FEBEX granular mixture	1.3	1.9	1.08	0.66	0.22	0.44	0.33	0.67	110	0.4	0.8	0.28	0	0
	1.5		0.8	0.56		0.34	0.39	0.61		1				
MX-80 granular mixture	1.49	2.12	0.45	0.37	0.21	0.16	0.58	0.42	45	2.5	0.45	0.75	0	0

Subscript 1: micro-structure, **Subscript 2:** Macro-structure e: Void Ratio, ϕ: Total porosity, $\bar{\phi}$: pore volume fraction, w: weight factor, **Po**: Air entry value, λ: Shape function for retention curve, **Sr**: Residual saturation.

Material	ρ_d: Mg/m^3	ρ_{d_Pellet}: Mg/m^3	e	ϕ	$\bar{\phi}_1$	$\bar{\phi}_{1\to2}$	w_1	$w_{1\to2}$	Po_1	$Po_{1\to2}$	λ_1	$\lambda_{1\to2}$	Sr_1	$Sr_{1\to2}$
MX-80 bentonite pellet	2.12	-	0.34	0.29	0.1	0.19	0.35	0.65	45	4.5	0.45	0.7	0	0

Subscript 1: micro-structure, **Subscript 1→2**: meso-structure

A.2.1. Water retention curves for compacted Boom Clay

The retention curves were obtained on artificially prepared (dry side statically compacted) powder obtained from natural Boom clay (Mol, Belgium). This moderately swelling clay (20-30% kaolinite, 20-30 illite, 10-20% smectite) has a liquid limit of w_L=56%, a plastic limit of w_P=29% and 50% of particles < 2mm (Romero et al., 1999).

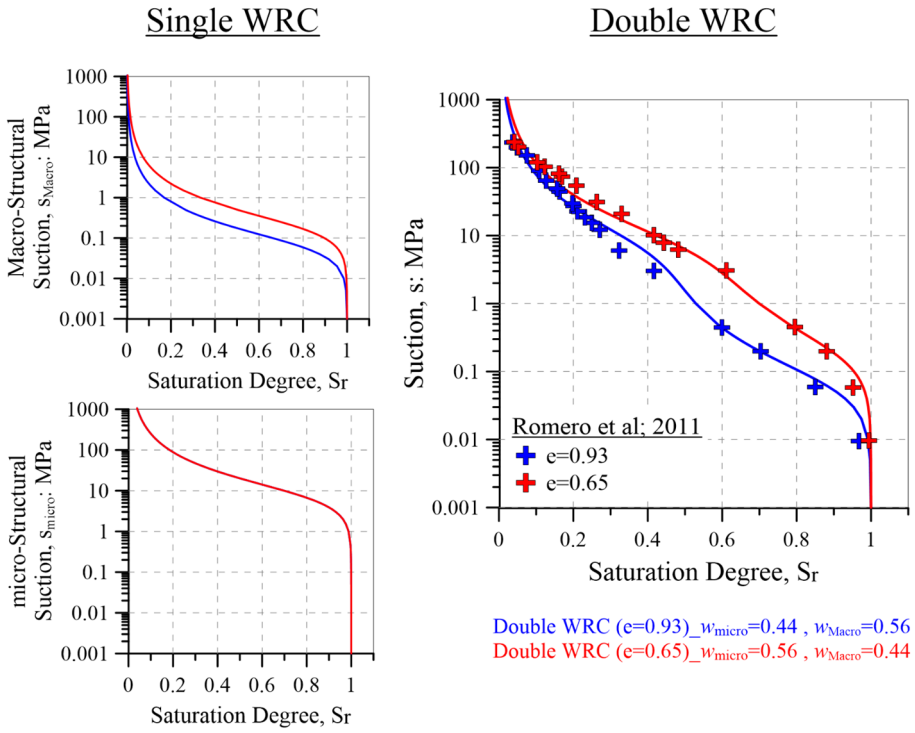

Figure A-1. Water retention curves for compacted Boom clay (Experimental data from Romero et al., 2011).

Figure A-1 shows the wetting WRC for two main soil packings of clay aggregates: high porosity with collapsible structure (γ_d=13.7 kN/m^3 and e=0.93) and low porosity structure with swelling tendency (γ_d=13.7 kN/m^3 and e=0.65). Axis translation technique, in constant volume condition, was used to obtain low suction data. Furthermore, the high suction values are measured with the vapour equilibrium methodology under free swelling.

The Van Genuchten micro-WRC is the same for both specimen, reflecting the water retention behaviour of the clay aggregates. In

contrast, the air entry value of the Macro-WRC is affected by the compaction level (See Table A-1 and Table A-2). MIP data offers quantitative information on the micro- and Macro-pore volume fractions. Therefore, the weighting parameter for each structural level and the multimodal WRC are easily assessed (Figure A-1). Good agreement with experimental data can be noted.

A.2.2. Water retention curves for compacted MX-80 bentonite

Seiphoori et al., 2014 investigated the water retention behaviour of compacted MX-80 (Wyoming) granular bentonite. The tested bentonite contains 85% sodium (Na)-smectite clay, which reflects the well-known high swelling capacity of the material.

Total suction at each hydration stage was measured by using a dew point potentiometer with a microcell to guarantee constant volume condition for specimens prepared at different dry densities (i.e. different void ratios) (Figure A-2).

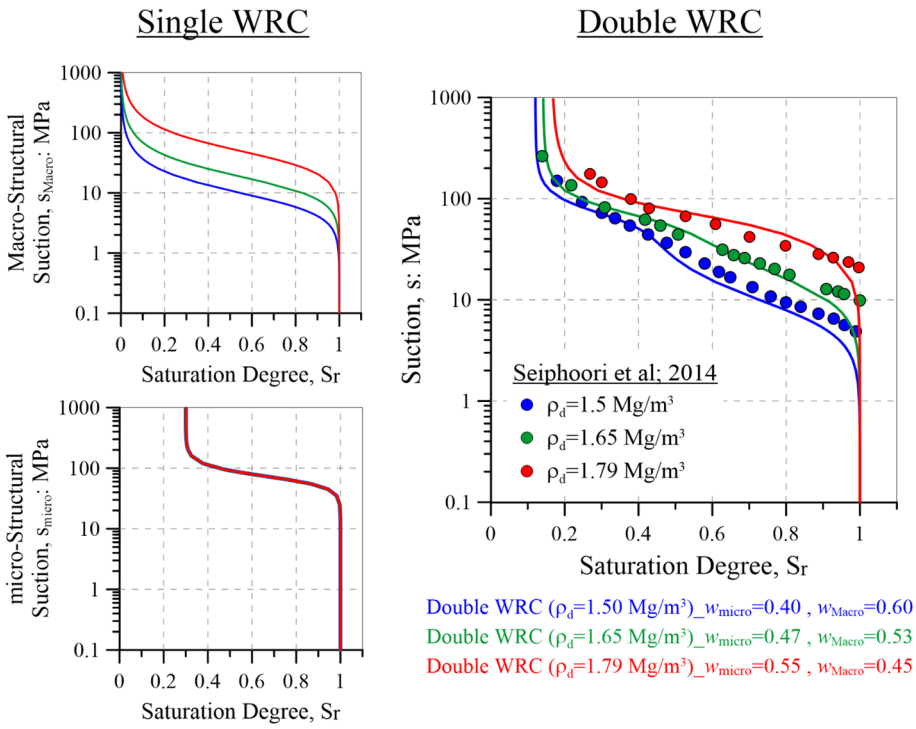

Figure A-2. Water retention curves for compacted MX-80 bentonite (Experimental data from Seiphoori et al., 2014).

Again, the micro-WRC is common for the three specimens and the Macro-structure air entry value evolves with the compaction level (Table A-1 and Table A-2). The computation of the multimodal WRC for the bentonite specimens reveals that denser states tends to mono-modal behaviour. This is due to the increasing of micro-pore volume fraction (hence, micro weighting parameter) (Figure A-2). The minor role of the Macro-structural level in heavily compacted bentonites does not imply the evolution towards single-structure medium. This transition from a double-structured to a single-structured fabric, by a permanent change of the microfabric, is found mainly in wetting-drying cycles.

A.2.3. Water retention curves for compacted granular mixtures of FEBEX bentonite

This water retention modelling is performed on compacted granular mixtures of FEBEX bentonite. In these types of mixtures, it is also possible to distinguish two basic structural levels:

- The Macro-structure corresponds to the granular skeleton of the clay mixture. It is composed of the arrangement of the clay pellets and the Macro-pores between them.
- The high-density pellets and the small pores inside them corresponds to the micro-structure.

Obviously, there are more pore levels in the analysis—for example, one could consider that, inside the clay pellets, there are clay aggregates, with their inter-aggregate and intra-aggregate pore space. In this case, three different types of pores can be distinguished: 1) the inter-pellet pores (i.e., the big macro-pores between pellets); 2) the inter-aggregate pores (i.e., pores between clay aggregates inside the pellets); and 3) the intra-aggregates pores (i.e., the pores inside the clay aggregates). However only two basic structural levels were considered, the pores types 2 and 3 are associated with the micro-structure.

The saturation degree-suction relationships were derived from wetting at constant volume tests performed on samples at dry density values of 1.3 and 1.5 Mg/m3 (Figure A-3). WRC of a bentonite pellet in free swelling condition is also available.

The experimental retention curves are well reproduced under the same reasoning used for the above compacted materials. It is also interesting to note that the retention model for micro-structural level does not fit with the experimental data from the bentonite pellet. A higher air entry value is required to reproduce the bentonite mixture behaviour. A plausible explanation is a minor hydraulic influence of a meso-scale pore family (i.e. inter-aggregate pores) in the water retention behaviour of the bentonite mixtures in a constant volume condition. Further ideas on the retention behaviour of bentonite pellets are given in the analysis of the next material.

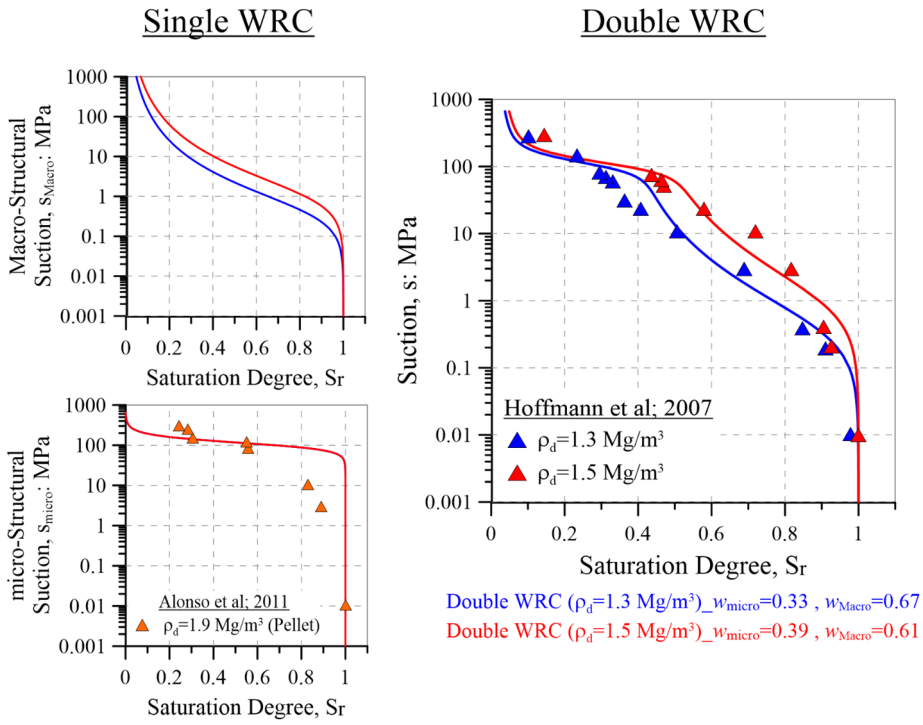

Figure A-3. Water retention curves for compacted granular mixtures of FEBEX bentonite (Experimental data from Alonso et al., 2011 and Hoffmann et al., 2007)

A closing remark on the effect of void ratio (compaction level) on the water retention behaviour is the phenomenological relation between the Macro air entry value and the Macro pore volume fraction. As pointed by Dieudonne et al., (2017), when the density increases, not only is the total volume of the voids reduced, but also the size of the Macro pores

decreases. Accordingly, Pores can sustain high suctions before emptying (Chapter 3). Table A-2 and Figure A-4 show the fitting of experimental data with a power law (Eq. 3-18).

Table A-2. Air entry values for Macro-structural level.

Material	Air entry value, P_{o_2}: MPa	Macro pore volume fraction, $\bar{\phi}_2$	Fitting parameters	
			A	B
Boom clay (Romero et al., 2011)	0.2	0.21	0.097	2.049
	0.07	0.35		
MX-80 (Seiphoori et al., 2014)	40.0	0.19	0.691	2.822
	15.0	0.26		
	8.0	0.34		
FEBEX granular mixture (Hoffmann et al., 2007)	1.0	0.34	0.342	3.501
	0.4	0.44		

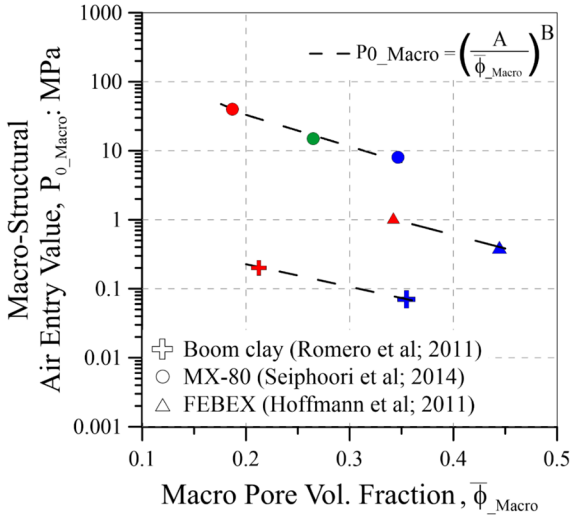

Figure A-4. Evolution of Macro-structure air entry values of compacted clays as function of Macro pore volume fraction, $\bar{\phi}_2$.

A.2.4. Water retention curve for compacted pellet/powder MX-80 bentonite mixture

This type of bentonite mixture has a complex fabric. Therefore, additional assumptions are required to fit its water retention behaviour with a double WRC model. Gens et al., (2011) pointed that the Macro-

structure refers to the large-scale arrangement of soil particle aggregates and the relatively large pores between them. It is expected that, initially, most of the Macro-structural pores belong to the bentonite powder. Accordingly, the micro and Macro pore volumes fractions are computed (Table A-1).

The experimental WRC of a single pellets (in free swelling condition) and the pellets/powder bentonite mixture is shown in Figure A-5. Similarly to the pellets mixture (Section A.2.3.), a satisfactory agreement with the bentonite mixture is reached, but a higher micro air entry value is required.

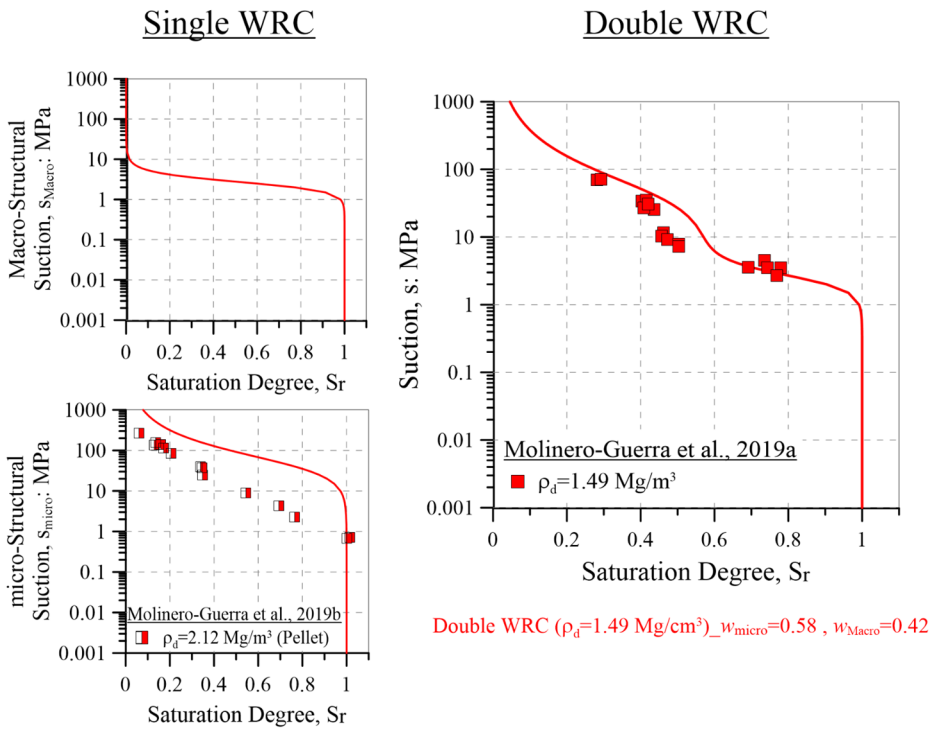

Figure A-5. Water retention curve for a compacted pellet/powder MX-80 bentonite mixture (Experimental data from Molinero-Guerra et al., 2019b, 2019a, 2017).

Important insights about the water retention behaviour of a bentonite pellet can be obtained from its modelling with a multimodal WRC. The good fitting of experimental data indicates that the bentonite pellet is a double-structure medium (Figure A-6). It is important to stress here that

micro WRC of the bentonite mixture correspond to the micro WRC used for the pellet. They reproduce the retention behaviour of the clay aggregates. Demonstrating the minor role of the meso-scale pores in the overall hydraulic behaviour of the pellets/powder mixture.

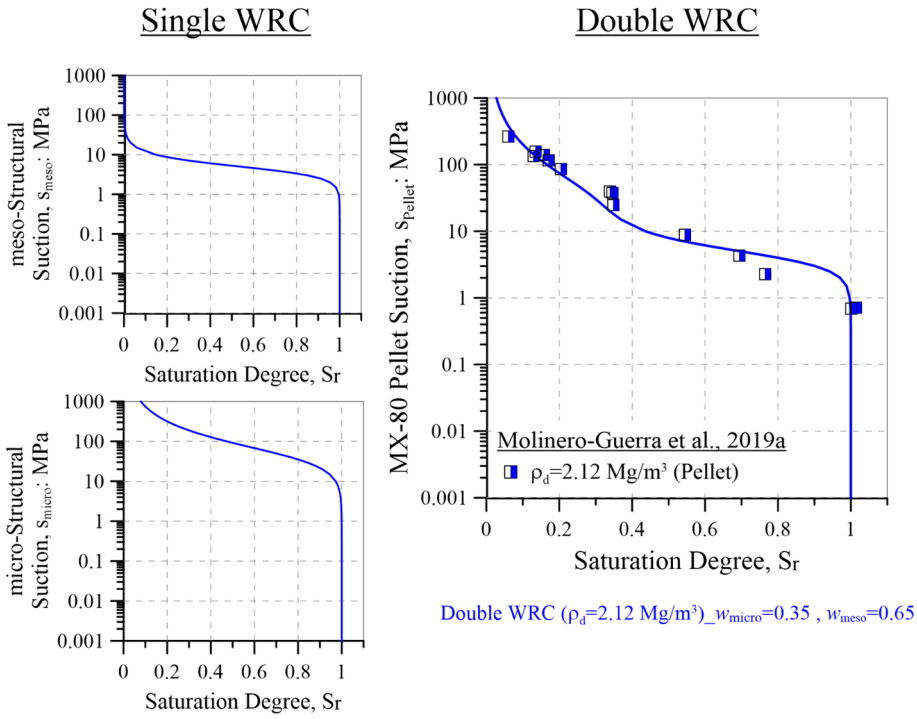

Figure A-6. Water retention curve for a MX-80 bentonite pellet (Experimental data from Molinero-Guerra et al., 2019b).

The difference between the micro WRC and the experimental data of bentonite pellets relies on the effect of volume constrain (Figure A-3 and Figure A-5). Dieudonne et al., (2017) shown that, for a given suction, the quantity of water stored under free swelling condition is greater than it is under prevented swelling. Figure A-7 illustrates the structural evolution of a MX-80 bentonite pellet upon wetting and free swelling condition. Suction changes yield significant swelling (in the order of several tens, even hundreds of percent of the initial volume) resulting in important changes of dry density.

In spite of the constrain volume of the pellets/powder bentonite mixture, the volume condition of pellets is related to the compaction level of the

mixture. The hydraulic relevance of the meso-scale pore family may increase in low compacted states.

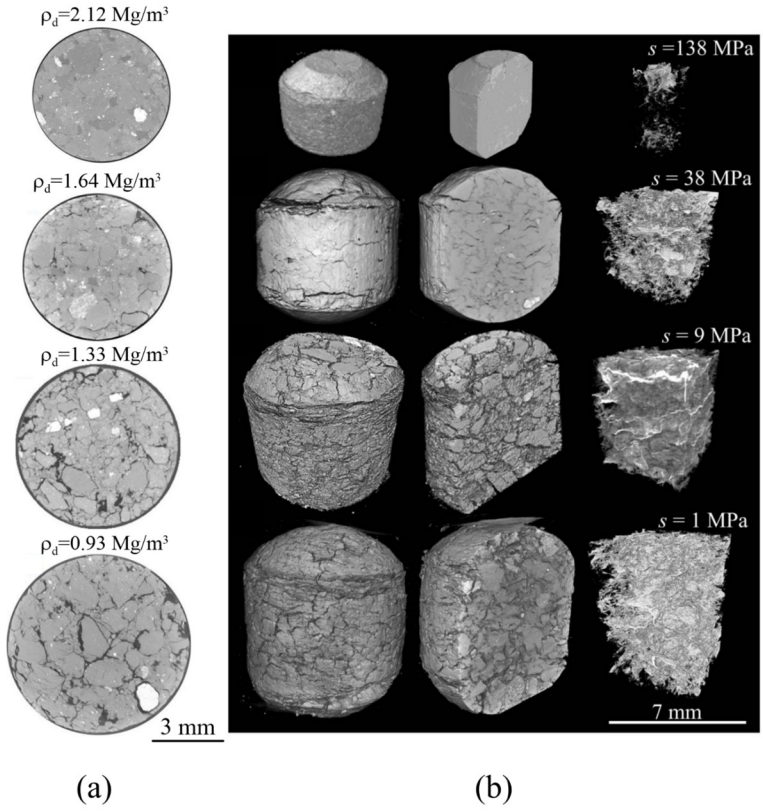

Figure A-7. Microstructure change of a MX-80 bentonite pellet upon wetting. a) X-ray computed microtomography (μ-CT) observations – horizontal section; b) 3D reconstruction image and network of cracks. (Molinero-Guerra et al., 2019b).

A.3. Conclusions

- The hydraulic constitutive model for double-structure formulation was used to reproduce the water retention behaviour of several compacted expansive materials.

- The main trends of behaviour where captured. Assumptions on the fabric of expansive clays with more than two pore families are required.

- The model does not take explicitly the effects of volume constrain. The consideration of bentonite behaviour under both confined and unconfined conditions is desirable for engineering purposes.

A.4. References

Alonso, E.E., Hoffmann, C., Romero, E., 2011. Hydromechanical behaviour of compacted granular expansive mixtures : experimental and constitutive study. Geotechnique 329–344.

Dieudonne, A.-C., Della Vecchia, G., Charlier, R., 2017. Water retention model for compacted bentonites. Can. Geotech. J. 54, 915–925.

Gens, A., Valleján, B., Sánchez, M., Imbert, C., Villar, M.V., Van Geet, M., 2011. Hydromechanical behaviour of a heterogeneous compacted soil: experimental observations and modelling. Géotechnique 61, 367–386.

Hoffmann, C., Alonso, E.E., Romero, E., 2007. Hydro-mechanical behaviour of bentonite pellet mixtures. Phys. Chem. Earth 32, 832–849.

Molinero-Guerra, A., Cui, Y.-J., He, Y., Delage, P., Mokni, N., Tang, A.-M., Aimedieu, P., Bornert, M., Bernier, F., 2019a. Characterization of water retention, compressibility and swelling properties of a pellet/powder bentonite mixture. Eng. Geol. 248, 14–21.

Molinero-Guerra, A., Delage, P., Cui, Y.-J., Mokni, N., Tang, A.M., Aimedieu, P., Bernier, F., Bornert, M., 2019b. Water-retention properties and microstructure changes of a bentonite pellet upon wetting/drying; application to radioactive waste disposal. Géotechnique 1-11 Submitted.

Molinero-Guerra, A., Mokni, N., Delage, P., Cui, Y.-J., Tang, A.M., Aimedieu, P., Bernier, F., Bornert, M., 2017. In-depth characterisation of a mixture composed of powder/pellets MX80 bentonite. Appl. Clay Sci. 135, 538–546.

Romero, E., Della Vecchia, G., Jommi, C., 2011. An insight into the water retention properties of compacted clayey soils. Géotechnique 61, 313–328.

Romero, E., Gens, A., Lloret, A., 1999. Water permeability, water retention and microstrucutre of unsaturated compacted boom clay. Eng. Geol. 54, 117–127.

Seiphoori, A., Ferrari, A., Laloui, L., 2014. Water retention behaviour and microstructural evolution of MX-80 bentonite during wetting and drying cycles. Geotechnique 64, 721–734.

Appendix B

Macro-micro Mechanical Interaction through Discrete Element Modelling

B.1. Introduction

The electro-chemical-mechanical phenomena occurring at clay aggregates (micro-structural level) are the root of the expansive nature of bentonite. However, the implication of these deformations on the aggregates arrangement (macro-structural level) is the core of the overall mechanical response. The occurrence of volumetric collapse as a function of compaction level and the subsequent progressive swelling are coming from this coupling mechanism.

The earliest double-structure expansive framework (Gens and Alonso, 1992) formulated the Macro-micro mechanical interaction as empirical laws based on the interpretation of physical phenomena and elastoplastic framework. Since the first mathematical formulation of the double-structural constitutive model (Alonso et al., 1999), exponential expressions have been used with a successful modelling results (see Charter 3).

The experimental evaluation of the mechanical interaction between both structural levels is not yet possible. Romero and Simms, (2008) correlates qualitatively the aggregates deformation with the global sample deformation, however, the stress state at both structural levels are uncontrolled (Figure B-1).

Discrete element modelling is an appealing numerical tool to evaluate the response of the system composed by expansive particles. This appendix presents a discrete modelling in which the behaviour of expansive

particles and global system provides new insights into the physical sources of their mechanical interaction.

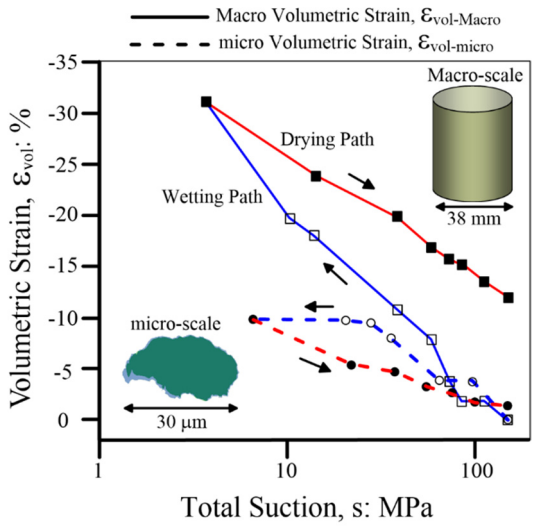

Figure B-1. (Also Figure 2-8) Volume change response along wetting-drying cycle at micro- and macro-scale. Volume changes at micro-structural level are tracking by ESEM observations (modified from Romero and Simms, 2008).

B.2. Discrete element modelling applied to expansive clays

The discrete element modelling is widely used in geomechanics. As an powerful tool, it allows a look inside the granular materials and the development of an understanding of the quantitative information on the material response.

The scale of clay particles and the nature of the inter-particle forces (surface interaction forces) have restricted the use of discrete element modelling on clays. Yao and Anandarajah, (2003) modelled a micrometrical 3D arrangement composed by platy particles which accounts the double-layer repulsive force, the van der Waals attractive force and the mechanical force. Aggregation phenomena and the global response against one-dimensional compression are well reproduced. The molecular-level modelling technique was used by Ahmed and Abduljauwad, (2017) to study the the processes and interactions occurring at the nano scale in the natural and compacted fabrics of the expansive soils (e.g. cation exchange capacity, moisture content,

exchangeable cations, interaction of clay minerals with non-clay minerals, among others)

Due to the complex clay particles interactions, it is convenient to analyse the behaviour of expansive clays from a macroscopic point of view. It means the computation of the interactions between expansive particles that emulate some physical entity (e.g. clay aggregates or bentonite pellets).

Darde et al., (2017) tackled the swelling behaviour of a bentonite powder/pellets mixture with an arrangement of swelling particles. In order to reproduce the stiffness decrease during humidification, the elastic modulus is progressively reduced according to experimental program realized on bentonite pellets (Darde et al., 2018).

As remarks O'Sullivan, (2011a), one of the purposes of DEM simulations is the development of constitutive models for continuum-based numerical analysis. In fact, this is the philosophy of the appendix. The main objective of the incoming simulations is evaluate the physical roots behind the mechanical interaction of structural levels in expansive clays.

B.2.1. Macro-micro mechanical interaction through discrete element modelling

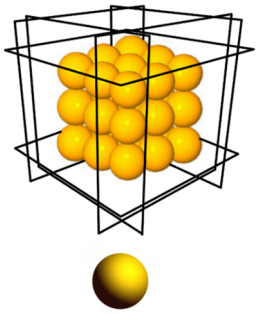

Figure B-2. Sketch of the expansive clays as discrete arrangement.

The general idea is to analyse the global response of a particulate system composed by expansive spheres at different stress states. The exact reproduction of an expansive clay with discrete elements is beyond the scope of this numerical work. Therefore, there is a similarity between the

expansive spheres and clay aggregates but they differ in dimensions by several order of magnitude (Figure B-2).

The modelling strategy is given by the following steps (Figure B-3):

a. The 3D DEM sample generation. According to the continuum-based formulation, a wide range of stress state levels is required (see Chapter 3).
b. Swelling and shrinkage of the spheres. The mechanical interaction mechanisms and the strains irreversibility as a function of stress state can be analysed

The expansive model was implemented on the PFC3D code (Itasca, 2017), which is used for all simulations.

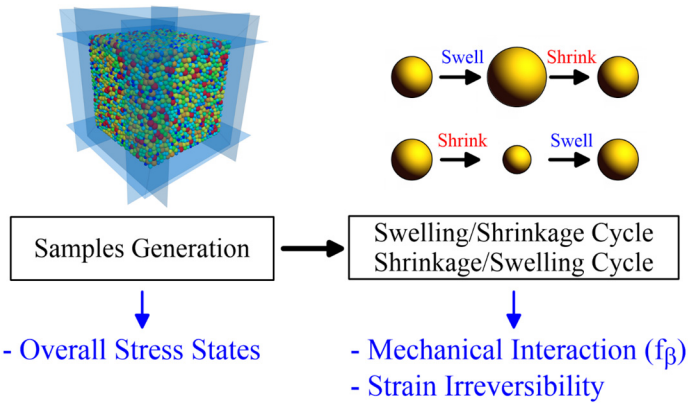

Figure B-3. Discrete modelling strategy.

B.2.1.1. DEM samples generation

In a DEM analysis a packing density and a stress level for the system under consideration cannot simply be specified as an input requirement. Rather a sample must be explicitly created and it must be in a state of equilibrium under the prescribed stress level (O'Sullivan, 2011b).

A cubic volume was filled with particles, using the ball distribution method to obtain a representative volumetric element (REV). The specimen boundaries were defined using frictionless 'wall' elements, which ensure that principal axes of stress and strain are coincident with the

cube axes. Gravity was set to zero. The grain size distribution of the specimen is shown in the Figure B-4.

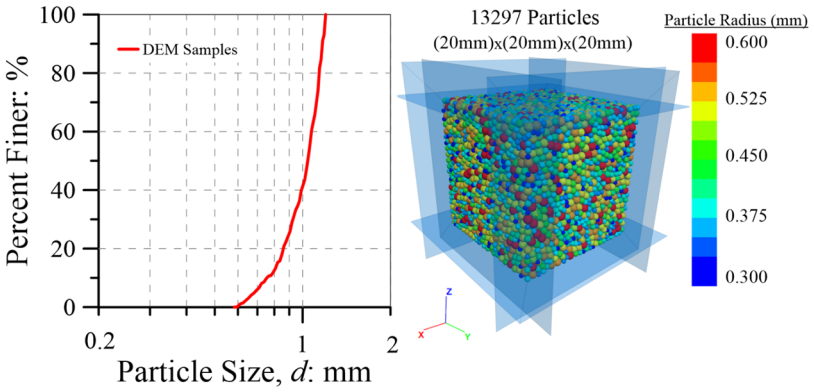

Figure B-4. Grain size distribution of the discrete specimen.

The samples preparation is performed in the following manner:

- An initial sample generated at mean stress of 1000 kPa. The artificial conditions of non-friction between spheres and free rotation are used to obtain a compacted specimen.

- Subsequent samples are generated releasing the stress from the above sample and taking into account realistic contact laws (Table B-1, Eq. B-1 and Eq. B-2). Here, friction between particles and fixed rotation are applied. There is not experimental evidence of clay aggregates rotations during expansive clay deformation.

The samples porosity as a function of stress state is presented in the Table B-2 and Figure B-5.

Table B-1. Contacts law between particles

	Parameter	Value
Friction *Coulomb Law*	φ (°)	25
Stiffness *Linear model-Deformability method*	E*(kPa)	1e8
	k*	1
	Damping ratio	0.7

$k_n = AE^*/L$ (Eq. B-1)

$k_s = k_n/k^*$ (Eq. B-2)

where:

- k_n and k_s are the normal and tangential stiffness respectively.
- A and L are contact particles dimensions (see Itasca, 2017).

Table B-2. Porosity and degree of compacnes at different stress levels.

Mean Stress, P (kPa)	Porosity (%)	Degree of Compactness P/P_{Max}
10	31.4	0.01
100	31.8	0.1
200	32.2	0.2
400	32.9	0.4
600	33.8	0.6
800	34.5	0.8
1000	35.6	1

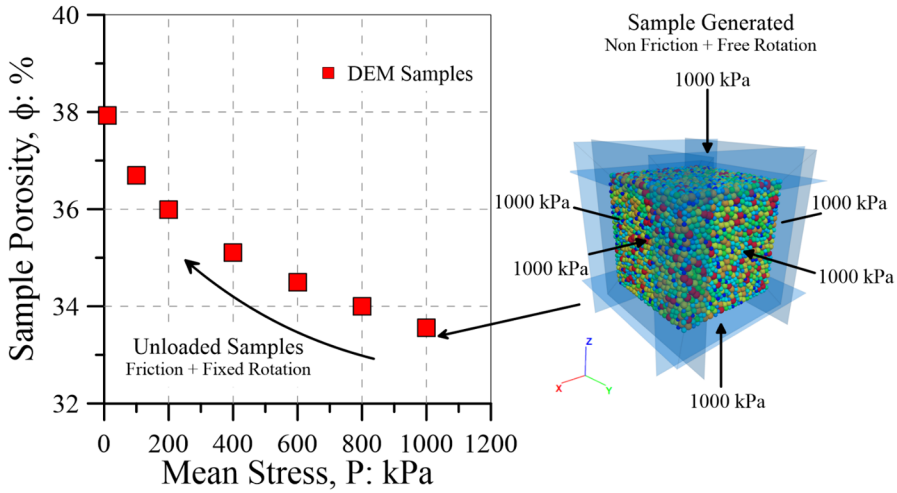

Figure B-5. Numerical procedure for different stress state at discrete samples.

B.2.1.2. Swelling and shrinkage of the spheres particles

From the different stress levels, swelling/shrinkage and shrinkage/swelling cycles are applied on the spheres particles. These actions are comparable with the wetting and drying of clay aggregates.

The particle radius changes linearly until 15 %, which means a volumetric particle strain of 32.25 % (Figure B-6). The experimental volumetric strain of a clay aggregate shows a hysteretic behaviour due to their porous nature (Figure B-1). The effects of hysteretic radius changes might be investigated.

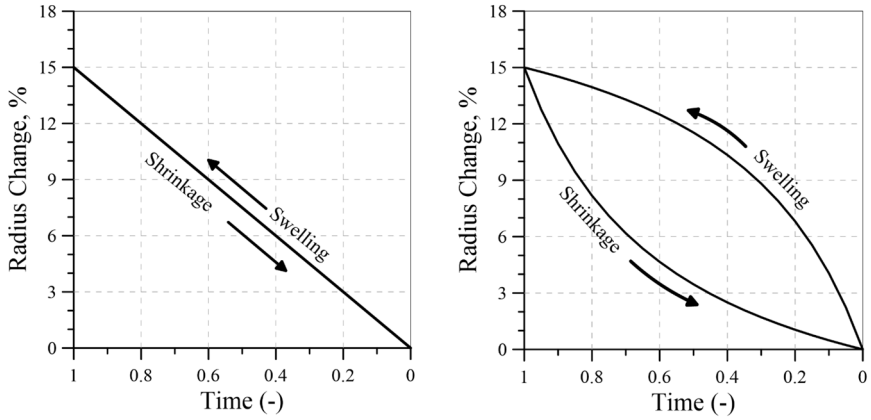

Figure B-6. Radius change cycle for spherical particles. Left: linear behaviour; Right: hysteretic behaviour (from Romero and Simms, 2008).

The volumetric strain for all samples is plotted in Figure B-7. The flat parts are due to the equilibration between wall boundaries and particles deformations. A remarkable outcome is the influence of the stress state level on the magnitude of samples swelling and shrinkage and the remained deformation after both cycles. This is in agreement with the constitutive double-structure formulation (see Chapter 3).

The numerical techniques in DEM can be divided in two categories: i) hard spheres models and ii) soft spheres models. The particles contact in the first category is binary-type, therefore it is mainly used in collision modelling. There is a prevalence of soft-sphere approaches in geomechanics O'Sullivan, (2011a). In the soft-sphere approach, a small amount of overlap is allowed at the contact points, and this overlap can be considered analogous to the deformation that occurs at the contacts among real soil particles. The magnitude of this overlap is related to the interparticle contact force, discussed previously.

Owing the high values of elastic stiffness the elastic overlapping between particles can be consider negligible. Thereby, the frictional slip (Coulomb

type) between particles is the main deformation mechanism at this strain level. This is comparable with the continuum-based formulation in which the Macro-micro elastic coupling is given under constant structural arrangement and small-strains (see Chapter 3).

The mechanical interaction functions between the particles and samples can be computed as follow:

$$f_{\beta}\_\text{microContraction} = \left.\frac{\text{Sample Vol Strain}}{\text{Sphere Vol Strain}}\right|_{\text{Sphere Shrinkage}} \quad \text{(Eq. B-3)}$$

$$f_{\beta}\_\text{microSwelling} = \left.\frac{\text{Sample Vol Strain}}{\text{Sphere Vol Strain}}\right|_{\text{Sphere Swelling}} \quad \text{(Eq. B-4)}$$

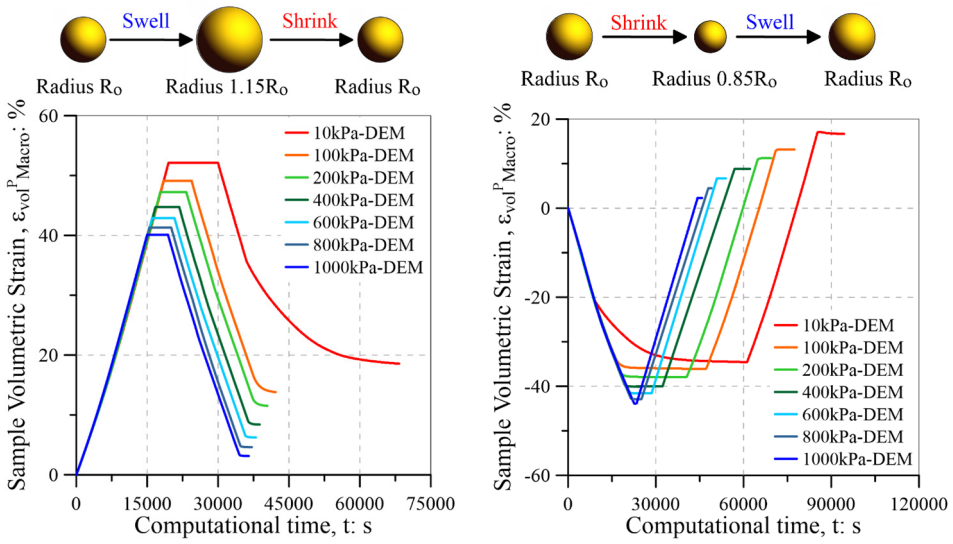

Figure B-7. Sample volumetric strain under swelling/shrinkage and shrinkage/swelling cycles.

The mechanical interaction functions from the discrete modelling and their reproduction through the exponential expressions used in the continuum-based model are plotted in the Figure B-8. The good agreement between the approaches validates the hypotheses of the constitutive double-structure model on the mechanical interactions of the Macro and micro structural levels.

The empirical nature of these interactions in the first formulations have been misunderstood with a fitting role of these functions on the double-

structure constitutive model. These discrete computations should help to dispel the above misuse. The physical source of structural interactions comes from the geometrical reorganization of the clay aggregates under hydro-mechanical actions. Respect to the discrete modelling, the spheres deformation (almost negligible) and the slip between them are the main responsible of geometrical reorganization. Contact stiffness and friction controls the system response. However, the clays aggregates interaction is more complicated; electrical forces and water menisci are involved.

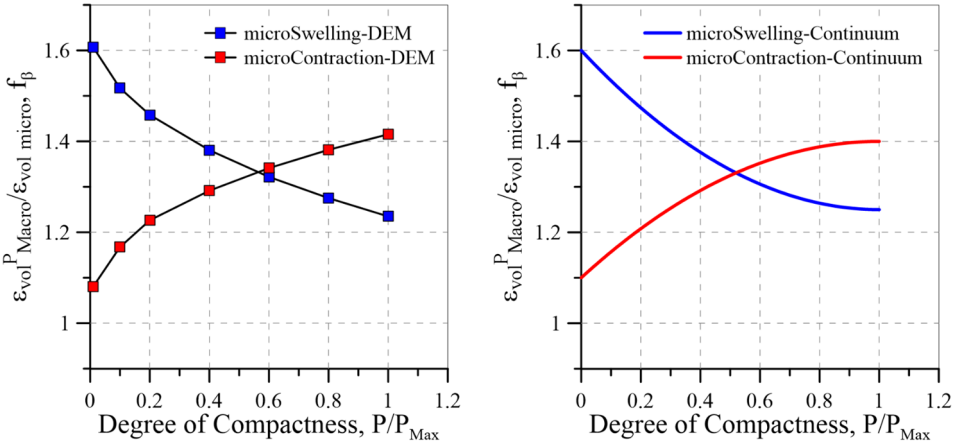

Figure B-8. Mechanical interaction functions. Left: discrete element modelling; Right: continuum approach (Table B-3) .

Table B-3. Input parameters for the Macro-micro mechanical interaction functions (see formulae in Chapter 3).

Parameter	Value
$\mathbf{f_{ms0}}$(-)	1.6
$\mathbf{f_{ms1}}$(-)	1.25
$\mathbf{n_{ms}}$(-)	2
$\mathbf{f_{mc0}}$(-)	1.1
$\mathbf{f_{mc1}}$(-)	1.4
$\mathbf{n_{mc}}$(-)	2

B.3. Conclusions

- The mechanical relationship between the two structural levels in the continuum-based formulation has been defined in a simple way. In spite

of this, the modelling of features of the unsaturated expansive clays can be carried out.

- The checking of the hypothesis behind the mechanical interaction mechanism in the double-structure constitutive model is a valuable analysis. The discrete element modelling (DEM) is a powerful numerical tool to overcome the lack of experimental data.

- A 3D discrete model has been used to evaluated the global response under the swelling and shrinkage of the particles at different stress state. The mechanical interaction functions between the sphere particles and global arrangement can be properly reproduced by the continuum-based formulae. Accordingly, the slip between sphere particles, as the driving factor for geometrical reorganization, is comparable with the clay aggregates reorganization during hydro-mechanical processes.

- The hysteretic deformation of clay aggregates due to suction change obeys to the intrusion/extrusion of water in their pore space. An option to reproduce this behaviour is the hysteretic spheres deformation. The global system response due to this might be investigated.

B.4. References

Ahmed, H.R., Abduljauwad, S.N., 2017. Nano-level constitutive model for expansive clays. Geotechnique 67, 187–207.

Alonso, E.E., Vaunat, J., Gens, A., 1999. Modelling the mechanical behaviour of expansive clays. Eng. Geol. 54, 173–183.

Darde, B., Tang, A.M., Pereira, J.-M., Roux, J.-N., Dangla, P., Talandier, J., Vu, M.N., 2018. Hydro-mechanical behaviour of high-density bentonite pellet on partial hydration. Géotechnique Lett. 8, 330–335.

Darde, B., Tang, M.A., Talandier, J., Pereira, J.-M., Roux, J.-N., Dangla, P., Vu, M.N., 2017. Swelling behaviour of pellet-based bentonite: grain-level experimental characterization and DEM simulations, in: The 7th International Conferences on Clays in Natural and Engeniereed Barriers for Radioactive Waste Confinemet. Clay Conference 2017, Davos, Switzerland. pp. 376–377.

Gens, A., Alonso, E.E., 1992. A framework for the behaviour of unsaturated expansive clays. Can. Geotech. J. 29, 1013–1032.

O'Sullivan, C., 2011a. Particle-based discrete element modeling: Geomechanics perspective. Int. J. Geomech. 11, 449–464.

O'Sullivan, C., 2011b. Particulate discrete element modelling. A geomechanics perspective. Taylor & Francis Group.

Pousada, E., 1984. Deformabilidad de arcillas expansivas bajo succión controlada (in spanish). PhD thesis, Universidad Politécnica de Madrid, Spain.

Romero, E., Simms, P.H., 2008. Microstructure investigation in unsaturated soils: A review with special attention to contribution of mercury intrusion porosimetry and environmental scanning electron microscopy. Geotech. Geol. Eng. 26, 705–727.

Yao, M., Anandarajah, A., 2003. Three-Dimensional Discrete Element Method Analysis of Cohesive Soil. J. Eng. Mech. 129, 585–596.